DRAFT DISCLAIMER

This contractor document was prepared for the U.S. Department of Energy (DOE), but has not undergone programmatic, policy, or publication review, and is provided for information only. The document provides preliminary information that may change based on new information or analysis, and is not intended for publication or wide distribution; it is a lower level contractor document that may or may not directly contribute to a published DOE report. Although this document has undergone technical reviews at the contractor organization, it has not undergone a DOE policy review. Therefore, the views and opinions of authors expressed do not necessarily state or reflect those of the DOE. However, in the interest of the rapid transfer of information, we are providing this document for your information.

Even # pages from 44 → 64 missing in original transmittal

SLTR97-0002
Pre-Experiment Thermal-Hydrological-Mechanical Analyses for the ESF Heated Drift Test

Nicholas D. Francis, Steven R. Sobolik, Clifford K. Ho,
Roger R. Eaton, Dale Preece
Nuclear Waste Management Center

Sandia National Laboratories
Albuquerque, NM 87185

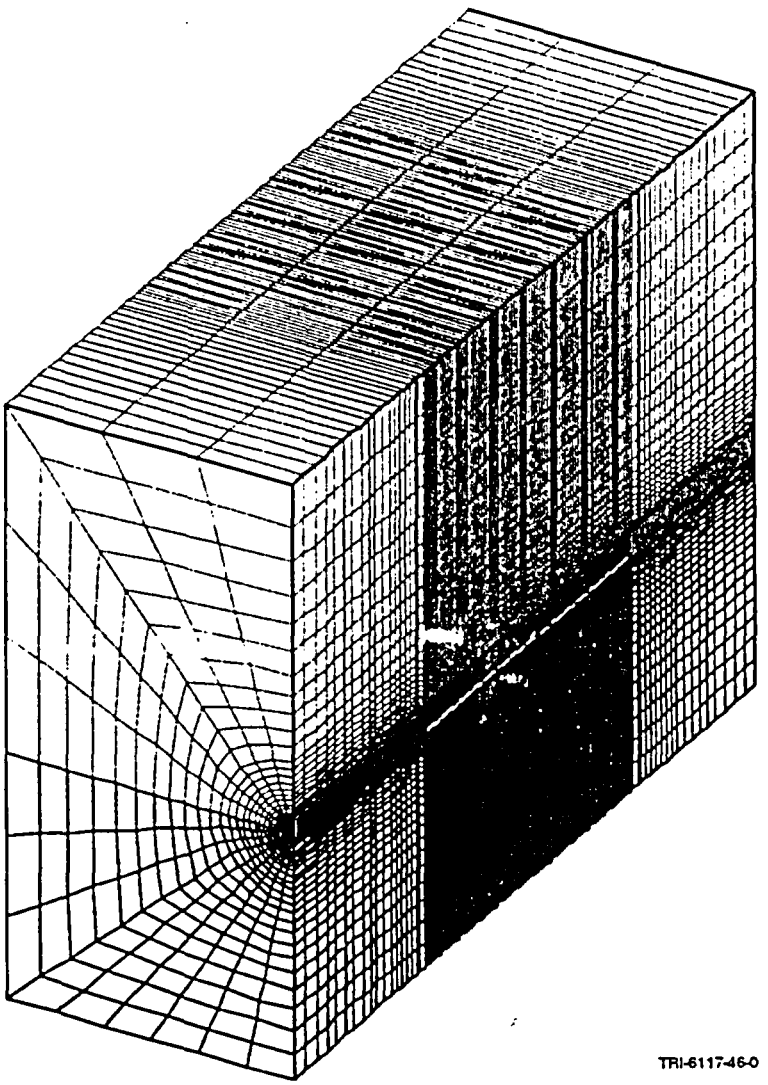

Three-Dimensional Mesh of the Heated Drift Used for the Thermal-Mechanical Calculations

SLTR97-0002
Pre-Experiment Thermal-Hydrological-Mechanical Analyses for the ESF Heated Drift Test

Nicholas D. Francis, Steven R. Sobolik, Clifford K. Ho,
Roger R. Eaton, Dale Preece
Nuclear Waste Management Center
Sandia National Laboratories
Albuquerque, New Mexico 87185

EXECUTIVE SUMMARY

This document describes pre-test analyses performed for the Heated Drift component of the Drift Scale Test in the Exploratory Studies Facility (ESF) at Yucca Mountain. The heating phase of the Heated Drift test is planned to begin in December 1997. The analyses documented in this report are pre-experiment thermal-hydrological-mechanical (T-H-M) analyses modeling the response of the the heated drift and surrounding rock induced by the horizontally-emplaced in-drift canister heaters and wing heaters with a total power output of approximately 210-220 kW. The experimental T-H-M response will be determined by measurements of temperature, moisture content, and displacement on and within the test block. The analyses performed include thermal-hydrological and thermal-mechanical calculations, with predictions of temperatures and displacements at selected locations in the drift where multi-point borehole extensometers (MPBX) will be installed. Input parameters for the calculations were obtained as much as possible from either the Heated Drift site or the nearby Single Heater Test site.

Thermal-hydrologic (T-H) modeling is performed using a two-dimensional (X-Z) cross-sectional model domain representing the center of the experiment, a two-dimensional (Y-Z) longitudinal model domain used to characterize edge cooling effects as a result of unheated rock mass at either end of the drift, and a three-dimensional "periodic boundary" model used to assess the effects of model dimensionality on the T-H model predictions. Temperature-time histories at ESF-HD-MPBX-7, 8, 9, and 10 are presented for the 2, 3, and 4 year heating scenarios with 2 year cooling. Time-histories predictions are given for both high and low permeability rock at this specified location. Additionally, temperature and liquid saturation contours are shown for each of the T-H models applied in the analyses. Temperature and liquid saturation profiles are given for both high and low permeability rock at 6 month intervals for the different heating scenarios.

Temperature-time history predictions near the center of the experiment (at the locations of the probes ESF-HD-MPBX-7, 8, 9, and 10) indicate maximum collar temperatures of 260°C, 300°C, and 330°C, respectively for 2, 3, and 4 year full power heating cycles. The high permeability results are approximately 10°C less. Temperature results at other borehole locations off center will be lower as a result of edge cooling into surrounding unheated rock mass. Both cases (low and high rock bulk permeability) indicate transport of energy by convection. The high bulk permeability cases indicate a constant temperature refluxing zone driven by buoyant convection.

Temperature contours indicate the location of important isotherms (96°C, 200°C) at different times during heating. Liquid saturation profiles indicate the location of dry-out zone and the extent of the condensate shedding. The low permeability cases indicate the formation of a symmetrical dry-out zone above and below the heater horizon. The high bulk permeability cases indicate the formation of an asymmetric dry-out zone with preferential drying below the heaters. It is note that for both cases, the formation of a large condensate zone forms below the heater due to water shedding. The longitudinal Y-Z model indicates the importance of edge cooling on both the temperature predictions as well as the location of water shedding around the unheated ends of the drift. Also, the 2-D X-Z cross-section model is compared to the 3-D periodic X-Y-Z model in order to assess the effects of dimensionality of the problem. It is noted that the 2-D model very accurately predicts the drift wall and surrounding rock temperatures. This is important as computational efficiency and the use of 2-D models will allow for extended analyses including the use of alternative conceptual models such as the dual permeability model.

Predictions of the displacement-time histories in the host rock during the heating and cooling phases of the heated drift test at selected MPBX anchor locations indicate maximum extension for any probe from collar to deepest anchor of about 15 mm. Displacement magnitudes were shown to be a strong function of the choice of thermal expansion coefficients. Also, predictions for the sequential drift mine-by MPBX's indicate that their measurements may be used as an indicator of rock mass elastic modulus because of the predicted difference in behavior between using an intact rock value of 36.8 GPa versus a value of 10 GPa obtained from nearby Goodman jack testing. Bulk permeability over the range of values measured at the heated drift site was not shown to be a strong factor in the general thermal-mechanical behavior or the magnitudes of thermally-induced displacements.

This work was performed by Sandia National Laboratories under Yucca Mountain Project WBS number 1.2.3.14.2. The SNL Work Agreement WA-0332 (SNL, 1996) details the SNL Quality Assurance procedures that governed the work described in this document. The completion of this document satisfies CRWMS M&O Level 4 Milestone SP9318M4. Table 1 outlines the criteria for these milestones and where they are met in this report. The completion of this milestone supports the M&O Level 3 Milestone SP3305M3, due July 16, 1997.

Table 1. List of Milestone Criteria Satisfied by This Report

Level 4 Milestone ID SP9318M4 is a letter report completed and reviewed by 6/13/1997. This report documents the results of thermal-hydrologic and thermal-mechanical analyses of the heated drift test which will predict the temperature, liquid saturation, and displacement profiles in the tunnel rock at intervals of one week for the first twelve weeks, and one month thereafter from the start of both the heating and cooling phases of the test.	
Criteria for SP9318M4	**Location**
Discussion of planned heated drift test geometry	Sections 3 and 4
Discussion of all thermal-hydrologic input parameters	Section 3
Discussion of thermal-hydrologic analyses	Sections 3 and 5.1
Temperature-time histories for selected thermocouples	Appendix A
Contour plots of temperatures at selected times	Appendix B and C
Contour plots of liquid saturation at selected times	Appendix B
Discussion of all thermal-mechanical input parameters	Section 4
Discussion of thermal-mechanical analyses	Sections 4 and 5.2;
Displacement-time histories for selected displacement sensors	Appendix D

Table of Contents

1. Introduction

This document describes pre-test analyses performed for the Heated Drift component of the Drift Scale Test in the Exploratory Studies Facility (ESF) at Yucca Mountain. The heating phase of the Heated Drift test is planned to begin in December 1997. The SNL Work Agreement WA-0332 (SNL, 1996) defines pre-experiment thermal-hydrological-mechanical (T-H-M) analyses modeling the response of the welded tuff in the heated drift and surrounding rock induced by the horizontally-emplaced in-drift and wing heaters with a total power output of approximately 210 kW. The experimental T-H-M response will be determined by measurements of temperature, moisture content, and displacement on and within the test block. The T-H-M analyses performed include thermal-hydrological and thermal-mechanical calculations. Input parameters for the calculations were obtained as much as possible from either the Heated Drift site or the nearby Single Heater Test site. This work was performed by Sandia National Laboratories under Yucca Mountain Project WBS number 1.2.3.14.2. The SNL Work Agreement WA-0332 (SNL, 1996) details the SNL Quality Assurance procedures that governed the work described in this document. The completion of this document satisfies CRWMS M&O Level 4 Milestone SP9318M4.

1.1 Background

The Exploratory Studies Facility (ESF) Thermal Test, shown schematically in Figure 1-1, is an integral part of the program of site investigations to characterize Yucca Mountain in Nye County, Nevada for the permanent disposal of spent nuclear fuel and high level nuclear waste. The purpose of the ESF Thermal Test is to understand better the coupled thermal, mechanical, hydrological, and chemical processes likely to exist in the rock mass surrounding the potential geologic repository at Yucca Mountain. Plans for a suite of in situ thermal tests to be conducted in the ESF began with the *Site Characterization Plan* (SCP) (DOE 1988). The planning basis documented in the SCP has evolved over the past several years to meet the changing needs and updated knowledge base of the project. The most recent iteration, in which the SCP thermal testing program was re-evaluated and consolidated, is discussed in *In Situ Thermal Testing Program Strategy* (DOE 1995). The ESF Thermal Test is being conducted in a facility specifically constructed for this purpose in the middle nonlithophysal (tptpmn) lithologic unit of the Topopah Spring Welded Tuff (TSw2) thermomechanical unit, the proposed repository horizon.

The ESF Thermal Test is comprised of a single heater test (SHT), and a drift scale test (DST) which is comprised of a sequential drift mining test (SDMT), a plate-loading test (PLT), and a heated drift test (HDT). In the DST, the local rock mass will be heated by electrical heaters placed in horizontal boreholes drilled into the ribs at the springline and canister within the Heated Drift itself. Ultimately, thermal-mechanical-hydrological-chemical (TMHC) behavior in the local rock mass and the performance prototype ground support systems will be measured in the main DST. Additional thermo-mechanical responses will be measured in the SDMT and the PLT portion of the DST.

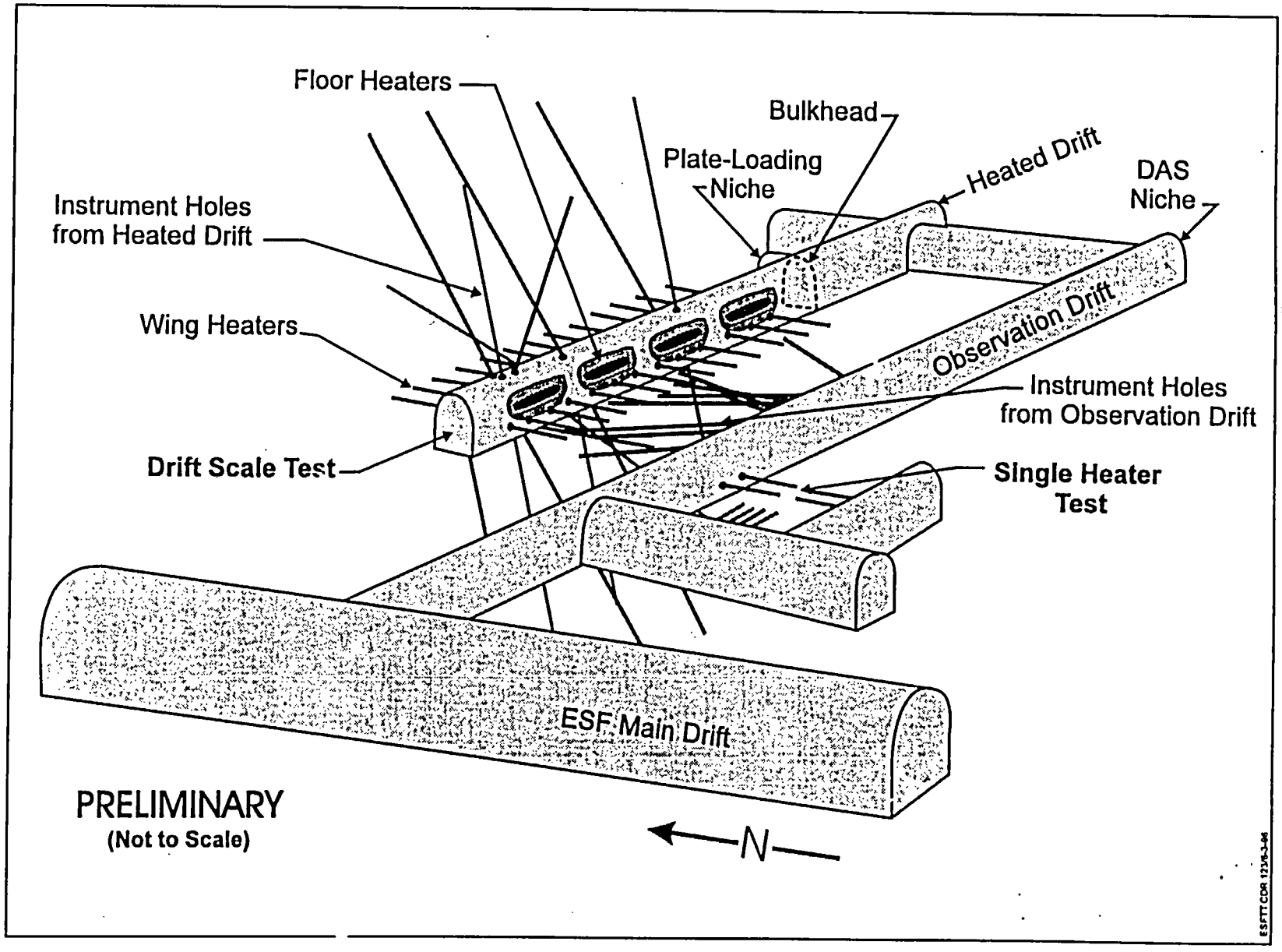

Figure 1-1. Schematic of ESF Thermal Test Facility

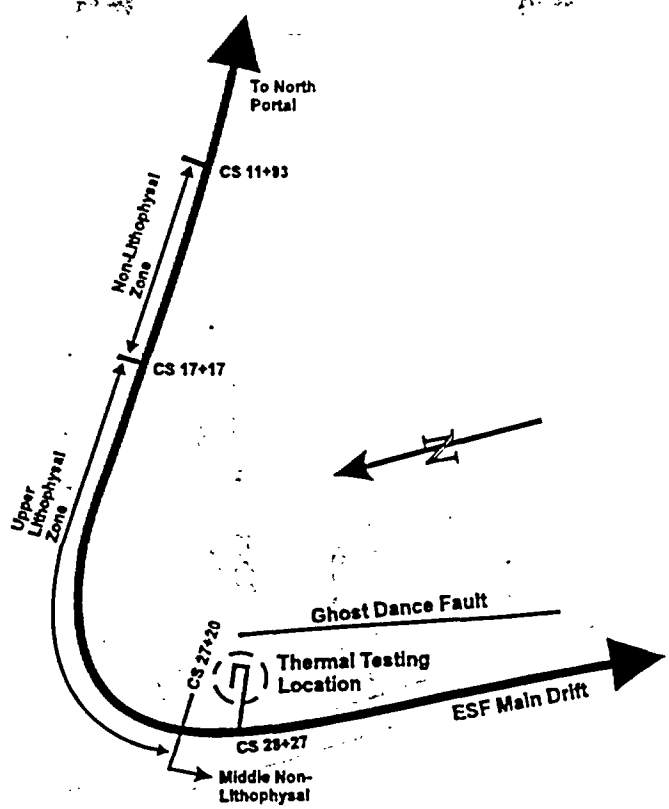

(a) ESF Location

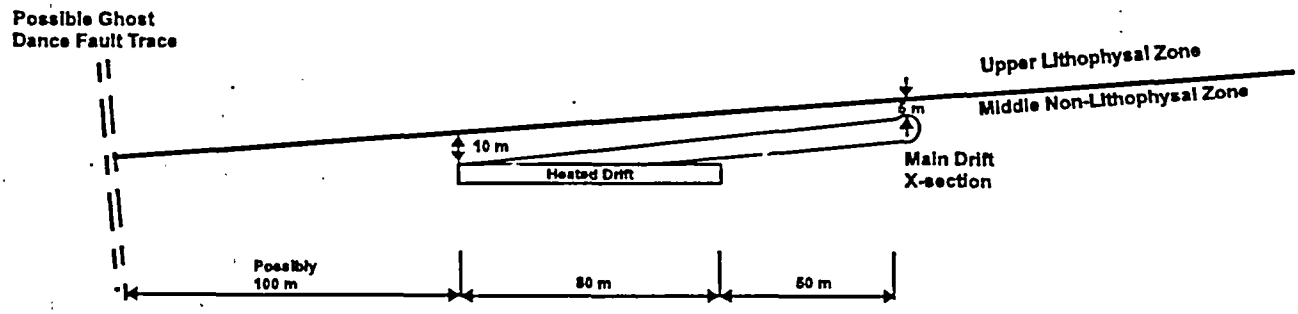

(b) Stratigraphic Location

REFERENCE ONLY
(Not to Scale)

ESFTT2.CDR.123/6-3-96

Figure 1-2. General Location of the ESF Thermal Test

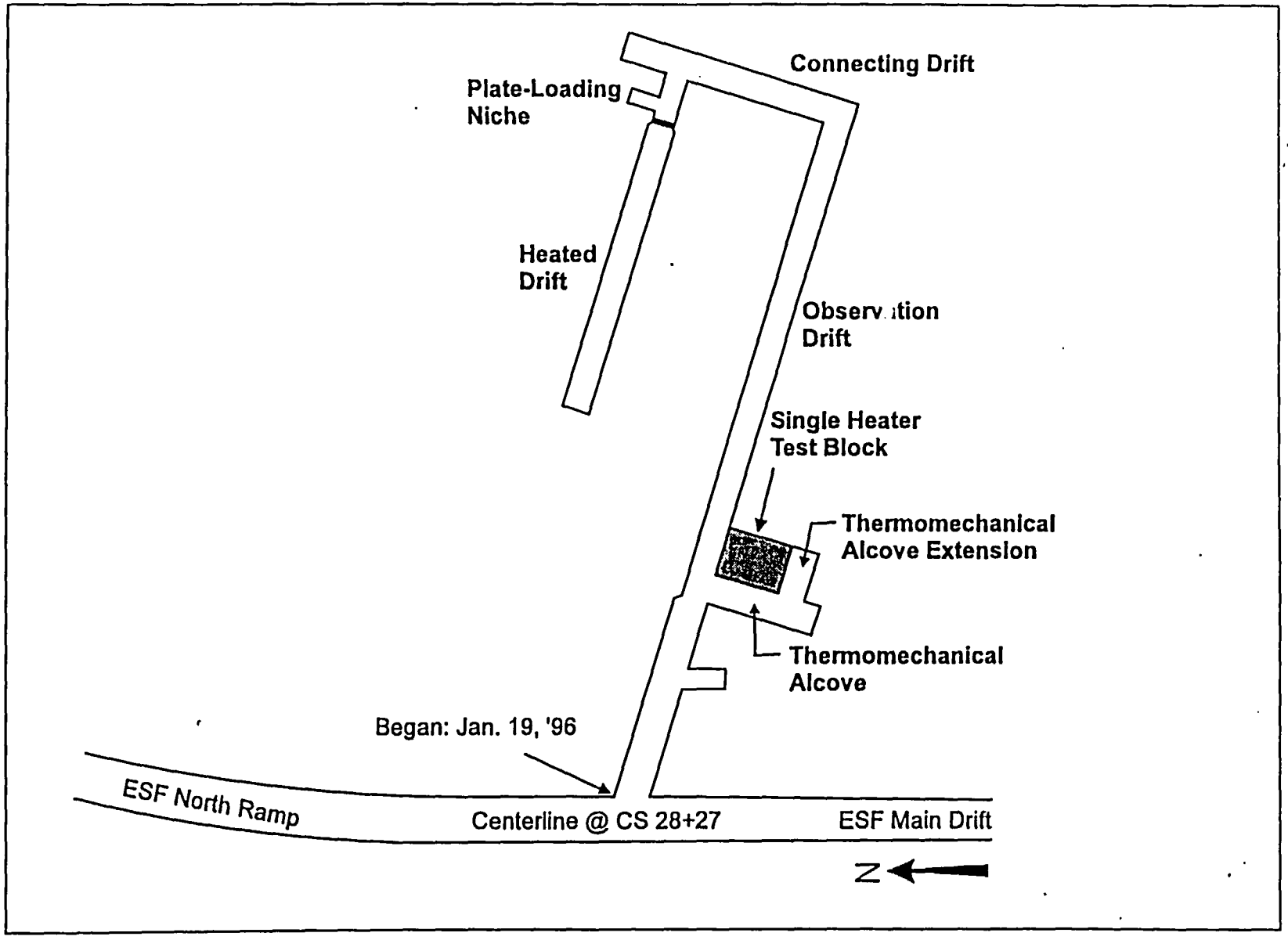

Figure 1-3. Plan View of the ESF Thermal Test Facility

The ESF Thermal Test facility general location and plan view are shown in Figures 1-2 and 1-3, respectively. The ESF Thermal Test will consist of an east-west observation drift driven downward from the ESF main drift, a connecting drift, and the heated drift constructed parallel to the observation drift. The orientation of the heated drift is nominally N72°W. Measurements will be made via instruments placed in boreholes drilled from the observation, connecting, and heated drifts.

1.1.1 Linkage of the ESF Thermal Test to the SCP and Subsequent Program Directives

The linkage of the ESF Thermal Test to the SCP and subsequent program directives has been well chronicled over the past eight years. The following citations represent current Yucca Mountain Site Characterization Project documents that describe scientific plans for the ESF Thermal Test. These documents, together with related study plans, include:

- *Site Characterization Plan* (DOE 1988) Studies
  - Section 8.3.1.15.1.5 Excavation Investigations
  - Section 8.3.1.15.1.6 In Situ Thermomechanical Properties
  - Section 8.3.1.15.1.7 In Situ Mechanical Properties
  - Section 8.3.4.2.4.4 Engineered Barrier System Field Tests

- *Technical Implementation Plan for WBS 1.2.3 Investigations* (YMP 1995)

- *In Situ Thermal Testing Program Strategy* (DOE 1995)

In Section 8.3 of the SCP, a number of in situ tests were proposed to investigate various aspects of thermal performance. These tests included measurement of thermal properties, investigations of TM effects on drift stability, and study of coupled TMHC processes that may affect the near-field and waste package performance or the far-field natural system performance. The objective of this suite of tests was to provide data for use in determining site suitability, for direct input into repository and waste package design, for model development and validation, and for performance assessments of preclosure safety and postclosure performance. In the SCP, the conceptual nature of the testing program was discussed along with the explicit ties to the data needs. Each test was expected to provide primary or confirmatory information for resolving specific performance and design issues within the SCP issues hierarchy. The tests were divided into two main categories: tests focused principally on TM processes to resolve preclosure and postclosure repository design issues (Section 8.3.1.15.1), and tests focused on resolving postclosure waste package design and near-field performance issues (Section 8.3.4.2.4). In addition to simple parameter measurement, the test objectives include the need to provide data to assist validation of thermal and mechanical models to be used for repository design and performance assessment, as well as the need to demonstrate that regulatory requirements could be met. The embodiment of these objectives into the test program resulted in tests that simulate the repository emplacement geometry and thermal loading strategy. Table 1-1 provides a summary of some of the issues and information/data needs addressed by the in situ thermal testing program. Note that not all aspects of the SCP will be addressed in the ESF Thermal Test. Rather it will focus primarily on obtaining a better understanding of the TMHC behavior in the local rock mass.

Table 1-1. SCP Issues and Data Needs

Testing Program	Issues	Information/Data Needs
Thermal/ Mechanical Tests	1.6 Ground Water Travel Time 1.10 Waste Package-Postclosure 1.11 Underground Configuration-Postclosure 1.12 Shaft and Borehole Seals 2.4 Waste Retrievability 4.2 Nonradiological Health and Safety 4.4 Preclosure Design/Feasibility	· Thermal properties of the rock mass · Thermal expansion · Deformation modulus at elevated temperature · Mechanical properties of fractures at elevated temperature · Thermal performance of backfill materials · Near-field permeability changes at elevated temperature · Thermal effects on ground support
Waste Package/ Near-Field Environment Tests	1.10 Waste Package-Postclosure 1.11 Underground Configuration-Postclosure 2.4 Waste Retrievability	· Near-field thermal history · Distribution of liquid water and saturation levels Changes in near-field mineralogy and fluid chemistry resulting from thermal loading · Changes in near-field hydrologic properties resulting from thermal loading · Rock-mass thermal and mechanical properties · Mechanical and hydrological properties of fractures

1.1.2 Information Needs Addressed by the Heated Drift Test

The information and data needs for the thermal testing program, identified in the SCP (DOE 1988) and further refined in the *In Situ Thermal Testing Program Strategy* (DOE 1995) are listed in Table 1-2. These needs which are described in three basic terms (bounded, conservative, and substantially finished), provide the anticipated status of information and data following the completion of the ESF Thermal Test.

The nomenclature of the ESF Thermal Tests used in Table 1-2 are defined as follows:

B(Bounded)—The extreme values (low and high) are known

C(Conservative)—Only one extreme value is known and it will contribute to conservative calculation of a corresponding behavior.

SF (Substantially Finished)—The information and data is mostly known

Also included in the table are the various end users of the data (Waste Package Design, Repository Design, and Performance Assessment) as well as the degree (conservative, bounded, or substantially finished) to which the data must be known for the initial license application.

Table 1-3 provides a comprehensive listing of information needs in terms of parameters to be measured in the ESF Thermal Test. Also included in the table are the corresponding instruments, which will measure these parameters in the SHT and/or DST.

1.1.3 Relevant Processes

Table 1-4 provides a matrix of thermally related processes and parameters which are considered relevant to the Heated Drift Test. Specifically, four types of processes are identified: thermal, mechanical, hydrological, and chemical. Each process consists of at least four subprocesses which are labeled in terms of their importance as either primary or secondary. Primary processes will receive much emphasis and will be addressed directly in the ESF Thermal Test. Secondary processes will receive less attention but their understanding will be advanced as a result of the ESF Thermal Test.

Discussion of the matrix of processes presented in Table 1-4 alludes to the appropriateness of the temporal and spatial scales in the ESF Thermal Tests. On a comparative basis, the temporal and spatial scales planned for the ESF Thermal Test are approximately equivalent or substantially longer and larger than other thermal tests associated with geologic disposal of nuclear waste (DOE, 1995). This favorable comparison with other thermal tests combined with the ESF Thermal Test objective to understand better the coupled TMHC processes ensures, to a large degree, that the planned temporal and spatial scales are appropriate. By linking the objective to the TMHC processes, investigators can address scaling issues properly because emphasis is placed on heating and cooling a substantial volume of rock such that observable dryout and rewetting zones are created.

In summary, the temporal and spatial scales are suitable for the ESF Thermal Test such that emphasis can be placed on understanding better the TMHC coupled processes which influence post-closure behavior. Characterizing other post-closure behavior is outside the scope of the ESF Thermal Test.

Table 1-2. Summary of Information Needs for the Thermal Testing Program (based on DOE 1995)

Data and Information Needs	Customers			
	Waste Package Design	Repository Design	Performance Preclosure	Assessment Postclosure
Near-field TMHC Processes				
Changes in Rock Saturation	B	N/A	N/A	B
Drift Humidity	B	C (Ventilation)	N/A	B
Water Chemistry (liquid reflux)	B	C (GS)	N/A	B
Propagation of "drying front"	N/A	N/A	N/A	B
Residual water saturation	B	N/A	N/A	B
Drainage/reflux of liquid by fracture flow (heterogeneity, heat pipes, fast paths)	B	N/A	N/A	B
Rock mass and fracture permeability changes (induced by construction and thermal load)	N/A	N/A	N/A	B
Conductive/convective heat transfer	B	N/A	N/A	B
Rock Mass Properties over a Range of Temperature				
Thermal heat capacity (specific heat)	SF	N/A	N/A	B
Thermal conductivity	SF	N/A	N/A	B
Thermal expansion	N/A	SF	SF	B
Deformation modulus	N/A	SF	SF	B
Strength	N/A	B	B	B
Normal and shear compliance	N/A	B	SF*	N/A
Shear strength of fractures	N/A	B	SF*	N/A
Cohesion of fractures	N/A	B	SF*	N/A
Drift Response/Stability under Thermal Conditions	B	B	B	B
Ground Support and Design Feature Interactions at Elevated Temperatures				
Rock mass/ground support	N/A	SF	B	N/A
Effect of materials on near-field water chemistry	C	C (GS)	C (GS)	C
TH properties of backfill	C	C (for emplacement)	N/A	C
In situ waste package material corrosion	C	N/A	N/A	C

* To achieve the stated level of confidence, laboratory or bench-scale tests are required. In situ tests can only provide gross estimates. Nomenclature: C-Conservative; B-Bounded; SF-Substantially Finished; GS-Ground Support;
N/A-Not Applicable

Table 1-3. Listing of Parameters and Corresponding Instrumentation

Information Needs/Parameters	Instrumentation Types
Heat Capacity (Specific Heat)	· Resistance Temperature Detectors (RTD) · Thermocouples · Rapid Evaluation of K and Alpha-Thermal Probes (REKA)
Thermal Conductivity	· Resistance Temperature Detectors (RTD) · Thermocouples · Rapid Evaluation of K and Alpha-Thermal Probes (REKA)
Thermal Expansion	· Multi-Point Borehole Extensometers (MPBX) · Wire Extensometers
Deformation Modules	· Goodman Borehole Jack · Plate-Loading
Rock-Mass Ground Support Interaction	· Rock Bolt Load Cells · Pull Tests · Multi-Point Borehole Extensometers (MPBX) · Wire Extensometers · Strain Gage Arrays
Changes in Rock Saturation	· Humicaps · Neutron Logging · Electrical Resistivity Tomography (ERT)
Propagation of "Drying Front"	· Humicaps · Neutron Logging · Electrical Resistivity Tomography (ERT) · Resistance Temperature Detectors (RTD)
Residual Water Saturation in "Dry Zone"	· Humicaps · Neutron Logging · Electrical Resistivity Tomography (ERT)
Drainage/Reflux of Liquid by Fracture Flow	· Infrared Imaging · Detailed Fracture Mapping · Fluid Sampling · Electrical Resistivity Tomography (ERT) · Resistance Temperature Detector (RTD)
Rock-Mass and Fracture Permeability Changes	· Gas Permeability Measurements · Gas Gage Pressure Transducers
In Situ Stress and Stress Orientation	· Hydraulic Fracturing
Convergence, Convergence Rate, and Rock-Mass Displacement	· Multi-Point Borehole Extensometers (MPBX) · Tape Extensometers · Wire Extensometers
Air Permeability	· Borehole Packers with Pressure Transducers
Moisture Content and Water Potential	· Borehole Packers with Psychrometers and Transducers
Relative Humidity and Drift Wall Moisture	· Humicaps · Infrared Imaging Camera

Table 1-4. Matrix of Processes Relevant to the Heated Drift Test

Heat Related Processes and Parameters	Heated Drift Test
Thermal	
Conduction	Primary
Convection	Primary
Radiation	Primary
Heat Pipes	Primary
Enhanced Diffusion	Secondary
Effect of Percolation on Temperature Distribution	Primary
Hydrological	
Sub-Boiling Mobilization (toward drift)	Primary
Sub-boiling Mobilization (away from drift)	Primary
Dry-out Zone Formation (boiling/sub-boiling)	Primary
Two Phase Water Movement From Dry-Out Zone	Primary
Vapor Movement from Condensation Zone	Primary
Shedding/Drainage from Condensation Zone	Primary
Imbibition in Condensation Zone	Primary
Vapor Removal (engineered system)	Secondary
Rewetting Time	Primary
"Downspout" Rewetting	Primary
Effect of Lateral Condensation on Downspout Rewetting	Primary
Mechanical	
Rock-Mass Properties	Primary
Drift Stability, Preclosure	Primary
Drift Stability, Postclosure	Primary
Fracture Aperture Change	Secondary
New Fracture Formation	Secondary
Near Field Stress/Displacement	Primary
Ground Support—Rock Mass Interaction	Primary
Chemical	
Return Water Chemistry (to waste package)	Primary
Evolution of Near Field Water Chemistry	Primary
Change to Hydrologic Pathways	Primary
Change to Matrix Transport Properties	Secondary

1.2 Heated Drift Test

Elements of the emplacement drift test and the plate source test as described in the report *In Situ Thermal Testing Program Strategy*, have been combined into the DST. As shown in Figure 1-1, the main test in the ESF Thermal Test is the heated drift, approximately 47.5 m long. Canister and wing heaters, simulating the thermal pulse from drift-emplaced waste packages in multiple drifts, will heat the local rock mass. Canister heaters are intended to simulate waste packages within the emplacement drifts whereas wing heaters simulate the influence of waste packages in adjacent emplacement drifts. The change in temperature of the rock will be measured at numerous locations by Resistance Temperature Detectors (RTDs) and thermocouples installed in boreholes drilled from the heated drift (HD), connecting drift, and the observation drift. Additionally, changes in rock displacement, moisture content, relative humidity, and chemistry will be measured by a variety of instruments inserted in boreholes strategically-located in the three drifts. Responses from instrumented ground support systems within the HD will also be measured as the local rock-mass temperature increases. It is possible the heating period in the DST will be as long as four years. Test results will be evaluated at the end of two years of heating to decide whether to continue heating and for how long. The heating phase will be followed by a cooling phase of comparable duration. The heated drift will be isolated by a bulkhead which will include an observation window and a vent to avoid and measure pressure buildup. The vent will be instrumented to measure flow rate, temperature, and humidity.

The objectives of the Drift Scale Test (DST) include the following:

- Examine the near-field TMHC environment that may impact the waste package such as
  - transient temperature distribution and possible formation of heat pipes
  - chemical changes from drying and reflux conditions
  - changes in rock saturation before, during, and after the test
  - propagation of the drying and subsequent re-wetting regions, including potential condensate cap and drainage, at intermediate rock-mass scale
  - residual saturation levels in the dry zones
  - drift humidity, temperature, and air pressure
  - changes in rock mass and fracture permeability
  - thermal expansion and deformation modulus of the rock
  - drift response and stability including ground support systems
- Provide a conceptual model and hypothesis test bed for thermal and coupled models used to examine the interrelationships between thermal, mechanical, hydrological, and chemical behavior such that realistic bounds can be developed on the expected near- field environment.
- Measure corrosion rates on typical waste package materials subjected to in situ conditions.
- Observe the effects of thermal loading on prototypical ground support systems.

It is a natural extension to the scope of the ESF Thermal Test to consider previous heater tests. Lessons learned from other heater tests, as documented by the DOE (1995), were an integral part of the planning process for the ESF Thermal Tests. Previous heated tests from which observations such as physical size, processes observed, failure occurrence, logistical problems,

and data interpretation, are listed below:

- G-Tunnel Underground Facility (Nevada)
- Waste Isolation Pilot Plant (New Mexico)
- Underground Research Laboratory (Canada)
- Basalt Waste Isolation Project (Washington)
- Stripa Underground Test Facility (Sweden)
- Avery Island (Louisiana)

Although a direct comparison is difficult, it appears the ESF Thermal Test is at least comparable and in many instances superior to other heater tests in the following categories:

- Volume of rock heated above 100°C (approximately 30,000 cubic m)
- Duration of heating (2 to 4 years) and cooling (2 years) periods
- Heater power (approximately 210 kW)
- Processes measured (4-TMHC)
- Number of sensors installed (approximately 5,000)
- Number of boreholes (approximately 210)
- Length of boreholes (approximately 4,000 m)

Note that the above statistics represent a composite of all components of the ESF Thermal Test which includes primarily the SHT and DST, although the DST is by far the larger component.

1.3 Schedule

The DST is scheduled to be started on December 8, 1997 (heater turn on). The heating period may continue for as long as four years while the cooling period may be two years or more. At the end of two years of heating, an evaluation will be conducted from which the DOE will decide whether to continue the heating and for how long.

2. Task Description

The Heated Drift test facility was still under construction as the analyses described in this report were being conducted. Therefore, some technical information required as input for these analyses, including heater locations and outputs, instrumentation locations, and DST site-specific T-H-M rock properties were based on design data and site-specific rock property data from the Singe Heater Test. The selection of all input for these analyses was based on information available on February 1, 1997, The testing scenario for the Heated Drift Test that will be modeled by the analyses described in this document is as follows:

- A Heated Drift facility approximately matching the Drift Scale Test facility description in Figures 1-1, 1-2, and 1-3 has been excavated. The tunnel is approximately 5 m in diameter with a concrete invert of 1.3 m maximum thickness installed, and 47.5 m in length.
- Nine canister heaters will be emplaced in the Heated Drift. The canister heaters are in the form of canisters containing linear heating elements with a combined output of 7.5 kW per canister. Fifty wing heaters will be located in the rock mass in boreholes drilled horizontal and perpendicular to the axis of the Heated Drift. Each wing heater will have an inner segment generating 1145 watts output at full power and an outer segment generating 1716 watts at full power. The estimated maximum power output for all the heaters is 210.55 kW. (On February 1, 1997, the best available estimate for total heater output was 215 kW; this value is used in the analyses described in this report.)
- Multi-point borehole extensometers (MPBXs), rod extensometers and anchor pins, srain gages, thermocouple probes, and moisture sensors will be installed into the rock per the test design as documented in the ESF Thermal Test design document (CRWMS M&O, 1996); their locations have been determined.
- The heaters are turned on at full capacity (~210 kW total) for a period of two, three, or four years, during which temperature, displacement, and moisture content measurements are taken. After the heating period, the heater is turned off; the measurements are continued for an additional period of two years.

The following tasks are defined to predict the T-H-M response of the TSw2 rock surrounding the Heated Drift during the Drift Scale Test.

Task 1: Thermal-Hydrological Predictions for the Heated Drift Test

A series of calculations to predict the thermal-hydrological response of the rock to the presence of the heaters were performed. The calculations were performed with the multi-phase, three-dimensional thermal-hydrological code TOUGH2 (Pruess, 1991), Version 3.2 in SNL's Software Configuration Management System. These calculations provide temporal predictions of temperature at the in situ locations of the thermocouples, and predictions of liquid saturation in the block over time for comparison with moisture-sensing gages (neutron probes, electrical resistivity tomography, and humicaps). Predicted two- and three-dimensional temperature and saturation behavior will be presented in this report with contour plots at selected times, and temperature-time histories at selected thermocouple locations. The predicted temperature histories for the entire test block were used as input to the thermal-mechanical calculations (Task 2).

Task 2: Thermal-Mechanical Predictions for the Heated Drift Test

A series of calculations to predict the thermal-mechanical response of the rock to the presence of the heater were performed. The calculations were performed with the finite element nonlinear structural mechanics code JAC3D (Biffle, 1993), Version 6.1-04 in SNL's Software Configuration Management System. These calculations provide temporal predictions of displacements at the in situ locations of the MPBXs and rod extensometers.

3. Thermal-Hydrologic Modeling Approach

3.1 Introduction

The thermal-hydrologic (T-H) calculations provide the temperature, liquid saturation, and gas phase pressure distributions in the host rock during the heating and cooling phases of the Drift-Scale Heater Test (DST) by solving the coupled conservation equations of energy and mass transfer. Heating phases of 2, 3, and 4 years are considered in the analyses coupled with 2 years of cooling after the heaters are turned off. The resulting temperature fields (at different times into heating and cooling) obtained from the T-H calculations are used as inputs to the thermal-mechanical (T-M) calculations used to provide predicted rock displacements during the experiment.

The T-H calculations are based on the early measured predictions by LBNL (personal communication from Yvonne Tsang, LBNL) of the range in bulk permeabilities obtained from the DST area. In each of the cases described in the following sections, T-H simulations have been completed for low and high bulk permeability cases. The site specific values used here are in the range of 2.19 millidarcy to 6.4 darcy for the low and high bulk permeabilities, respectively. More recent permeability data obtained by LBNL indicate that the high bulk permeability value used may be overestimated by a factor of about 3. Although the upper end value used in the analysis is higher, it is still considered a bounding value for a high bulk permeability simulation. This range of values obtained from the DST area is nearly the same as those previously obtained from the SHT block (DTN LB960500834244.001,TDIF 305605). The potential solutions may fall within the range considered. It is also noted, based on the ongoing results obtained from the single heater test (SHT) area, that the lower bulk permeabilities are potentially more representative of the experimental location, particularly for early heating times.

The source of heat for this experiment includes 9 waste package type canister heaters placed inside the heated drift and 100 (50 on each side of the heated drift) wing-heaters that are borehole emplaced directly into surrounding host rock adjacent to the heated drift. Each side contains 25 inside wing heaters and 25 outside wing heaters. The inside wing heaters operate at a slightly lower power output than the outside units. This heater specification results in roughly 220 kW of total power input into the overall test area.

The following sections will describe the T-H models used to characterize the test area, the conceptual model used in the analyses, descriptions of the thermal and hydrologic properties applied in the simulations, a description of the test (and modeled) geometry, and a specific description of the approach applied to each of the T-H models used to provide temperature data input for the T-M models.

Finally, it is noted that all available DST data, including site-specific hydrologic properties such as permeability and/or any test geometry and layout information, were frozen for this set of T-H analyses as of 02/07/97. Any additional changes in geometric layout or hydrologic or thermal properties that occurred after this date can be readily incorporated into any future calculations for the DST.

3.2 General Description of the Thermal-Hydrologic Models

Three different thermal-hydrologic models are developed in order to characterize the T-H DST heating results. Due to the extensive size of the experimental test area and the limiting geometry of the wing heaters (i.e., small diameter), two representative 2-D models and a simplified "unit cell" 3-D model are used to determine the temperature fields encompassing the entire test area. The development of a full 3-D T-H model for the entire test area (including the drift and other surrounding features) including the necessary grid refinement required for each of the wing heaters would result in a very computationally intensive model domain with an excessive number of volume elements needed to describe the fundamental fluid and heat flow processes. Therefore, a modified product solution (refer to Section 4.3) was used to obtain pseudo-3-D temperature predictions for the entire test area based on the results of the simplified 2-D T-H model simulations. The 3-D "unit cell" model can be used in a limited way to assess the accuracy of the approximate solution used to obtain the overall pseudo-3-D temperature fields.

A two-dimensional cross-section model is used to determine the temperatures in the X-Z plane (where Z is vertical and hence parallel to the gravity vector). This model is a symmetry plane (i.e., near the center of the test area) and assumes that the drift length is infinitely long (i.e., infinite in the Y direction parallel to the axis of the drift). This 2-D model, however, is unable to accurately account for the edge cooling effects near the ends of the heated drift. This model domain will be the basis model in the product solution used to generate a 3-D temperature field for the thermal-mechanical calculations (refer to Section 4.3).

A second two-dimensional model is used to determine the effects of edge cooling along the ends of the heated drift. This longitudinal model domain is used to determine the temperatures in the Y-Z plane. This model uses an areal averaged amount of the total heat input (~ 220 kW) to the DST, including the heater cans in drift and the borehole emplaced wing heaters. The heat input is then scaled to the appropriate modeled area. This model includes the concrete invert in the drift floor as well as the insulated bulkhead and the concrete liner at the end of the heated drift. The longitudinal model domain will serve as the scaling component in the product solution and is used to account for edge effects near the ends of the drift (refer to Section 4.3).

A three-dimensional "unit cell" T-H model is used to determine the effects of dimensionality near the center of the heated drift (results given in Appendix B). This model is also used to guide the determination of the appropriate scaling factors for the product solution used to obtain the 3-D temperature results of the entire test area from the lower dimensional models.

3.3 General Description of the Conceptual Model

The porous medium at the DST area contains both fractures and rock matrix, each with its own set of characteristic properties. Typical conceptual models used to characterize such a system include an equivalent continuum model (i.e., an equivalent porous medium with averaged fracture and matrix properties), a dual permeability model (DKM) (i.e., a porous medium containing separate fracture and matrix continua), and a random, discrete fracture model. This T-H model analysis makes use of the equivalent continuum model (ECM) for computational

efficiency. It may be determined, based on the scale of the problem, that a DKM may be a more accurate representation of condensate drainage during the heating cycle.

The ECM assumes that thermodynamic equilibrium exists between the fractures and matrix. The fracture and matrix properties are pore volume averaged to produce parameters that represent a single effective porous material. The effective porous material can behave as matrix or fracture depending on the phase of the fluid and the bulk liquid saturation of the material. Using an ECM formulation for heat and mass transfer, effective material properties can be defined as the following:

$$\phi_b = \phi_f + (1-\phi_f)\phi_m \tag{3-1}$$

$$S_b = \frac{S_f\phi_f + S_m(1-\phi_f)\phi_m}{\phi_f + (1-\phi_f)\phi_m} \tag{3-2}$$

$$K_b = K_f\phi_f + K_m(1-\phi_f) \tag{3-3}$$

where ϕ_b is the effective porosity, S_b is the effective liquid saturation, K_b is the effective (bulk) permeability, all a function of rock matrix (subscript *m*) and fracture (subscript *f*) properties. It is assumed in the T-H analyses that the test area properties are homogeneous as well as isotropic. That is, the material properties do not vary with location or direction (X, Y, Z).

The unsaturated zone is characterized by two-phase gas and liquid. Water is represented in both the liquid and gas phases. For two-phase flow in a partially saturated porous medium, functions relating liquid saturations and liquid relative permeability to capillary pressure are required. The van Genuchten (1980) two-phase characteristic functions for capillary pressure and liquid phase relative permeability are used with the ECM formulations defined above.

3.4 General Description of the Hydrologic and Thermal Properties

3.4.1 Hydrologic Properties

Hydrologic properties such as porosity (fracture and matrix), permeability (fracture and matrix), characteristic curve data (fracture and matrix), and in situ liquid saturations are required for the T-H calculations performed using the code TOUGH2 (Pruess, 1991). Some of the data comes from the DST area itself (i.e., bulk permeability ranges), while other data comes from the Single Heater Test area (SHT) (i.e., fracture frequency). Other hydrologic data come from borehole measurements and are representative of the Middle Nonlithophysal (Tptpmn) unit properties obtained by Flint, 1996. Table 3-1a lists all the hydrologic input values used for the DST analyses and the sources for each. When necessary, DST hydrologic properties are consistent (or calculated in a consistent manner) with the hydrologic property calculations performed for the SHT (Sobolik et al., 1996).

Table 3-1a. Hydrologic Values Used in the T-H Calculations

Hydrologic parameter	Value	Source, Comments
Bulk permeability, m^2 Low value High value	 2.16×10^{-15} 6.35×10^{-12}	Initial (1/97) air-permeability test results for the DST See Comment 1 below.
Matrix porosity	0.11	See Comment 2 below.
Matrix permeability, m^2 (and corresponding saturated hydraulic conductivity, m/s)	4.0×10^{-18} (4.0×10^{-11})	DTN's GS940808312231.008, GS950608312231.006, GS960808312231.001
Fracture density, fractures/m^3	7.6	Sobolik et al., 1996 (for the Single Heater Test calculations).
Fracture porosity Low value High value	 1.143×10^{-4} 1.639×10^{-3}	Derived value; see Comment 3 below.
Fracture permeability, m^2 Low value High value	 1.885×10^{-11} 3.8736×10^{-9}	Derived value; see Comment 3 below.
Matrix van Genuchten α, 1/Pa	6.40×10^{-7}	See Comment 2 below.
Matrix van Genuchten β	1.47	See Comment 2 below.
Matrix residual saturation	0.18	See Comment 2 below.
Initial (in situ) liquid saturation	0.92	DTN GS950408312231.004; see Comment 2 below.
Fracture van Genuchten α, 1/Pa Low value High value	 1.044×10^{-4} 1.497×10^{-3}	Derived value; see Comment 3 below.
Fracture van Genuchten β	3.0	Altman et al., 1996; see Comment 4 below.
Fracture residual saturation	0.03	Altman et al., 1996; see Comment 4 below.

In addition to hydrologic properties for the host rock, hydrologic properties (porosity, permeability, initial liquid saturation, etc.) for the concrete invert and concrete end liner were required for the T-H analyses (refer to Table 3-1b). These values are approximated from values obtained from the WIPP (Waste Isolation Pilot Plant) database for material properties and/or from handbook values (Merritt, 1968). The characteristic relative permeability curves are assumed to follow the Brooks-Corey representation while the capillary pressure curve follows the Leverett's function given in TOUGH2 (Pruess, 1991).

Table 3-1b. Hydrologic Values Used for Concrete in the T-H Calculations

Hydrologic parameter	Value	Source, Comments
Bulk permeability, m^2	1.0×10^{-14}	WIPP database for concrete materials.
Porosity	0.05	WIPP database for concrete materials.
Initial liquid saturation	0.80	Handbook value for an average aggregate size (Standard Handbook for Civil Engineers, Merritt, 1968).
Residual liquid saturation	0.0	-

Comments regarding the hydrologic values listed in Table 3-1a:

1. Rock bulk permeability ranges are obtained from the initial (early results 1/97) air permeability field tests conducted at the DST. This range of values obtained from the DST area is nearly the same as those previously obtained from the SHT block (DTN LB960500834244.001,TDIF 305605).

2. The matrix porosity, van Genuchten curve fitting parameters α and β, residual saturation, and in situ liquid saturation values are all average values based on measurements from eight boreholes in the Middle Nonlithophysal unit (Tptpmn). The documentation of the values for these parameters can be found in Flint, 1996. The datasets which contain the data used for these parameters are the following:

DTN GS950408312231.004	Physical properties and water potentials of core from borehole USW SD-9
DTN GS940508312231.006	Core analysis of bulk density, porosity, particle density and in situ saturation for borehole UE-25 UZ#16
DTN GS950608312231.007	Physical properties and water content of core from borehole USW NRG-6
DTN GS951108312231.009	Physical properties, water content, and water potential for borehole USW SD-7
DTN GS951108312231.011	Physical properties, water content, and water potential for borehole USW UZ-7a
DTN GS951108312231.010	Physical properties and water content for borehole USW NRG-7/7A
DTN GS950308312231.002	Laboratory measurements of bulk density, porosity, and water content for USW SD-12

3. The fracture porosity, permeability, and van Genuchten curve fitting parameter α for the low and high bulk permeability cases may be calculated in terms of the bulk and matrix parameters. The equation for the relationship between bulk, matrix, and fracture permeability is given in equation (3-3). The fracture porosity is related to the fracture aperture δ and the fracture frequency *ff* by the equations $\phi_f = ff \times \delta$, where *ff* = (7.6 fractures/m^3)×(1 m^2), and $K_f = \delta^2/12$. The intrinsic fracture permeability is subsequently computed using equation (3-3) with all other quantities known. The van Genuchten α for the fractures is related to the air entry pressure and based on the commonly-used relationship with surface tension σ of water at 25°C, $\alpha_f = \delta/2\sigma$, where σ=0.072 N/m.

4. The van Genuchten β for fractures has not been measured. It has been common practice in the Yucca Mountain Project to assign β_f a high value (such as the value of 3.0 used here) to produce a steep gradient in the moisture retention curve, thereby simulating either totally empty or totally full, clean, parallel fractures. The residual saturation in the fractures of 0.03 has been used in previous literature (e.g., Altman et al., 1996).

5. The bulk permeability of the drift elements were assumed equal to that of the rock.

The tortuosity of the path followed during the gas phase diffusional process is assumed constant for this analysis and the tortuosity coefficient is maintained for the thermal-hydrologic runs at τ=0.2. Also, it was assumed for these analyses that matrix and fracture porosity and permeability do not vary as a result of thermal-mechanical processes; this coupling may be incorporated in future analyses.

3.4.2 Thermal Properties

Thermal properties of the host rock include such quantities as thermal conductivity (both wet and dry), heat capacity, grain density, and thermal expansion are required for the T-H calculations performed using TOUGH2 and the T-M calculations performed with JAC3D. The properties used in the T-H analyses are given in detail in this section. Some of the thermal properties used in the DST analyses come from site-specific data from the nearby SHT (i.e., dry thermal conductivity); others come from borehole data from the Middle Nonlithophysal unit (Tptpmn), in which the DST resides. Also required for the T-H analyses, thermal properties for the heater materials where obtained using handbook properties of copper, bulkhead properties using handbook values of an insulation material, and handbook values of concrete properties applied to the invert and end liner. Table 3-2 lists all the thermal property input values used for the DST analyses and the sources for each.

Table 3-2. Thermal Values Used in the T-H-M Calculations

Thermal parameter	Value	Source, Comments
Rock Grain density, kg/m³	2526.	DTN GS950408312231.004 (Physical properties and water potentials of core from borehole USW SD-9); average particle density for 105C oven-dried samples, Middle Nonlithophysal zone (Tptpmn) 728.8-845.8 ft.
Thermal conductivity K_{th} (dry) of the rock mass, W/m-K	1.67	DTN SNL22080196001.001, TDIF 305593 see Comment 1.
Thermal conductivity K_{th} (wet) of the rock mass, W/m-K	2.1	RIB value for the wet value of thermal conductivity at the repository horizon (TSw2).
Heat capacity of the rock grain c_p, J/kg-K	928.	DTN SNL01C12159302.002, TDIF 305182; see Comment 2 below.
Thermal conductivity. density, and heat capacity of air	K_{th}= 0.03 W/m-K; ρ=0.995 kg/m³; c_p=1009 J/kg-K	Handbook values for air (Incropera and DeWitt, 1985).
Thermal conductivity. density, and heat capacity of air (the radiation equivalent thermal conductivity)	K_{th}= 60 W/m-K; ρ=0.995 kg/m³; c_p=1009 J/kg-K	see Comment 3 below for explanation of the treatment of radiation heat transfer in the heated drift.
Thermal conductivity. density, and heat capacity of the insulation bulkhead	K_{th}= 0.0447 W/m-K; ρ=32 kg/m³; c_p=835 J/kg-K	Handbook values for insulation (Sobolik et al, 1996).
Thermal conductivity. density, and heat capacity of the concrete liner and invert	K_{th}= 1.40 W/m-K; ρ=2300 kg/m³; c_p=880 J/kg-K	Handbook values for concrete (Incropera and DeWitt, 1985).
Thermal conductivity and heat capacity of the heater material	K_{th}=401 W/m-K; ρ=8933 kg/m³ c_p=385 J/kg-K	Handbook properties for copper (Incropera and DeWitt, 1985).

Comments regarding the thermal values listed in Table 3-2:

1. Thermal conductivity measurements were performed on four tuff samples from the SHT test block (DTN SNL22080196001.001, TDIF 305593). A total of 36 measurements were taken at temperatures ranging from 30°C to 289°C. The samples were exposed to ambient room conditions for some time before testing, which likely resulted in drying of the samples. No testing was performed to distinguish between "wet" and "dry" thermal conductivity of the material, so for the DST calculations reported here, these values were assumed to produce a "dry" average thermal conductivity of 1.671 W/m-K for all samples.

2. Thermal capacitance (ρc_p) measurements were taken from Middle Nonlithophysal (Tptpmn) samples over a temperature range of 25°C to 300°C (DTN SNL01C12159302.002, TDIF 305182). Average values of thermal capacitance were obtained for two temperature ranges - 25°C to 75°C, and 100°C to 300°C - and then those two values were averaged to obtain an average value for the entire temperature range. Using the rock's grain density and porosity, the thermal capacitance of water, and a liquid saturation of 0.2 (derived from moisture content data of room-dried samples from the SHT test block; DTN SNL22080196001.002), the heat capacity of the dry rock of 928 J/kg-K was obtained.

3. The air thermal conductivity is modified (increased by over three orders of magnitude) in the heated drift section in order to approximate the radiant heat transfer from the canister heaters to the floor and walls of the drift. It is assumed that the canister heater and the walls will behave as blackbodies during the radiant heat transfer process. The enhanced value of the air thermal conductivity is based on an average heater canister and wall temperature after 2 years of heating. The form of the equivalent thermal conductivity used to approximate radiation heat transfer inside the drift is computed with the following:

$$\lambda_r = \sigma (T_1 + T_2)(T_1^2 + T_2^2)\Delta x \qquad (3\text{-}4)$$

where Δx is the distance between the radiating surface and the receiving surface, T_1 and T_2 are the absolute temperatures of each surface, and σ is the Stefan-Boltzmann constant. It was found that, for the temperature ranges experienced by the drift wall and canister heaters during the experiment, the equivalent drift thermal conductivity may range from K_{th} = 60 to 90 W/m-K. The canister surface temperature remains nearly constant for approximate drift air thermal conductivities of 20 W/m-K or greater based on sensitivity analyses. The rate of energy transfer from the drift wall surface into the host rock is conduction limited and is controlled by the resistance to heat transfer associated with the host rock as shown in Ho and Francis, 1996 (in particular for the lower permeability cases).

3.5 General Description of the Test (and Modeled) Geometry

Figure 3-1 displays a simplified schematic of the heated drift test layout. This figure is intended to indicate the major modeled features included in the T-H analyses such as the surrounding wing heaters, nine canister heaters, insulated bulkhead, and the concrete liner at the end of the heated drift. Not shown in this figure but included in the analysis is the concrete invert that runs the entire length of the drift. It is noted that this figure is not to scale and the relative positions of the canister heaters (which very nearly fill the entire heated drift) are shown only in a qualitative sense. In order that one may apply the automated MESHMAKER feature included in TOUGH2 for model domain gridding purposes, the actual cylindrical geometry of the experiment is approximated by transforming it into a surface area equivalent rectangular (X-Y-Z) coordinate system. The resulting (X-Z) cross-sectional model (refer to Section 3.6) and the (Y-Z) longitudinal model (refer to Section 3.7) are shown in Figures 3-2 and 3-3, respectively. The "unit cell" 3-D model (refer to Section 3.8) location is oriented through the center canister (canister number 5 of 9) and spans to the midpoint between adjacent canisters. Therefore, it

includes one-half of a drift heater canister with its periodic boundary (in the Y direction) falling mid-way between two canister heaters while including the heat for approximately one and one-half wing heaters on a side. Each of the wing heaters are separated by 1.83 m. The (X-Z) model is representative of an infinitely long drift. The results of this 2-D cross-section model are used to approximate the results of the actual test very near the center of the experiment where the temperatures are the highest. The (Y-Z) longitudinal model will capture the effects of the unheated rock mass at either end of the heated drift and will be used to characterize the effects of edge cooling during the heating and cooling phases of the experiment.

3.5.1 Construction of the Model Domains

Since heat transfer is a surface area phenomenon, the total surface area of the actual cylindrical geometry is maintained as a constant when constructing the rectilinear grid representation of the test. Therefore, as an example, the heated drift diameter of 5 m is transformed into a total surface area equivalent parallelepiped with a drift dimension of 3.93 m on a side (refer to Figure 3-2). The length of the heated drift is the actual value of 48 m (refer to Figure 3-3). Additionally, the relative mass of concrete invert (i.e., the volume fraction of concrete invert in the heated drift) and the actual mass of concrete liner at the end of the heated drift have been preserved in the working rectilinear numerical model domains.

3.5.1.1 Heated drift and wing heater geometry

The height of the surface area equivalent drift (3.93 m) is computed using the heated drift radius of 2.5 m as:

$$h_{drift} = \tfrac{1}{2}\pi r_{drift} = 3.93\,meters \qquad (3\text{-}5)$$

This relationship neglects the surface area of the ends of the drift itself. This assumption is considered reasonable due to the fact that length of the heated drift (48 m), and subsequently its surface area, is much greater than the end of the drift and its diameter (5 m), and subsequently its surface area. The modeled wing heater geometry is also computed using equation (3-5). For a wing heater diameter of 0.096 m, the modeled surface area equivalent wing heater height is 0.0754 m. As before, the ends are neglected due to the very large aspect ratio between wing heater length and diameter.

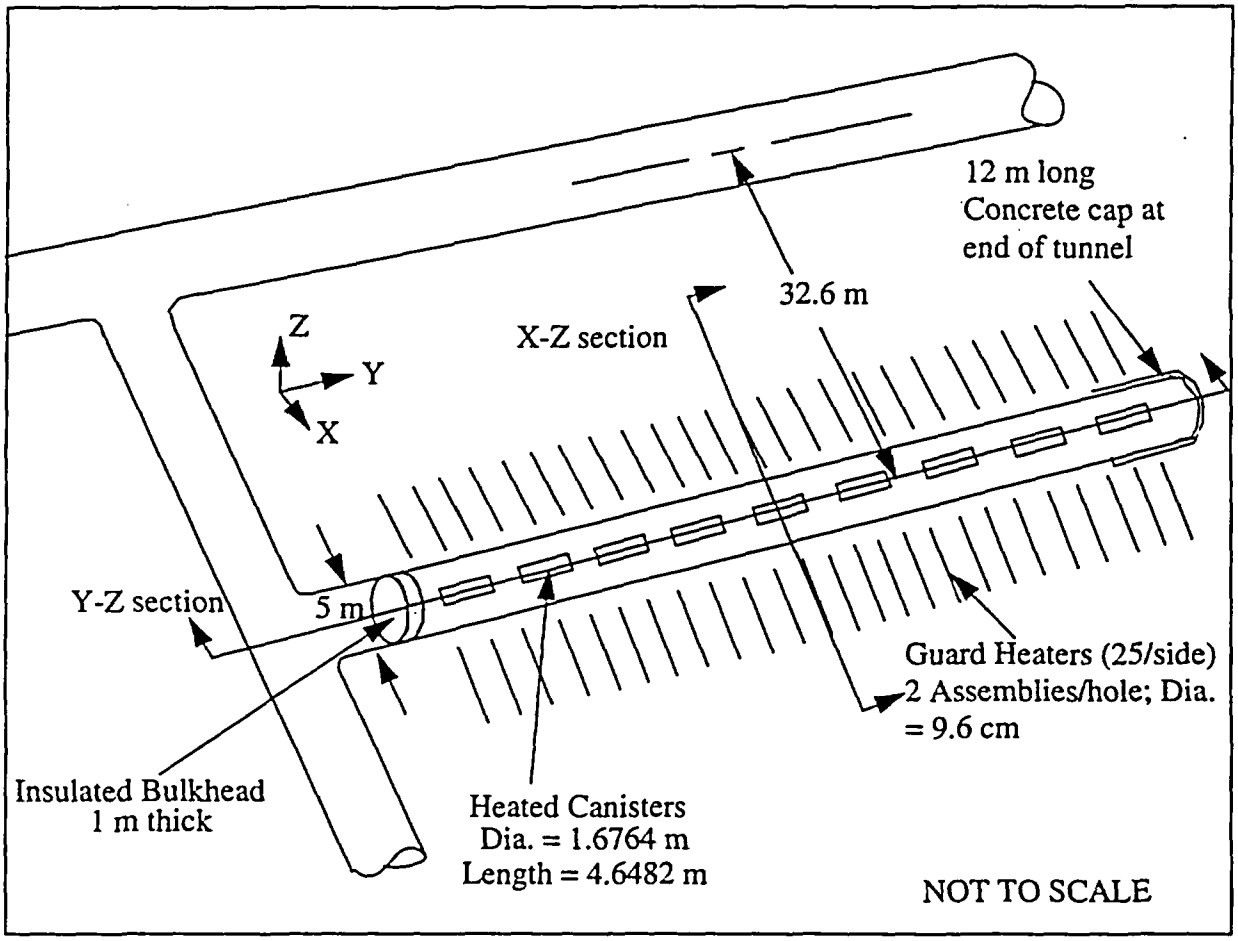

Figure 3-1. Schematic of the Heated Drift Layout

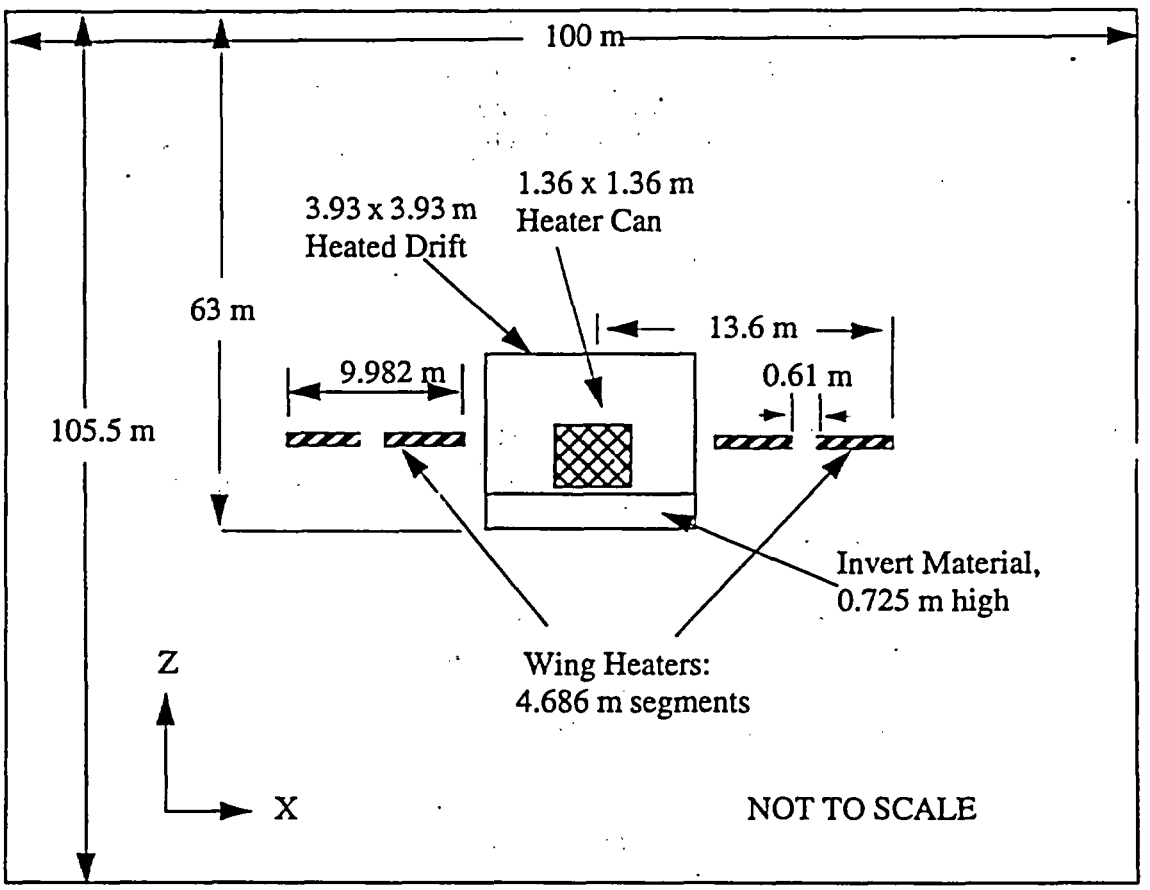

Figure 3-2. X-Z Two-Dimensional Cross-Section Through the Mid-Section of the Test

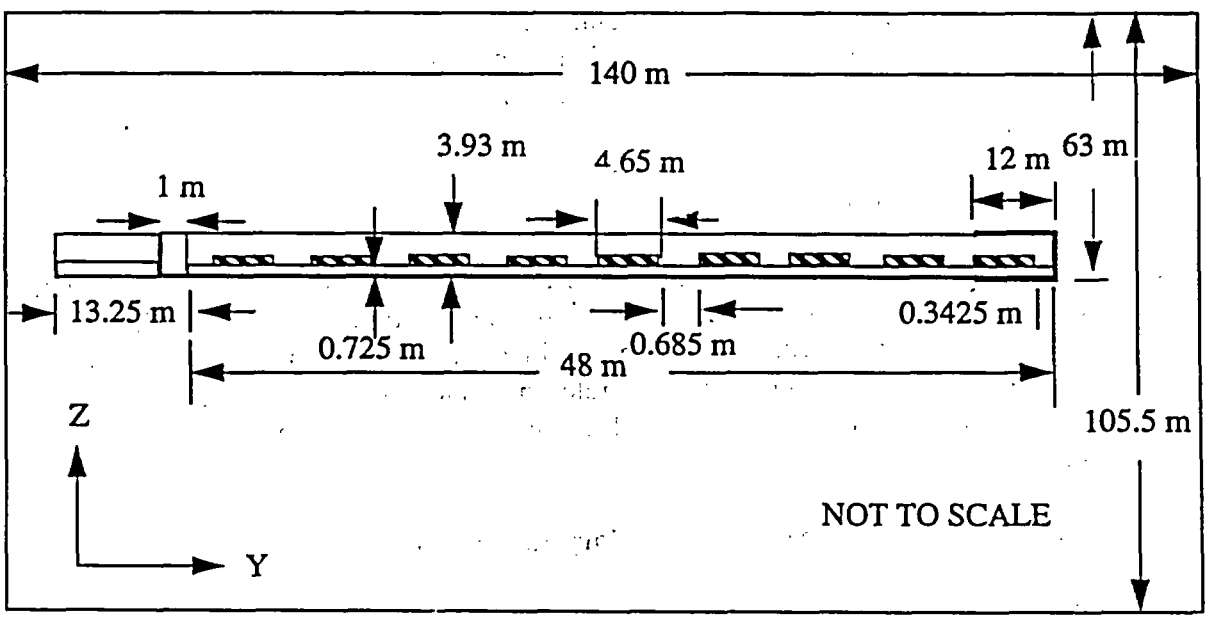

Figure 3-3. Y-Z Longitudinal Model Used to Determine Edge Effects

3.5.1.2 Canister heater geometry

The same type of calculation is used to transform the cylindrical canister heater into a surface area equivalent parallelepiped. In this case, however, the area of the ends of the canisters are included since the heater length and diameter are of the same order. This results in a modeled heater canister of 1.36 m on a side. The following equation is used to obtain the canister height dimension:

$$2\pi r_{can} l_{can} + 2\pi r_{can}^2 = 4h_{can} l_{can} + 2h_{can}^2$$
$$\therefore \qquad (3\text{-}6)$$
$$h_{can} = 1.36 meters$$

where r_{can} is the radius of the actual heater canister, l_{can} is the length of the canister and h_{can} is the unknown surface area equivalent height of the modeled, rectilinear, canister heater.

3.5.1.3 Concrete invert geometry

The maximum actual height of concrete invert is approximately 1.2 m. Based on this and the radius of the heated drift, the resulting area represented by the invert is approximately 3.624 m^2 out of the total cross-sectional area of the heated drift. The modeled height of the concrete invert as placed into transformed, rectilinear, coordinates is computed with the following relationship:

$$h_{inv} = \frac{4A_{inv,act}h_{drift}}{\pi d_{drift}^2} = \frac{4(3.624m^2)(3.93m)}{\pi(5.0m)^2} = 0.725 meters \qquad (3\text{-}7)$$

It is noted from this relationship that the volume fraction of concrete invert in the actual drift is identical to that of the surface area equivalent (i.e., rectilinear geometry) drift. That is, the relative amounts of concrete invert mass are exactly identical for both the actual test and the modeled geometry.

3.5.1.4 Concrete liner geometry

The total amount of concrete mass in the end liner is conserved in the T-H calculations (this information applies to the longitudinal model domain only, Figure 3-3). Equating concrete mass actual to the modeled mass equivalent, the end liner thickness used in the modeled, rectilinear, geometry is approximately 0.3 m. The concrete liner is a total of 12 m in length at the end of the heated drift. The concrete liner is assumed to have the same thermal and hydrologic properties as the concrete invert.

3.5.2 Determination of the Outer Boundary Locations

The extent and approximate location of the modeled T-H domain (i.e., the outer boundaries for the X-Z, Y-Z, and X-Y-Z models) is based on a one-dimensional, transient heat conduction

solution for a constant temperature boundary (the drift wall) at four years of heating into a semi-infinite medium. The resulting temperature distribution is governed by an error function (ERF) solution and is dependent on the thermal diffusivity of the material. For an average thermal conductivity (wet plus dry divided by 2), the temperature distribution approaches the initial value approximately 40 to 60 m away from the source. Therefore, within and beyond this distance, the medium is not aware of the high temperature source. The assumption of negligible thermal influence at this distance from the drift wall (40-60 m) is assumed to be a limiting case for the T-H analyses for the DST. This is due to the fact that the error function temperature solution assumes that all energy transport (conducted) is in only one direction.

The T-H analyses includes, at a minimum, multi-dimensional heat transfer, therefore, reducing the thermal influence in any one direction. Therefore, for the case of low or no convection, it is assumed that an outer boundary approximately no less than 40 m away from the drift wall is adequately removed from the source for the multi-dimensional cases and in the time frames considered. This outer boundary location (i.e., 40 m removed from the thermal source) is applied for side or bottom boundaries only. In the case of higher bulk permeabilities, energy transport is not limited by conduction heat transfer. Therefore, in all cases considered, the top boundary is located no less than 60 m away from the drift wall in order to accommodate the convection component of energy transfer away from the source.

3.6 General Description of the 2-D X-Z Cross-Section

3.6.1 Description of Mesh

A two-dimensional X-Z cross-section of the drift-scale heater test has been simulated using TOUGH2. The numerical mesh consists of 36 columns of rectangular elements that span 100 meters in the X-direction and 35 rows of rectangular elements that span 105 meters in the Z-direction, comprising a total of 1260 elements. As discussed earlier, the size of the domain was chosen so that the thermal perturbation would occur well within the boundaries of the modeled domain. The non-uniform grid is refined in the vicinity of the drift to accommodate the canister heaters and the borehole emplaced wing heaters. Conversely, the mesh is coarser further away from the drift towards the boundaries.

The two-dimensional X-Z model consists of a heater situated on concrete invert inside a drift. Because the grid elements are rectangular, the simulated dimensions of the drift and canister heater were chosen to preserve the surface area of the actual materials (for heat transfer). The height of the invert was chosen to yield the same volumetric ratio of invert to heated drift. Wing heaters, consisting of inner- and outer-heating elements, also extend horizontally away from the drift into the surrounding rock (TSw2). Figure 3-4a shows the location of the centroids of the elements representing the different materials, including the boundary elements along the perimeter of the model. Figure 3-4b shows an expanded view of Figure 3-4a in the vicinity of the drift. Tables 3-1a, 3-1b, and 3-2 present the thermal and hydrologic properties of the different materials used in the simulations.

3.6.2 Initial Conditions

The model domain was equilibrated before the heater was "turned on" by allowing the system to reach an ambient steady-state during a one million year equilibration run. During the equilibration run, the entire domain was comprised of only TSw2 material. The heater, drift, and invert materials were omitted. A geothermal gradient of approximately 0.02 °C/m (Sobolik et al., 1996) was established by fixing the upper and lower boundaries (shown in Figure 3-4a) at temperatures of 25°C and 27.25°C, respectively. A liquid saturation of 0.92 was imposed at the lower boundary, and hydrostatic conditions were established throughout the domain. Following the equilibration run, the heater, drift, and invert materials were added, and a relative humidity of 100% was specified within the drift, which was calculated using the simulated temperatures and pressures of the equilibrated elements located in the drift domain.

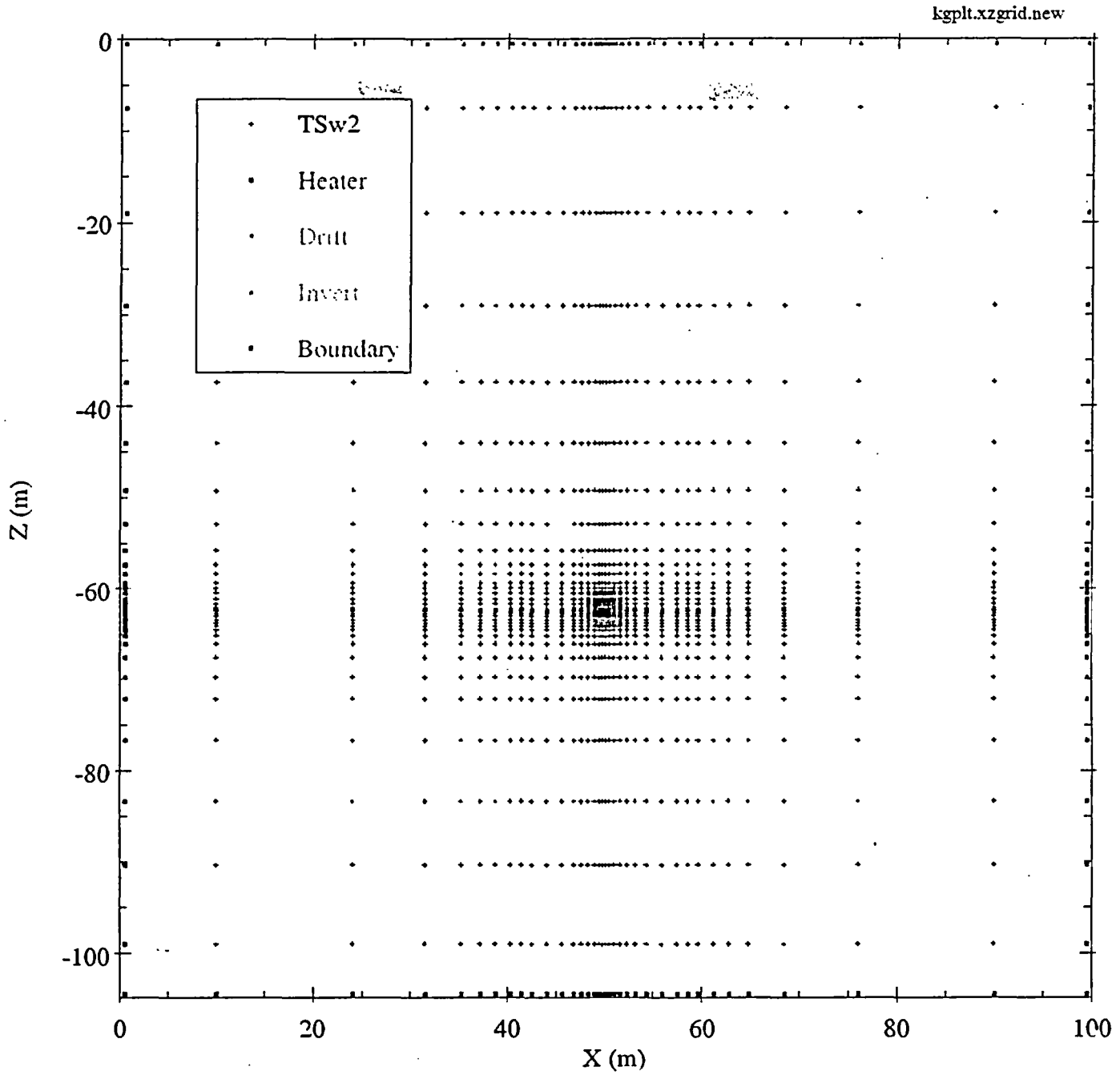

Figure 3-4a. Element centroids and associated materials for two-dimensional X-Z grid.

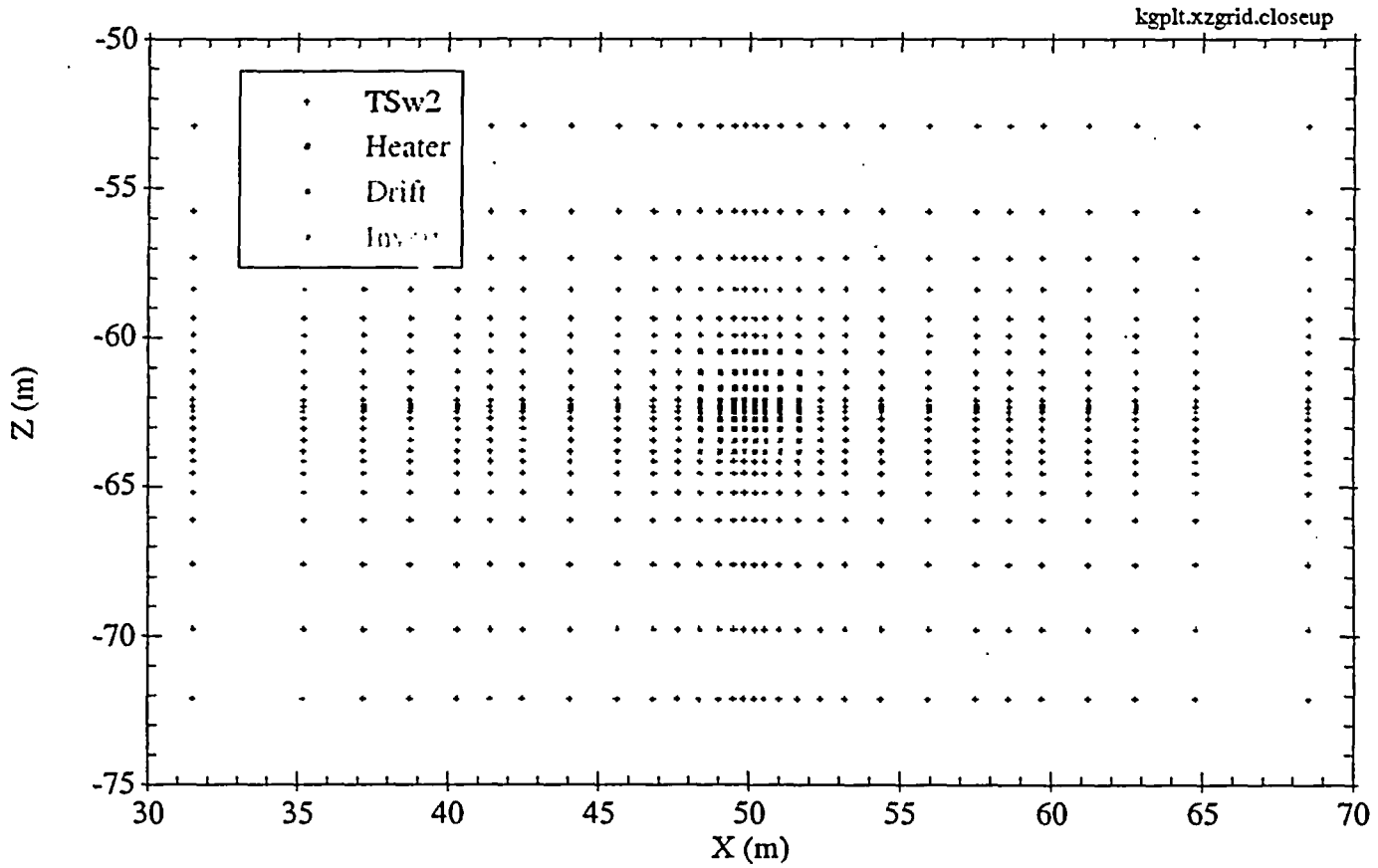

Figure 3-4b. Expanded view of element centroids and associated materials for two-dimensional X-Z grid.

3.6.3 Boundary Conditions

The equilibrated pressures, liquid saturations, and temperatures along the four boundaries of the modeled domain were then fixed in preparation for the heating phase. These perimeter elements allowed liquid, gas, and heat fluxes to occur across the boundaries during the heating simulation, but the values of their state variables remained constant. No infiltration was applied during the simulations.

The simulated heat generation in the two-dimensional X-Z model was calculated using the reported heat output of the canister heaters (8000 W) and wing heaters (1145 W inner; 1719 W outer). The heat output was scaled accordingly to yield a generation rate for the canister heater, inner wing heater, and outer wing heater per unit depth in the Y-dimension. The spacing between each heater can was calculated to be 4.65 m + 0.685 m = 5.335 m. The simulated heat generation for the canister heater was therefore 8000/5.335 = 1499.5 W/m. Similarly, the simulated heat generation of the inner and outer wing heaters was calculated, based on a wing heater spacing of 1.83 m, to be 625.68 W/m and 939.34 W/m, respectively. The generation rates were held constant during the heating phase of the simulations.

3.6.4 Simulation Procedure

Three heating scenarios consisting of 2, 3, and 4 year heating periods were considered. In each case, a 2 year cooling period (no heat output) followed each heating period. In addition, both high- and low-permeability scenarios were considered to simulate the possible range of bulk permeabilities associated with the fractured tuff (TSw2) surrounding the drift. Therefore, a total of six simulations were performed using the two-dimensional X-Z model. In each, state variables were processed at pre-determined times during the heating and cooling periods. These temperatures were then passed on to the thermal-mechanical simulations.

3.7 General Description of the 2-D Longitudinal Model Domain

3.7.1 Longitudinal Mesh

This T-H model domain is required in order to determine the influence of the unheated rock mass at either end of the heated drift. Figure 3-3 represents a schematic for the longitudinal model domain necessary to determine edge effects. The working numerical MESH including color indicators at volume element centroids for the different material types is shown in Figure 3-5a. An expanded view of the drift represented in the longitudinal numerical MESH is shown in Figure 3-5b. In the heated portion of the drift, the air thermal conductivity is enhanced using equation (3-4) in order to include the effects of radiant heat transfer from the canister heaters to the drift walls and invert in an empty drift. In the initial drift region not containing canister heaters, the air thermal conductivity is the standard handbook value for air (≈ 0.03 W/m-K). This drift region is separated from the heated drift by a 1 m thick insulation bulkhead. The heated drift region is 48 m in total length with nine heaters emplaced 0.3425 m from the ends of the drift and about 0.685 m apart inside of the drift. The concrete liner is located in the remaining 12 m of heated drift and encompasses approximately 2.2 heated canisters. The modeled domain contains 35 rows of rectangular elements that span approximately 105 m in the Z-direction. The Y-direction contains 68 rows of rectangular elements that span 140 m. Grid refinement occurs within and around the drift. The model domain becomes more coarse away from the drift moving towards the outer boundaries. The Y-Z model domain contains 2380 elements and is very computationally efficient.

3.7.2 Initial Conditions

The initial conditions for the T-H test geometry applied to Figures 3-5 are selected as representative values at the depth of the Middle Nonlithophysal tuff. A constant geothermal gradient of approximately 0.02°C/m is assumed throughout this region. The temperature at the top of the test geometry is specified to be 25°C. The temperature at the bottom of the heater test modeled geometry is thus calculated to be 27.25°C. The bottom boundary is also assigned a constant gas-phase pressure of 0.87 bar. The initial liquid saturation is specified to be 0.92 throughout the model domain; this value is based on nearby SD-9 borehole data. The model domain is then "equilibrated" for 1,000,000 years without the heater in place (Pruess and Tsang, 1993) in order to obtain nearly steady state initial conditions for the temperature, gas-phase pressure, and liquid saturation at the onset of the heating process. The top boundary is specified as a constant temperature boundary, while the gas-phase pressures and liquid saturations are calculated with TOUGH2 by running out to a steady state condition. The bottom boundary is a fixed location at the specified liquid saturation (S_{liq}=0.92), temperature (T=27.25°C), and gas phase pressure (P_{gas}=0.87 bar). The TOUGH2 code then calculates steady state values for temperature, gas-phase pressure, and liquid saturation at all other locations in the modeled domain (refer to Figure 3-5a for grid refinement). In this equilibrated case, an initial hydrostatic pressure distribution is obtained for the gas phase. The initial distribution of temperature is governed by the geothermal gradient. It should be noted that the constant property boundary condition implies that the "equilibrated values" of (T, S_{liq}, P_{gas}) are maintained as constants during the heated simulations.

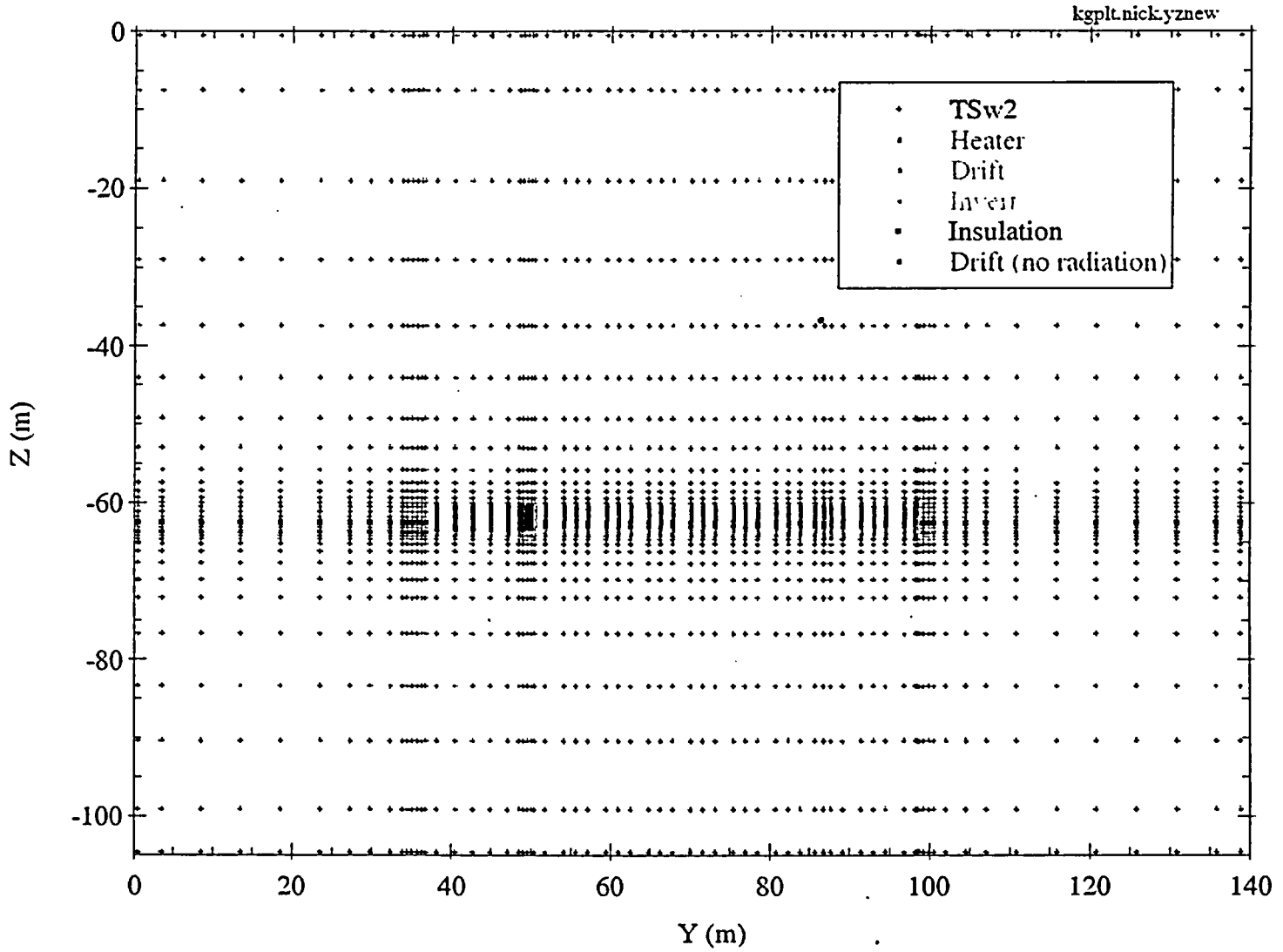

Figure 3-5a. Element centroids and associated materials for two-dimensional Y-Z grid.

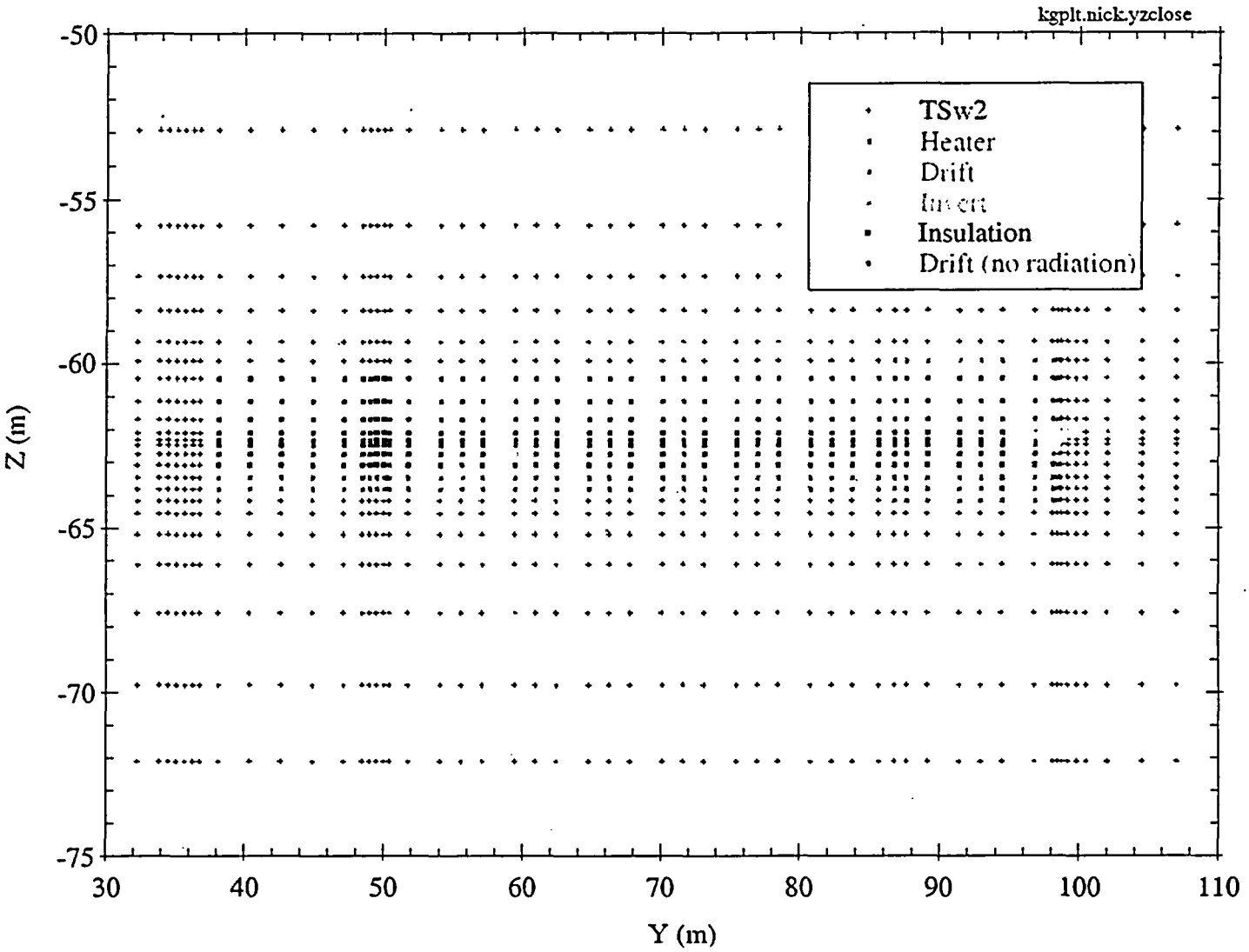

Figure 3-5b. Expanded view of element centroids and associated materials for two-dimensional Y-Z grid.

3.7.3 Boundary Conditions

3.7.3.1 Perimeter elements

The boundary conditions (T, S_{liq}, P_{gas}) for the 2-D longitudinal model domain are illustrated using Figure 3-3 or 3-5a. The surrounding boundaries are assumed to be located far enough away from the heat source (refer to the discussion in section 3.5.2) such that the thermodynamic properties at the outer locations remain constant in time during the heating process (for constant power heating times limited to 4 years total). The top (Y, Z = 0 m)and bottom boundaries (Y, Z = - 105.5 m) are maintained constant at all times at the values obtained or specified during the TOUGH2 equilibration procedure. These properties do not vary in space (Y is perpendicular to gravity). The two side boundaries, (Y = 0 m, Z) and (Y = 140 m, Z), are maintained constant at all times during the heating process at the values obtained during the equilibration procedure. Unlike the top and bottom boundaries, these properties vary in space (Z is parallel to the direction of gravity), but not in time.

3.7.3.2 Heat generation elements

The average areal power density obtained for the DST is equated to the average areal power density applied to the longitudinal (Y-Z) model domain. Therefore, an equivalent fractional amount of heat will be input to the 2-D modeled geometry as is input to the actual areal extent of the heater experiment. In order to obtain an approximate experimental total heat output of 220 kW, the canister heaters output 8 kW each (9 total), the inside wing heaters output 1.145 kW each (50 total), and the outside wing heaters output 1.719 kW each (50 total). Based on the plan area of the heated drift test, this corresponds to a specified areal power density of the test.

The actual areal power densities of each heat source (canister heater, inside wing heater, and outside wing heater) are computed as the following:

$$APD_{can} = \frac{N\dot{Q}_{can}}{A_{can}} = 211.3\frac{W}{m^2} \qquad (3\text{-}8)$$

where equation (3-8) represents the areal power density for all canister heaters, N is the total number of drift heaters (=9), and A_{can} is the plan area of the drift and stand-off between the drift wall and the inside wing heaters. A similar areal based expression is obtained for the inside wing heaters as the following:

$$APD_{inwing} = \frac{N\dot{Q}_{inwing}}{A_{inwing}} = 122.8\frac{W}{m^2} \qquad (3\text{-}9)$$

Finally, for the outside wing heaters:

$$APD_{outwing} = \frac{N\dot{Q}_{outwing}}{A_{outwing}} = 208.5\frac{W}{m^2} \qquad (3\text{-}10)$$

The area averaged total for the DST is obtained from the following expression:

$$APD_{avg} = \frac{A_{can}}{A_{total}} APD_{can} + \frac{A_{inwing}}{A_{total}} APD_{inwing} + \frac{A_{outwing}}{A_{total}} APD_{outwing} = 176.5 \frac{W}{m^2} \quad (3\text{-}11)$$

averaged over the footprint of the DST. Equation (3-11) is equated to the power density of the longitudinal model as the following:

$$APD_{avg} = \frac{\dot{Q}_{model}}{A_{model}} \quad (3\text{-}12)$$

where the A_{model} is known and the model heat generation rate is computed from equations (3-11) and (3-12). The total model heat output (i.e., the scaled value based on the 2-D longitudinal model domain area) is concentrated into the nine canister heaters in order to establish, overall, the effects of the unheated rock mass surrounding the experiment with respect to the entire amount of heat input by the canisters as well as the emplaced wing heaters (i.e., equations 3-11 and 3-12).

3.7.4 Simulation Procedure

The simulation procedure is carried out in a two step process. The first step is to obtain a fully equilibrated model domain that serves as the initial conditions (of the host rock) for each of the heating simulations. This step occurs with refined gridding for the drift and other features already in place, however, all material elements are first initialized as those of the surrounding host rock. After 1,000,000 years simulated (without the heat source), the rock model domain contains equilibrated values for the gas-phase pressure, liquid saturation, and formation temperature. These serve as the initial conditions for the specific host rock elements as shown in Figure 3-5. For an equilibrated model domain with the host rock elements in place; drift, concrete invert and liner, and bulkhead properties are then placed in the numerical MESH file as well as in the initial conditions file. Therefore, model initial conditions are specified for each of the materials in the domain with the rock in equilibrium based on the hydrologic properties and the in situ saturation of this region.

The specific details of the numerical mesh are shown in Figure 3-5 with each of the different material identifiers in place. The engineered material specific elements (i.e., concrete invert, etc.) possess initial conditions based on assumption or established handbook data (Merritt, 1968). The drift element initial conditions are for a constant temperature of 25°C and an air mass fraction based on an assumed drift relative humidity of approximately 100%. The concrete invert and end liner initial liquid saturation is 0.8 based on an average aggregate size (Merritt, 1968). The bulkhead and heater elements are initially dry.

With the equilibrated rock and specialty elements (i.e., drift, invert, liner, heater, etc.) in place, the heating simulations may proceed. This is step two in the calculation procedure. Individual heat outputs for each of the generating elements of volume V_i in the model domain are obtained

from equation (3-12) and scaled by the total volume of all generating elements. Therefore, a consistent amount of heat output is placed into the 2-D model domain that is consistent with the actual test.

Heating simulations were performed for 2, 3, and 4 years of heating with 2 additional years of cooling. The T-H simulations included both low and high bulk permeability representations applied to an equivalent continuum conceptual model. It is assumed that the drift permeability (i.e., the convection of the gas-phase in the drift) is limited by that of the rock. Therefore, the drift bulk permeability is assumed identical to that of the surrounding rock. It may be that convection developed within the drift is greater than that in the rock, this feature will in general be contained inside the drift as the resistance to fluid flow (gas and vapor) in the rock is indeed controlled by the rock fracture properties. Additionally, convection heat transfer in the drift will not be the dominant mode of heat transfer as radiation is the primary (approximated by a very large air thermal conductivity in this analysis) mode of heat transfer from the canister heater surface to the drift walls at the temperatures predicted by the analyses.

3.8 General Description of the 3-D X-Y-Z Model Domain

3.8.1 Description of Mesh

A three-dimensional TOUGH2 model of the drift-scale heater test was created by further discretizing the two-dimensional X-Z model in the Y-dimension. The numerical mesh consists of 36 columns in the X-direction, 35 rows in the Z-direction, and 6 columns of elements in the Y-direction. The X- and Z-discretization are identical to the two-dimensional X-Z model. The boundaries in the Y-direction reflect symmetry at the midpoint of a canister heater and at the midpoint of the spacing between canister heaters. Figure 3-6 shows a plan view (X-Y) of the modeled three-dimensional domain that illustrates the location of the heater can relative to the drift elements, as well as the wing heaters. The three dimensional model consists of the same materials presented in the two-dimensional X-Z model: a canister heater, wing heaters (inner and outer), concrete invert, drift, and TSw2.

3.8.2 Initial Conditions

The three-dimensional model was equilibrated for one million years in the same manner described for the two-dimensional models. A specified geothermal gradient was established by fixing the top and bottom boundary temperatures of the model, and hydrostatic liquid saturations were simulated using a constant bottom liquid saturation of 0.92. Following the equilibration run, the heater, drift, and invert materials were added, and a relative humidity of 100% was specified within the drift, which was calculated using the simulated temperatures and pressures of the equilibrated elements located in the drift domain.

3.8.3 Boundary Conditions

The equilibrated pressures, liquid saturations, and temperatures along the six boundaries of the modeled domain were then fixed to maintain boundary conditions for the three-dimensional heating simulations. These perimeter elements allowed liquid, gas, and heat fluxes to occur across the boundaries during the heating simulation, but the values of their state variables remained constant. No infiltration was applied during the simulations.

The simulated heat generation in the two-dimensional X-Z model was calculated using the reported heat output of the heater can (8000 W) and wing heaters (1145 W inner; 1719 W outer). Because only half a canister heater was modeled, the simulated heat generation for the three-dimensional model was 4000 W. The heat output of the simulated wing heaters was calculated by scaling the heat output by the ratio of the length of the modeled domain (in the Y-dimension) to the spacing of the wing heaters. This ratio was equal to 2.6675/1.83 = 1.46. Therefore, the simulated heat generation of the inner and outer wing heaters was 1671 W and 2510 W, respectively. The generation rates were held constant during the heating phase of the simulations.

3.8.4 Simulation Procedure

Three heating scenarios consisting of 2, 3, and 4 year heating periods were considered for the three-dimensional simulations. In each case, a 2 year cooling period (no heat output) followed the heating period. Only the low-permeability scenario was considered for the three-dimensional runs. In each simulation, state variables were processed at pre-determined times during the heating and cooling periods. These temperatures were then passed on to the thermal-mechanical simulations.

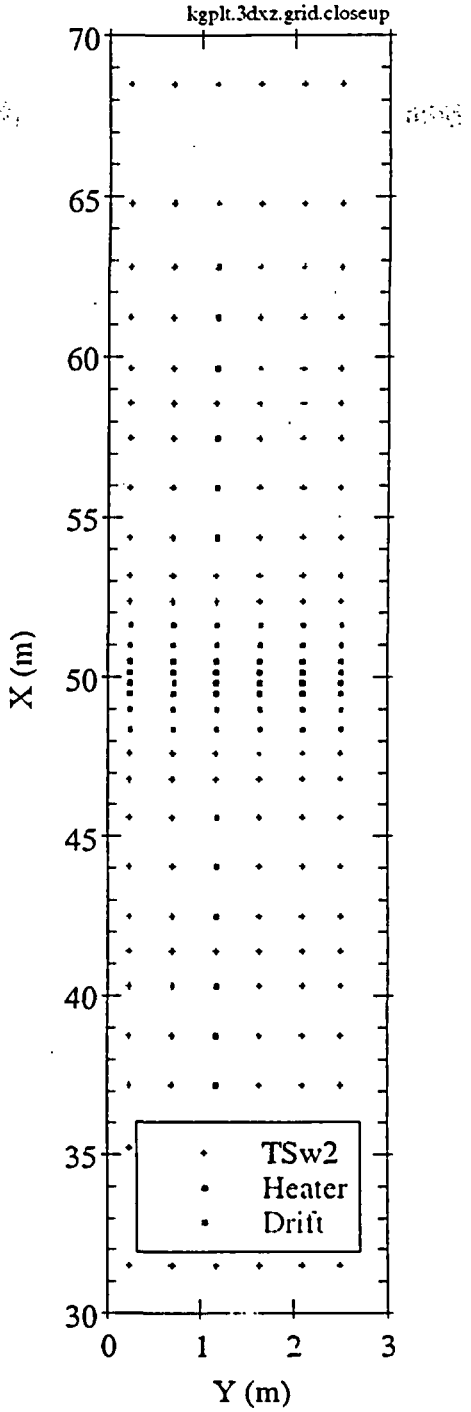

Figure 3-6. Expanded plan view (X-Y) of element centroids and associated materials for three-dimensional X-Y-Z grid.

4. Thermal-Mechanical Modeling Approach

4.1 Introduction

The thermal-mechanical (T-M) calculations predict the displacement and stress distributions in the host rock during the heating and cooling phases of the Drift-Scale Heater Test (DST) by solving temperature-dependent, quasi-static mechanics equations in three dimensions. Heating phases of 2 and 4 years are considered in the analyses coupled with 2 years of cooling after the heaters are turned off. The resulting temperature fields (at different times into heating and cooling) obtained from the T-H calculations are used as inputs to the T-M calculations used to provide predicted rock displacements during heating.

The results of the calculations are used to predict the temperature-dependent displacements at the gage locations for each of the MPBX's installed. Two MPBX's have been located in boreholes drilled parallel to the heated drift's axis, primarily for evaluating the thermal expansion of the rock mass at varying temperatures. Three sets of four MPBX's are planned at stations within the heated drift to measure radial displacements and potential asymmetric behavior. Typical MPBX measurements are made using anchors attached to connecting rods which are themselves connected to gages mounted in a protective "head" mounted at the borehole collar.

The thermal-mechanical code JAC3D (Biffle, 1993) was run individually for each predicted temperature field at the temperature time-planes provided from the TOUGH2 calculations. These calculations, produced predictions of displacements and stresses the same times as for the thermal-hydrologic calculations.

4.2 General Description of the Thermal-Mechanical Models

The three-dimensional T-M calculations were performed with the following assumptions:

- The heaters are turned on at full power for 2 or 4 years. The calculations simulate the thermal-mechanical response of the test block through the period the heater is on.
- The temperature fields from the 2-D longitudinal and 2-D cross-section thermal-hydrological calculations described in Section 3 were used as input to the JAC3D calculations. A product solution routine was created to convert the two 2-D temperature fields into an approximate 3-D field; this routine is described in Section 4.3.
- The thermal conductivity used for the rock mass in the T-H calculations was taken from the values measured from intact rock samples. This decision is based upon the assumption that the presence of the fractures and test instrumentation will have negligible influence on the rock mass thermal conductivity.
- Isotropy was assumed for all thermal-mechanical properties.
- The existence of the thermocouples, MPBXs, boreholes, and all other instrumentation, wiring, and grout in the test block are assumed to have no effect on the thermal-mechanical properties of the rock mass.
- Overburden was included in the thermal-mechanical analyses, and stress changes resulting from overburden, mechanical relief from tunneling, and thermal expansion were calculated.

The calculations were performed as follows. First, the entire computational domain, including the original in situ rock located in the heated drift before the tunnel excavation occurred, was modeled with the appropriate overburden (calculated to be 3.80 MPa) as the top boundary condition. Second, the tunnel "rock" was removed (by the use of "element death" in JAC3D), and the resulting stress changes were simulated. Third, the temperature fields from the thermal-hydrologic calculations were input to JAC3D to calculate stresses and displacements.

- The rock mass elastic modulus used in the T-M calculations was taken from both SHT and DST data. Two values are used for these calculations. The value which was used as our "base case" value was taken from a combination of intact rock modulus measurements from samples from the heated drift, and rock mass quality measurements of the heated drift and connecting drifts. The other value is a rock mass value based on Goodman Jack testing near the SHT site. For these analyses, the rock mass modulus is assumed to be constant with regard to temperature.
- The thermal expansion characteristics used for the rock mass in the T-M calculations were taken from the values measured from the Single Heater Test site. Two sets of data are used to simulate the thermal expansion characteristics. One set of data is from measurements from intact rock samples from the SHT. The other set includes approximate rock mass values computed from displacement and temperature measurements from the SHT; this approach for thermal expansion includes the effects of the constrained rock mass and of fractures.
- The effect of different values of bulk permeability is addressed in two sets of calculations, using the low and high values described in Section 3.

Figure 4-1 shows the three-dimensional computational mesh used for the thermal-mechanical calculations. The view presented features the vertical plane of symmetry through the axis of the heated drift. Figure 4-1 is presented in color to show the excavated tunnel, tunnel invert and liners, and the bulkhead, which have all been explicitly identified in the mesh with their appropriate properties.

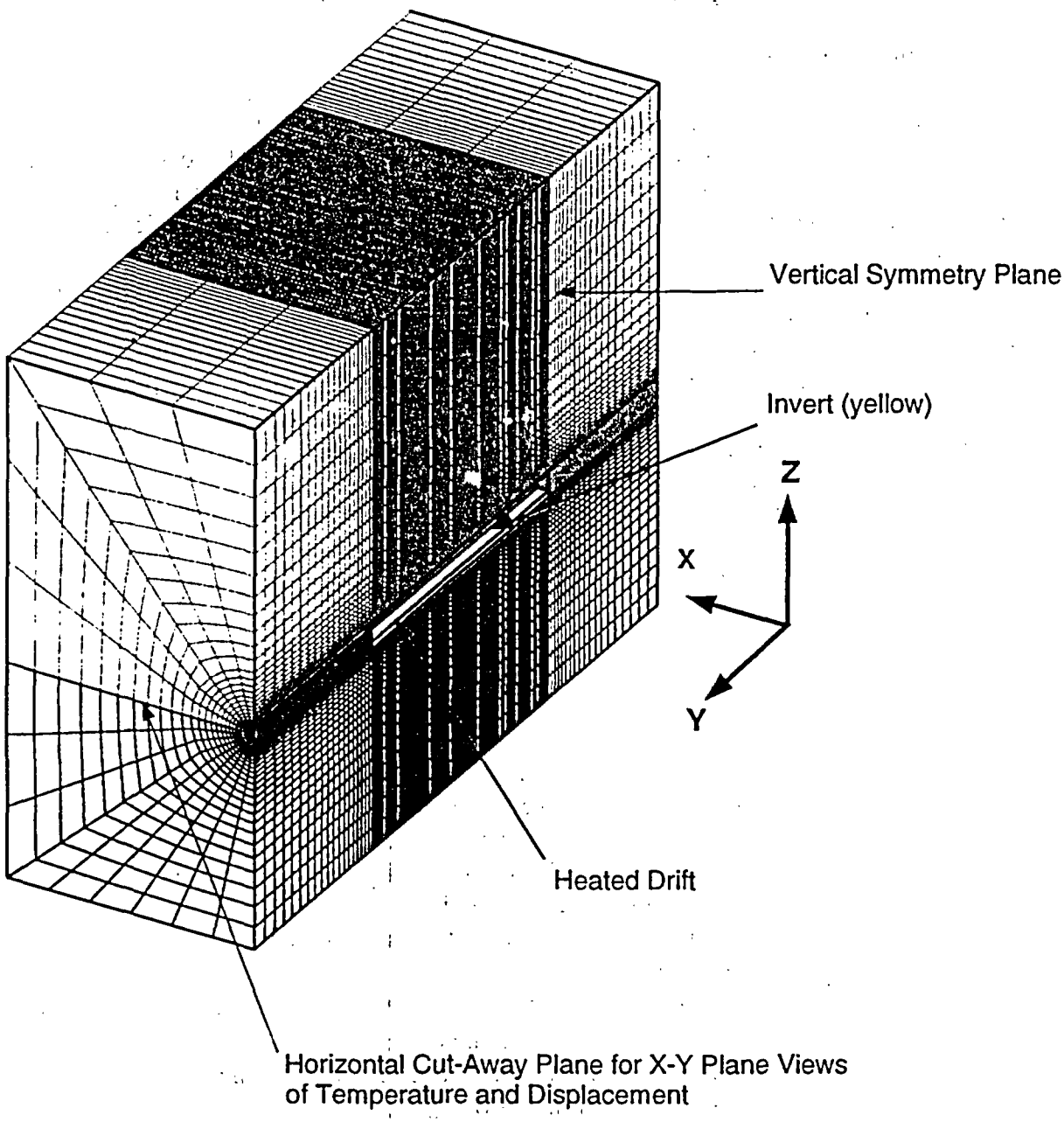

Figure 4-1. Three-Dimensional Mesh of the Heated Drift Used for the JAC3D Thermal-Mechanical Calculations

4.3 General Description of the Conceptual Model

The calculations were performed with the finite element nonlinear structural mechanics code JAC3D (Biffle, 1993). The temperature predictions from TOUGH2 described in Section 3 were used as the input temperatures for the thermal-mechanical calculations. The temperatures from the two-dimensional longitudinal (Y-Z plane) and two-dimensional cross-section (X-Z plane) thermal-hydrologic calculations were used to produce three-dimensional temperature contours for the thermal-mechanical mesh at each time step. The X-Z TOUGH2 calculations simulate a "symmetry" plane in the middle of the drift, with wing heaters on each side. Therefore, the temperature contours from the X-Z calculations were assumed to more appropriately model the axial conductive and convective heat transfer, and thus chosen as the standard results for each time step. Accordingly, the temperature contours of the 3-D T-M mesh near the center of the tunnel should match those for the 2-D cross-sectional calculations, and the 2-D longitudinal calculations should be used to modify the cross-sectional contours for edge effects. This scenario was used to produce the mathematical model used to translate the 2-D T-H temperature results to the 3-D T-M mesh:

$$T(t)_i = T_{0,i} + \theta_\ell^* \left(\frac{T_{c,i} - T_{0,i}}{T_{c,max} - T_{0c,max}} \right) \left(T_{c,max} - T_{0c,max} \right),$$

$$\theta_\ell^* = 1 + \left(\max\left(1, \frac{y_i - y_{mid}}{y_{end} - y_{mid}} \right) \right)^2 \left[\left(\frac{T_{\ell,i} - T_{0,i}}{T_{\ell,max} - T_{0\ell,max}} \right) - 1 \right]. \qquad (4\text{-}1)$$

where
- $T(t)_i$ = Temperature at T-M mesh node i at time t,
- $T_{0,i}$ = Temperature at time t=0 (before heating) at T-M mesh node i
- $T_{c,i}$ = Interpolated temperature at time t at a point with the same X and Z coordinates as T-M mesh point i in the 2-D cross-sectional simulation
- $T_{c,max}$ = Maximum temperature at time t in the 2-D cross-sectional simulation
- $T_{0c,max}$ = Temperature at time t=0 at the same point as $T_{c,max}$ in the 2-D cross-sectional simulation
- $T_{\ell,i}$ = Interpolated temperature at time t at a point with the same Y and Z coordinates as T-M mesh point i in the 2-D longitudinal simulation
- $T_{\ell,max}$ = Maximum temperature at time t in the 2-D longitudinal simulation
- $T_{0\ell,max}$ = Temperature at time t=0 at the same point as $T_{\ell,max}$ in the 2-D longitudinal simulation
- y_i = Y coordinate at T-M mesh point i
- y_{mid} = Y coordinate at the middle of the heated section of the drift
- y_{end} = Y coordinate at a point 10 meters past the end of the canisters in the drift

Equation 4-1 preserves the radial temperature profiles (due to the explicit modeling of both the in-drift heater canisters and the wing heaters) predicted by the 2-D cross-sectional T-H calculations at the middle of the drift, and allows the 2-D longitudinal profiles to define the shape of the temperature contours near the drift ends. Appendix C shows plots of the estimated 3-D temperature fields at 2 and 4 years of heating. Several views are used: two views showing the temperature

Table 4-1. Mechanical Values Used in the T-H-M Calculations

Mechanical parameter	Value	Source, Comments
Dry bulk density of SHT block rock, kg/m³	2263.	DTN SNL22080196001.002, TDIF 305602 (from SHT data)
RMR values for the thermal test alcoves' surfaces by rock mass quality category	Category: Value 1: 67.4 2: 76.1 3: 80.1 4: 83.3 5: 87.1	DTN SNF32020196001.015, TDIF 306063; see Comment 1 in this section.
Thermal expansion of TSw2 rock surrounding tunnel, μm/m-°C	From 7.47-51.47 as a function of temperature; See Table 4-2 below.	DTN SNL22080196001.001, TDIF 305593 (from SHT intact rock data); see Comment 3 below.
Thermal expansion of concrete in invert and liners, μm/m-°C	12.6	Handbook data
Thermal expansion of SHT in situ rock during heating phase, μm/m-°C	5.27 for T<60°C, 5.02 for T>60°C	(DTN SNF35110695001.004, TDIF 306088); see Comment 3 below
Young's modulus for intact rock, GPa	36.8	DTN SNL02100196001.001, TDIF 306126 (intact rock data from Heated Drift samples)
Young's modulus for rock mass based on RMR values, GPa	Category: Value 1: 27.2 2: 36.8 3: 36.8 4: 36.8 5: 36.8	Derived values; see Comment 2 in this section.
Young's modulus (rock mass) chosen for the T-M calculations, GPa	36.8 (base case value) 10.0 (Goodman jack)	See Comment 2 below
Poisson's ratio for intact rock (and for rock mass)	0.201	DTN SNL02100196001.001, TDIF 306126 (intact rock data from Heated Drift samples)
Overburden pressure on JAC3D DST computational domain, MPa	3.80	Calculated from data in Engstrom and Rautman, 1996

Comments regarding the mechanical values listed in Table 4-1:

1. RMR values were calculated using the approach described in Bieniawski (1979) from data taken along the thermal test alcoves connecting the ESF Main Drift to the end of the Heated Drift (DTN SNF32020196001.015, TDIF 306063). For determining rock mass elastic moduli, the RMR was calculated without adjustment for joint orientation. The RMR values were grouped into five categories of rock mass quality based on frequency of occurrence of 5%, 20%, 40%, 70% and 90% (Rock Mass Quality Categories 1, 2, 3, 4, and 5, respectively). The procedures employed in these calculations follow the Drift Design Methodology (Hardy and Bauer, 1991).

2. Serafim and Periera (1983) developed a correlation between the RMR and rock mass elastic modulus that was recommended for use by Hardy and Bauer (1991) and is shown by the equation

Table 4-2. Thermal Expansion and Thermal Strain Data from Specimens from the Thermal Test Alcove

(from DTN SNL22080196001.001, TDIF 305593)

Temperature Range (°C) Heating Cycle		MCTE	Thermal Strain	Temperature Range (°C) Cooling Cycle		MCTE	Thermal Strain
Low	High	µm/m-°C	m/m	High	Low	µm/m-°C	m/m
	25		0	300	275	26.49	4.025×10^{-3}
25	50	7.47	1.867×10^{-4}	275	250	36.1	3.122×10^{-3}
50	75	8.88	4.087×10^{-4}	250	225	32.77	2.303×10^{-3}
75	100	9.64	6.497×10^{-4}	225	200	23.77	1.709×10^{-3}
100	125	10.01	9.000×10^{-4}	200	175	18.98	1.234×10^{-3}
125	150	10.72	1.168×10^{-3}	175	150	14.21	8.790×10^{-4}
150	175	11.26	1.449×10^{-3}	150	125	12.08	5.770×10^{-4}
175	200	12.78	1.769×10^{-3}	125	100	10.82	3.065×10^{-4}
200	225	15.66	2.165×10^{-3}	100	75	10.27	4.975×10^{-5}
225	250	19.47	2.652×10^{-3}	75	50	9.18	-1.798×10^{-4}
250	275	29.69	3.394×10^{-3}	50	35	8.43	-3.062×10^{-4}
275	300	51.7	4.687×10^{-3}				

An estimate of the in situ thermal expansion characteristics was made from the MPBX and thermocouple measurements from the SHT (DTN SNF35110695001.004, TDIF 306088). The in situ value is less than the intact rock value by about 30% for the lower temperature ranges, and the discrepancy increases for higher temperatures. Both the SHT intact rock and SHT in situ values for thermal expansion are evaluated in the T-M calculations.

- Alternate rock mass elastic modulus value of 10 GPa,based on preliminary results Goodman Jack tests near SHT site (reported by authors), all other base case values remaining the same
- Temperatures from the high bulk permeability simulation, $K_b=6.35\times10^{-12}$ m², all other base case values remaining the same
- Alternate thermal expansion values based on in situ values calculated from SHT temperature and displacement test data (5.27 µm/m-°C) (DTN SNF35110695001.004, TDIF 306088)

In addition, calculations for two years of cooling following two years of heating were also performed. Predicted three-dimensional temperature contours are presented in Appendix C, and displacement-time histories of selected MPBX anchor locations are discussed in Section 5.

the conceptual model used to describe the mechanism of heat and fluid flow, and the homogeneity of the surrounding host rock. The following results are described for the ECM conceptual model with isotropic and homogeneous rock properties. Additional analyses should be conducted implementing the actual complexities seen in the surrounding host rock while incorporating conceptual models that may better describe the actual mechanism of fluid and heat flow.

The temperature-time history results at the collar locations indicate the highest predicted temperatures at all of the borehole locations. The low bulk permeability results at the collar of ESF-HD-MPBX-7 indicate a maximum drift wall temperature of approximately 260°C, 300°C, and 330°C, respectively for 2, 3, and 4 year continuous full power heating. The higher rock bulk permeability temperature predictions at this (collar) location are approximately 10°C less than the lower permeability rock. In general, the low permeability temperature predictions are greater than the high permeability temperature predictions. At very early times, however, a slight increase in the convection heat transfer aids in the transport of energy away from the heat source towards the rock wall. The higher bulk permeability rock will result in a slightly greater temperature as heat is convected more readily from the canister heater to the drift wall. This process occurs while the medium is below the boiling point and the drying front is just beginning to move away from the drift wall. At further locations along the borehole (i.e., anchors 1 through 4), convection effects become more pronounced in the higher bulk permeability simulations as is evident by the prolonged constant temperature regions (T = 96°C) and the bumps (i.e., inflection points) in the temperature predictions of both permeability cases. At the furthest point along the MPBX in the borehole, anchor 4, convective heat transfer results in a slight increase in the predicted temperatures of the high permeability rock when compared to the low bulk permeability cases.

The same general trends are observed in the temperature predictions for ESF-HD-MPBX-9 and -10 as well. Convection heat transfer influences the temperature predictions with increasing distance from the collar at later times particularly for the higher bulk permeability cases. It is noted that the predicted temperature at the collar of ESF-HD-MPBX-10 is slightly greater than the collar predictions at the other locations due to the proximity of this specific collar location to the canister heaters.

5.1.2 Temperature and Liquid Saturation Contours

Contour plots (refer to Appendix B) of predicted temperatures and liquid saturations are shown at 6 month intervals for each of the thermal-hydrologic models used to analyze the heated drift area. The Y-Z longitudinal model results illustrate the impact of edge cooling while the X-Z model results provide T-H predictions at the center of the heated drift experiment. The 3-D X-Y-Z model results are shown only for the low bulk permeability case with a 2 year heating and cooling cycle.

The heating results for the low bulk permeability case are shown for each of the heating cycles. It is noted that identical times (later in the simulation) are not repeated for the longer heating cycles (3 and 4 year heating). For example, consider 3 year heating, 2 year cooling; the displayed results begin at 30 months simulated since the early heating times (6 - 24 months) are

network begins to flow. Subsequently, the condensate water would enter the fracture domain and leave the system via the connected fracture network out the bottom of the test.

An additional theory should also be investigated. It is an argument regarding the formation of a dry-out zone and subsequently a condensate zone based on the degree of fracture connection. It is possible that the in situ water located in unconnected pore volumes within the matrix will not readily evaporate (due to large pore pressures) and thus mobilize in vapor form to regions where condensation may occur. This implies a reduction in the growth of the dry-out zone and thus the formation of such a large condensate zone. In situ water around connected fracture features will readily mobilize in the form of vapor. Water in matrix pore space not near connected fractures may be transport limited by the permeability of the matrix itself. Therefore, water will not be readily mobilized with some moisture remaining in the system at temperatures much higher than 96°C.

The high permeability results are qualitatively similar to the low permeability liquid saturation predictions. In this case, however, the condensate shedding and high saturation build-up below the heater horizon is somewhat larger in extent and duration than in the low permeability cases. Additionally, the formation of the dry-out zone is asymmetrical and is somewhat larger in extent and duration.

5.1.2.2 Temperature and liquid saturation contours for the Y-Z longitudinal model

The temperature contours from the Y-Z longitudinal model domain are used to establish the effects of edge cooling near the ends of the heated drift. At early times (i.e., 6-12 months), the temperature profiles are quite tabular indicating small effects due to unheated rock mass at the drift ends and bulkhead. With continued heating (12-18 months), the temperature profiles become elliptical in shape thus indicating an increasing influence due to the unheated rock mass near the ends surrounding the drift. The 96°C isotherm indicates that edge cooling is an important phenomenon approximately 18-24 months into full power heating. This trend (increasing importance of edge cooling effects at late times) continues for the longer heating cycle scenarios considered. These results are similar for the high bulk permeability cases, but they are delayed in time by approximately 6 months.

The high bulk permeability temperature profile indicates a very flat 96°C isotherm above the drift and somewhat below (not as large in extent) due to the development of the refluxing zones sustained by the buoyant gas-phase convection. At later times during the high permeability simulations, 24 months and beyond, temperatures greater than the 96°C isotherms indicate that edge cooling is an important effect and should not be neglected in model analyses. It may also be important to consider the ventilation effects on the bulkhead side of the heated drift in future analyses.

Liquid saturation results indicate the development of a condensate zone with water shedding around the far end (adjacent to the concrete liner) of the heated drift. Regions of high liquid saturation exist both above and below the drift (above and below the dry-out zone) with more extensive high saturations forming below the dry-out zone. Water shedding finally occurs entirely around the bulkhead end of the drift during the 4 year heating scenario at about 48

5.2 Thermal-Mechanical

Appendix D contains predictions of the displacement in the host rock during the heating and cooling phases of the heated drift test at selected MPBX anchor locations. Heating scenarios of 4 years heating, and 2 years heating-2 years cooling, are presented in Appendix D. The 3-D temperature fields used as input to the T-M calculations were obtained from the T-H calculations by the process described in Section 4.3, and selected temperature fields are included in Appendix C. The displacement-time history results presented in Appendix D are for: ESF-HD-MPBX-7, -9, and -10, located at the approximate midpoint of the heated drift experiment (boreholes 154-157; refer to Section 5.1); ESF-HD-MPBX-1, which runs horizontally along the length of the heated drift approximately 7 m south of the center line; and SDM-MPBX-2, located in the sequential mining borehole which is at the same Y-coordinate as the borehole 154 through 157 (roughly the midpoint of the heated drift). All the predictions presented in Appendix D are of displacement of the host rock at each anchor location relative to its corresponding collar.

The sensitivity of the predictions to different determinations of rock mass elastic modulus, rock mass thermal expansion, and bulk permeability has been addressed in the T-M calculations. As described in Section 4.5.3, four cases are used for simulation: 1) a "base case" with a rock mass elastic modulus E=36.8 GPa and thermal expansion values α=7.47-51.47 μm/m-°C as a function of temperature, both based on intact rock measurements, and a low bulk permeability $K_b=2.16\times10^{-15}$ m²; 2) an in situ elastic modulus case, where E=10 GPa based on Goodman Jack measurements near the SHT; 3) an in situ thermal expansion case, where α=5.27 μm/m-°C based on SHT displacement and temperature data; and 4) the high bulk permeability case, $K_b=6.35\times10^{-12}$ m², for which a different set of temperature predictions from the T-H calculations is input to the T-M calculations. The base case calculations were run for both the heating scenarios described above (the 2-year heating, 2-year cooling and the 4-year heating scenario). The other three cases were run to simulate the 4-year heating scenario to provide comparisons with the base case.

5.2.1 Displacement Predictions at the Middle of the Heated Drift

The displacement-time history results presented Figures D-1 through D-15 in Appendix D are for ESF-HD-MPBX-7, -9, and -10 (boreholes 154-157), located 21 m from the heated drift bulkhead, at the approximate center of the heated drift experiment . ESF-HD-MPBX-7 will be located in a borehole drilled into the ceiling of the drift at an orientation of 30° from the vertical, with the collar location at the drift wall about 1.3 m from the centerline. ESF-HD-MPBX-9 will be located vertically upward from the top of the drift. ESF-HD-MPBX-10 will be located vertically downward from the top of the concrete invert.

Figure D-1 shows the predicted displacement relative to the collar of the four anchors in MPBX-7 for the 2-years heating, 2-years cooling scenario. Anchors 1, 2, 3, and 4 are 1, 2, 4, and 15 m, respectively, from the collar. (As the MPBXs had not yet been installed when these analyses were performed, for the purposes of these analyses the collar is assumed to be at the rock surface, or the invert surface for those with vertical-down orientation.) Note that during the two-year heating period, the anchors 1, 2, and 3 extend outward from the drift wall equally for the first month or so, indicating that only Anchor 1 is experiencing rock deformation due to thermal

interaction with the liners and end effects. A preliminary look at the results of the T-M calculations indicates these results are indeed predicted by the computational model. Time constraints did not allow for a thorough examination and presentation of the T-M calculations at these locations in this report, but the authors will examine these results more closely in the next few months and intend to report their findings in early FY98.

5.2.2 Displacement Predictions Along the Length of the Heated Drift

The displacement-time history results presented Figures D-16 through D-21 in Appendix D are for ESF-HD-MPBX-1, which runs horizontally along the length of the heated drift at an (X-Z) location of (7.0 m, 3.5 m). MPBX-1 has six anchor stations, located 7.5, 15, 25, 27, 39, and 45 m away from the collar (Anchor 1 through 6, respectively).

Figure D-16 shows the predicted displacement relative to the collar of the six anchors in MPBX-1 for the 2-years heating, 2-years cooling scenario. Anchor 1 is outside the heated region, and all the other anchors are within it. Note that the heat in the drift is pushing Anchor 1 toward the collar, and causing the other anchors to extend away from the collar. After the heater is turned off, the contraction of the rock to initial conditions is slow due to the heat capacity of the rock and the large volume that is heated. Figures D-17 through D-20 show displacements for the 4 year heating scenario for the four rock property cases. Three of the cases predict very similar results, with the alternate rock mass modulus case (E=10 GPa) providing the largest predicted displacements. A direct comparison of the four cases at Anchor 6 is presented in Figure D-21. The SHT in situ thermal expansion coefficient predicts significantly less displacements than the other cases.

5.2.3 Radial Displacement Predictions from the Sequential Mining Drift

The displacement-time history results presented Figures D-22 through D-28 in Appendix D are for SDM-MPBX-2, which is located in a borehole drilled from the primary thermal test alcove (or observation drift) toward the heated drift for the sequential drift mining experiment. The location of this borehole (number 43) is at the same Y-coordinate as the borehole 154 through 157. Borehole 43 is drilled at an angle of 11 below horizontal and is 26.5 m long, with the end of the borehole within 1 m of the wall of the heated drift. SDM-MPBX-2 has six anchor stations, located 16, 18, 20, 22, 24, and 25 m away from the collar (Anchor 1 through 6, respectively). As the collar for this borehole is in the observation, the displacements plotted in Figures D-22 through D-27 are relative to a point far away from this test.

Figures D-22 through D-25 show the predicted displacement relative to the collar of the six anchors in SDM-MPBX-2 for the 4-years heating scenario, for all four of the rock mass properties cases. As the heaters turn on, all four cases show all six anchors with negative displacement, meaning that the expanding rock near the heated drift is compressing the rock between there and the observation drift. However, for all the cases except the alternate rock mass modulus (E=10 GPa) case, the two anchor stations furthest from the collar (i.e., closest to the heated drift) eventually move in extension with respect to the collar, probably indicating that the rock near the heated drift is expanding into the drift and resulting in some tunnel closure; this is consistent with the other MPBX results. The fact that the E=10 GPa case does not predict a

6.0 Summary

Thermal-hydrological and thermal-mechanical analyses were performed to predict temperatures, saturations, and displacements in and around the heated drift. The results presented in Appendices A through D are to be used as first-cut predictions of the T-H-M parameters being measured during the heated drift experiment.

Temperature-time history predictions near the center of the experiment (at the locations of the probes ESF-HD-MPBX-7, 8, 9, and 10) indicate maximum collar temperatures of 260°C, 300°C, and 330°C, respectively for 2, 3, and 4 year full power heating cycles. The high permeability results are approximately 10°C less. Temperature results at other borehole locations off center will be lower as a result of edge cooling into surrounding unheated rock mass. Both cases (low and high rock bulk permeability) indicate transport of energy by convection. The high bulk permeability cases indicate a constant temperature refluxing zone driven by buoyant convection.

Temperature contours indicate the location of important isotherms (96°C, 200°C) at different times during heating. Liquid saturation profiles indicate the location of dry-out zone and the extent of the condensate shedding. The low permeability cases indicate the formation of a symmetrical dry-out zone above and below the heater horizon. The high bulk permeability cases indicate the formation of an asymmetric dry-out zone with preferential drying below the heaters. It is note that for both cases, the formation of a large condensate zone forms below the heater due to water shedding. The longitudinal Y-Z model indicates the importance of edge cooling on both the temperature predictions as well as the location of water shedding around the unheated ends of the drift. Also, the 2-D X-Z cross-section model is compared to the 3-D periodic X-Y-Z model in order to assess the effects of dimensionality of the problem. It is noted that the 2-D model very accurately predicts the drift wall and surrounding rock temperatures. This is important as computational efficiency and the use of 2-D models will allow for extended analyses including the use of alternative conceptual models such as the dual permeability model.

The formation of extensive condensate zones both above and below the heater horizon (surrounding the dry-out zone) indicate large scale movement of water during the heating phase of the experiment. Water is removed from the dry-out zone and transported to cooler regions where condensation allows for an increase in the matrix saturation. This condensate zone persists even into the cooling phase. The extent and duration of the water build-up in the experimental system may be driven by the application of the equivalent continuum model (ECM) used to characterize heat and fluid flow in the model. The assumptions governing the ECM will restrict water transport in the matrix (low permeability) until the matrix is very nearly saturated (i.e., a result of capillary pressure equilibrium). Liquid flow will be maintained at relatively low velocities. Fracture like water flow will not occur in this model until this condition is obtained. Therefore, the development of a very large condensate zone will result in response to the assumption in conceptual model (refer to Appendix B)

In reality, fracture/matrix non-equilibrium will allow fractures to flow at matrix saturations much less than 1.0. Therefore, water can exit the system without the matrix saturations approaching highly saturated conditions. If this is the case, water may drain from the system as it is vaporized and later condensed and removed from the system for good as it flows out of the

References

Altman, S.J., B.W. Arnold, C.K. Ho, S.A. McKenna, R.W. Barnard, G.E. Barr, and R.R. Eaton, 1996. *Flow Calculations for Yucca Mountain Groundwater Travel Time (GWTT-95)*, SAND96-0819, Sandia National Laboratories, Albuquerque, New Mexico.

Bieniawski, Z.T., 1979. *Engineering Rock Mass Classification*, Wiley-Interscience Publication, John Wiley & Sons, New York.

Biffle, J.H, 1993. *JAC3D - A Three-Dimensional Finite Element Computer Program for the Nonlinear Quasi-static Response of Solids with the Conjugate Gradient Method*, SAND87-1305, Sandia National Laboratories, Albuquerque, New Mexico.

CRWMS M&O, 1996. *Test Design, Plans and Layout Report for the ESF Thermal Test*, M&O Report BAB000000-01717-4600-00025 Rev 01, September 20, 1996, Yucca Mountain Site Characterization Project, TRW Environmental Safety Systems, Las Vegas, Nevada.

Data Tracking Number (DTN) GS940508312231.006, Technical Data Information Form (TDIF) No. 303221 (Core analysis of bulk density, porosity, particle density and in situ saturation for borehole UE-25 UZ#16).

Data Tracking Number (DTN) GS940808312231.008, Technical Data Information Form (TDIF) No. 303458, "Physical and Hydrologic Properties of Rock Outcrop Samples at Yucca Mountain, Nevada," USGS OFR 95-280, by L.E. Flint, A.L. Flint, C.A. Rautman, and J.D. Istok.

Data Tracking Number (DTN) GS950308312231.002, Technical Data Information Form (TDIF) No. 304164 (Laboratory measurements of bulk density, porosity, and water content for USW SD-12 from Mar. 19 to Aug. 11, 1994).

Data Tracking Number (DTN) GS950408312231.004, Technical Data Information Form (TDIF) No. 304288 (Physical properties and water potentials of core from borehole USW SD-9).

Data Tracking Number (DTN) GS950608312231.006, Technical Data Information Form (TDIF) No. 304420 (Water Permeability of Core from SD-9, Feb. 28 to Apr. 17, 1995).

Data Tracking Number (DTN) GS950608312231.007, Technical Data Information Form (TDIF) No. 304427 (Physical properties and water potentials of core from borehole USW NRG-6, Mar. 19, 1994 to Mar. 27, 1995).

Data Tracking Number (DTN) GS951108312231.009, Technical Data Information Form (TDIF) No. 305056 (Physical properties, water content, and water potential for borehole USW SD-7).

from the Single Heater Test Area in the Thermal Testing Facility at Yucca Mountain, Nevada).

Engstrom, D.A., and C.A. Rautman, 1996. *Geology of the USW SD-9 Drill Hole, Yucca Mountain, Nevada*, SAND96-2030, Sandia National Laboratories, Albuquerque, New Mexico.

Flint, L., 1996 (in review). *Matrix Properties of Hydrogeologic Units at Yucca Mountain, Nevada*, USGS Water Resources Investigations Report 96-XX, U.S. Geological Survey, Las Vegas, Nevada.

Francis, N.D., S.R. Sobolik, and S. Ballard, 1997 (in review). "Thermal-Hydrologic-Mechanical Analyses of the In Situ Single Heater Test, Yucca Mountain, Nevada," Sixth Symposium on Multiphase Transport in Porous Media, 1997 ASME International Mechanical Engineering Congress and Exposition.

Hardy, M.P., and S.J. Bauer, 1991. *Drift Design Methodology and Preliminary Application for the Yucca Mountain Site Characterization Project*, SAND89-0837, Sandia National Laboratories, Albuquerque, New Mexico.

Ho, C.K., and N.D. Francis, 1996. "The Effects of Conduction, Convection, and Radiation on the Thermodynamic Environment Surrounding a Heat-Generating Waste Package," Proceedings of the Thermal Hydraulics Division of the American Nuclear Society, presented at the 1996 National Heat Transfer Conference, Houston, TX.

Incropera, F.P., and D.P. DeWitt, 1985. Introduction to Heat Transfer, John Wiley and Sons, New York.

Merritt, F.S., 1968. Standard Handbook for Civil Engineers, McGraw-Hill Book Company, New York.

Pruess, K.. 1991. *TOUGH2--A General-Purpose Simulator for Multiphase Fluid and Heat Flow*, LBL-29400, Lawrence Berkeley Laboratory, Berkeley, California.

Pruess, K., and Y. Tsang, 1993. "Modeling of Strongly Heat-Driven Flow Processes at a Potential High-Level Nuclear Waste Repository at Yucca Mountain, Nevada," Proceedings, Fourth High Level Radioactive Waste Management International Conference, April 26-30, 1993, Las Vegas, Nevada.

Sandia National Laboratories (SNL), 1996. "Drift Scale Test: Test Design," Work Agreement WA-0332, Sandia National Laboratories, Albuquerque, New Mexico.

Serafim, J.L., and J.P. Periera, 1983. "Consideration of the Geomechanical Classification of Bieniawski," *Proceedings, International Symposium on Engineering Geology and Underground Construction*, pp. 1133–1144.

Appendix A: Predicted Temperature-Time Histories for the Heated Drift from the 2-D Cross-Section Thermal-Hydrologic Calculations

ESF-HD-MPBX-7,8 (Collar Location)
2 Year Heating, 2 Year Cooling

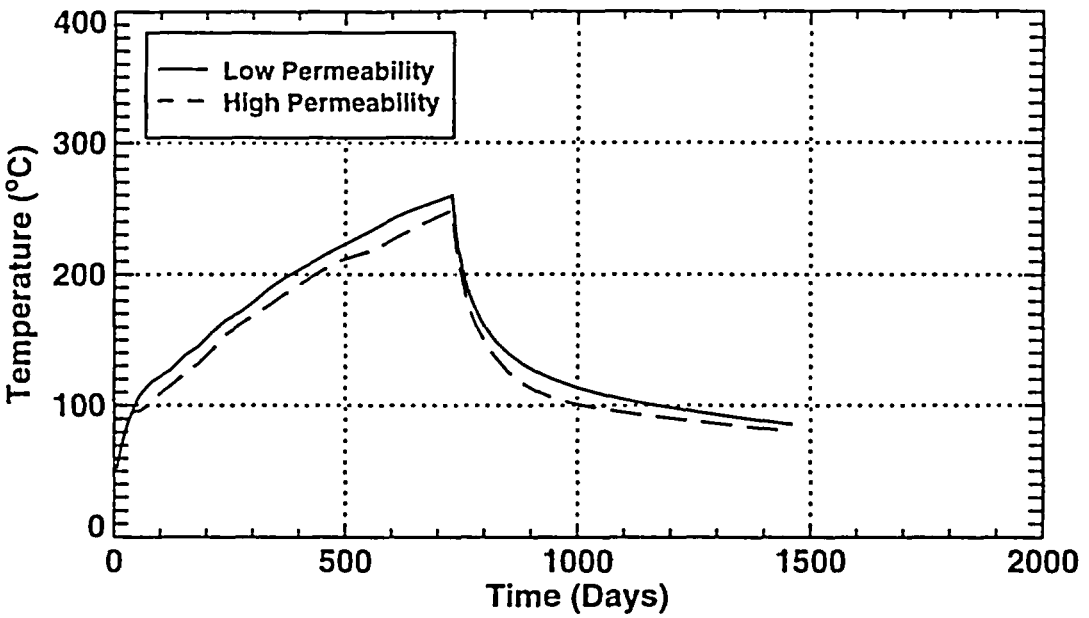

ESF-HD-MPBX-7,8 (Anchor 1)
2 Year Heating, 2 Year Cooling

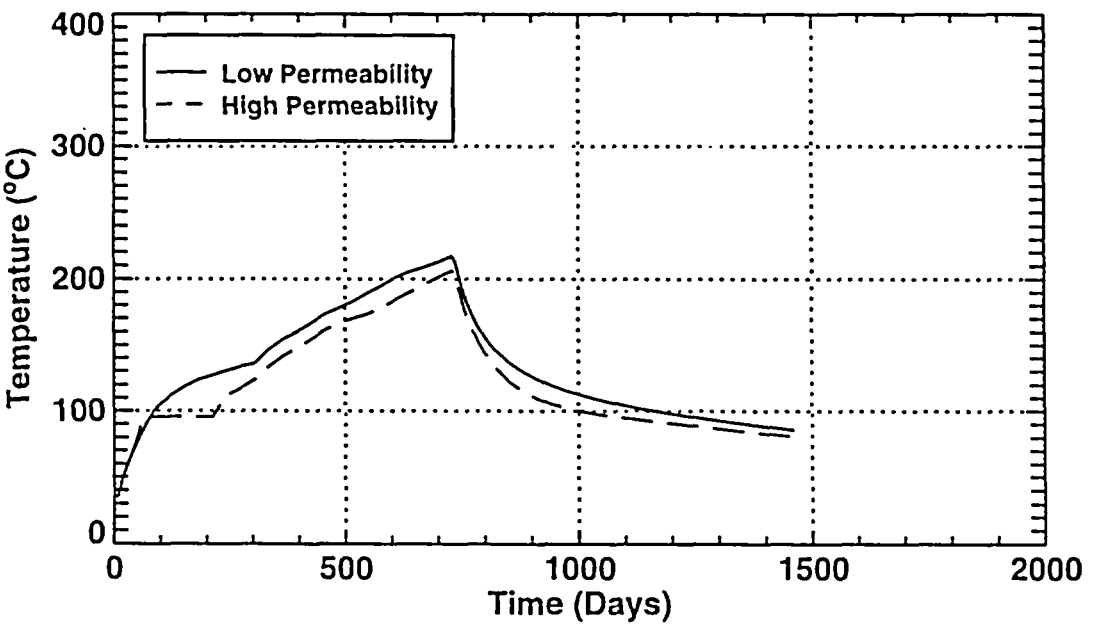

ESF-HD-MPBX-7,8 (Anchor 2)
2 Year Heating, 2 Year Cooling

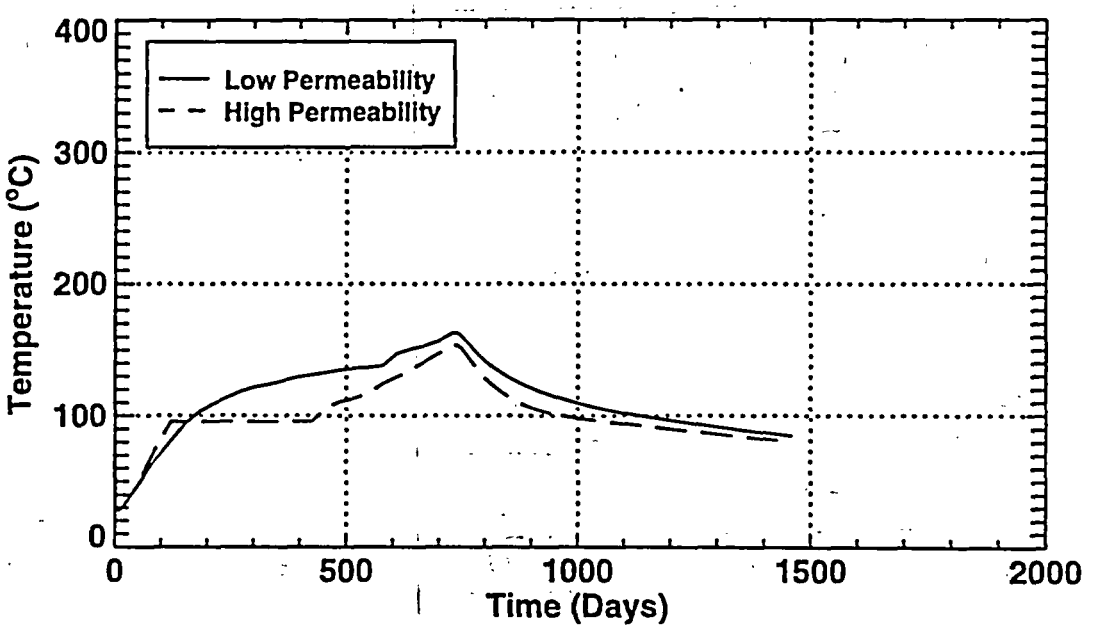

ESF-HD-MPBX-7,8 (Anchor 3)
2 Year Heating, 2 Year Cooling

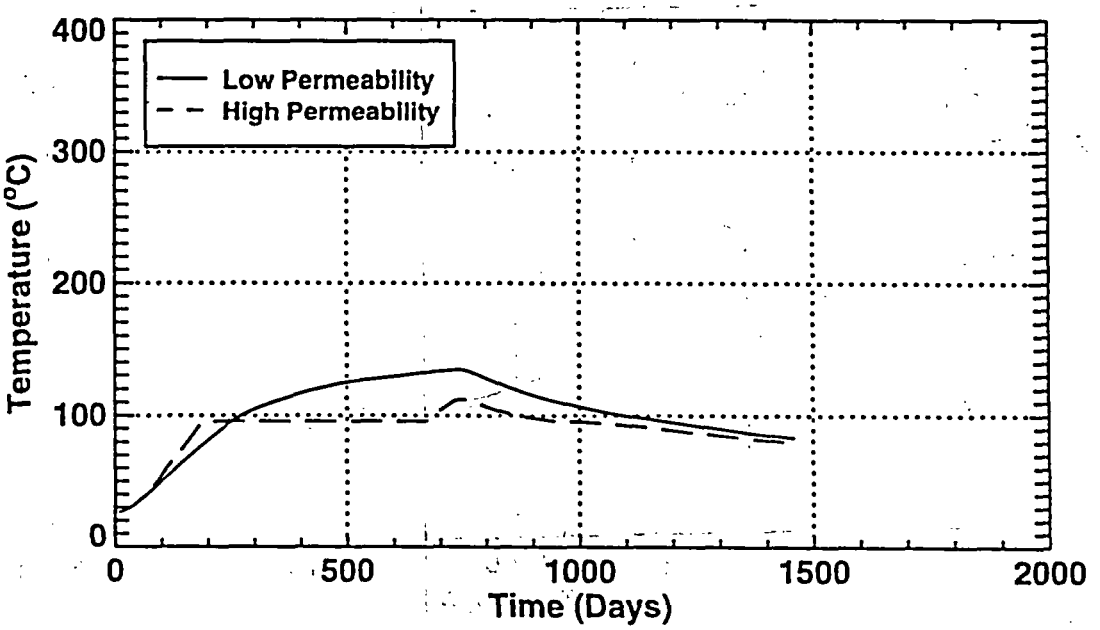

ESF-HD-MPBX-7,8 (Anchor 4)
2 Year Heating, 2 Year Cooling

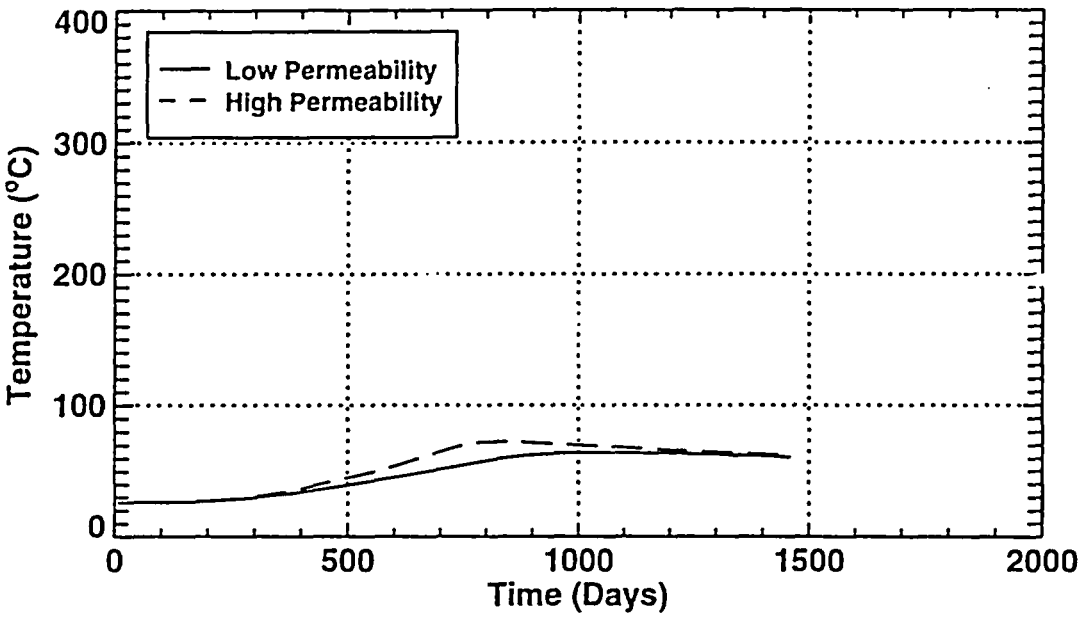

ESF-HD-MPBX-9 (Collar Location)
2 Year Heating, 2 Year Cooling

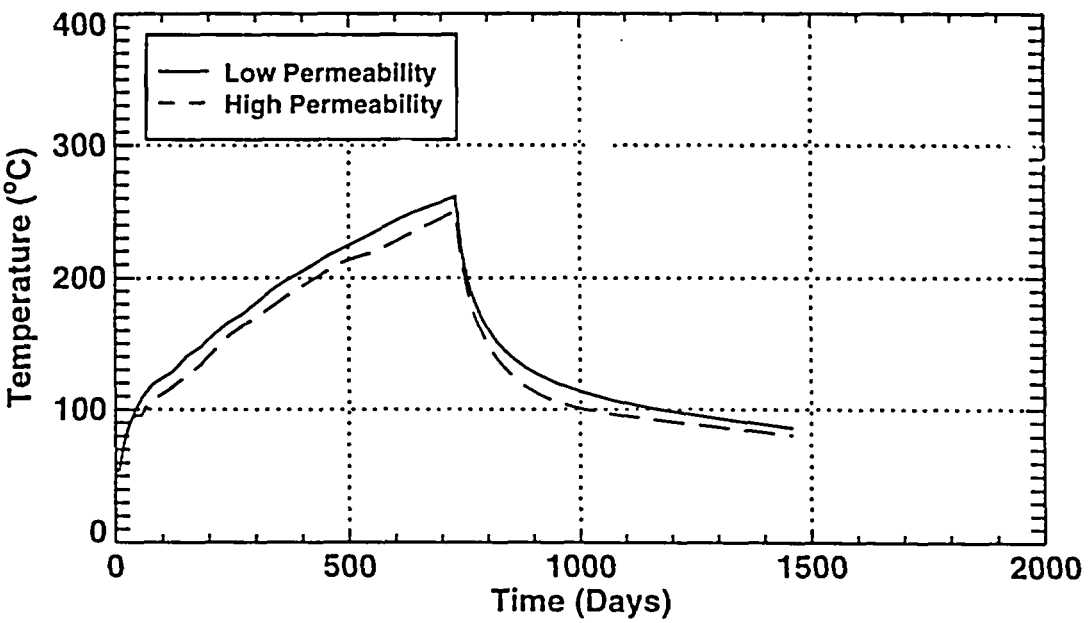

ESF-HD-MPBX-9 (Anchor 1)
2 Year Heating, 2 Year Cooling

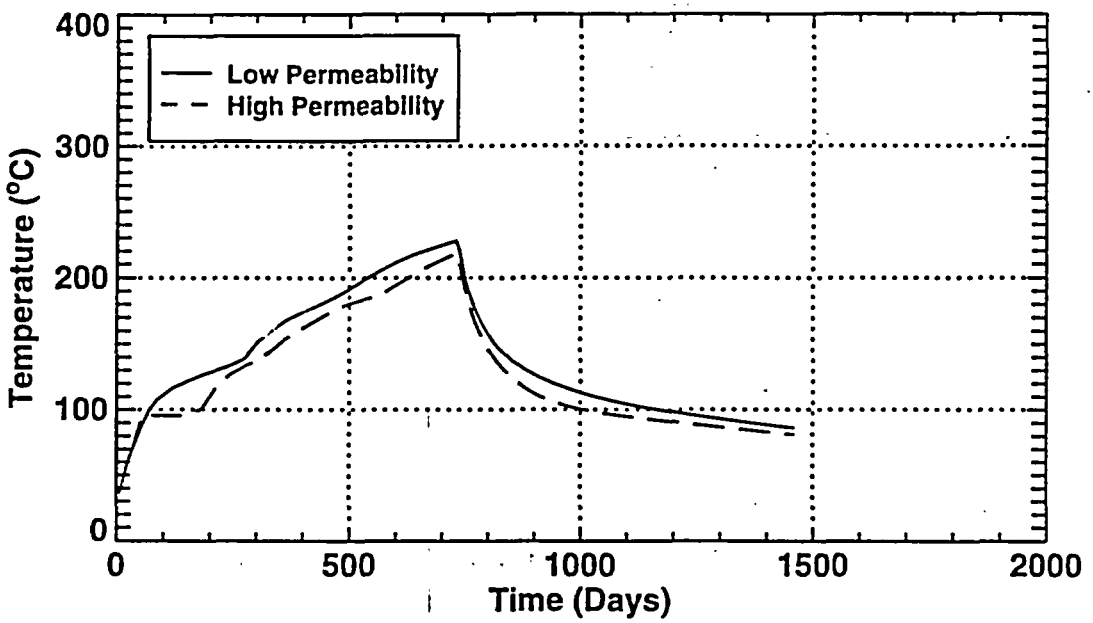

ESF-HD-MPBX-9 (Anchor 2)
2 Year Heating, 2 Year Cooling

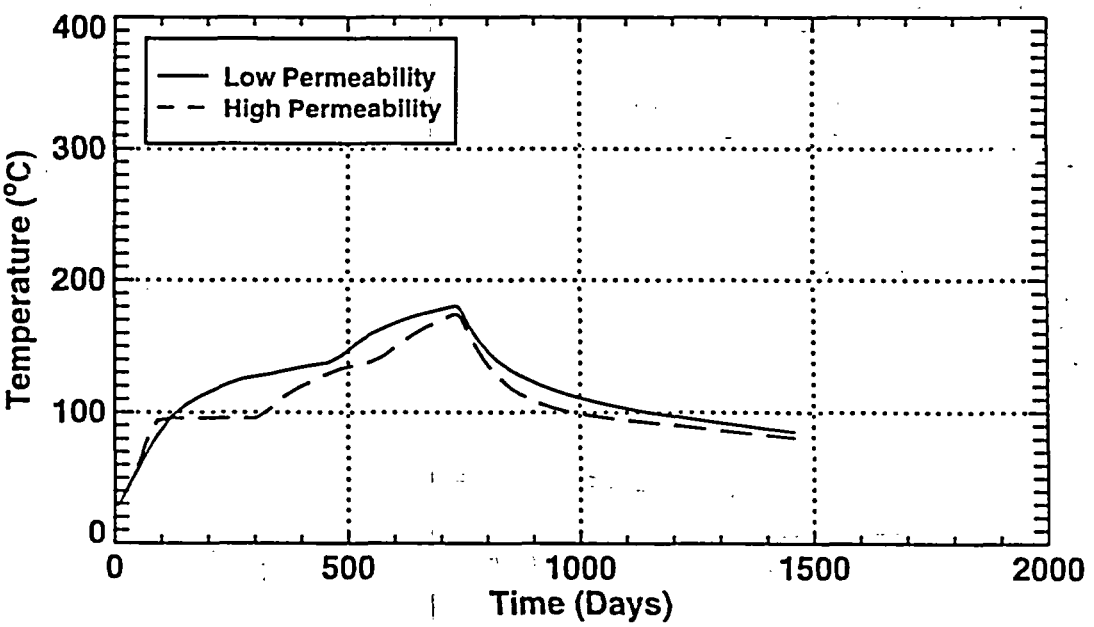

ESF-HD-MPBX-9 (Anchor 3)
2 Year Heating, 2 Year Cooling

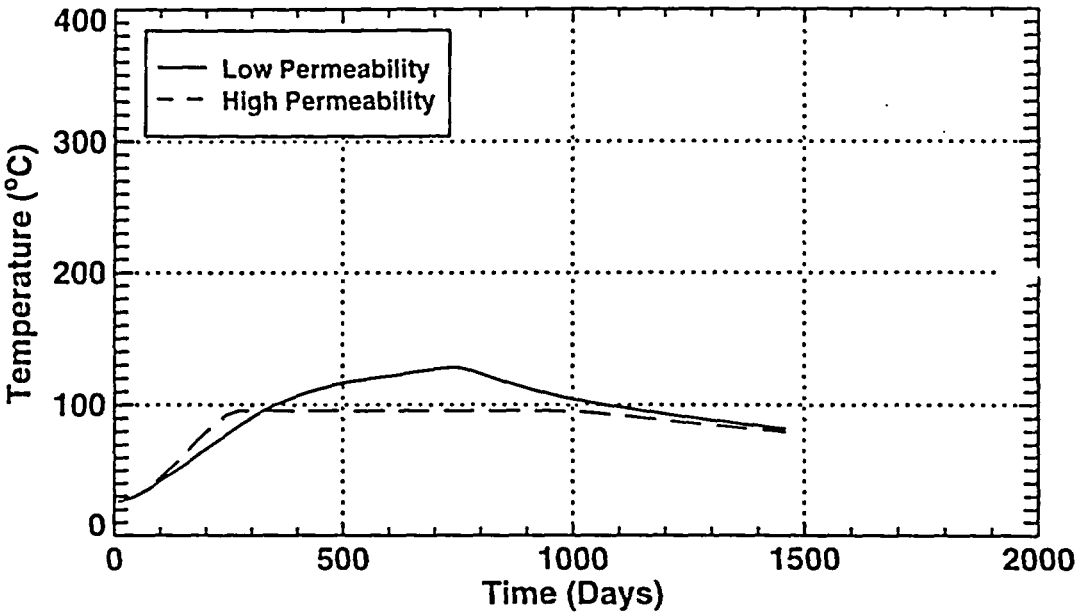

ESF-HD-MPBX-9 (Anchor 4)
2 Year Heating, 2 Year Cooling

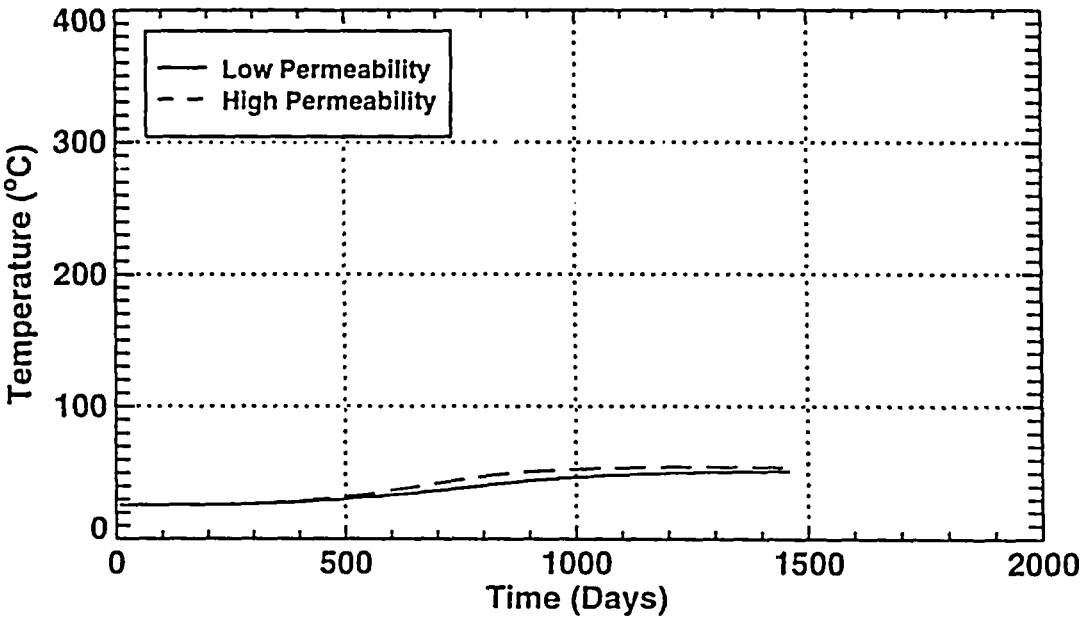

ESF-HD-MPBX-10 (Collar Location)
2 Year Heating, 2 Year Cooling

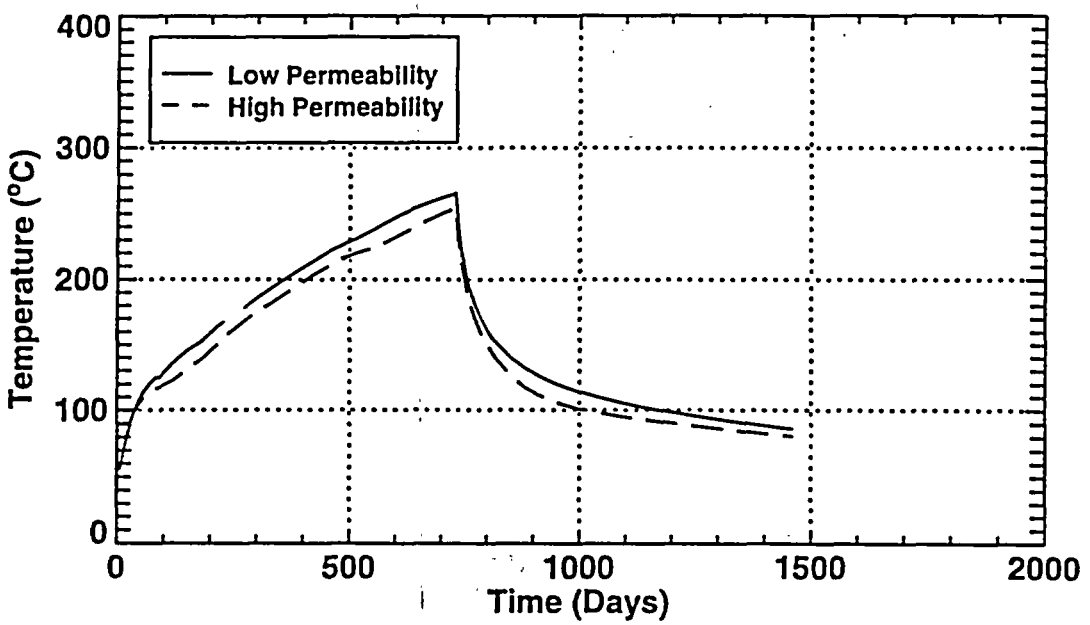

ESF-HD-MPBX-10 (Anchor 1)
2 Year Heating, 2 Year Cooling

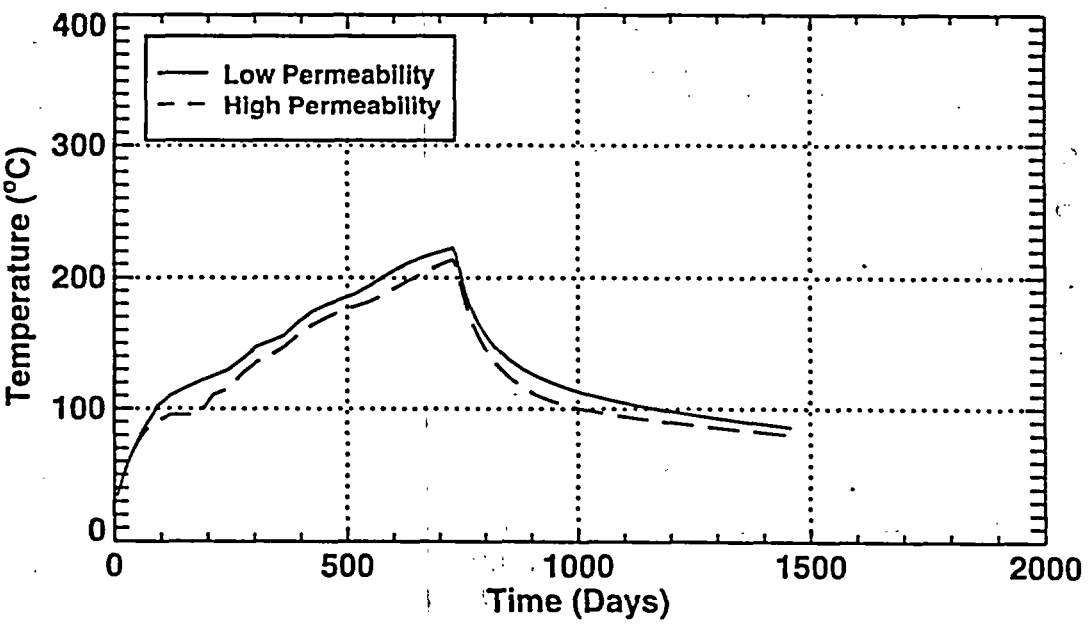

ESF-HD-MPBX-10 (Anchor 2)
2 Year Heating, 2 Year Cooling

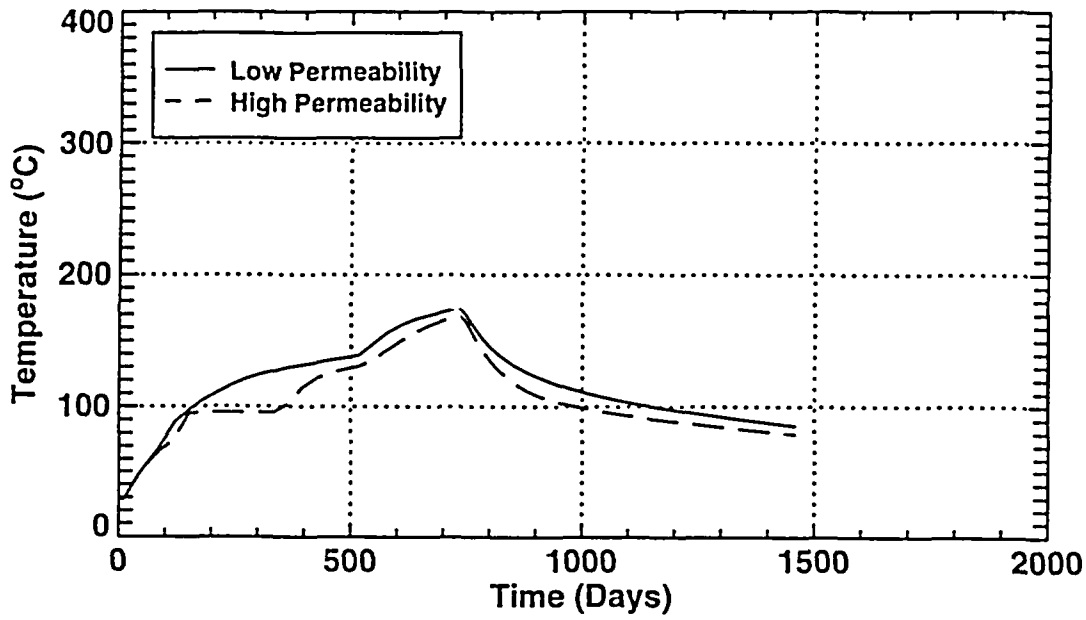

ESF-HD-MPBX-10 (Anchor 3)
2 Year Heating, 2 Year Cooling

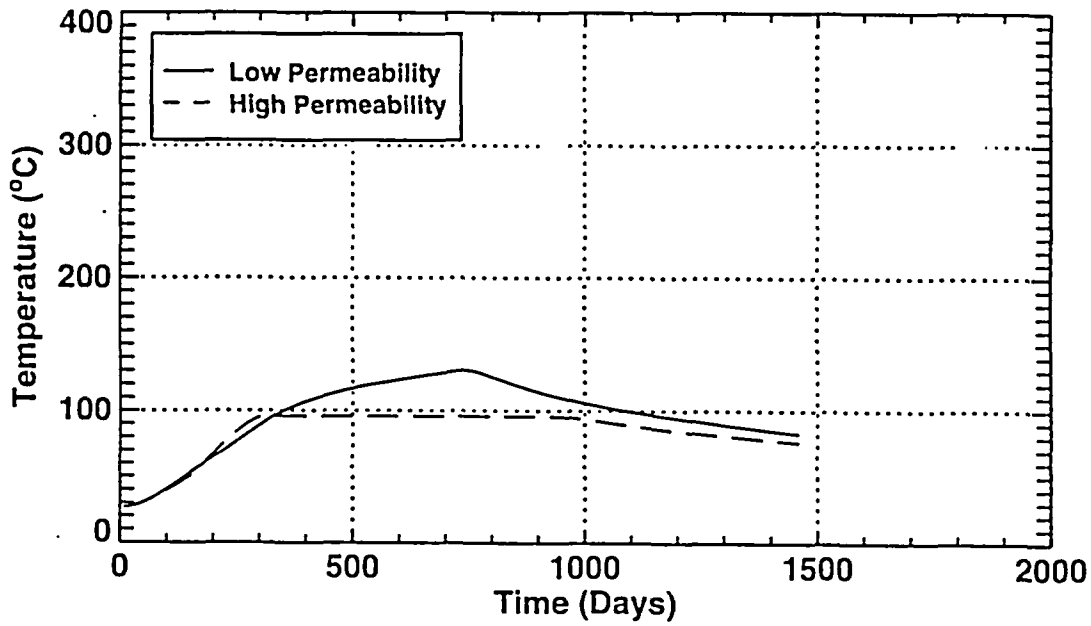

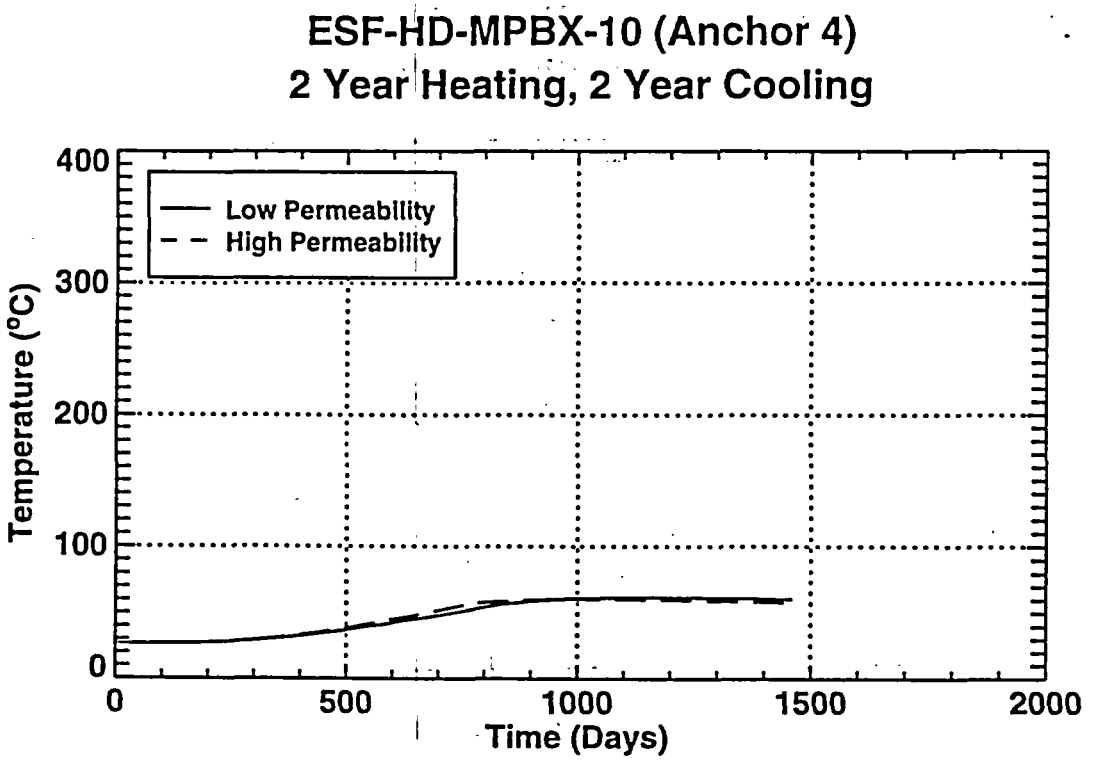
ESF-HD-MPBX-10 (Anchor 4)
2 Year Heating, 2 Year Cooling
Low Permeability
High Permeability
Temperature (°C)
400
300
200
100
0
0
500
1000
1500
2000
Time (Days)

ESF-HD-MPBX-7,8 (Collar Location)
3 Year Heating, 2 Year Cooling

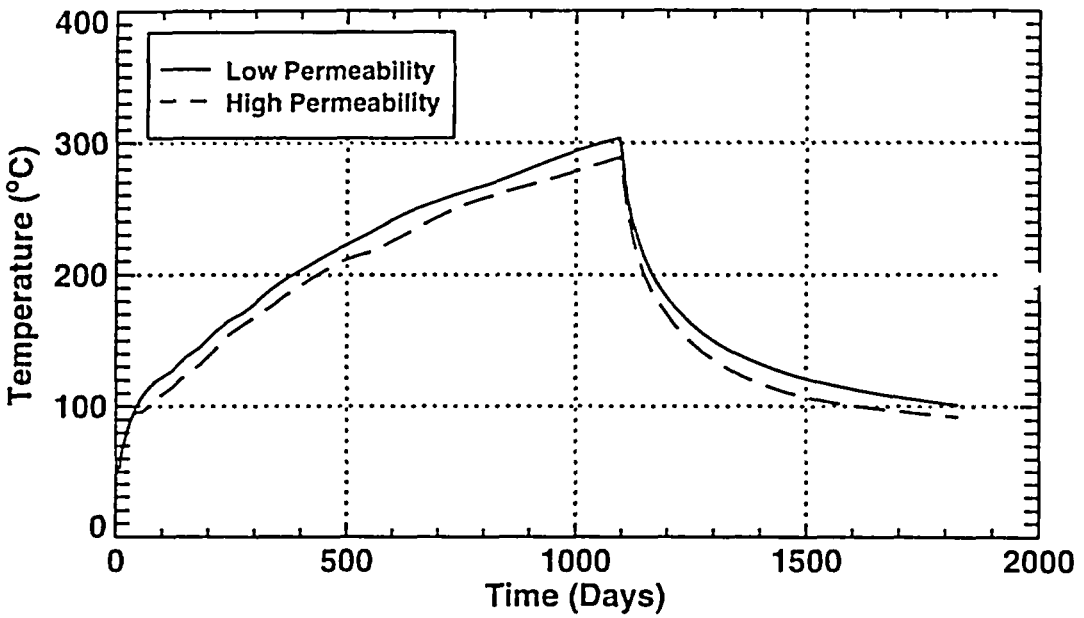

ESF-HD-MPBX-7,8 (Anchor 1)
3 Year Heating, 2 Year Cooling

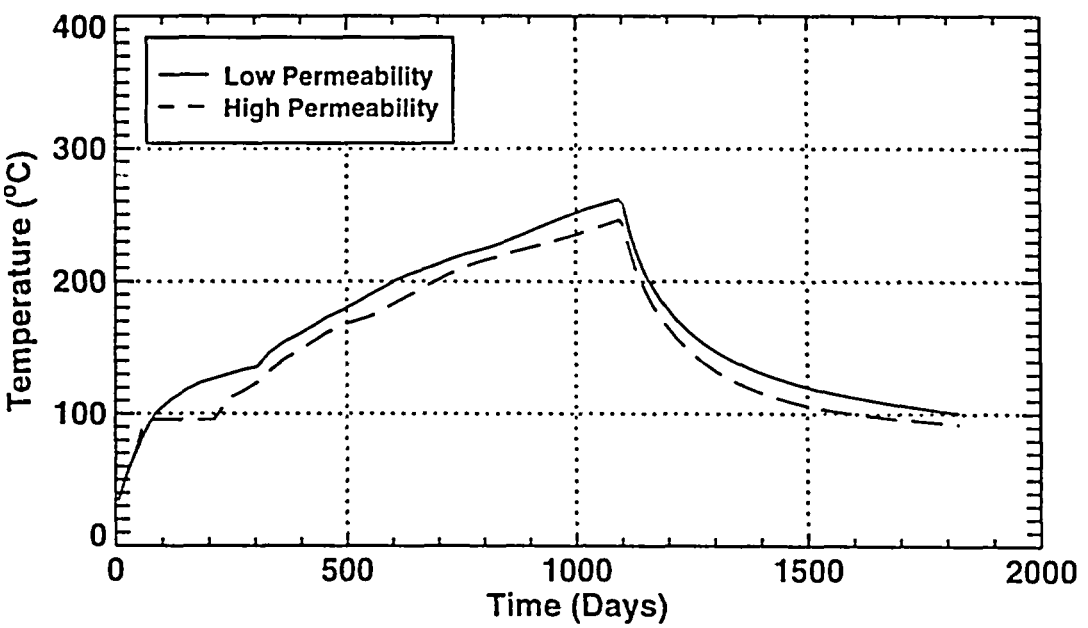

ESF-HD-MPBX-7,8 (Anchor 2)
3 Year Heating, 2 Year Cooling

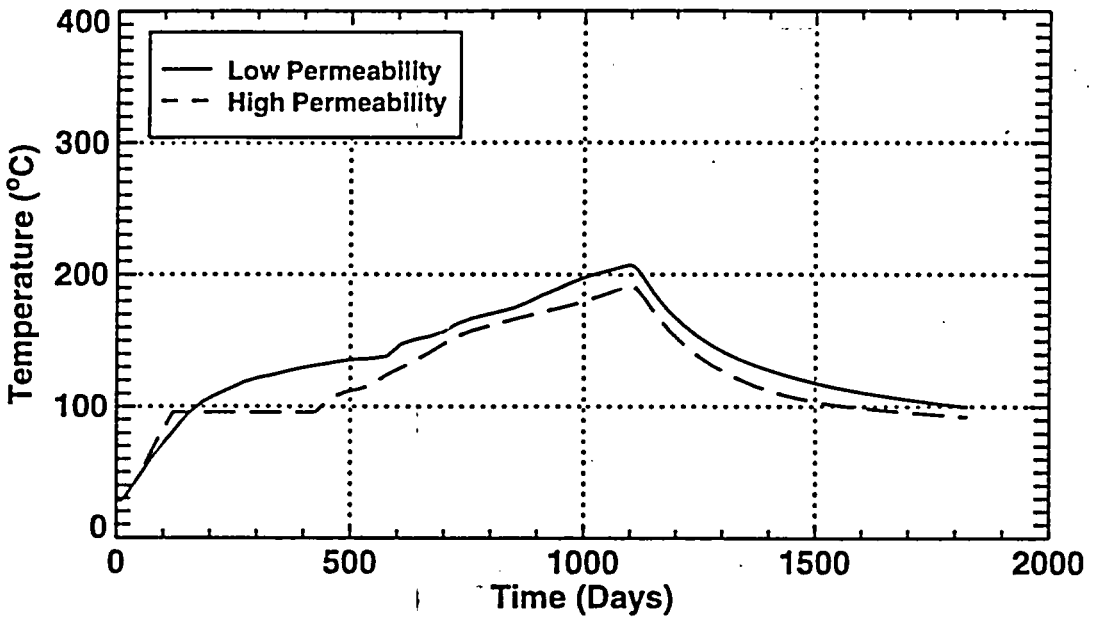

ESF-HD-MPBX-7,8 (Anchor 3)
3 Year Heating, 2 Year Cooling

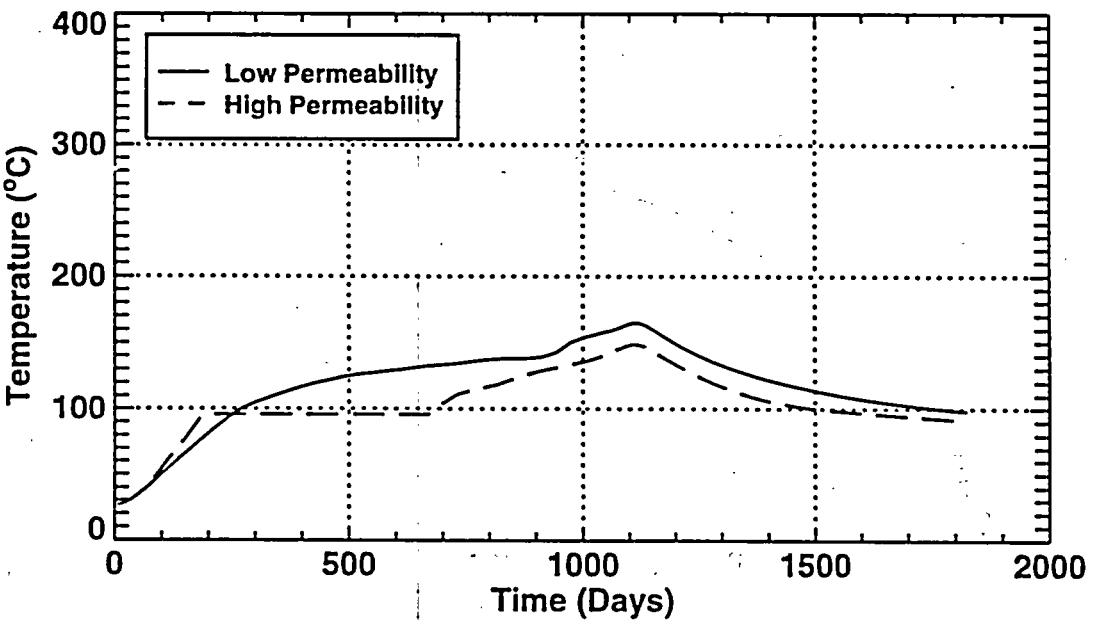

ESF-HD-MPBX-7,8 (Anchor 4)
3 Year Heating, 2 Year Cooling

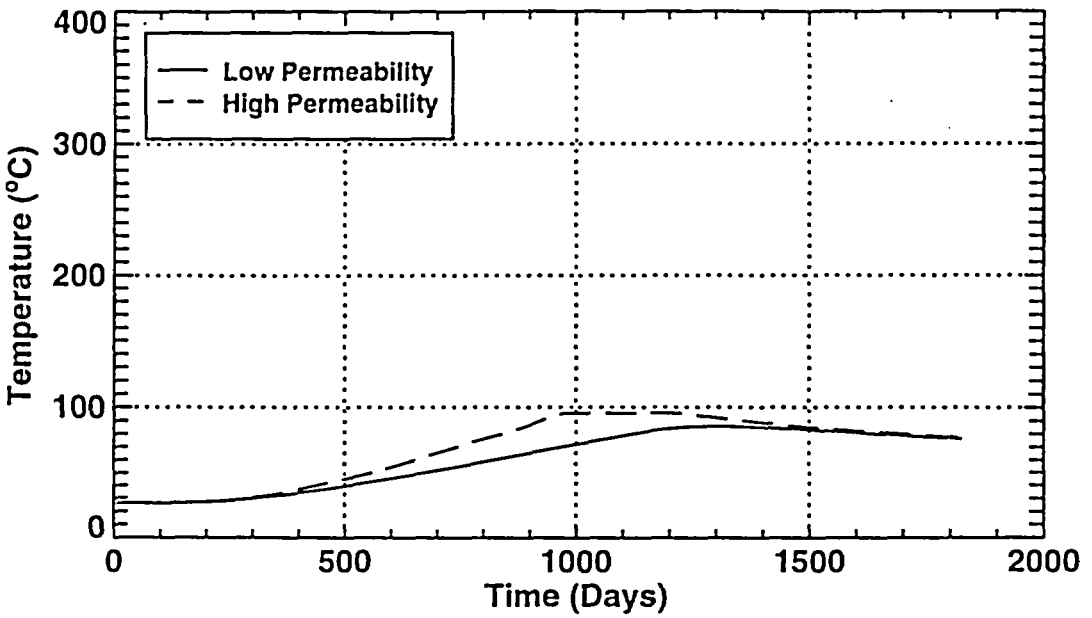

ESF-HD-MPBX-9 (Collar Location)
3 Year Heating, 2 Year Cooling

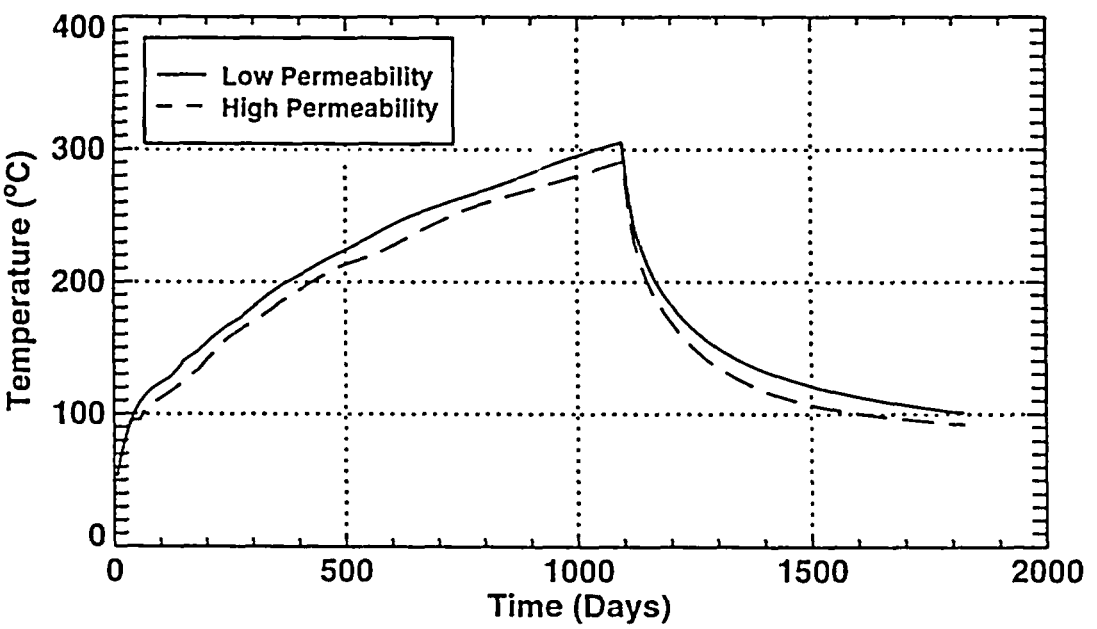

ESF-HD-MPBX-9 (Anchor 1)
3 Year Heating, 2 Year Cooling

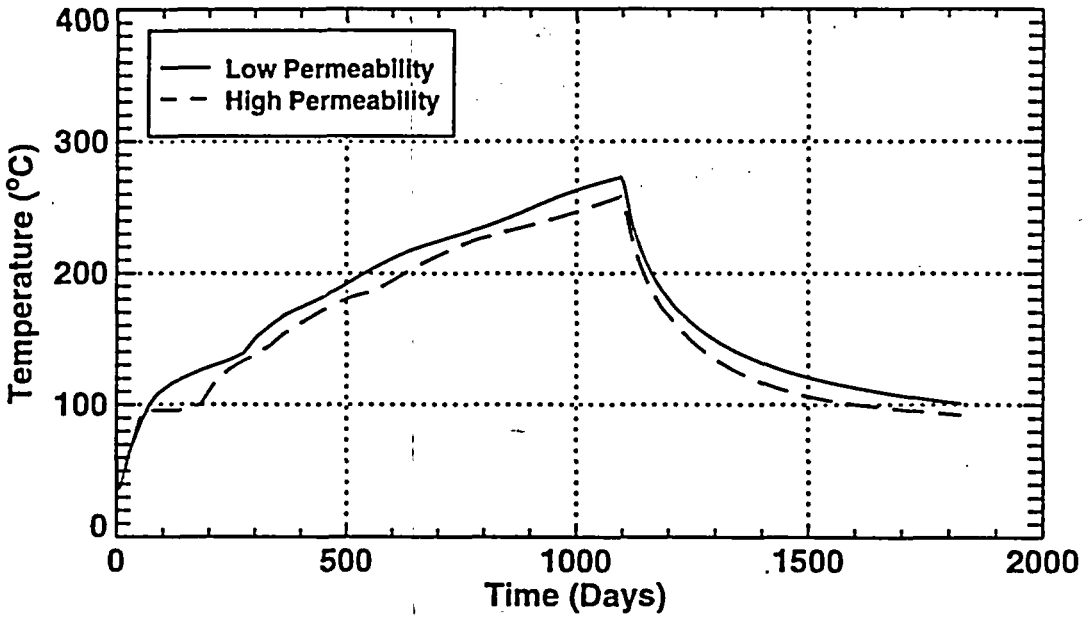

ESF-HD-MPBX-9 (Anchor 2)
3 Year Heating, 2 Year Cooling

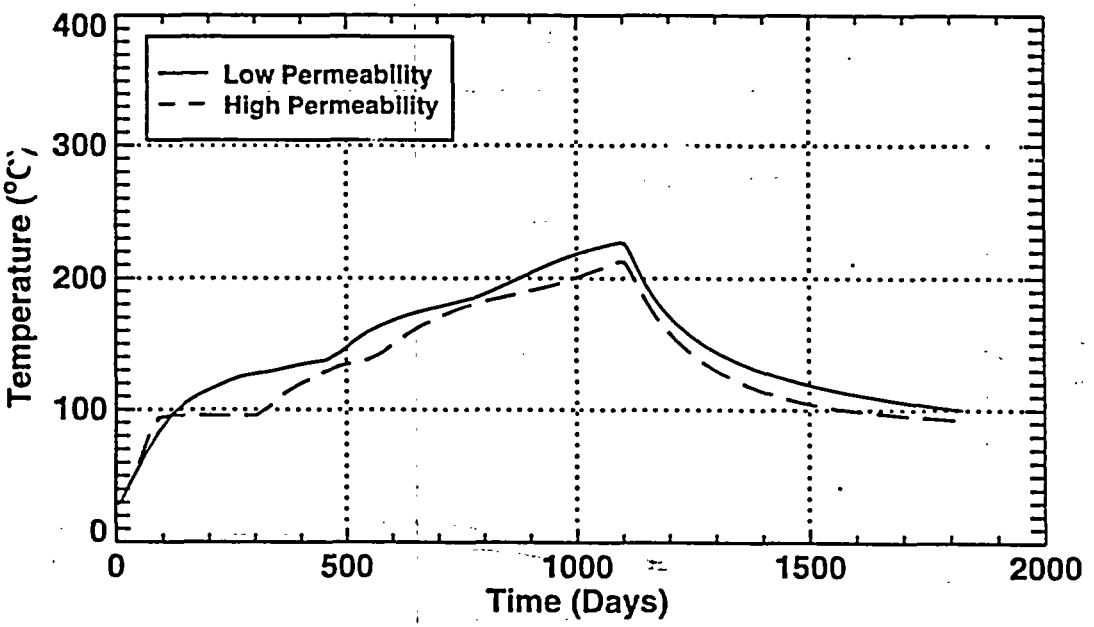

ESF-HD-MPBX-9 (Anchor 3)
3 Year Heating, 2 Year Cooling

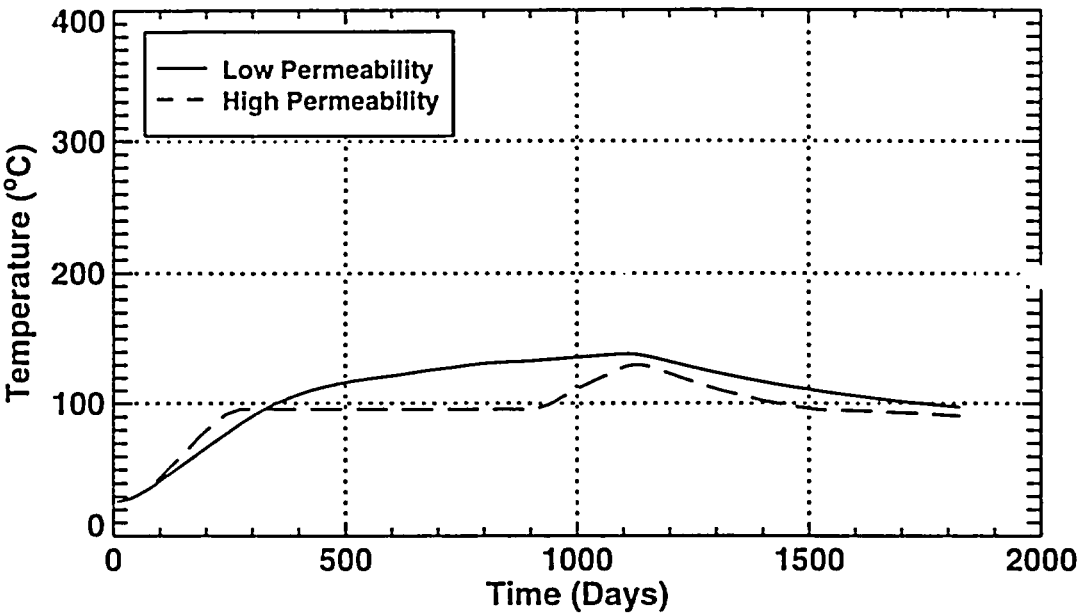

ESF-HD-MPBX-9 (Anchor 4)
3 Year Heating, 2 Year Cooling

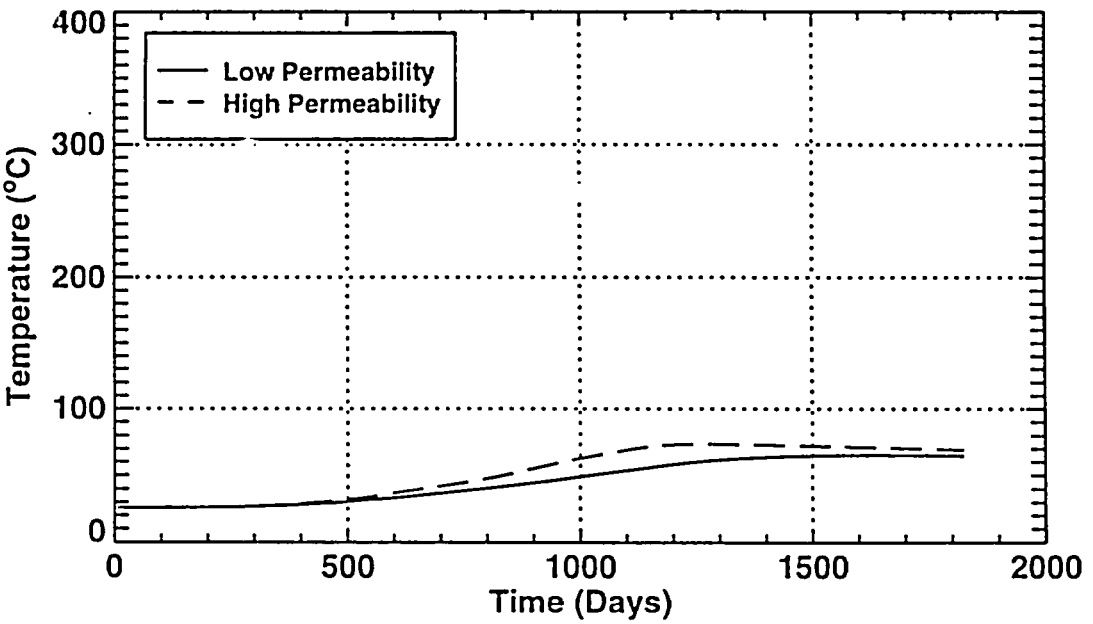

ESF-HD-MPBX-10 (Collar Location)
3 Year Heating, 2 Year Cooling

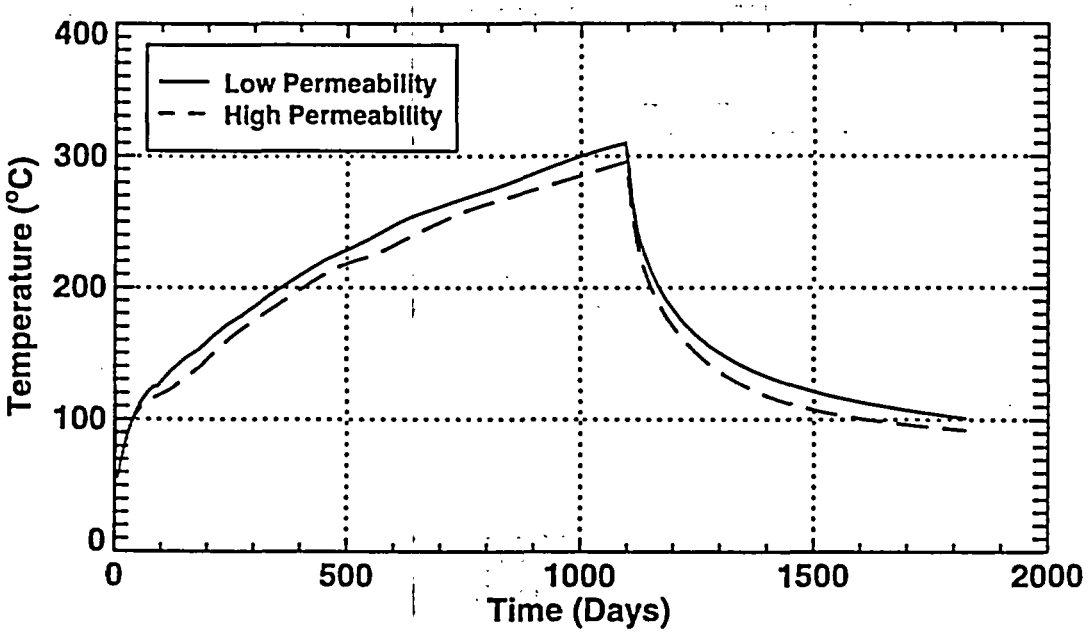

ESF-HD-MPBX-10 (Anchor 1)
3 Year Heating, 2 Year Cooling

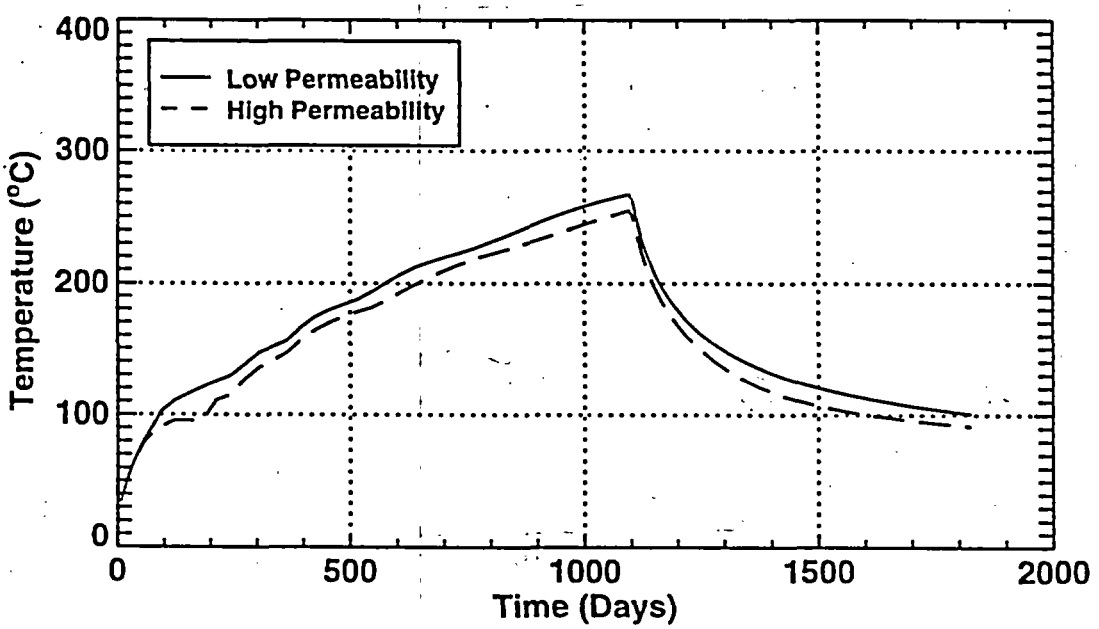

ESF-HD-MPBX-10 (Anchor 2)
3 Year Heating, 2 Year Cooling

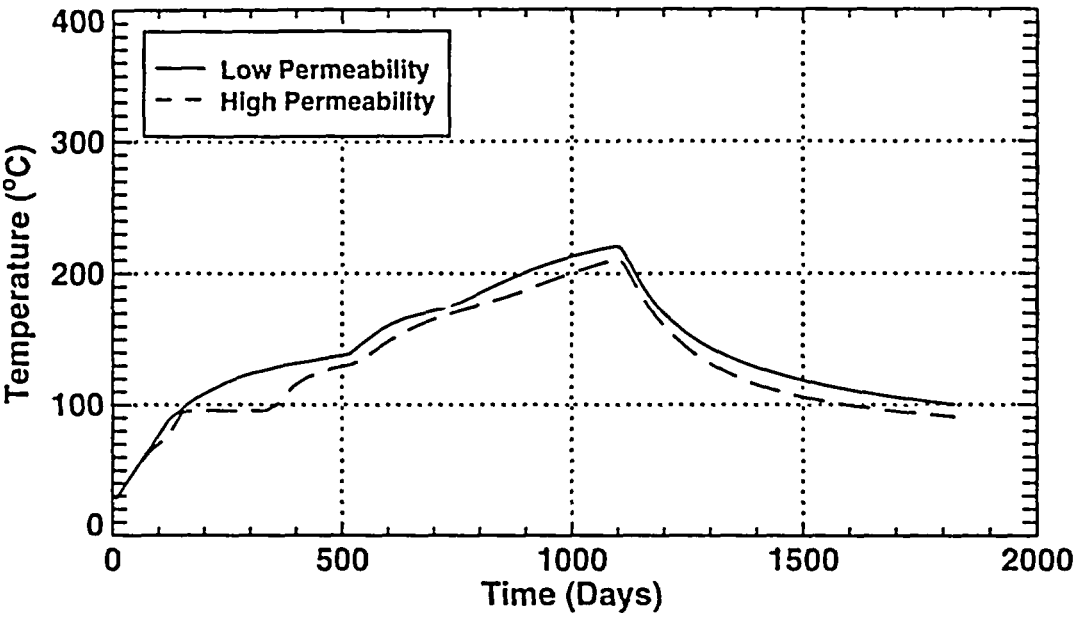

ESF-HD-MPBX-10 (Anchor 3)
3 Year Heating, 2 Year Cooling

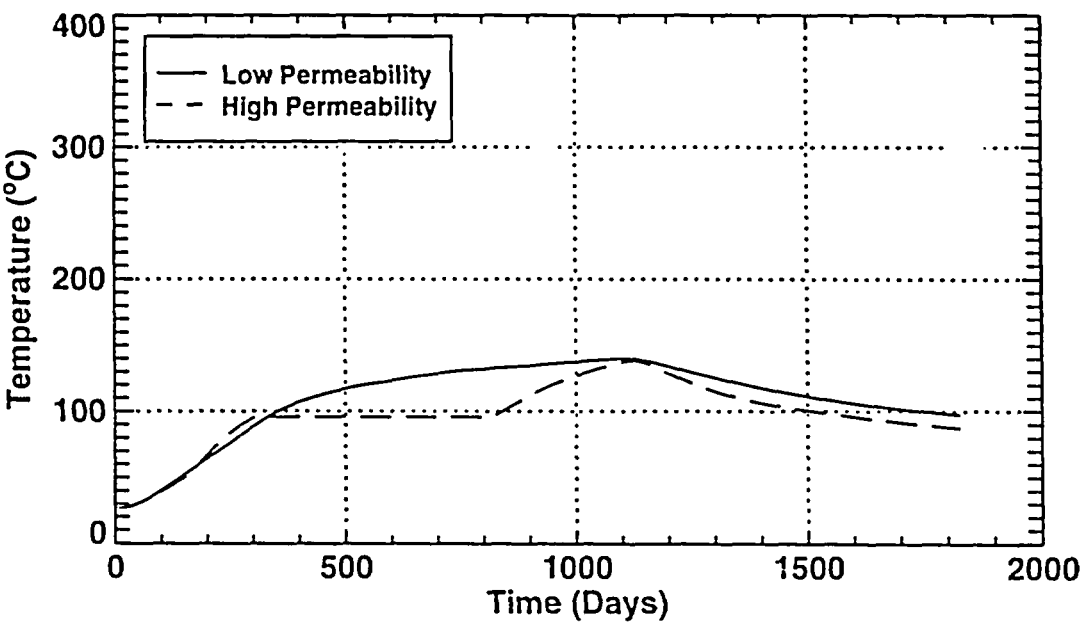

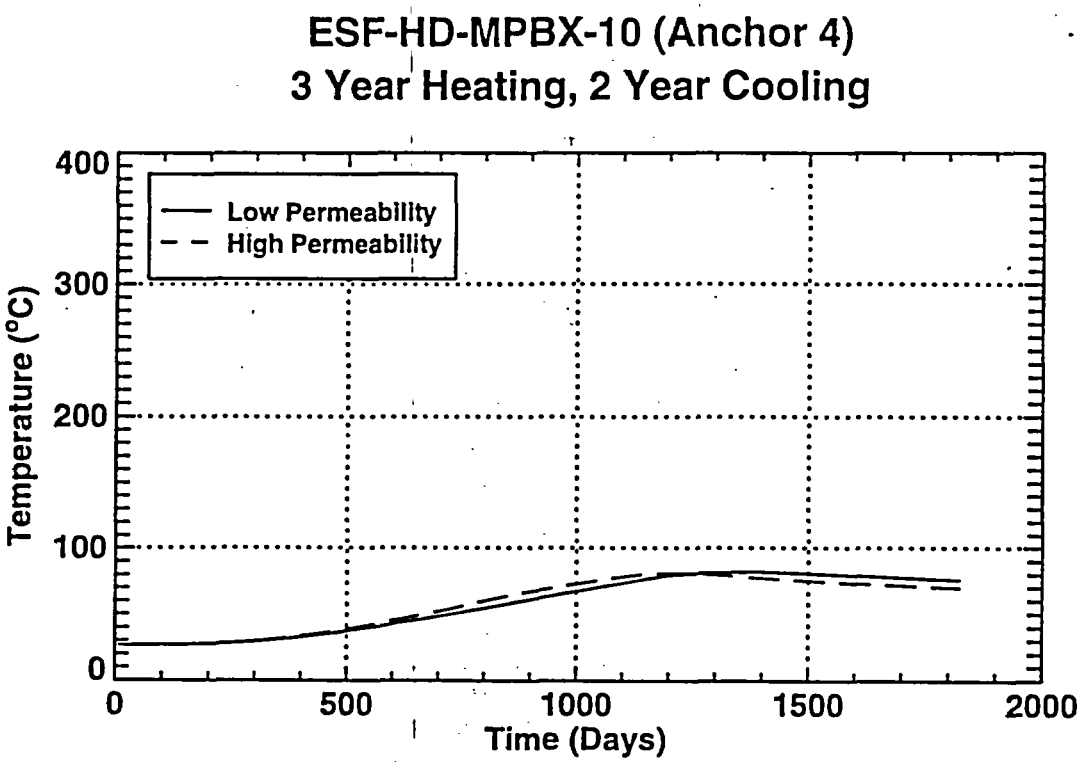
ESF-HD-MPBX-10 (Anchor 4)
3 Year Heating, 2 Year Cooling
Low Permeability
High Permeability
Temperature (°C)
400
300
200
100
0
0
500
1000
1500
2000
Time (Days)

ESF-HD-MPBX-7,8 (Collar Location)
4 Year Heating, 2 Year Cooling

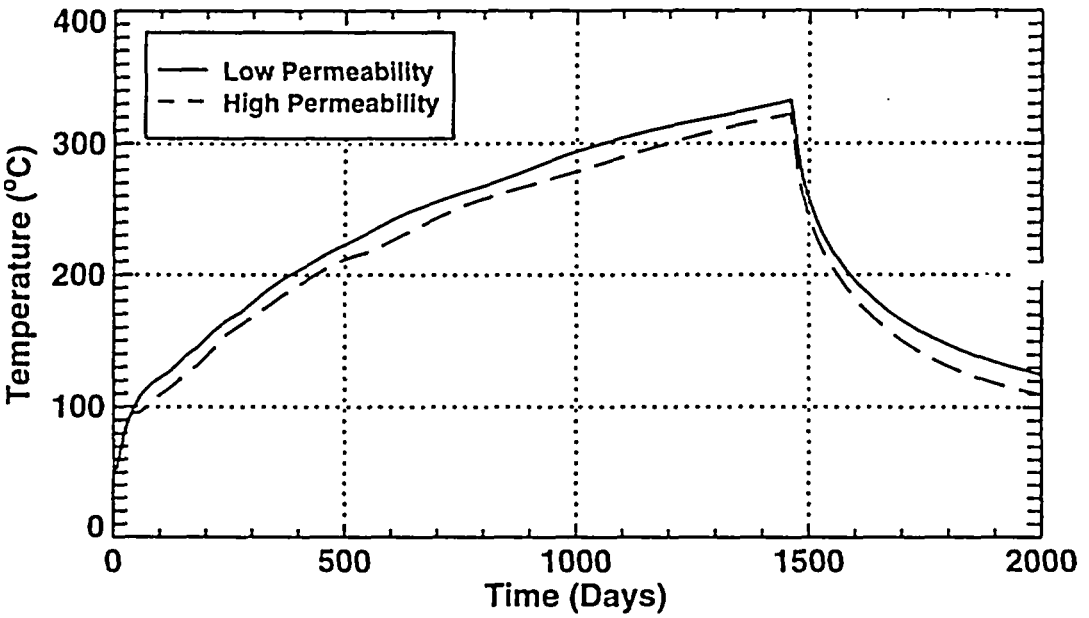

ESF-HD-MPBX-7,8 (Anchor 1)
4 Year Heating, 2 Year Cooling

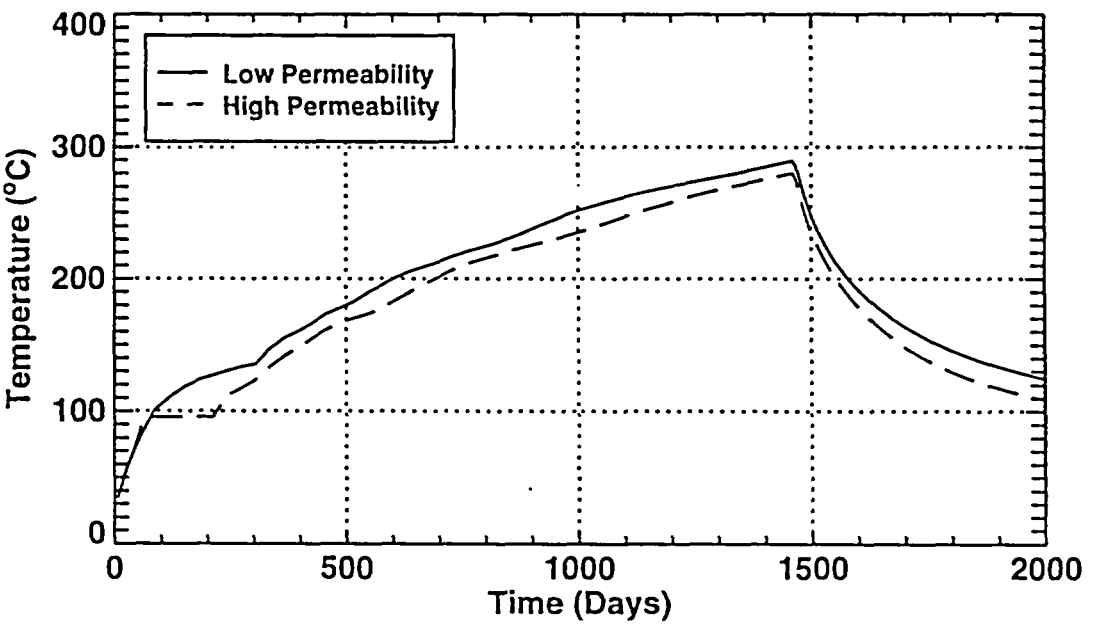

ESF-HD-MPBX-7,8 (Anchor 2)
4 Year Heating, 2 Year Cooling

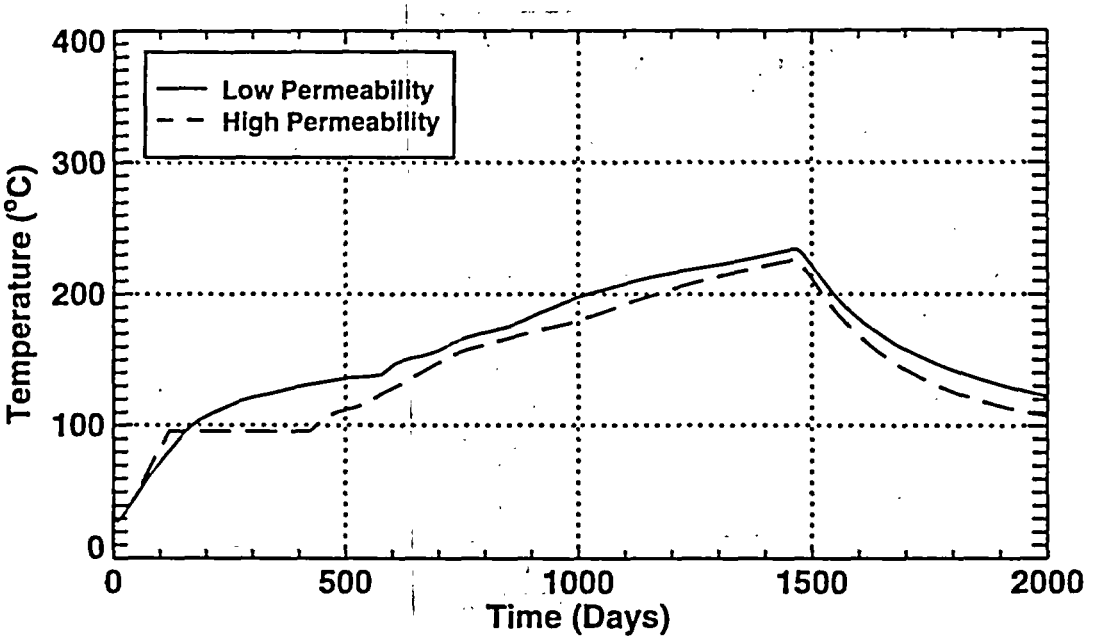

ESF-HD-MPBX-7,8 (Anchor 3)
4 Year Heating, 2 Year Cooling

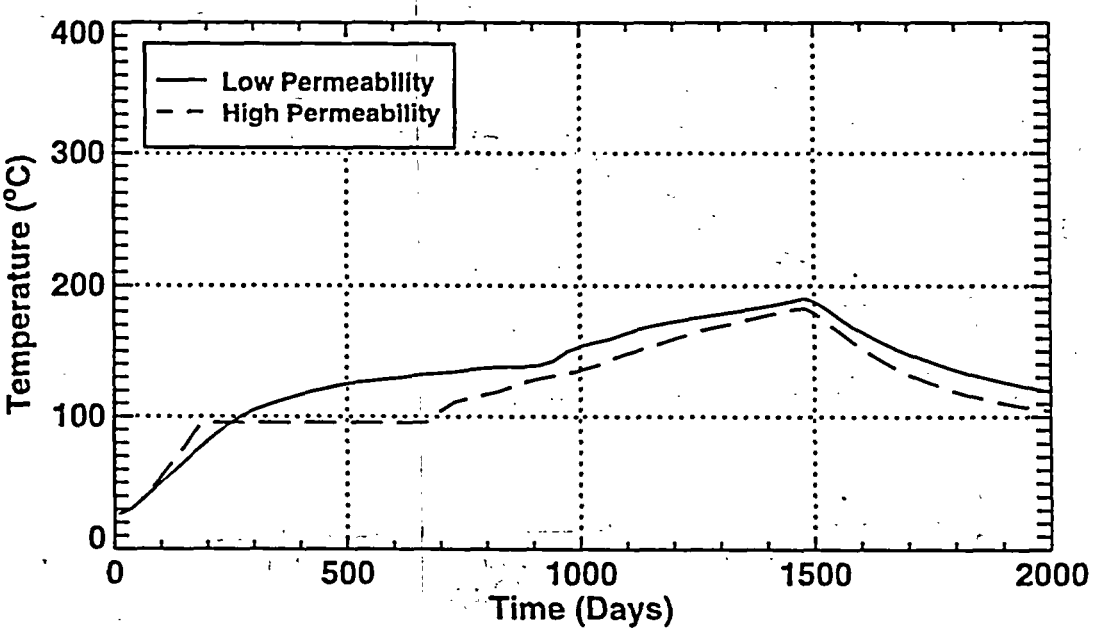

ESF-HD-MPBX-7,8 (Anchor 4)
4 Year Heating, 2 Year Cooling

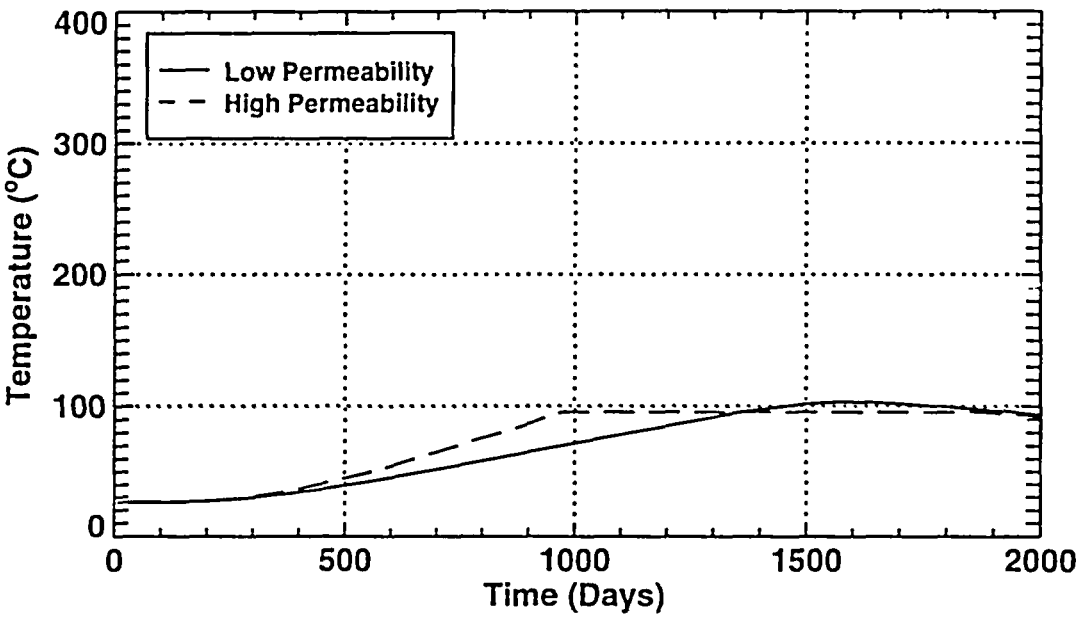

ESF-HD-MPBX-9 (Collar Location)
4 Year Heating, 2 Year Cooling

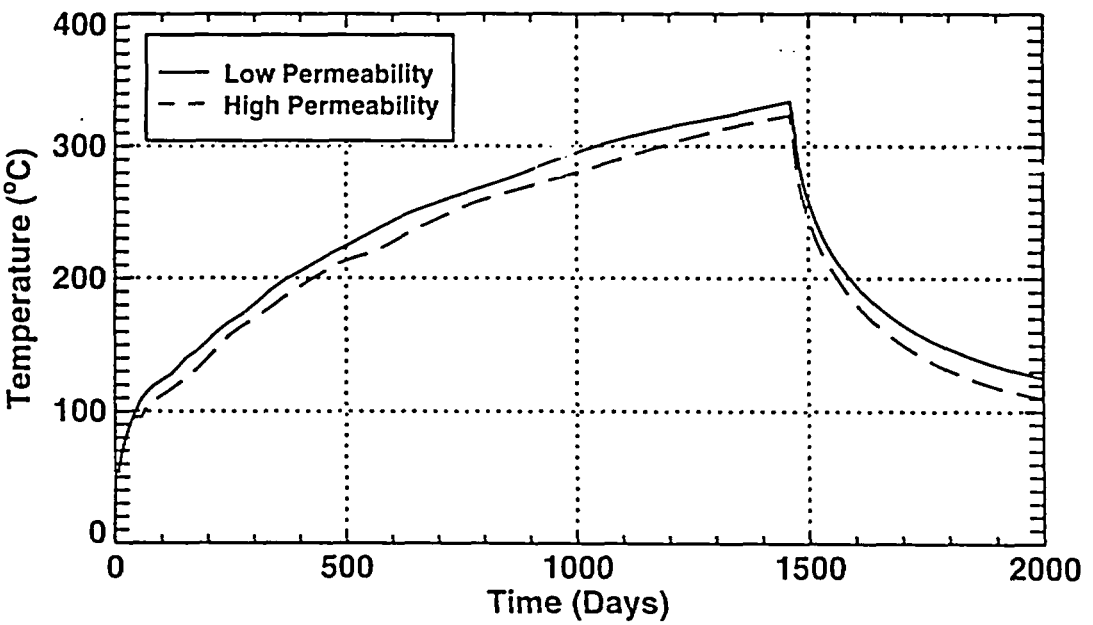

ESF-HD-MPBX-9 (Anchor 1)
4 Year Heating, 2 Year Cooling

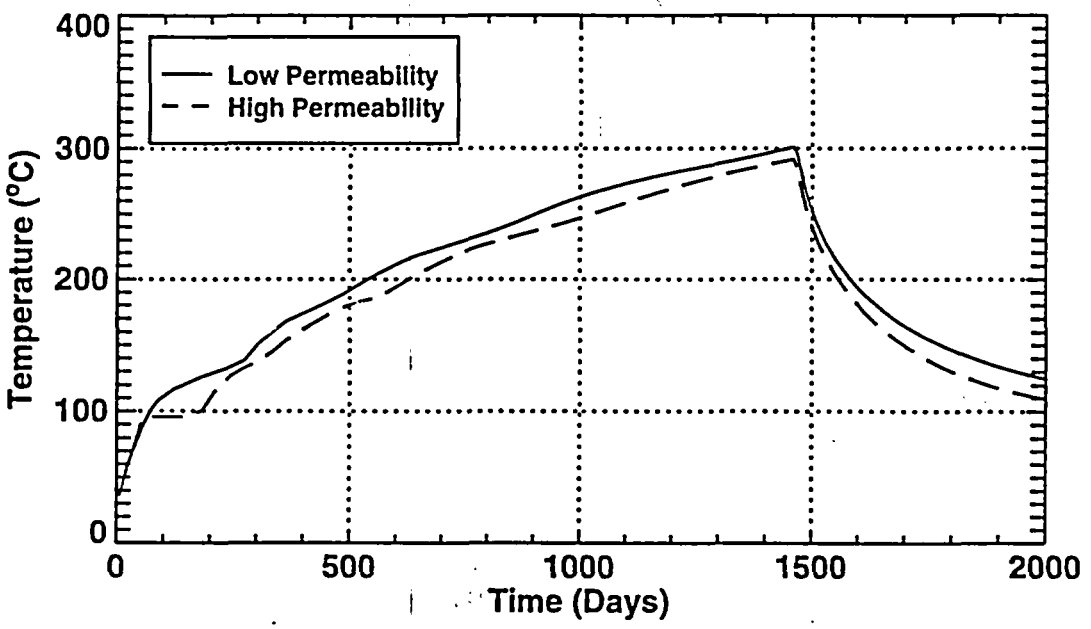

ESF-HD-MPBX-9 (Anchor 2)
4 Year Heating, 2 Year Cooling

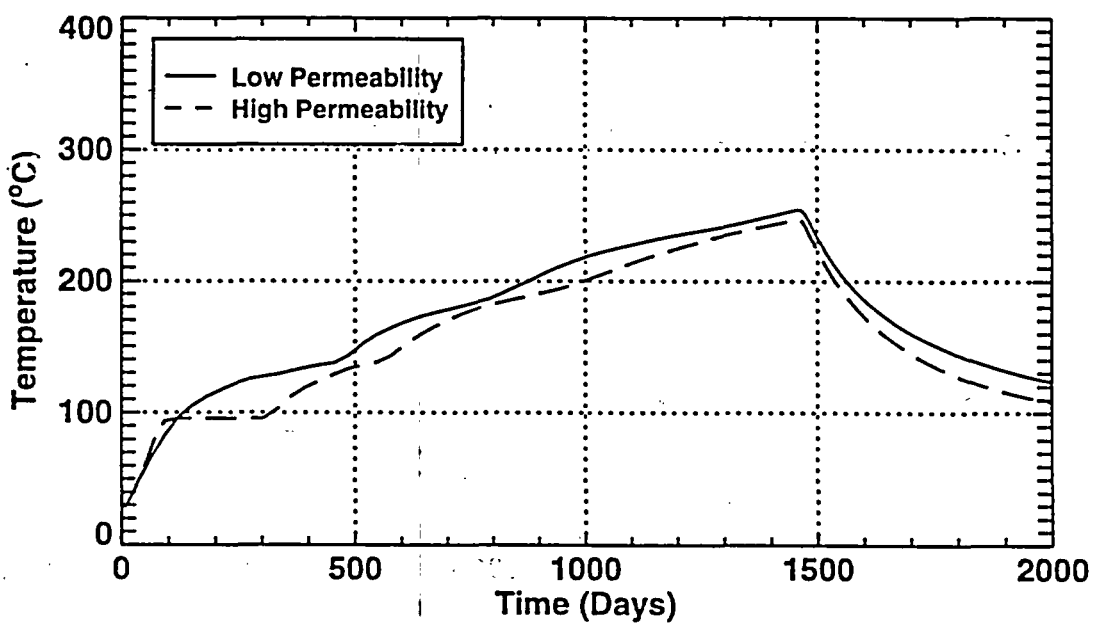

ESF-HD-MPBX-9 (Anchor 3)
4 Year Heating, 2 Year Cooling

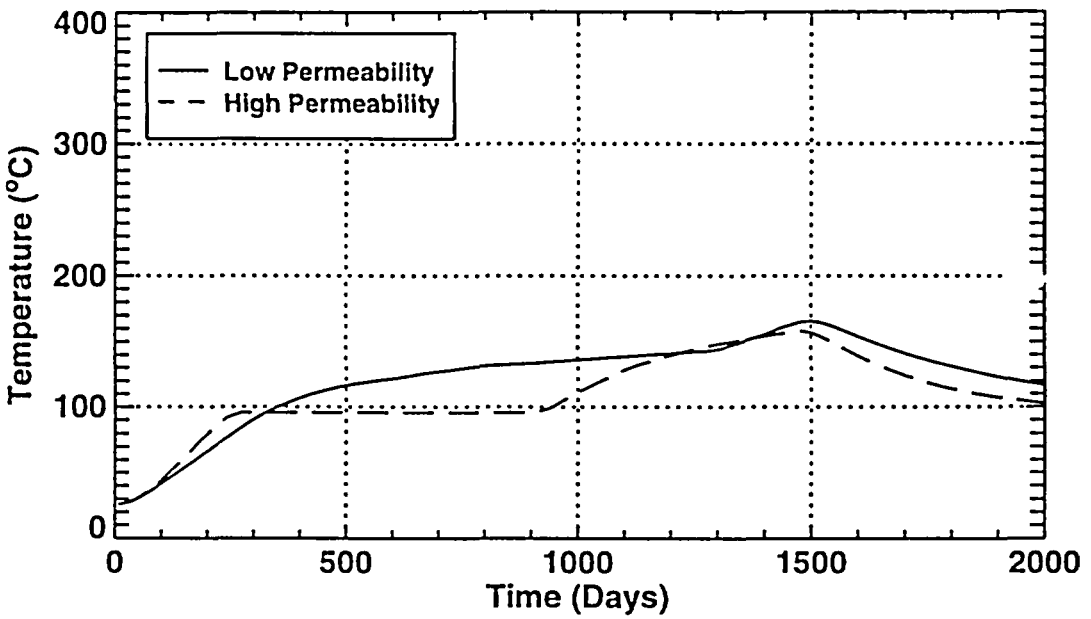

ESF-HD-MPBX-9 (Anchor 4)
4 Year Heating, 2 Year Cooling

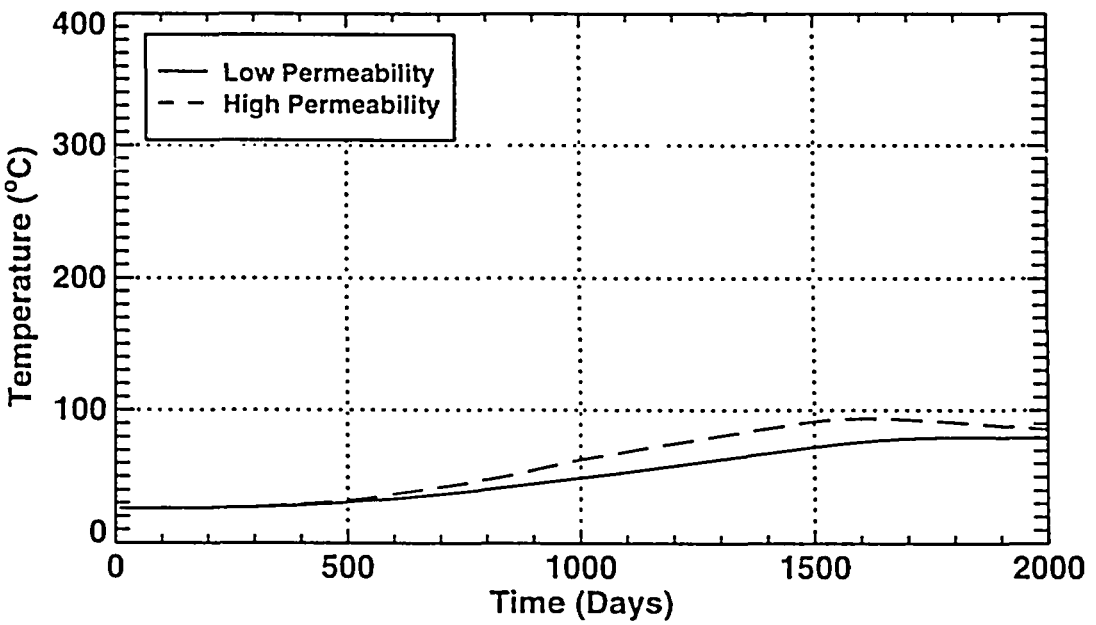

ESF-HD-MPBX-10 (Collar Location)
4 Year Heating, 2 Year Cooling

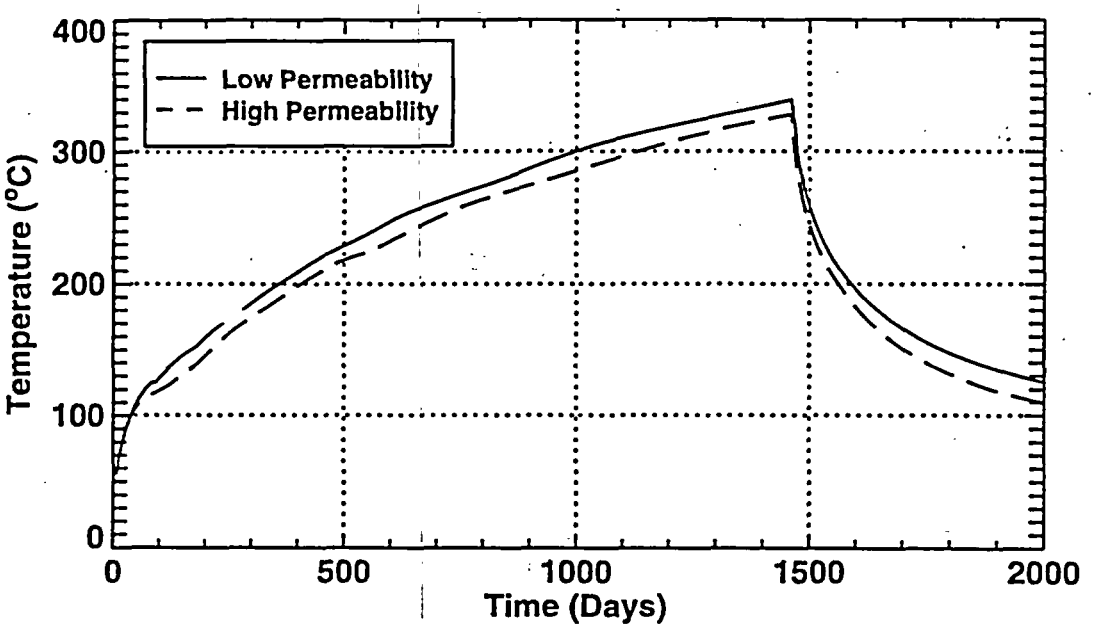

ESF-HD-MPBX-10 (Anchor 1)
4 Year Heating, 2 Year Cooling

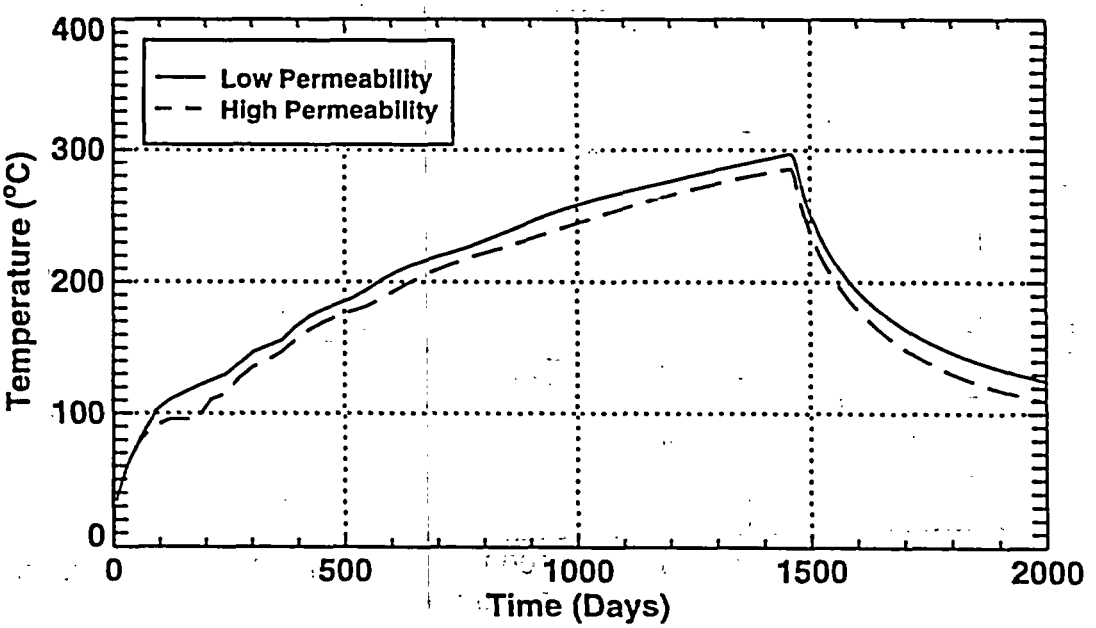

ESF-HD-MPBX-10 (Anchor 2)
4 Year Heating, 2 Year Cooling

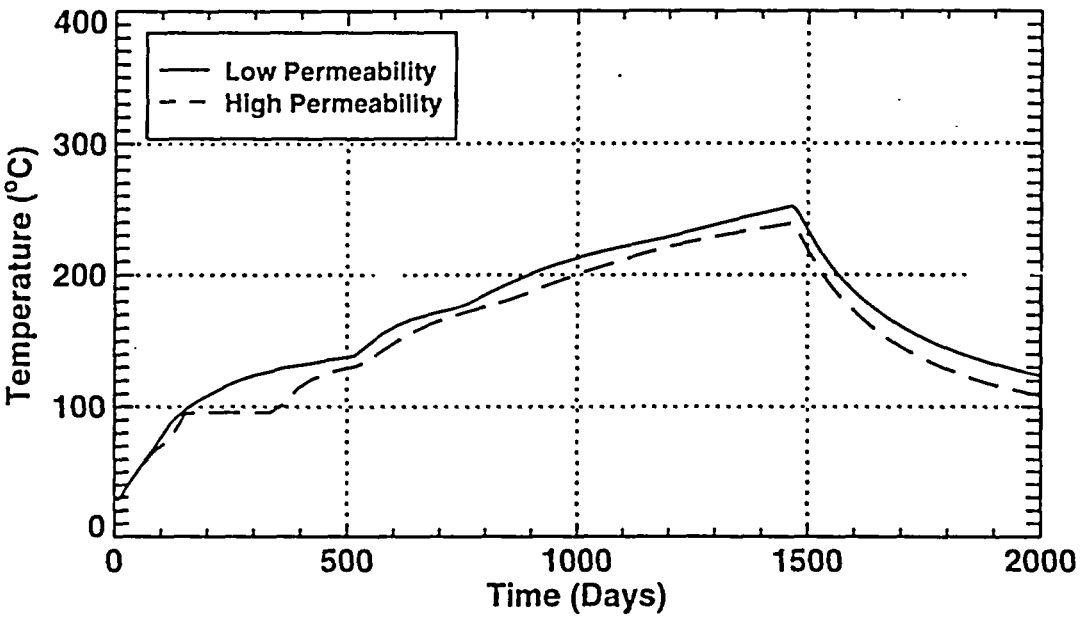

ESF-HD-MPBX-10 (Anchor 3)
4 Year Heating, 2 Year Cooling

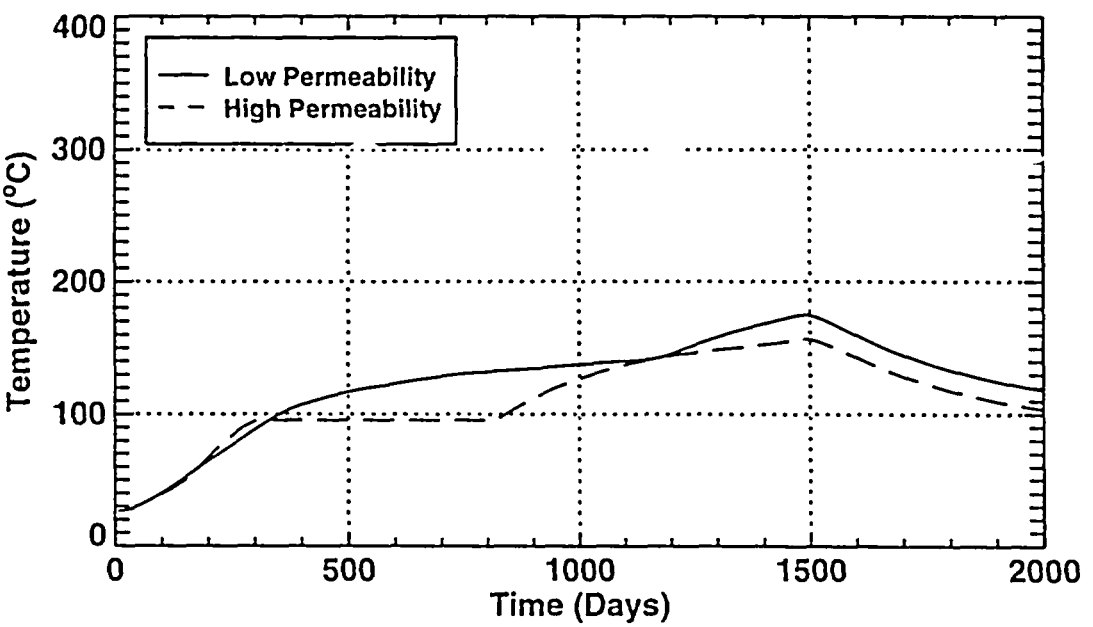

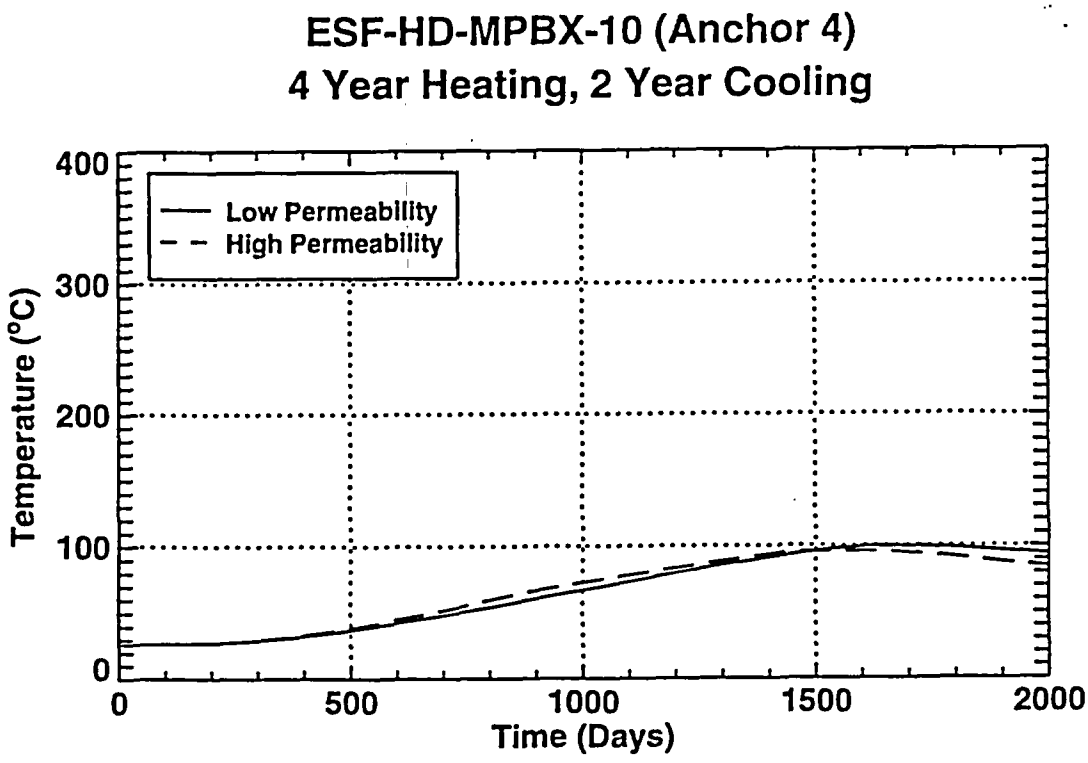
ESF-HD-MPBX-10 (Anchor 4)
4 Year Heating, 2 Year Cooling
Low Permeability
High Permeability
Temperature (°C)
400
300
200
100
0
0
500
1000
1500
2000
Time (Days)

Appendix B: Contour Plots of Predicted Temperatures and Liquid Saturations from the Thermal-Hydrologic Calculations

X-Z Cross Section Model
Low Bulk Perm., 2 Years Heating, 2 Years Cooling
Temperature

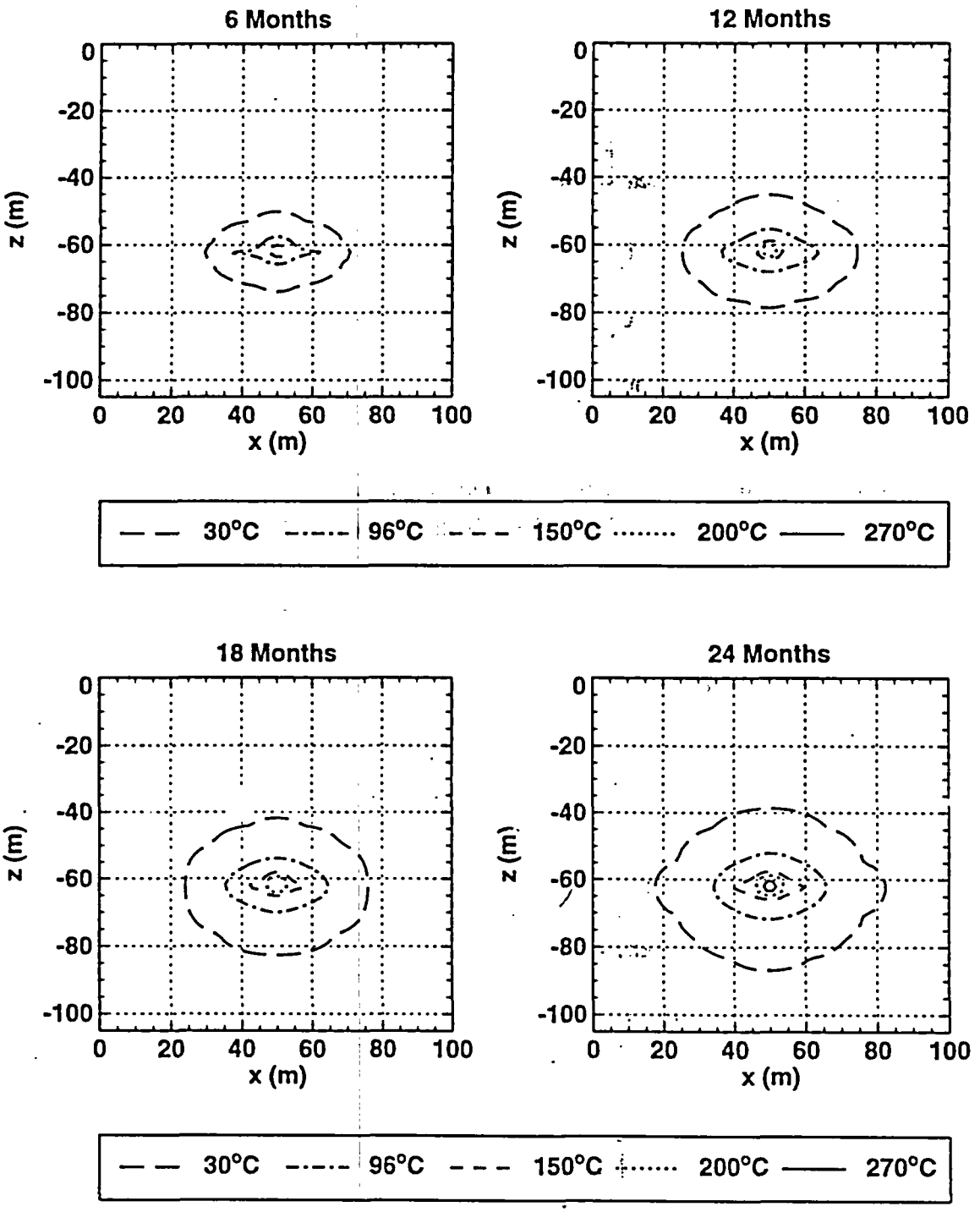

X-Z Cross Section Model
Low Bulk Perm., 2 Years Heating, 2 Years Cooling
Temperature

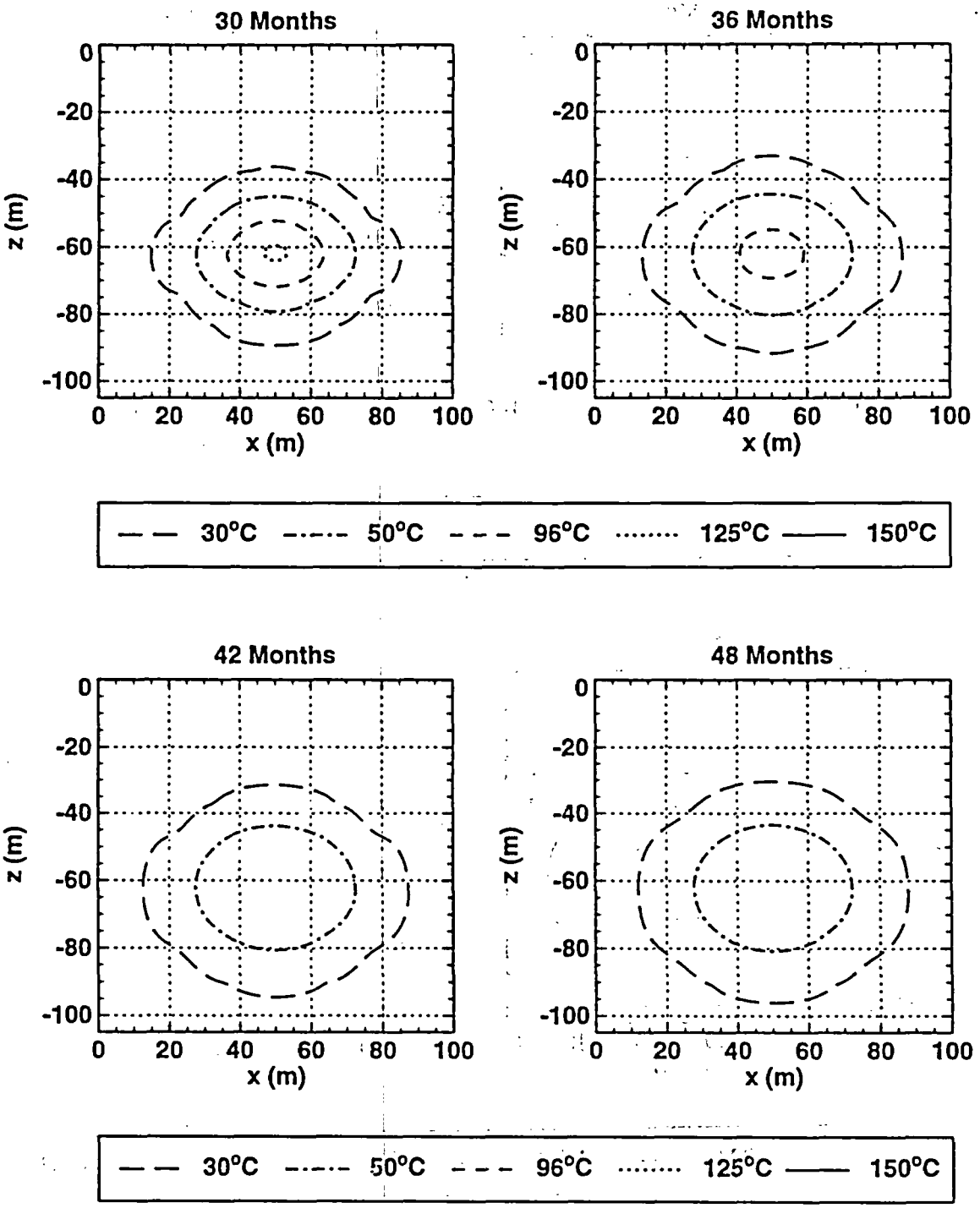

X-Z Cross Section Model
Low Bulk Perm., 3 Years Heating, 2 Years Cooling
Temperature

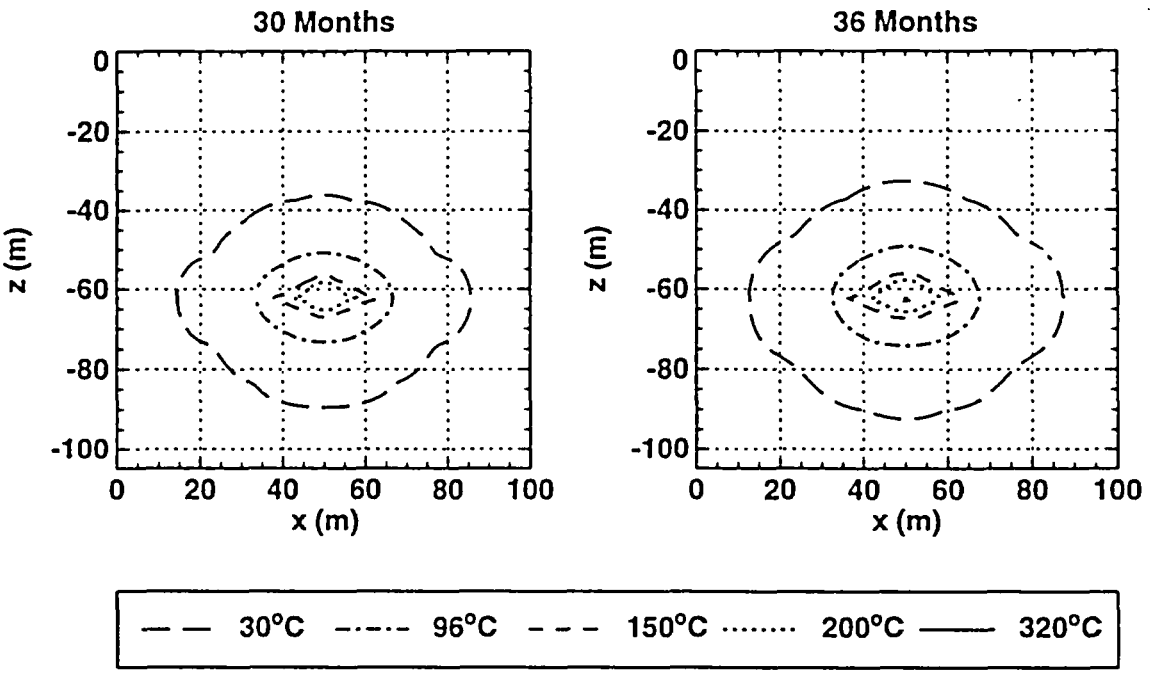

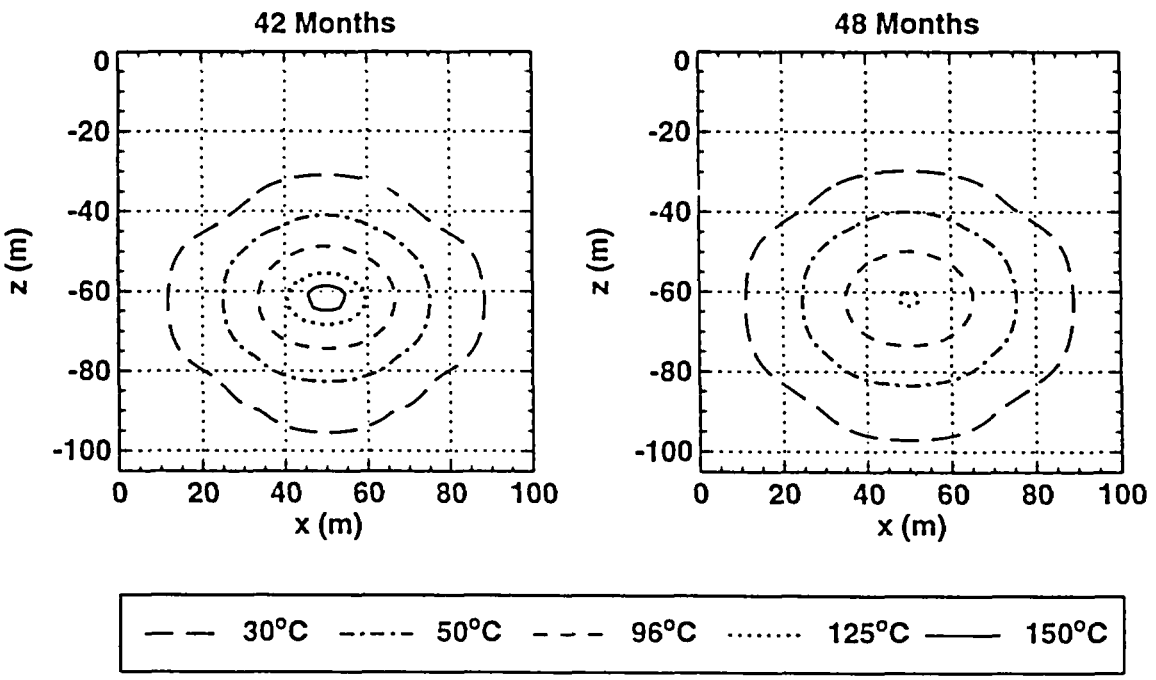

X-Z Cross Section Model
Low Bulk Perm., 3 Years Heating, 2 Years Cooling
Temperature

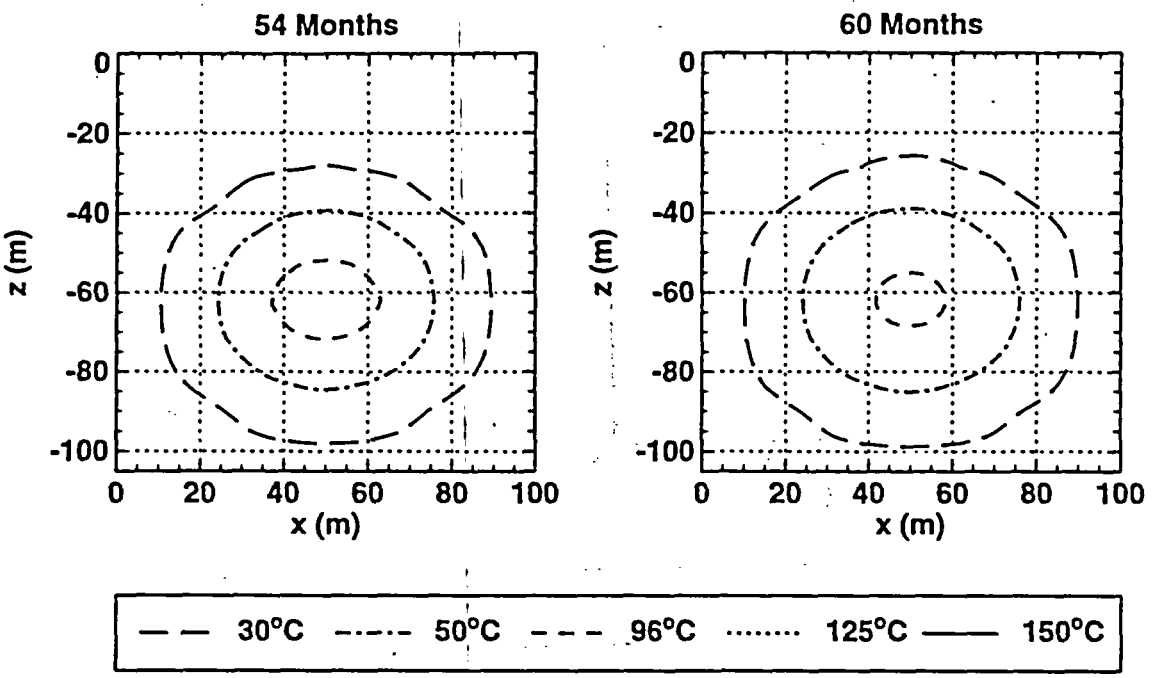

X-Z Cross Section Model
Low Bulk Perm., 4 Years Heating, 2 Years Cooling
Temperature

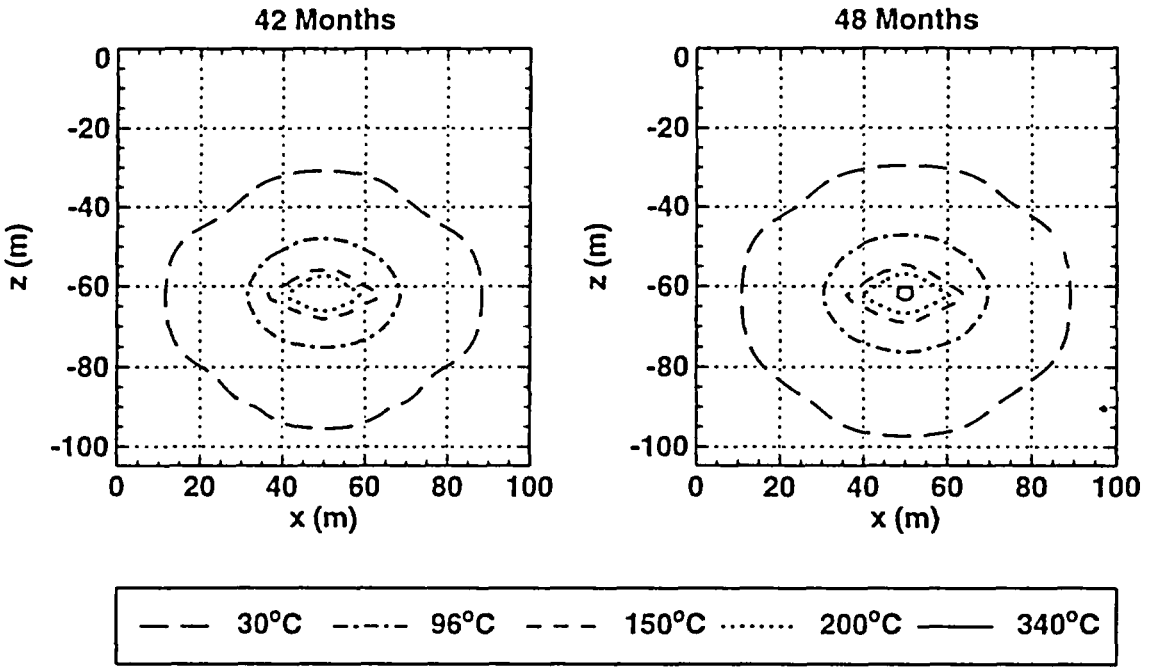

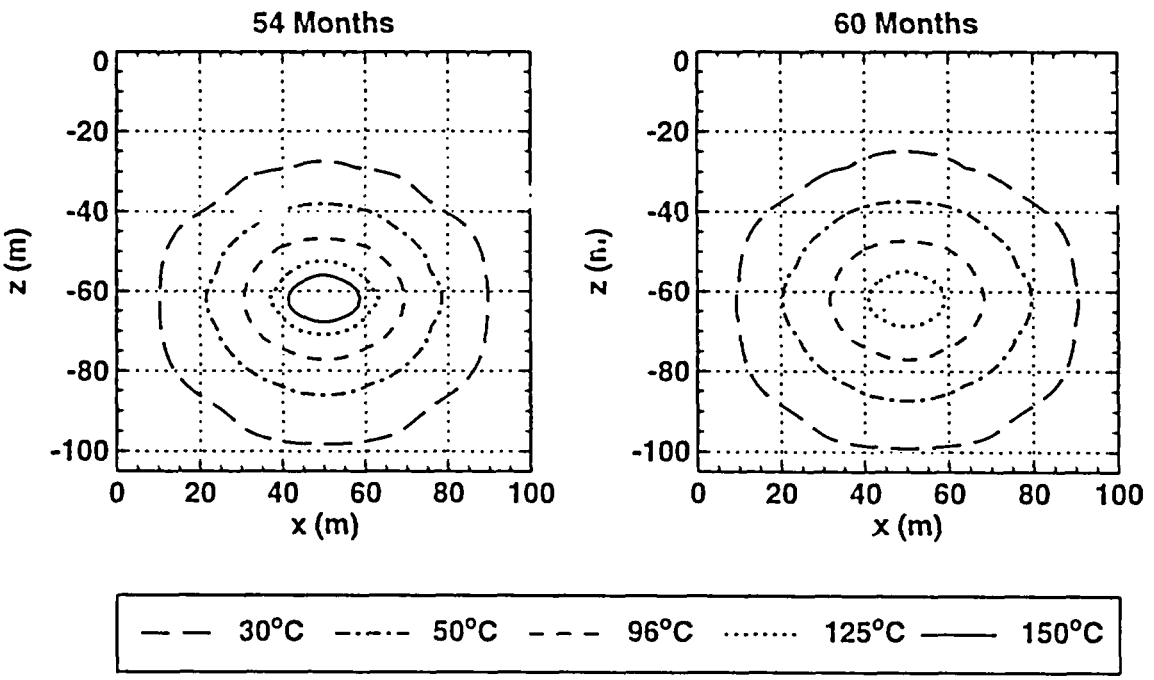

X-Z Cross Section Model
Low Bulk Perm., 4 Years Heating, 2 Years Cooling
Temperature

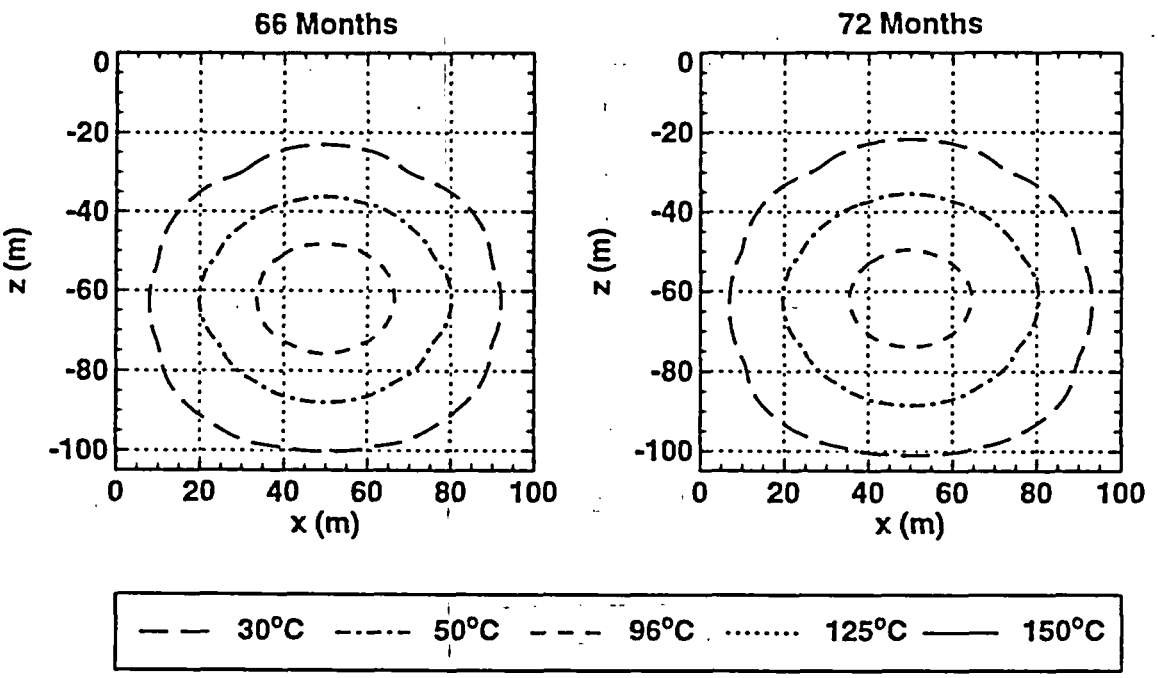

X-Z Cross Section Model
High Bulk Perm., 4 Years Heating, 2 Years Cooling
Temperature

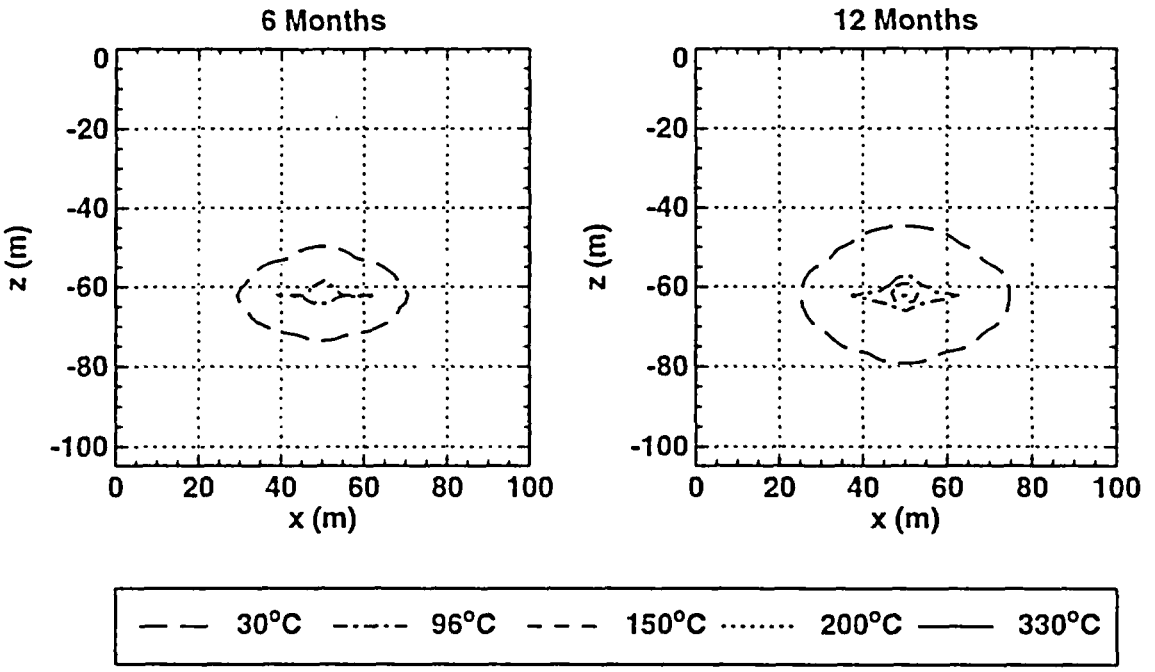

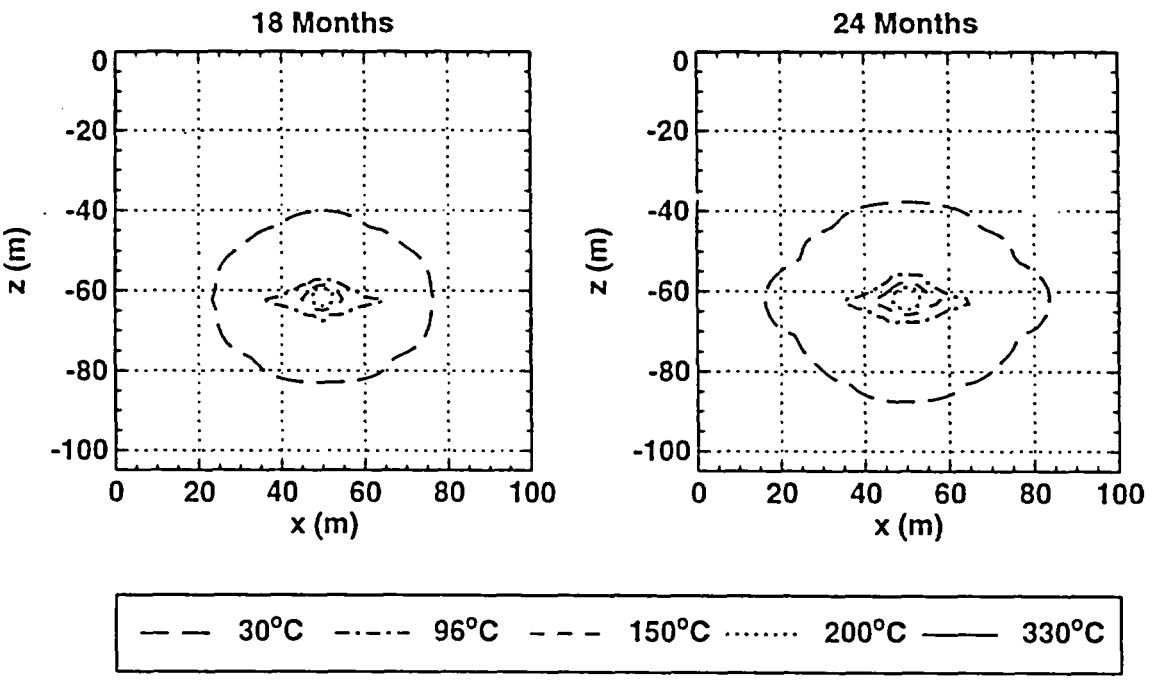

X-Z Cross Section Model
High Bulk Perm., 4 Years Heating, 2 Years Cooling
Temperature

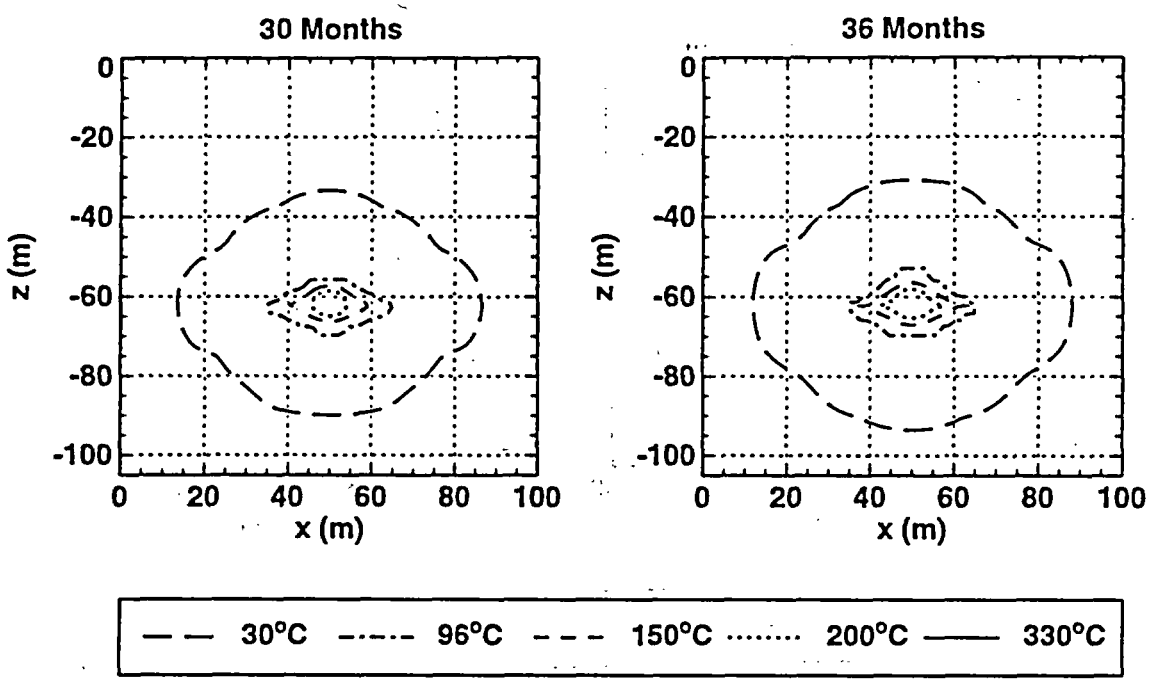

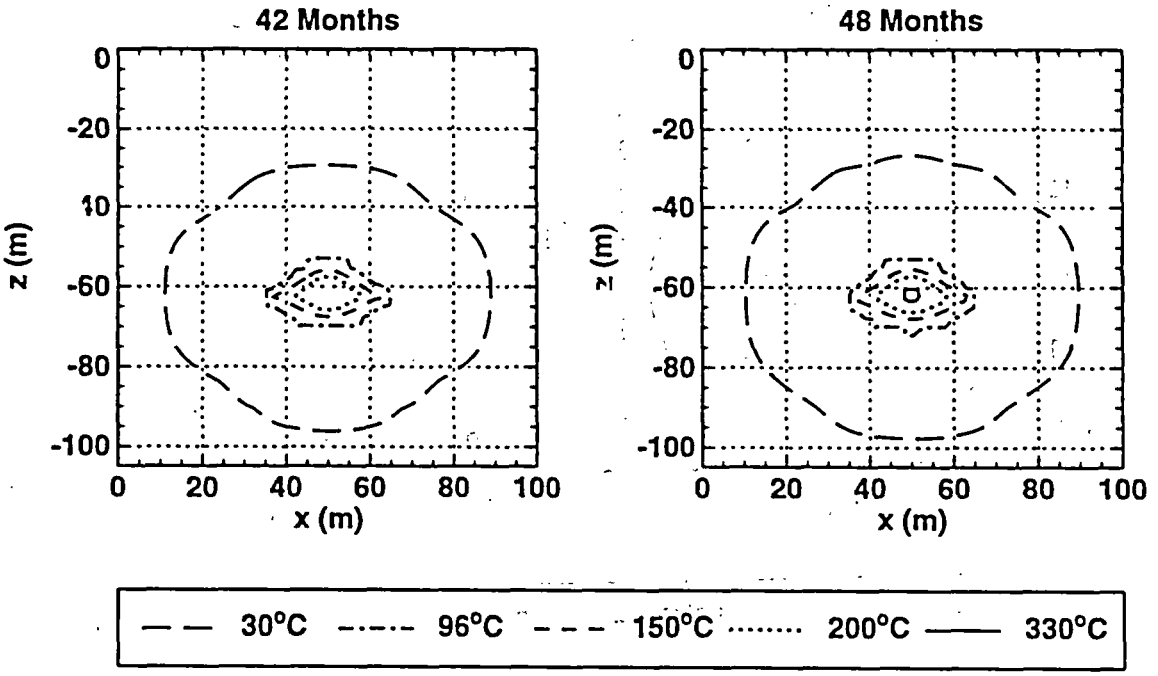

X-Z Cross Section Model
High Bulk Perm., 4 Years Heating, 2 Years Cooling
Temperature

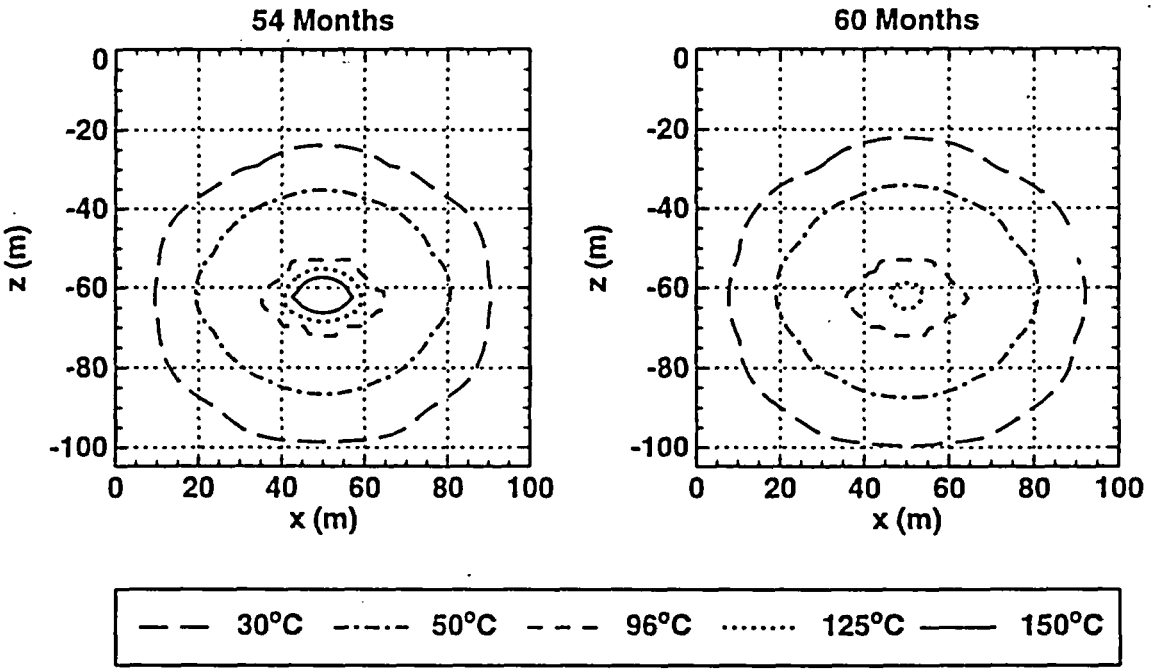

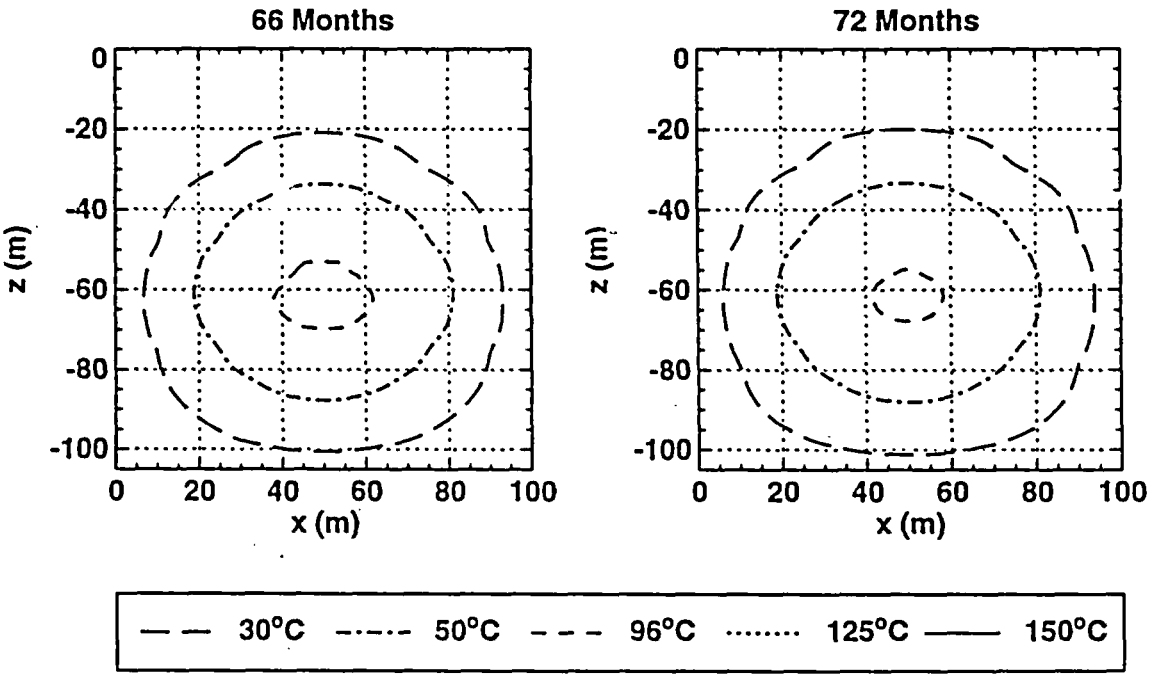

X-Z Cross Section Model
Low Bulk Perm., 2 Years Heating, 2 Years Cooling
Liquid Saturation

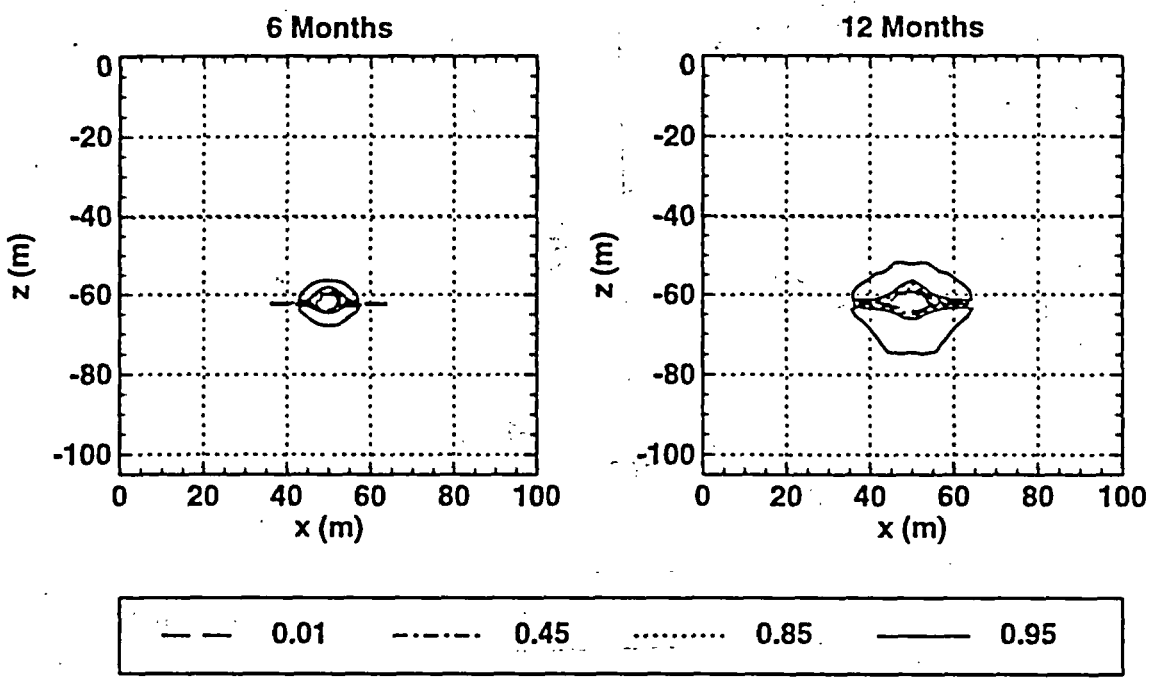

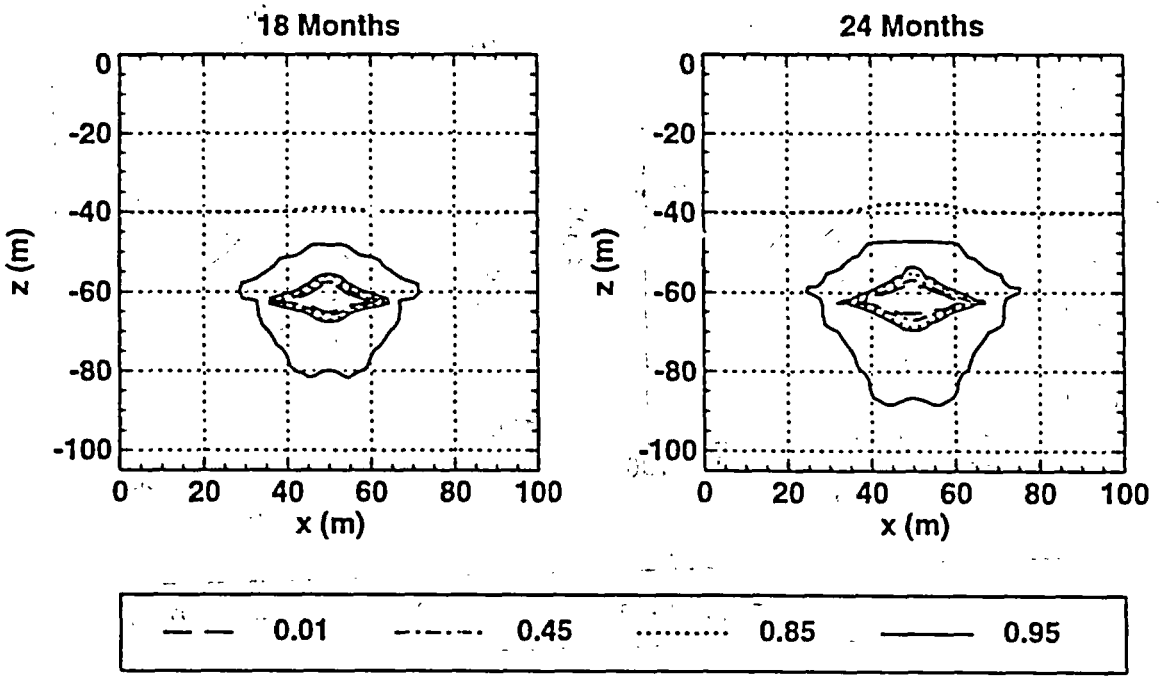

X-Z Cross Section Model
Low Bulk Perm., 2 Years Heating, 2 Years Cooling
Liquid Saturation

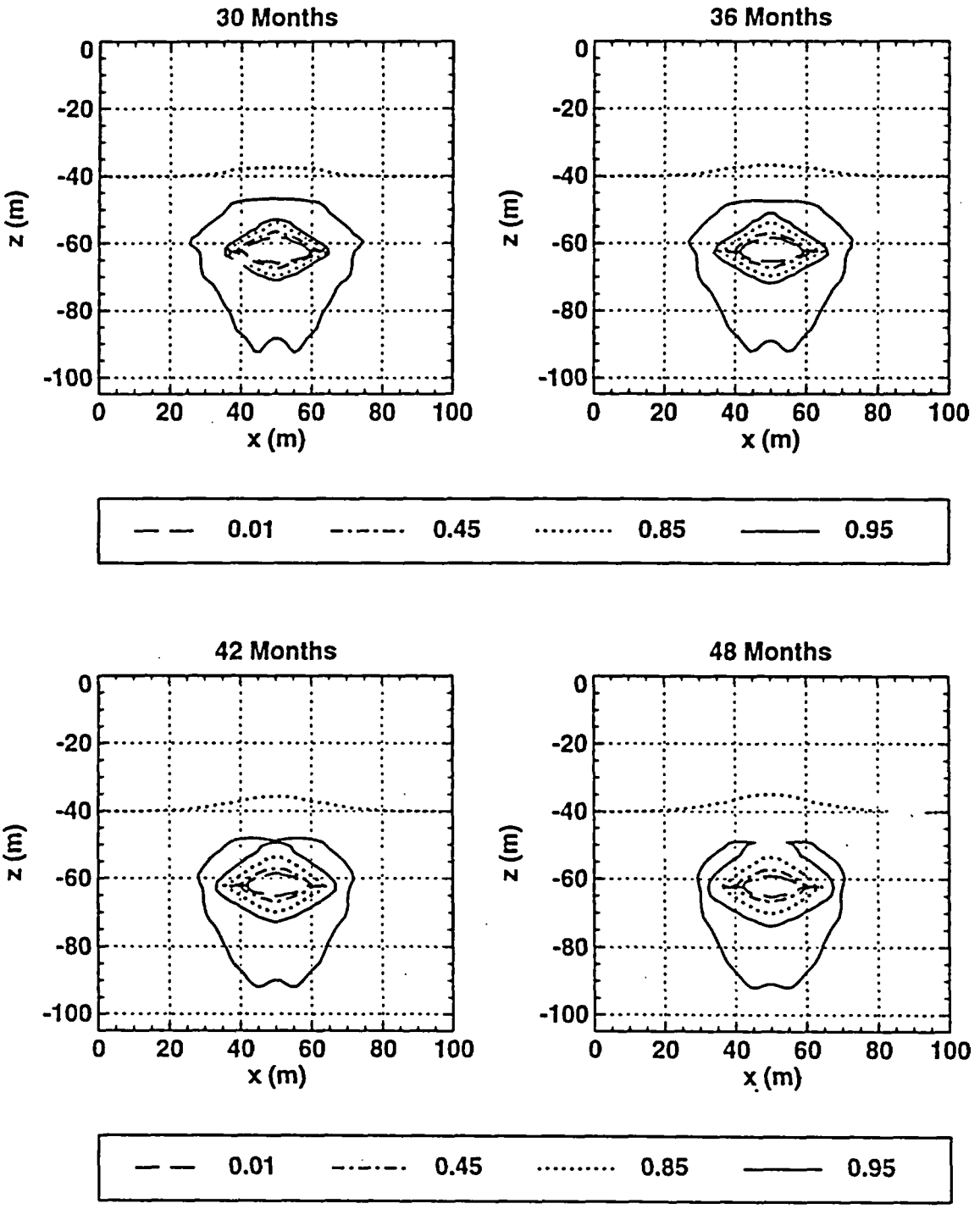

X-Z Cross Section Model
Low Bulk Perm., 3 Years Heating, 2 Years Cooling
Liquid Saturation

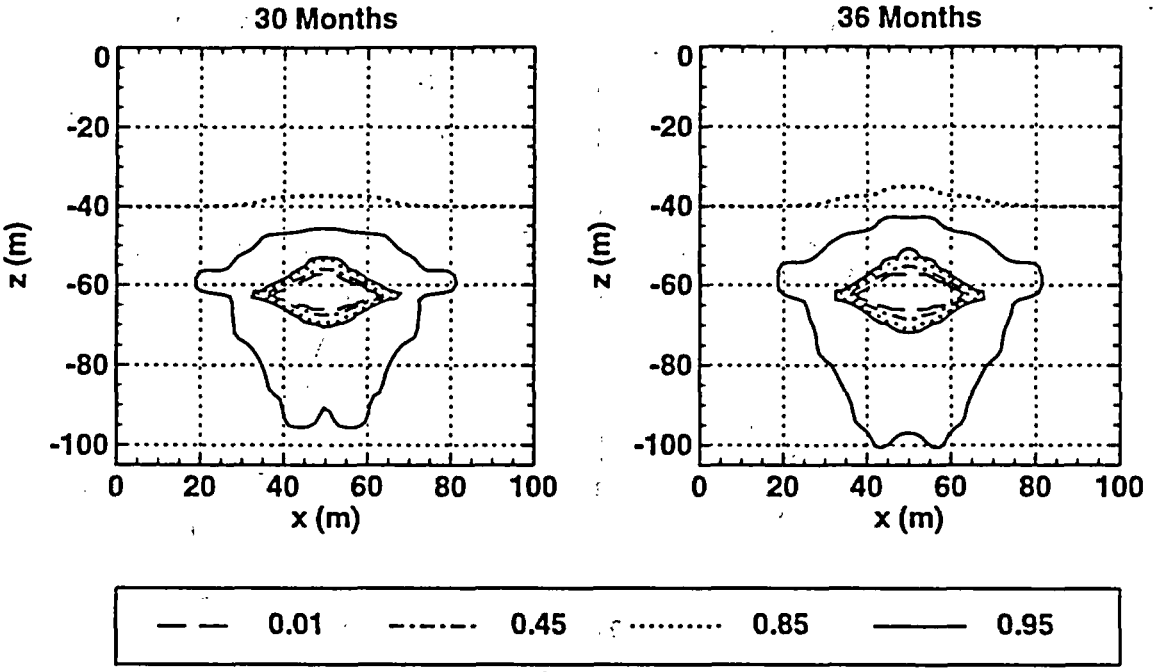

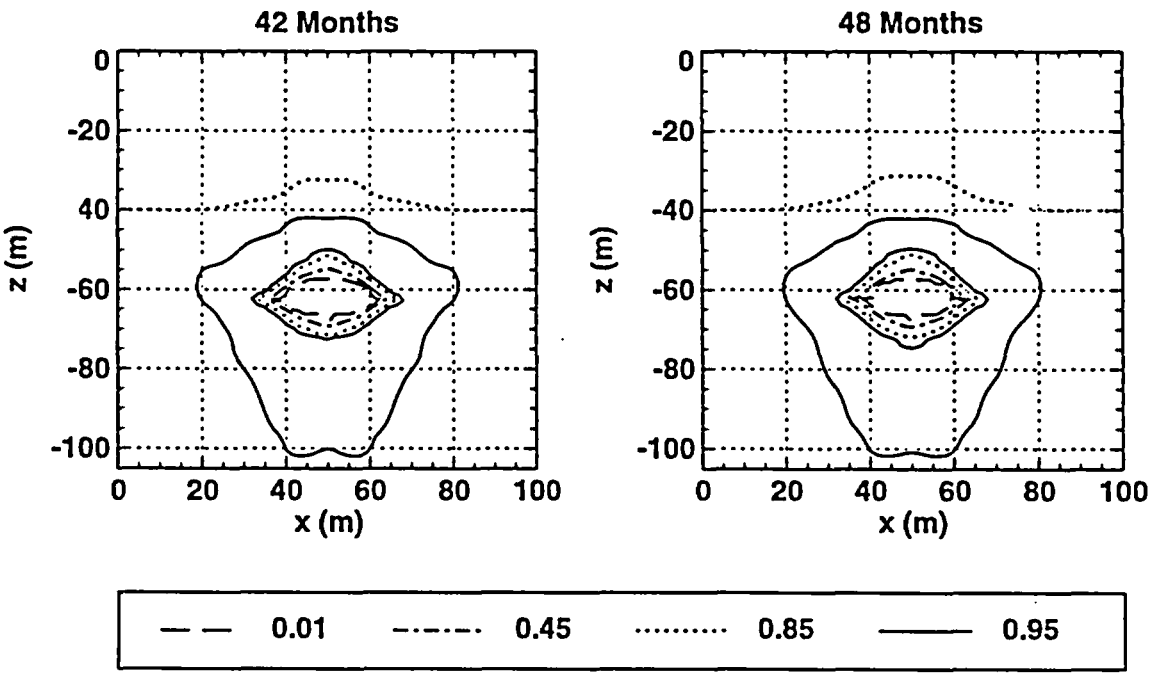

X-Z Cross Section Model
Low Bulk Perm., 3 Years Heating, 2 Years Cooling
Liquid Saturation

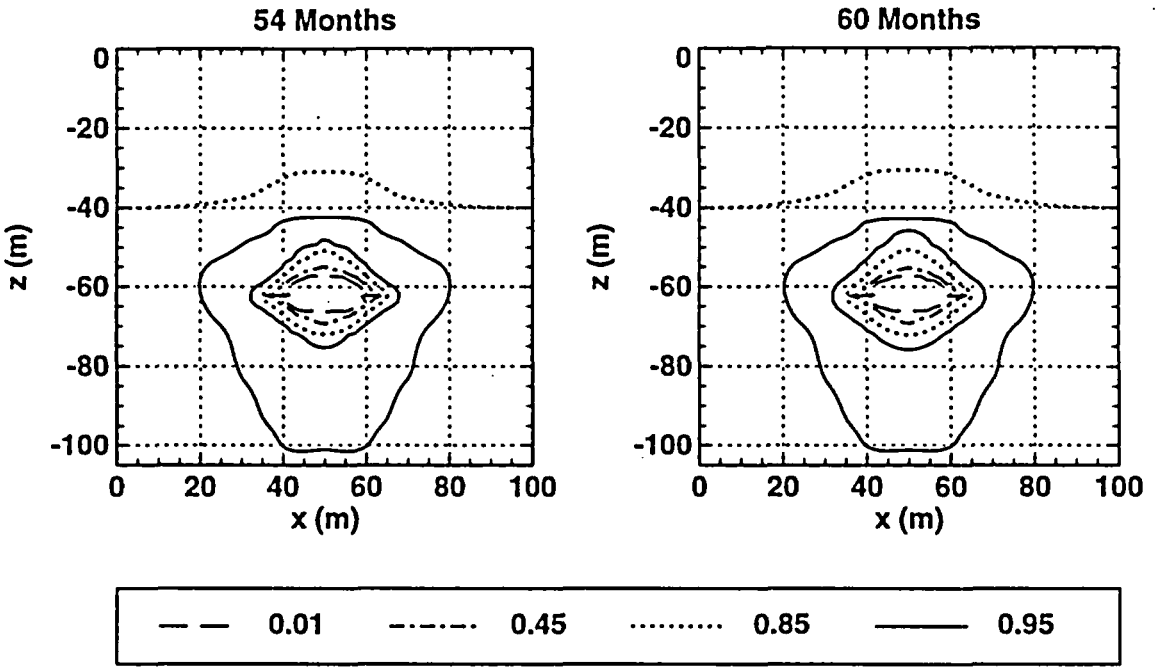

X-Z Cross Section Model
Low Bulk Perm., 4 Years Heating, 2 Years Cooling
Liquid Saturation

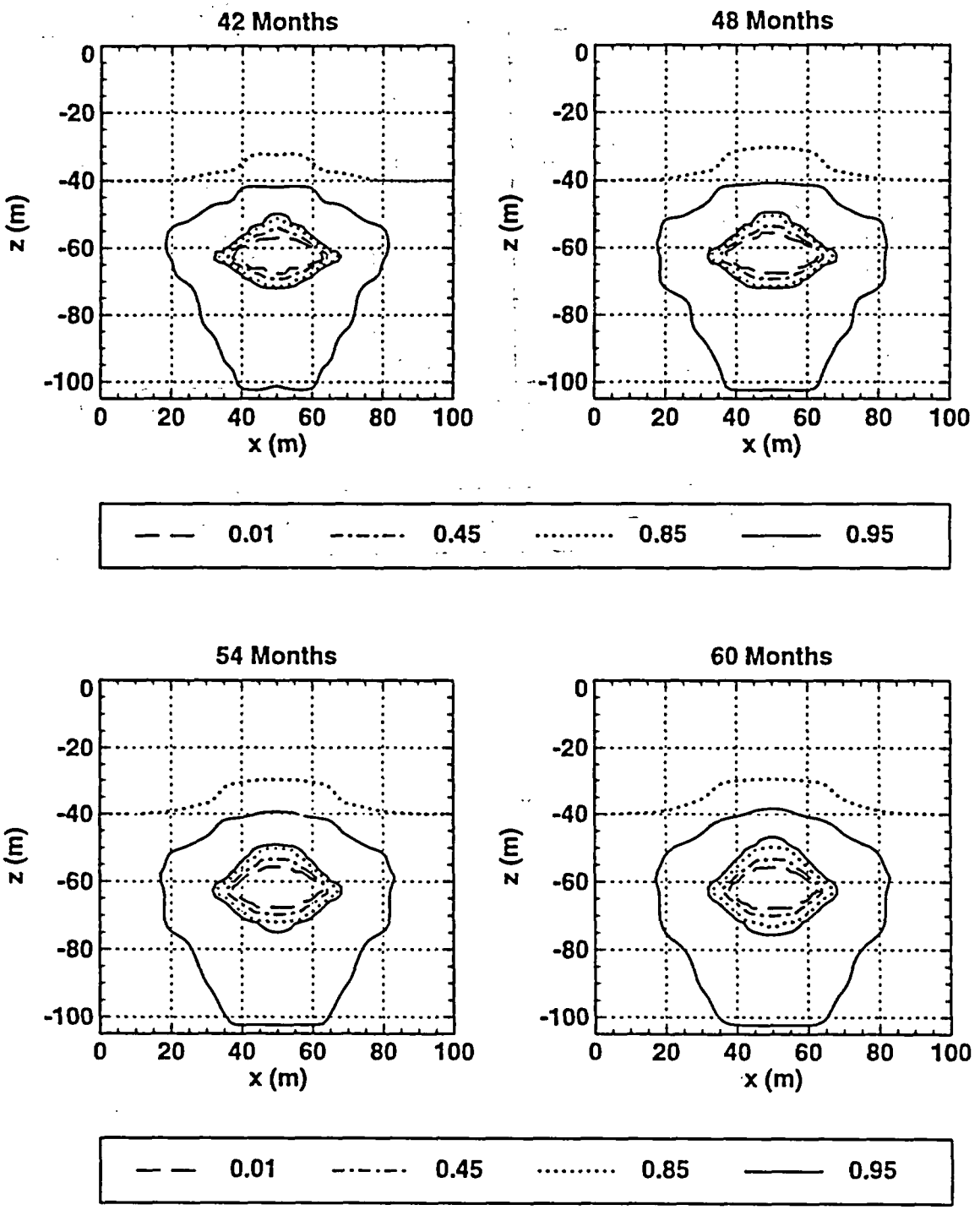

X-Z Cross Section Model
Low Bulk Perm., 4 Years Heating, 2 Years Cooling
Liquid Saturation

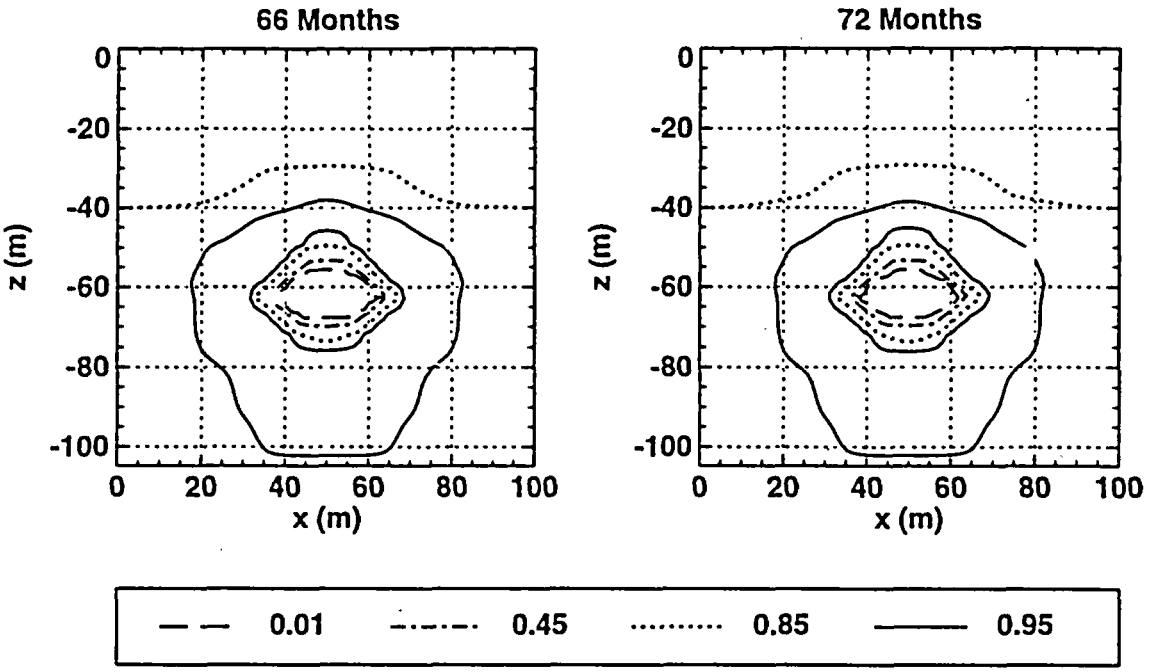

X-Z Cross Section Model
High Bulk Perm., 4 Years Heating, 2 Years Cooling
Liquid Saturation

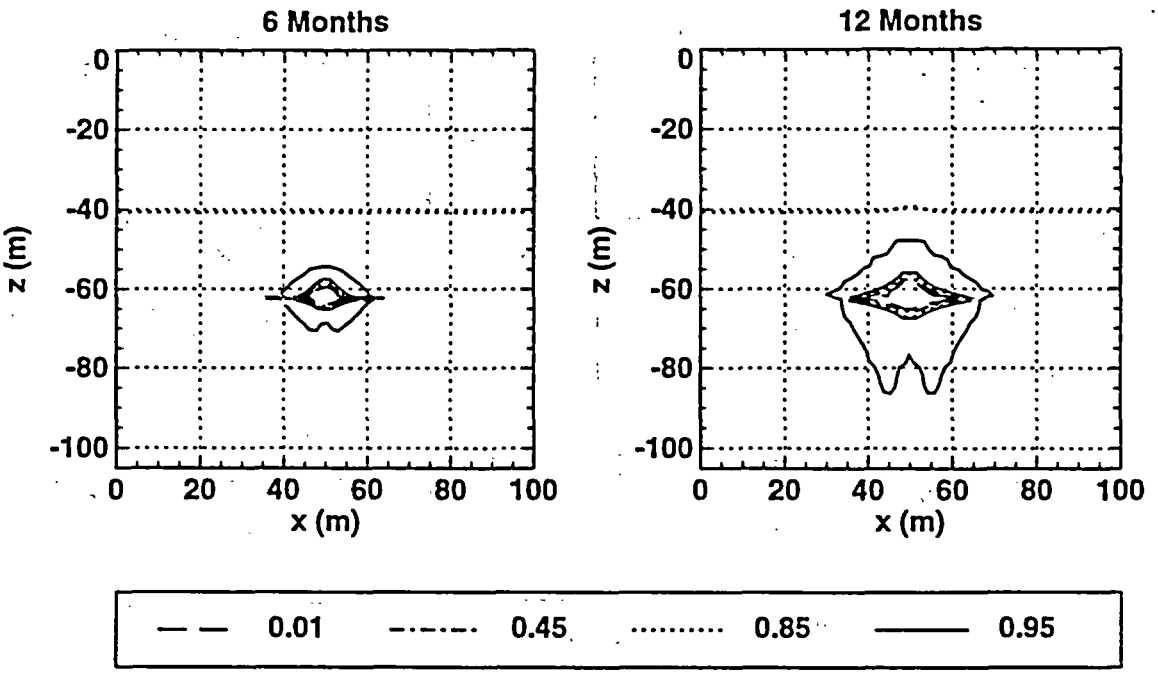

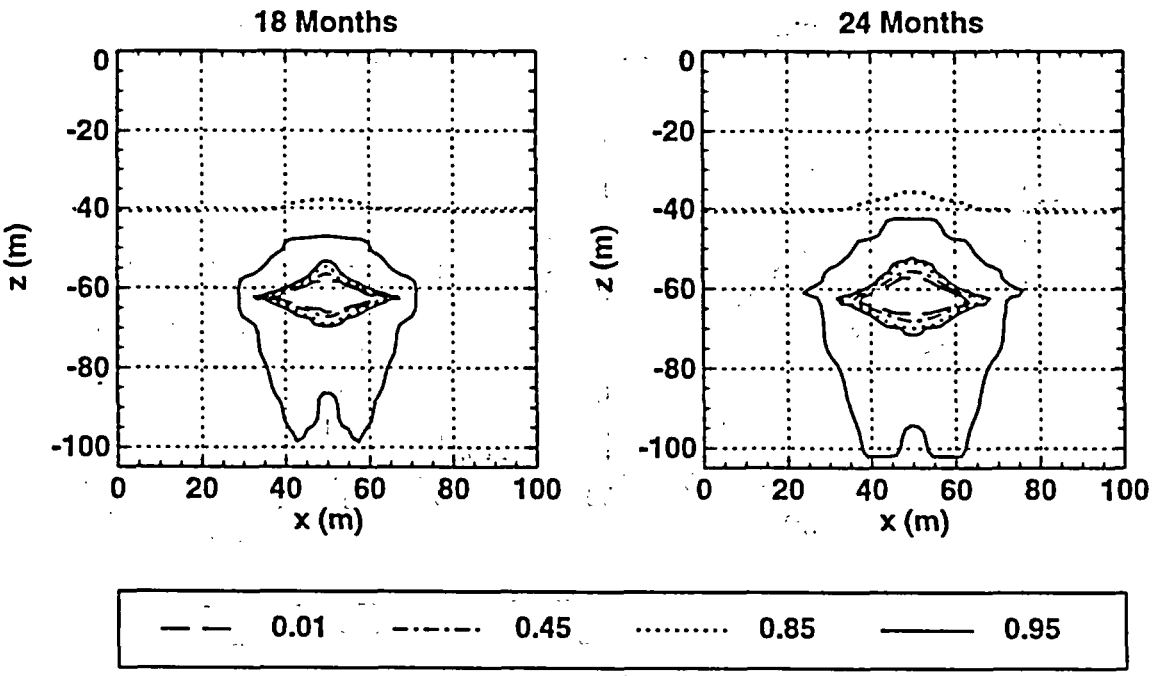

X-Z Cross Section Model
High Bulk Perm., 4 Years Heating, 2 Years Cooling
Liquid Saturation

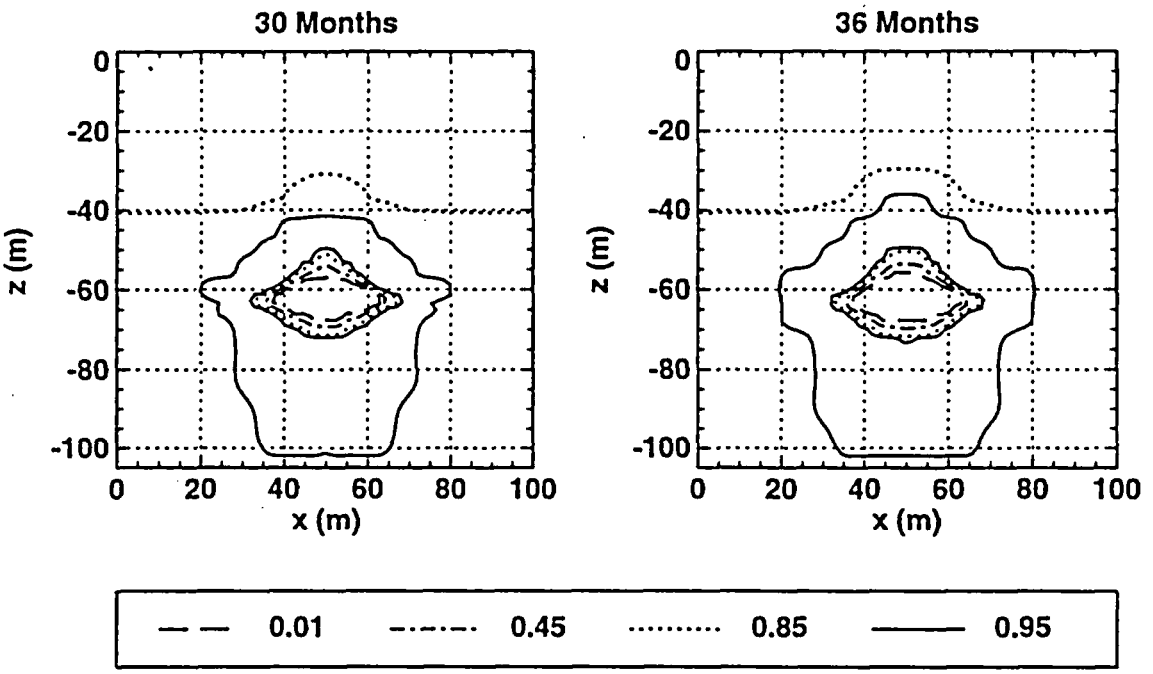

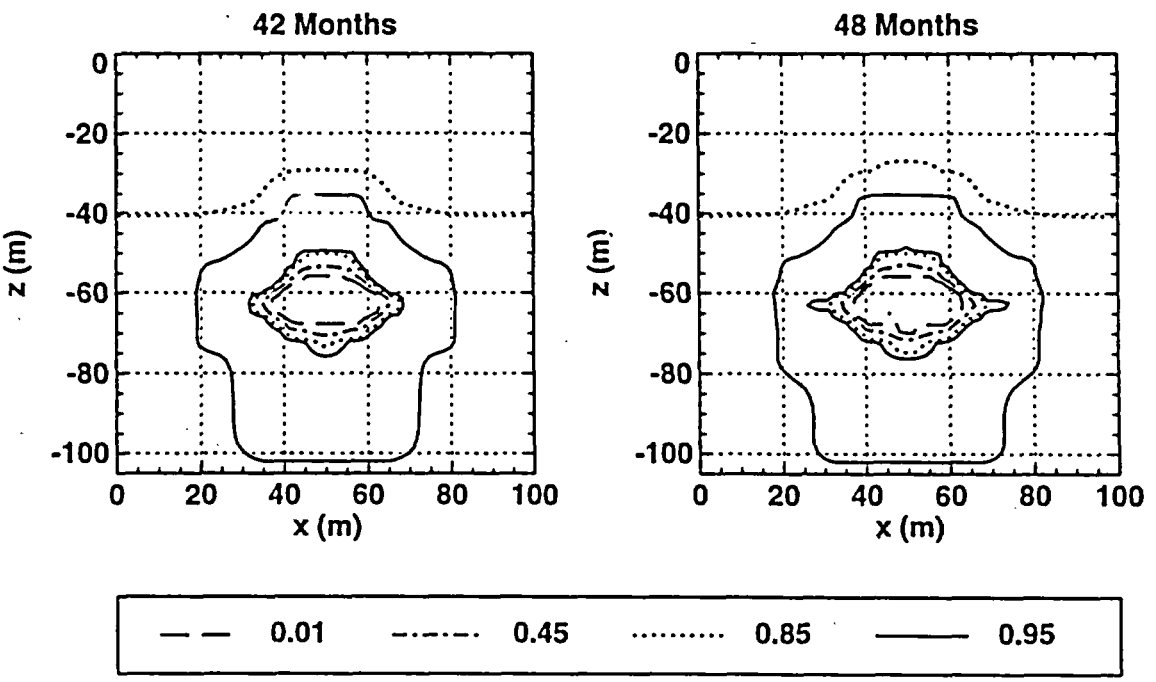

X-Z Cross Section Model
High Bulk Perm., 4 Years Heating, 2 Years Cooling
Liquid Saturation

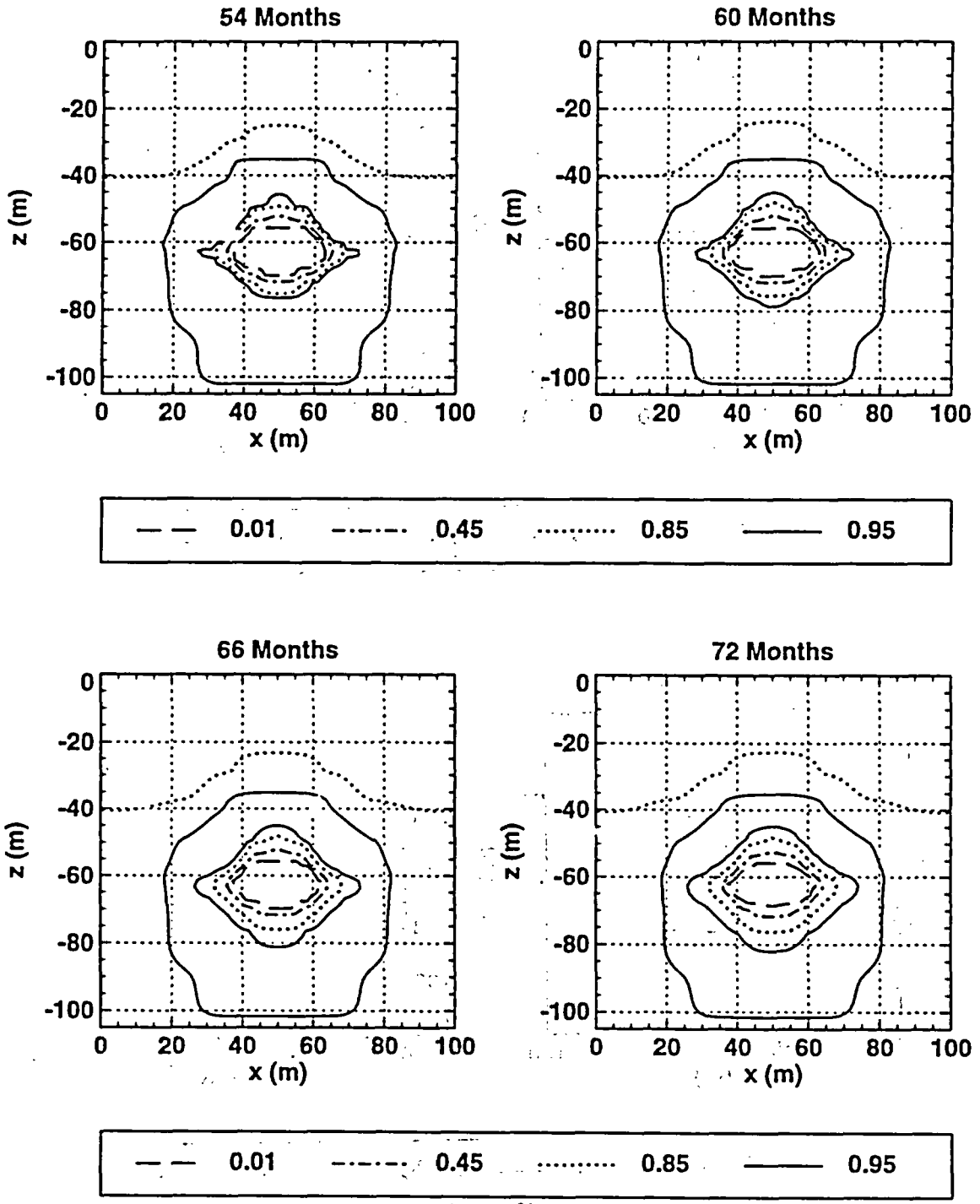

Y-Z Longitudinal Model
Low Bulk Perm., 2 Year Heating, 2 Year Cooling
Temperature

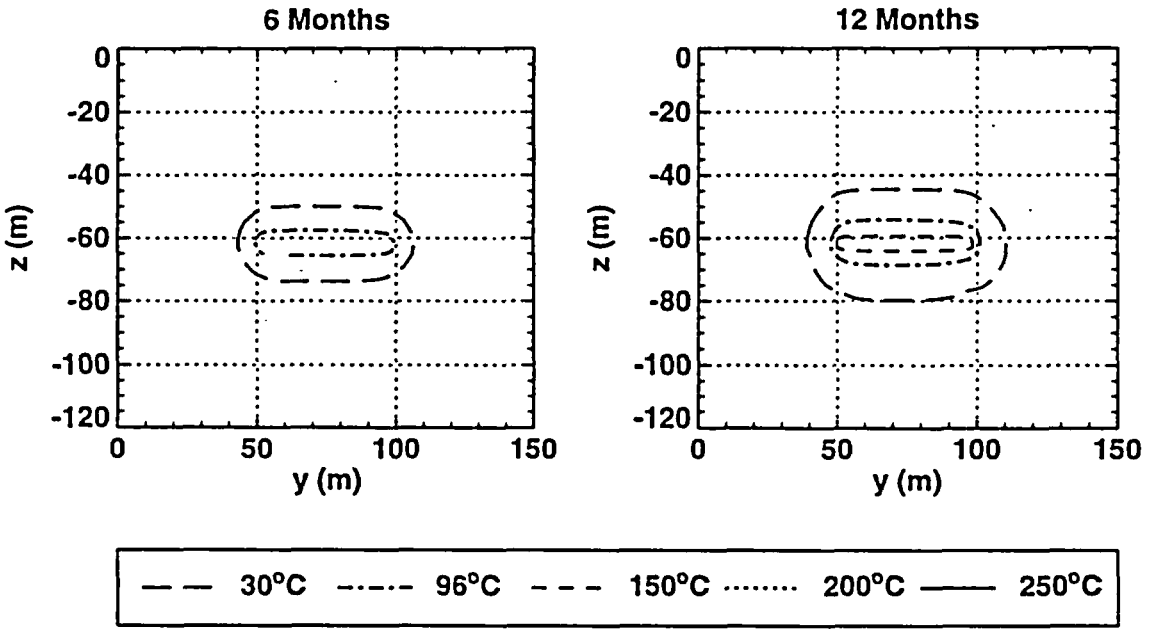

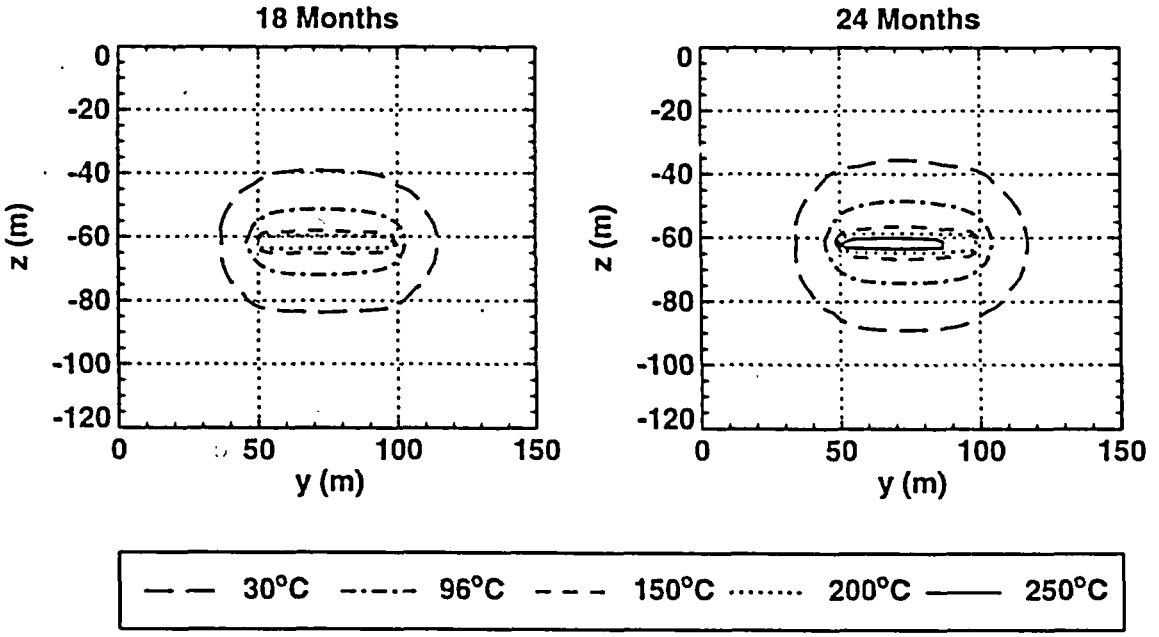

Y-Z Longitudinal Model
Low Bulk Perm., 2 Year Heating, 2 Year Cooling
Temperature

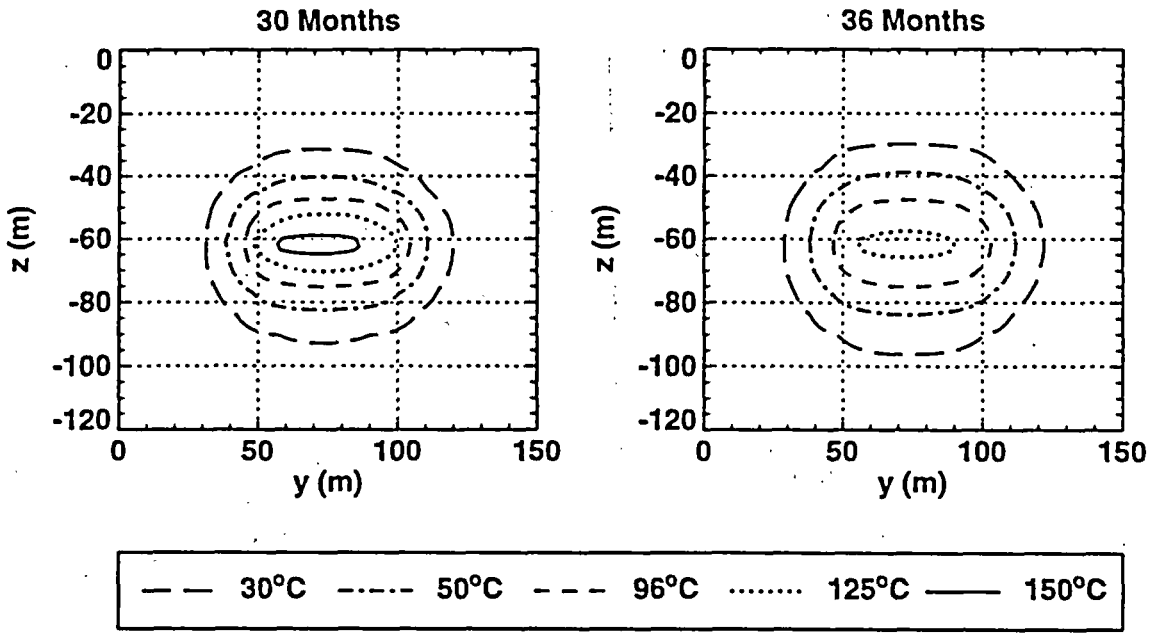

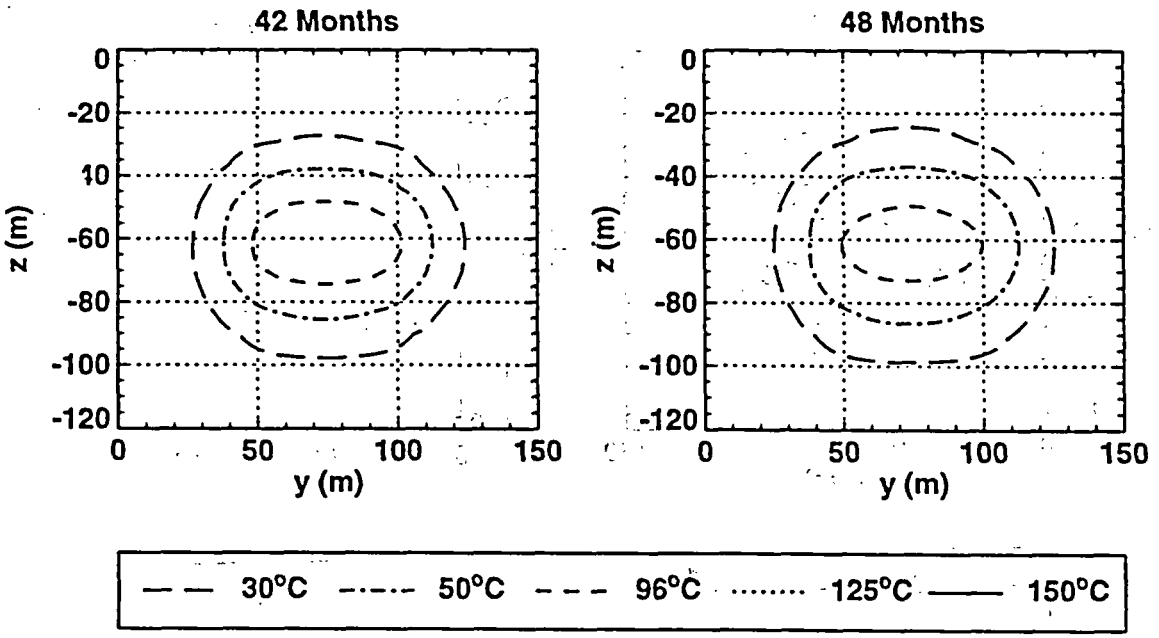

Y-Z Longitudinal Model
Low Bulk Perm., 3 Year Heating, 2 Year Cooling
Temperature

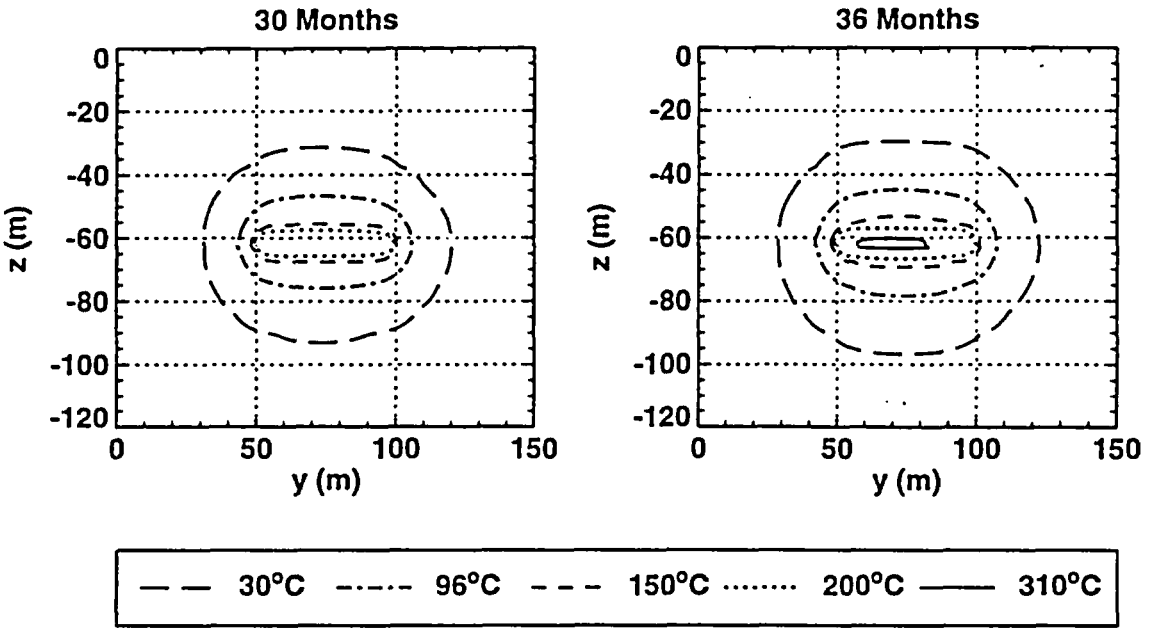

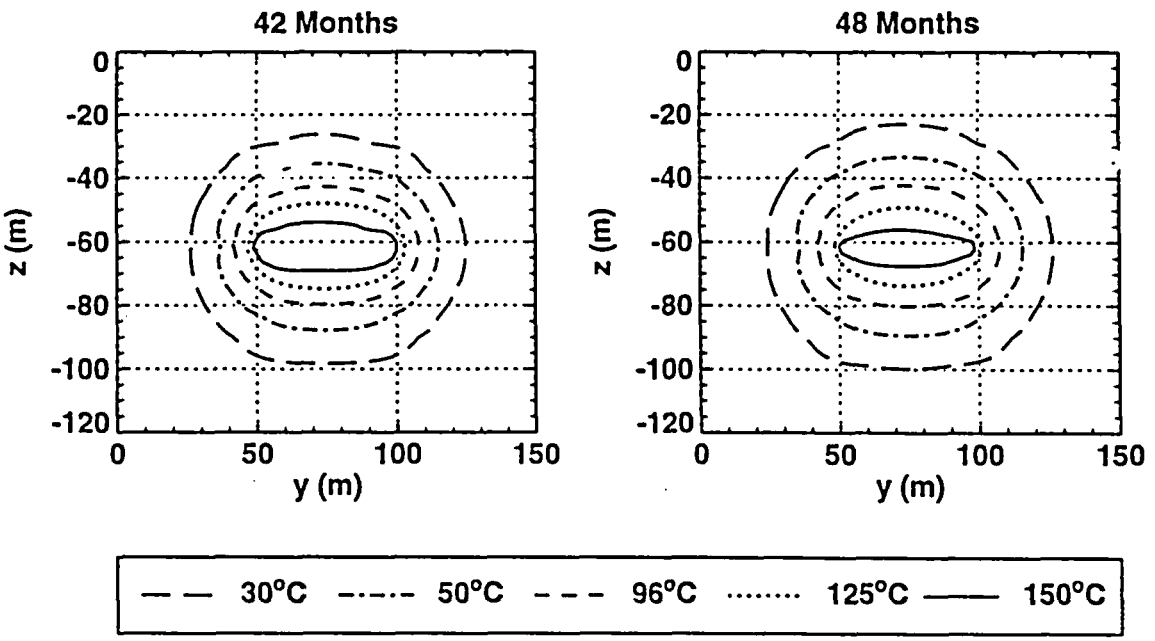

Y-Z Longitudinal Model
Low Bulk Perm., 3 Year Heating, 2 Year Cooling
Temperature

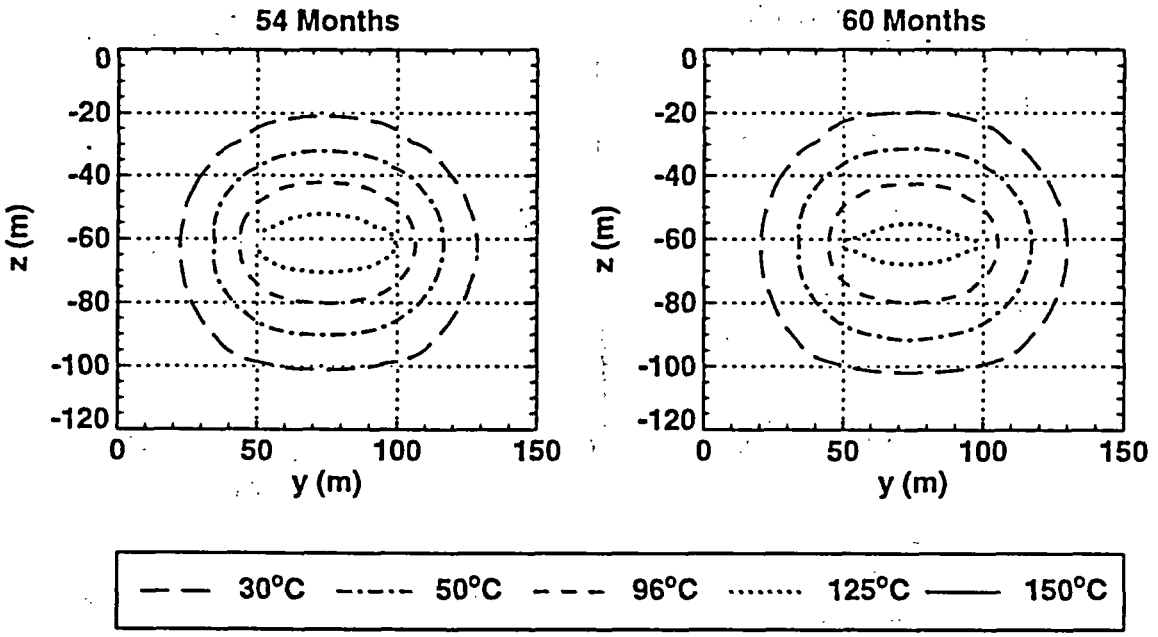

Y-Z Longitudinal Model
Low Bulk Perm., 4 Year Heating, 2 Year Cooling
Temperature

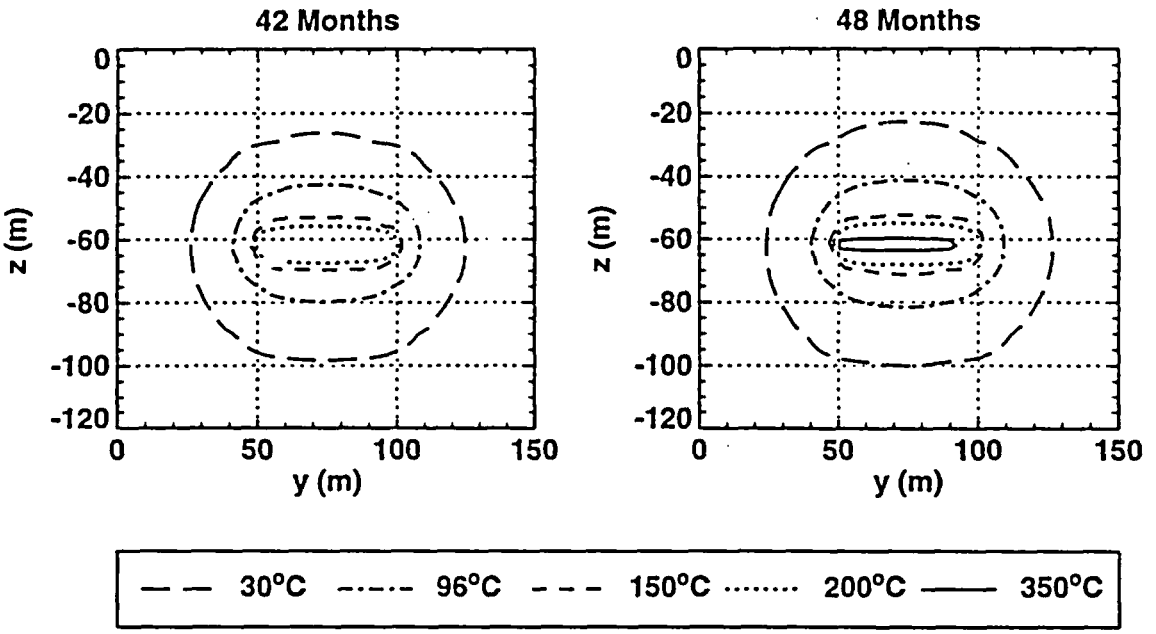

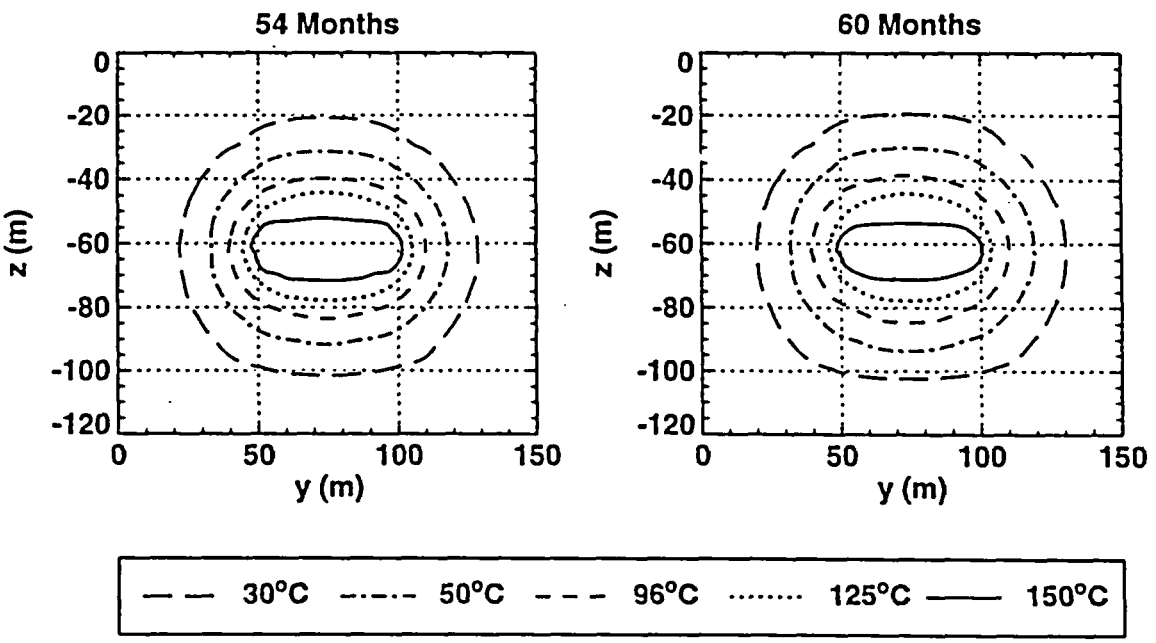

Y-Z Longitudinal Model
Low Bulk Perm., 4 Year Heating, 2 Year Cooling
Temperature

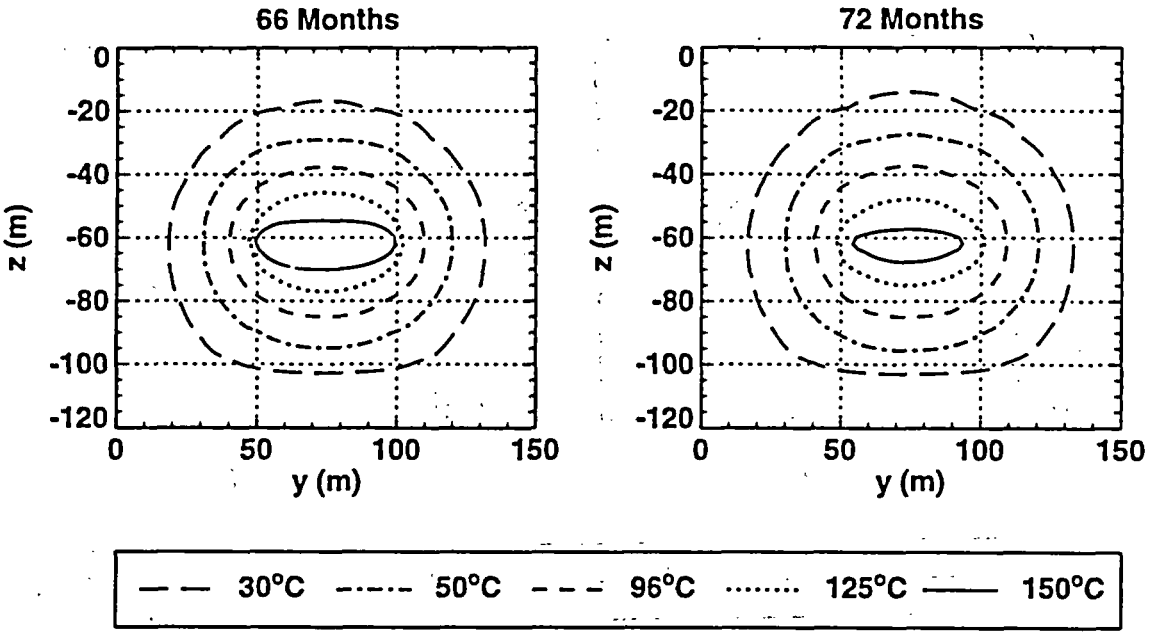

Y-Z Longitudinal Model
High Perm, 4 Year Heating, 2 Year Cooling
Temperature

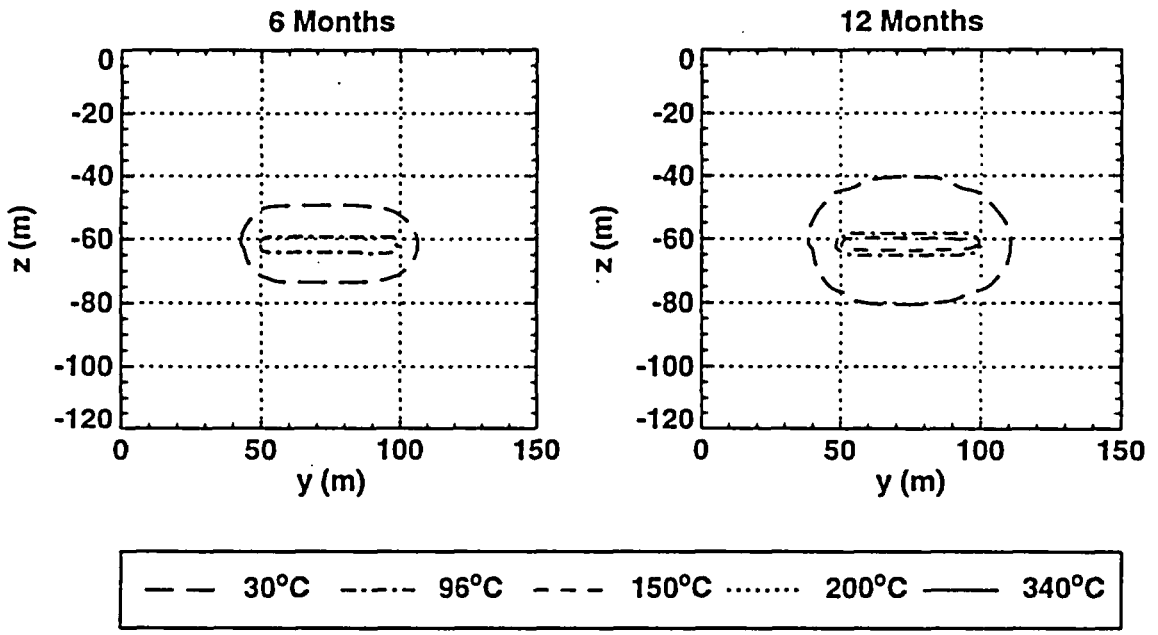

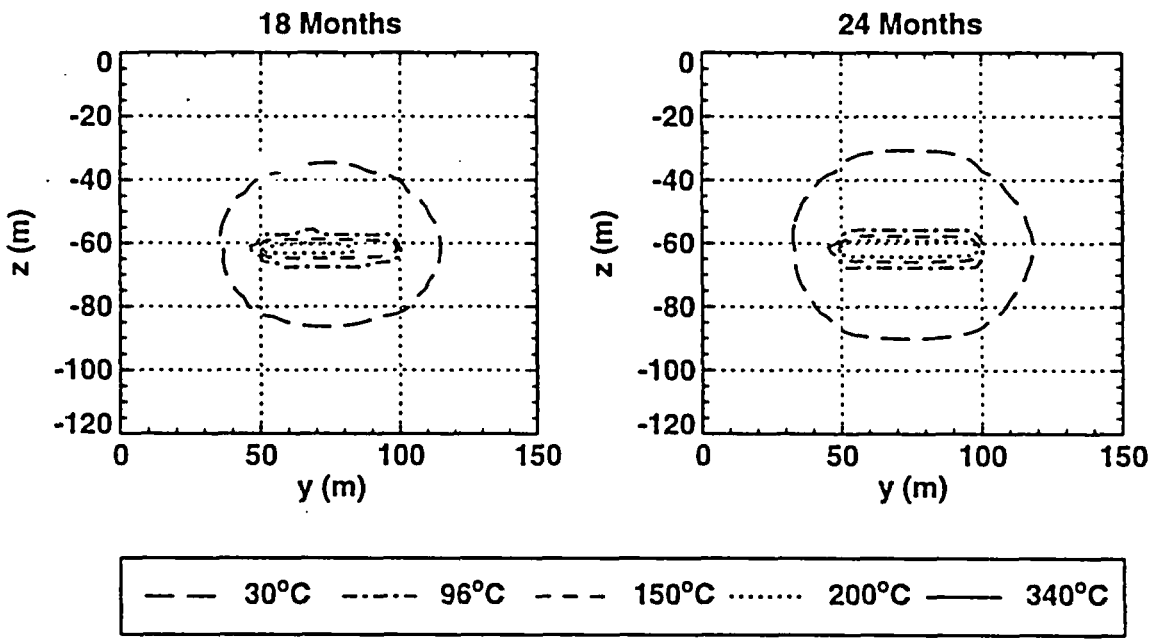

Y-Z Longitudinal Model
High Perm, 4 Year Heating, 2 Year Cooling
Temperature

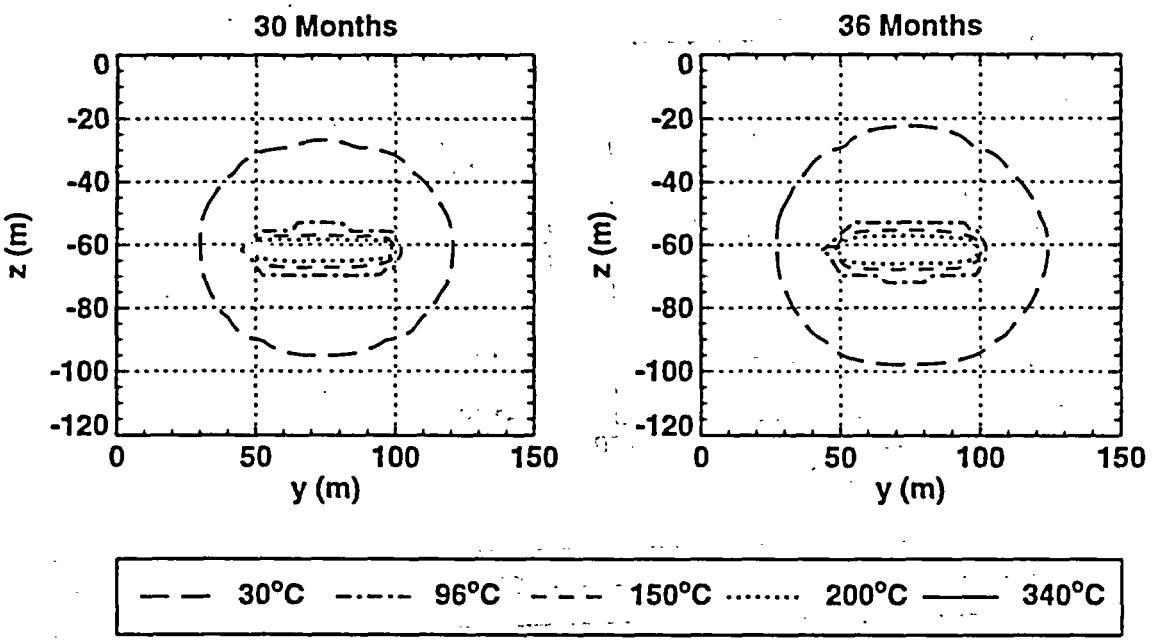

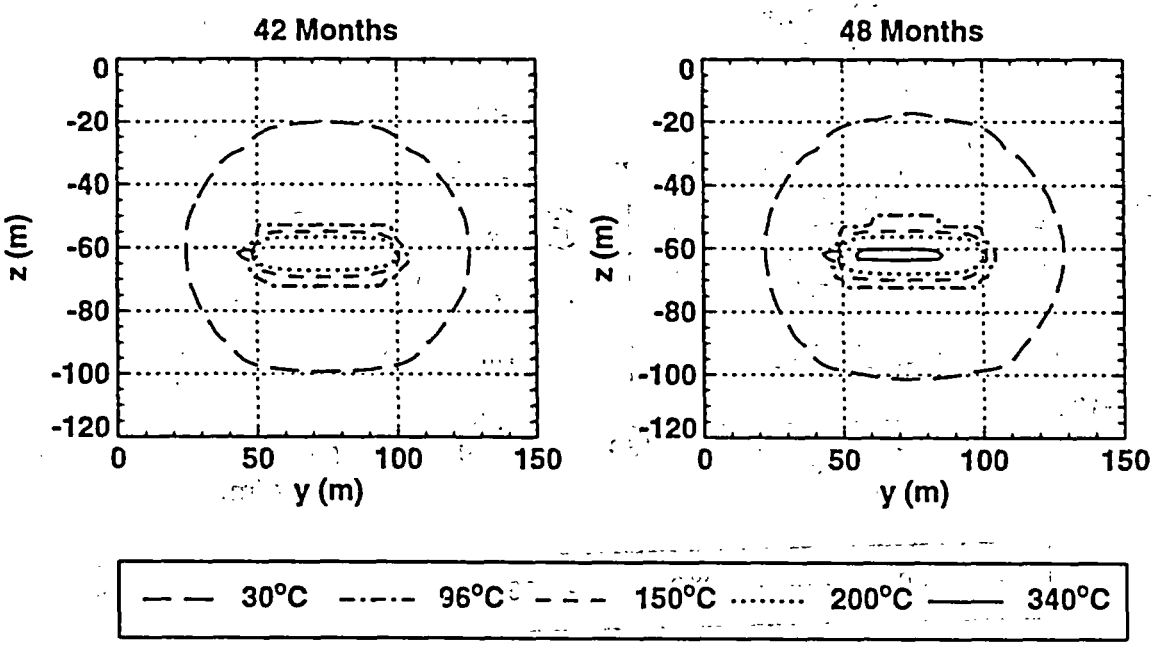

Y-Z Longitudinal Model
High Perm, 4 Year Heating, 2 Year Cooling
Temperature

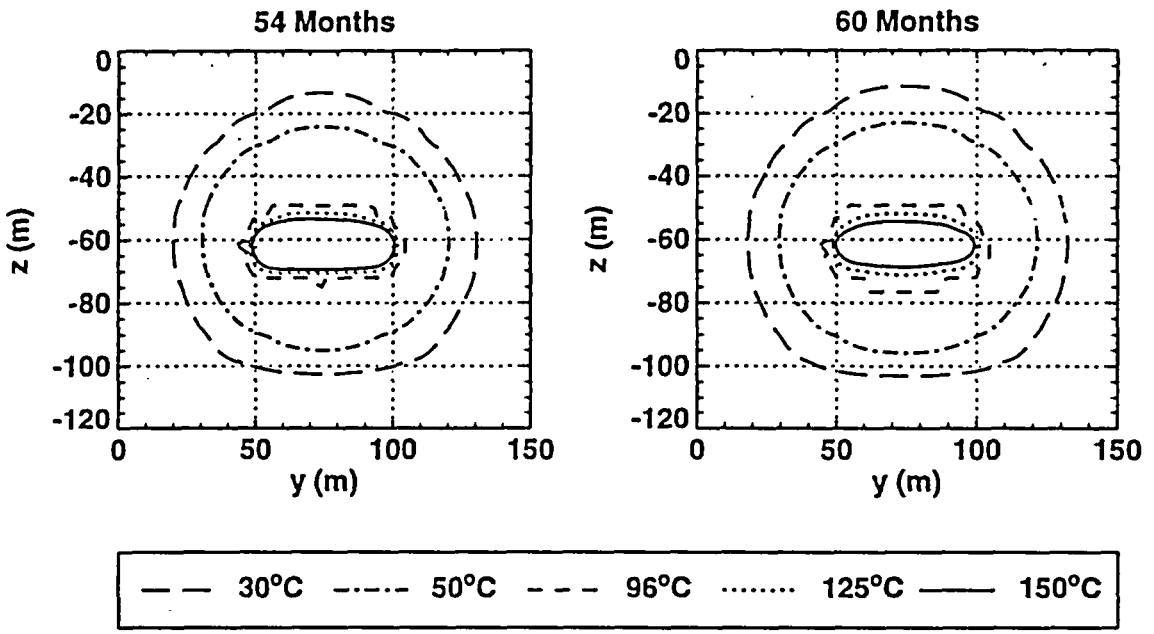

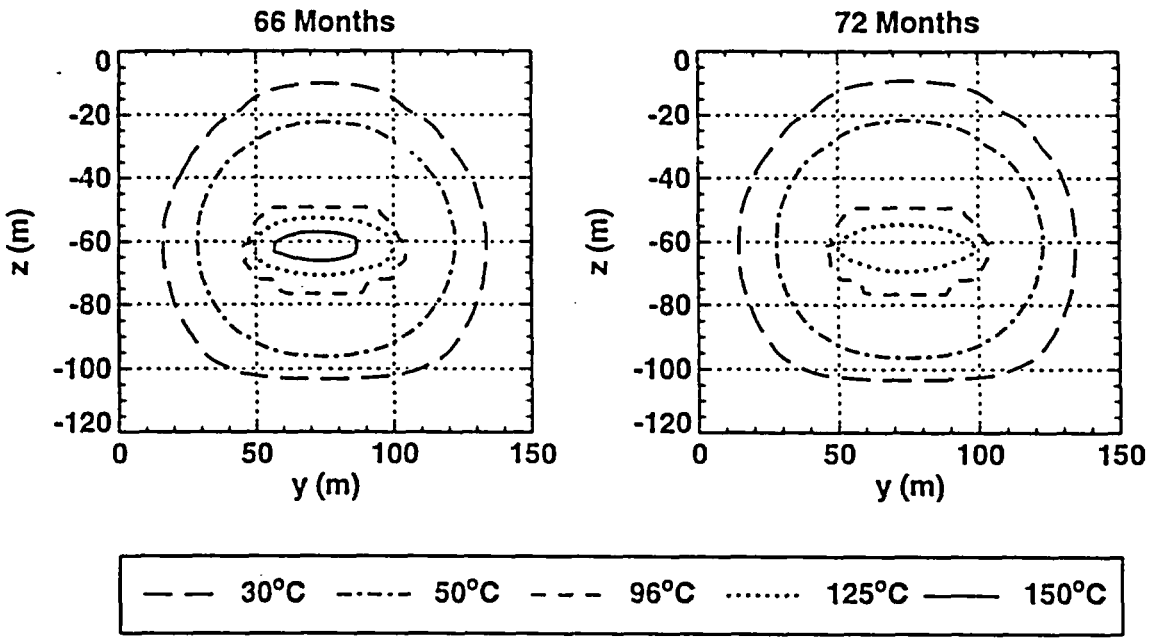

Y-Z Longitudinal Model
Low Bulk Perm., 2 Year Heating, 2 Year Cooling
Liquid Saturation

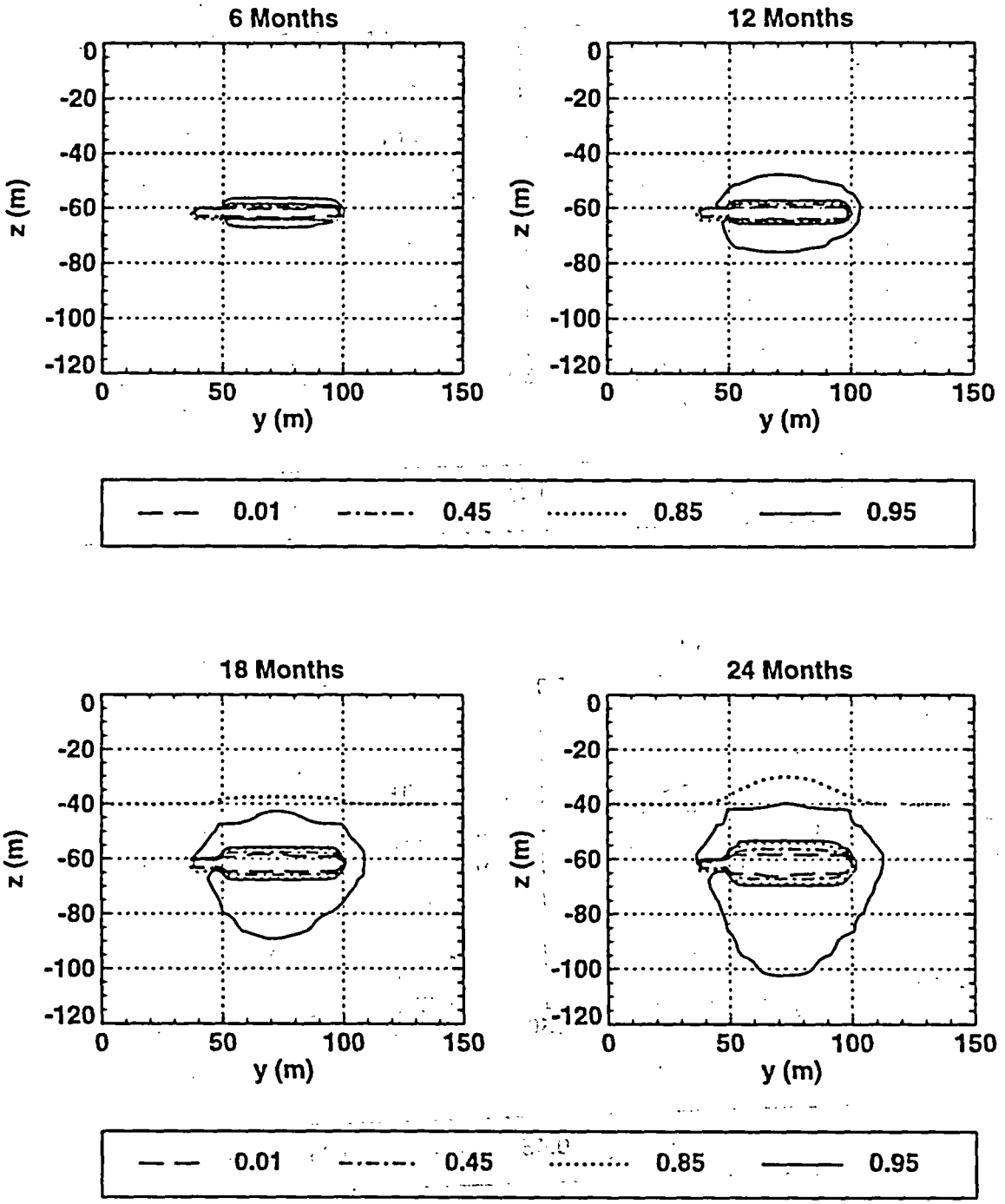

Y-Z Longitudinal Model
Low Bulk Perm., 2 Year Heating, 2 Year Cooling
Liquid Saturation

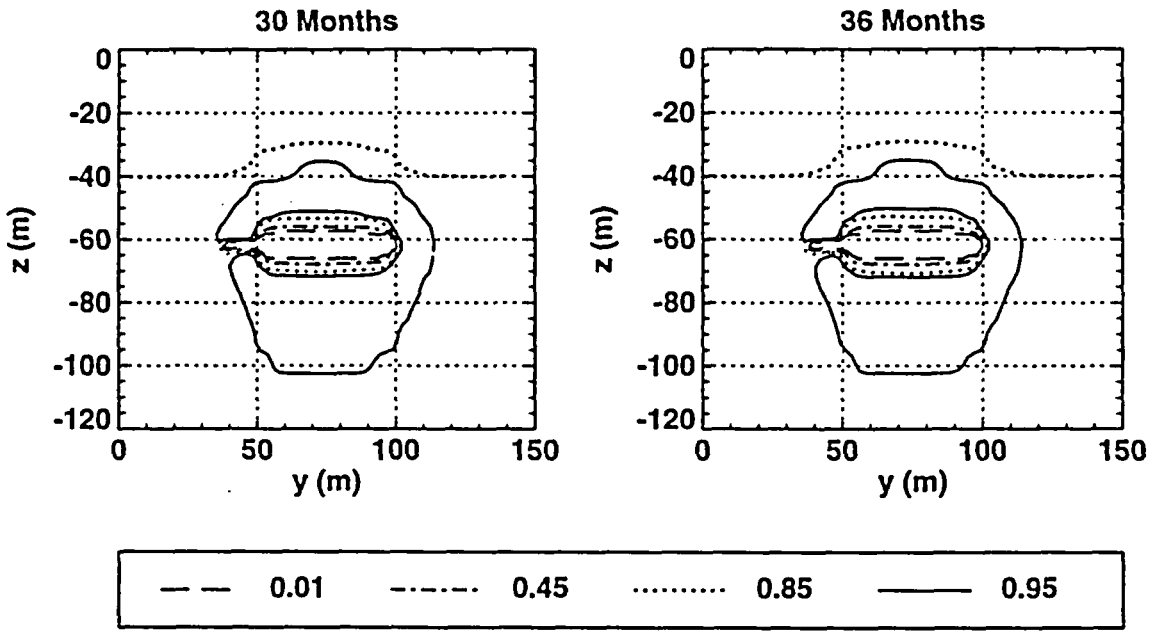

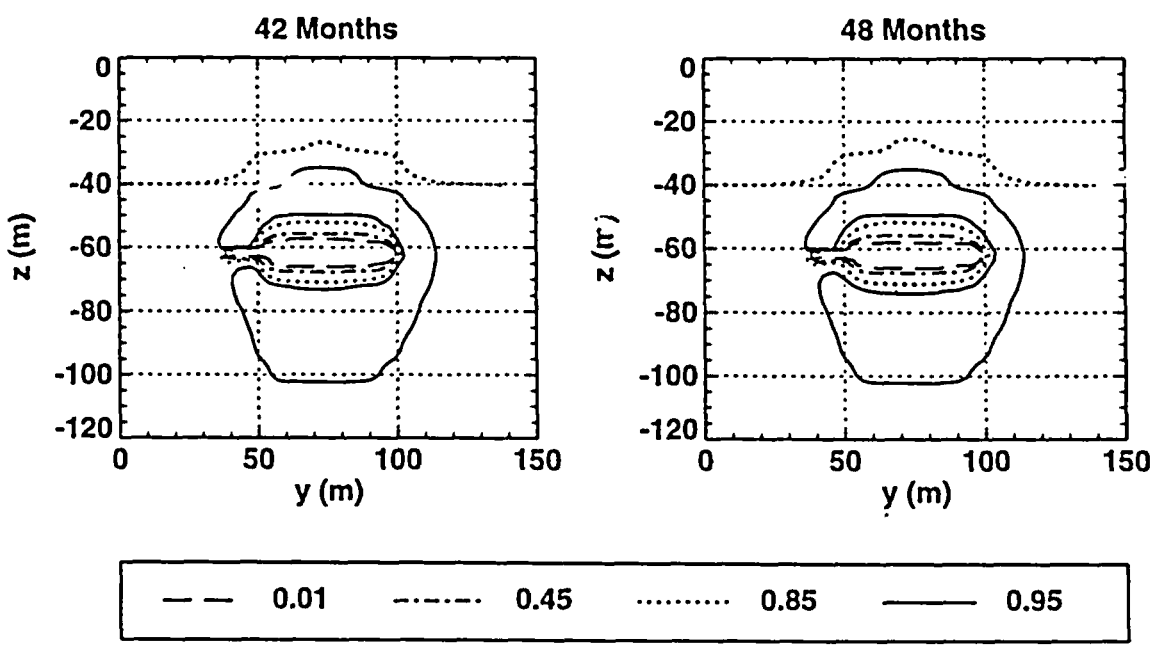

Y-Z Longitudinal Model
Low Bulk Perm., 3 Year Heating, 2 Year Cooling
Liquid Saturation

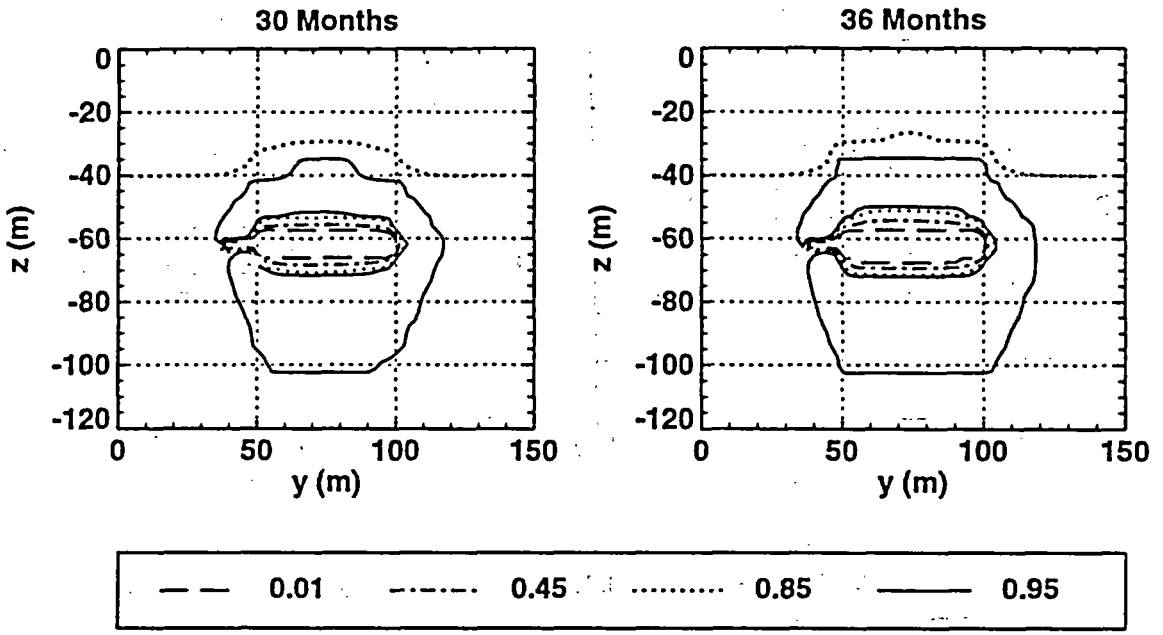

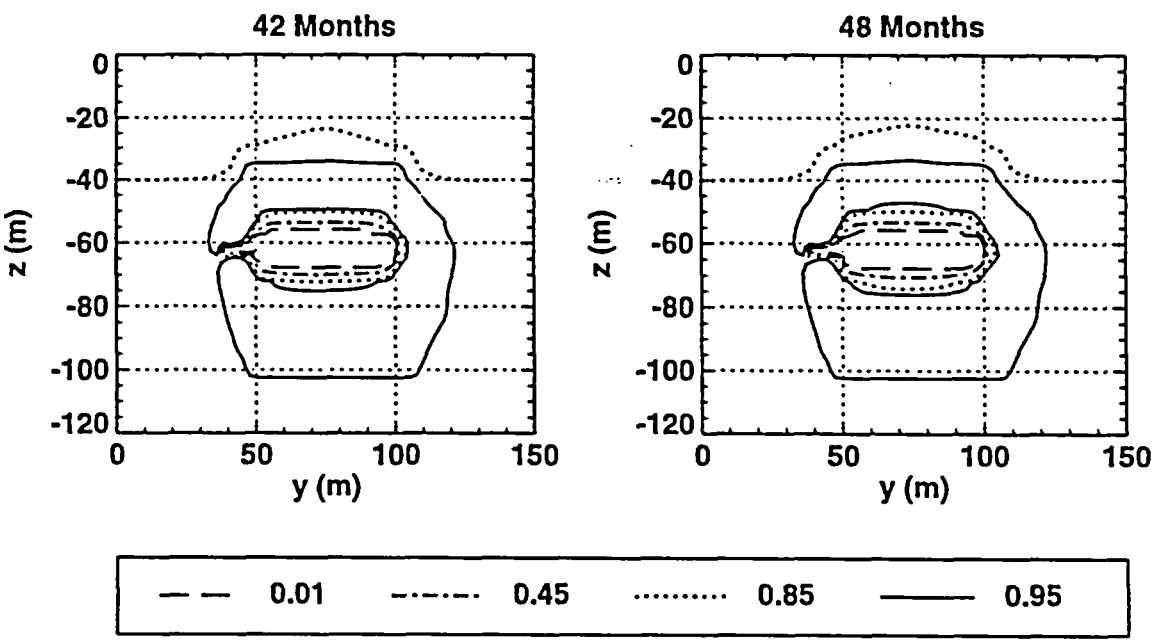

Y-Z Longitudinal Model
Low Bulk Perm., 3 Year Heating, 2 Year Cooling
Liquid Saturation

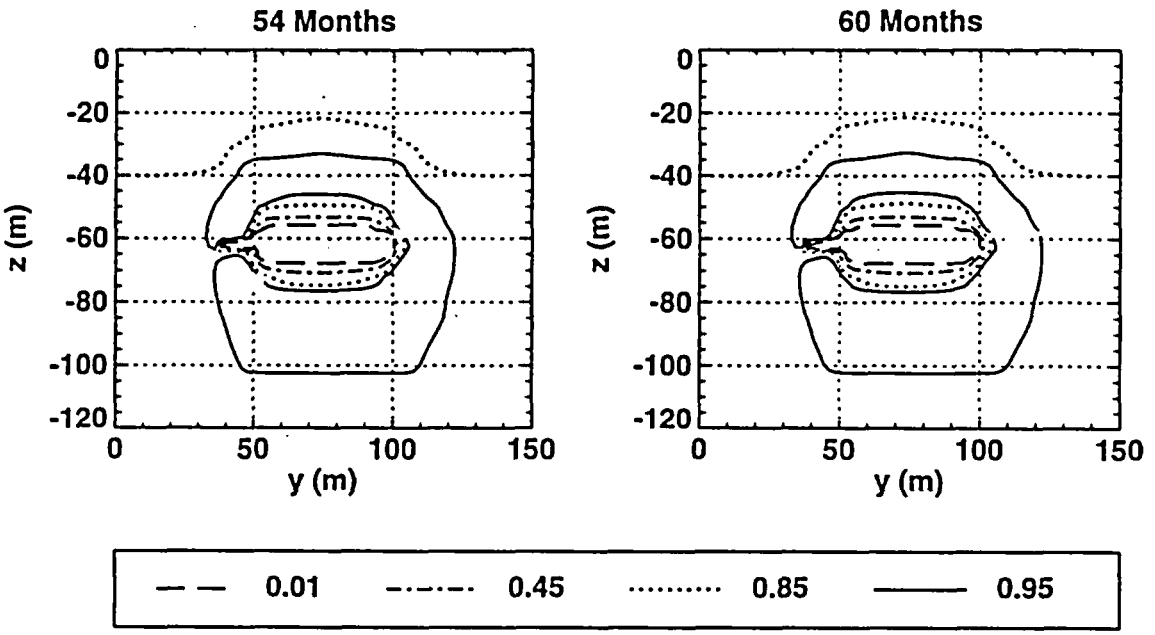

Y-Z Longitudinal Model
Low Bulk Perm., 4 Year Heating, 2 Year Cooling
Liquid Saturation

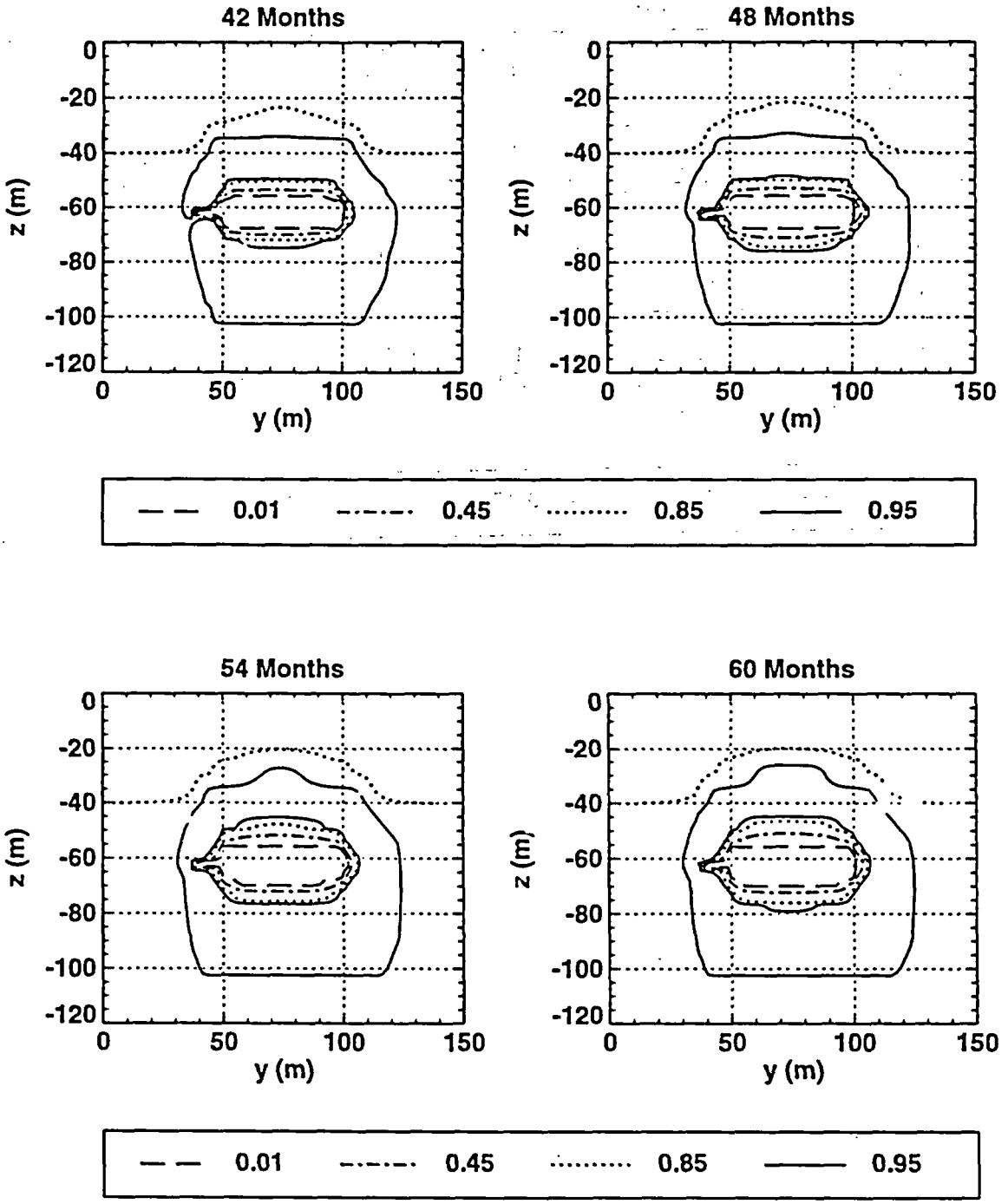

Y-Z Longitudinal Model
Low Bulk Perm., 4 Year Heating, 2 Year Cooling
Liquid Saturation

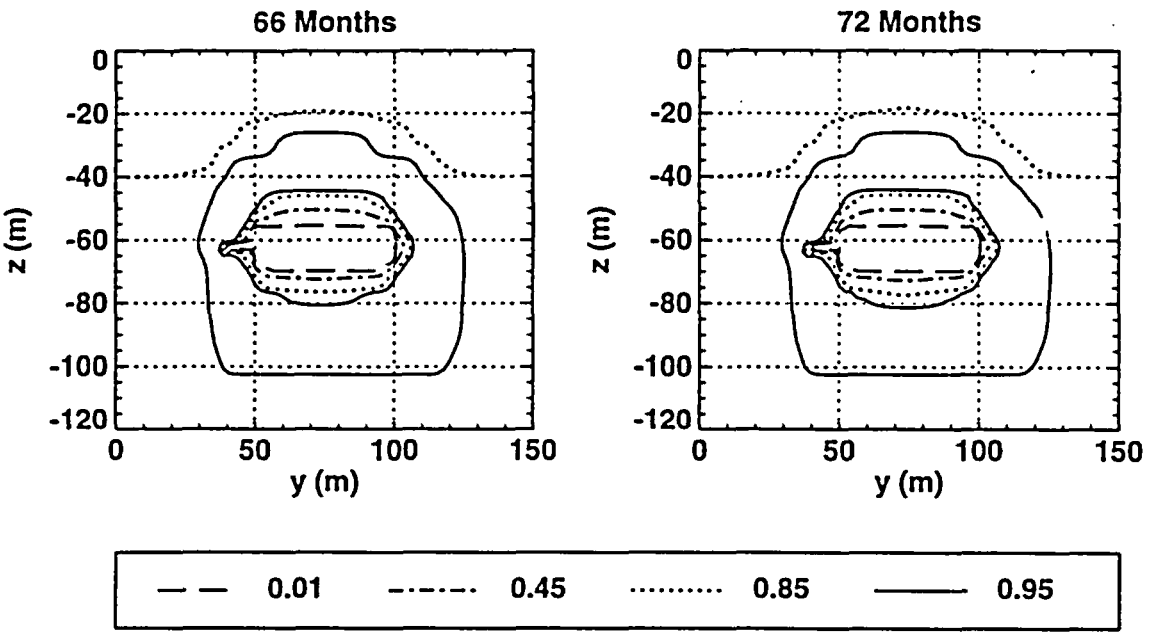

Y-Z Longitudinal Model
High Bulk Perm., 4 Year Heating, 2 Year Cooling
Liquid Saturation

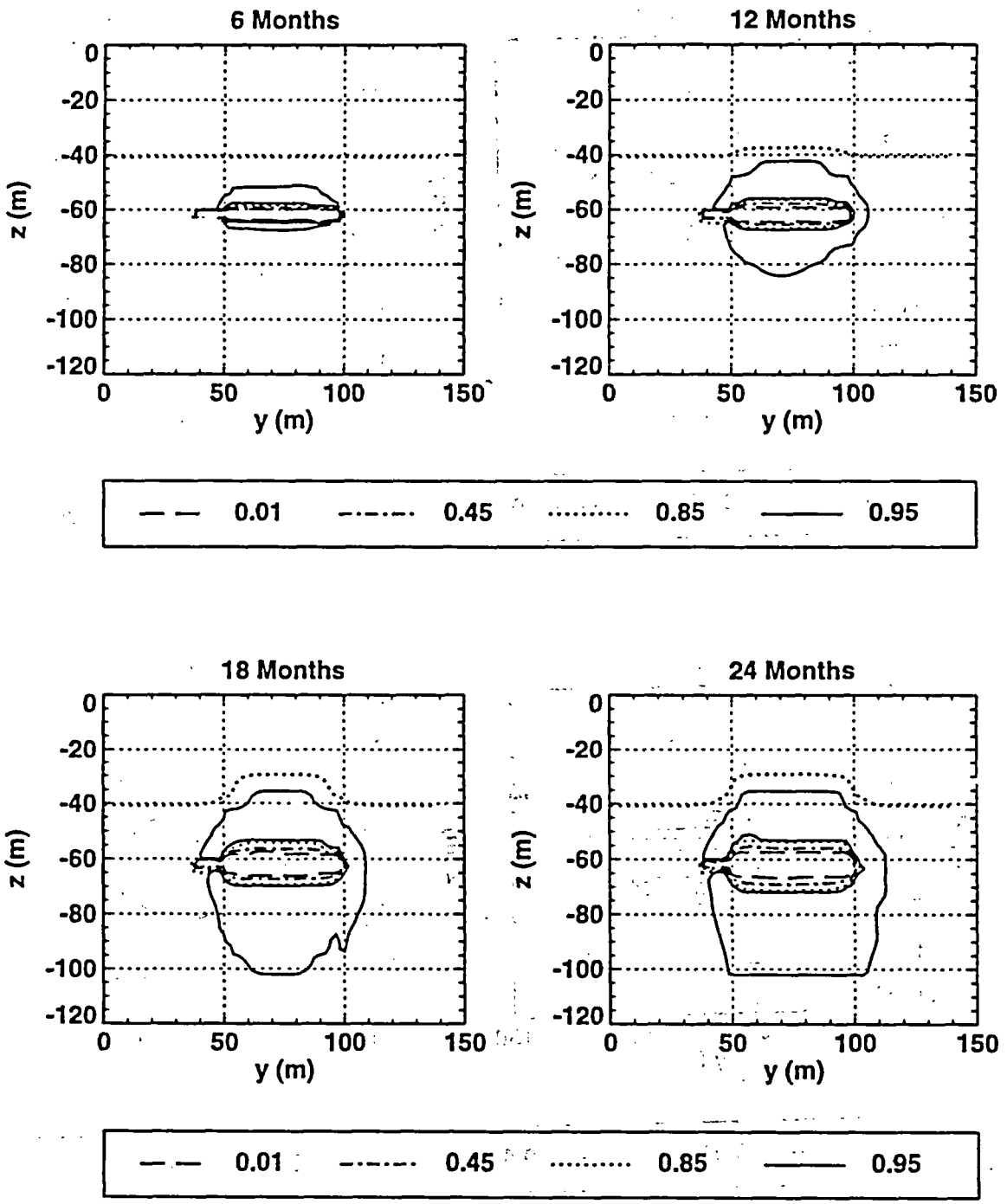

Y-Z Longitudinal Model
High Bulk Perm., 4 Year Heating, 2 Year Cooling
Liquid Saturation

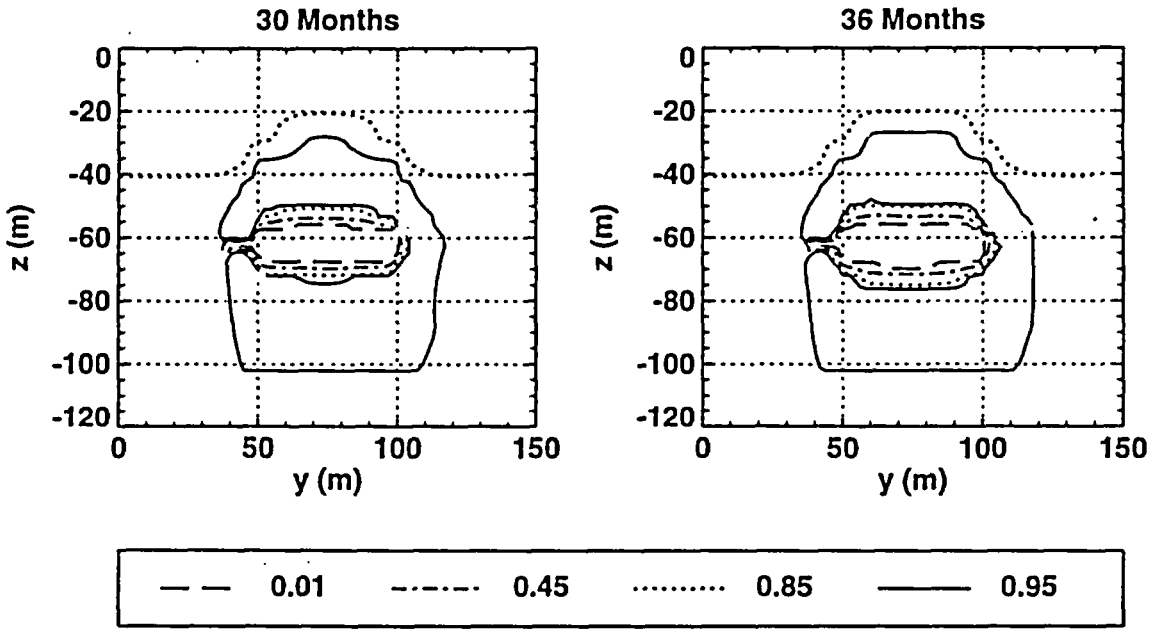

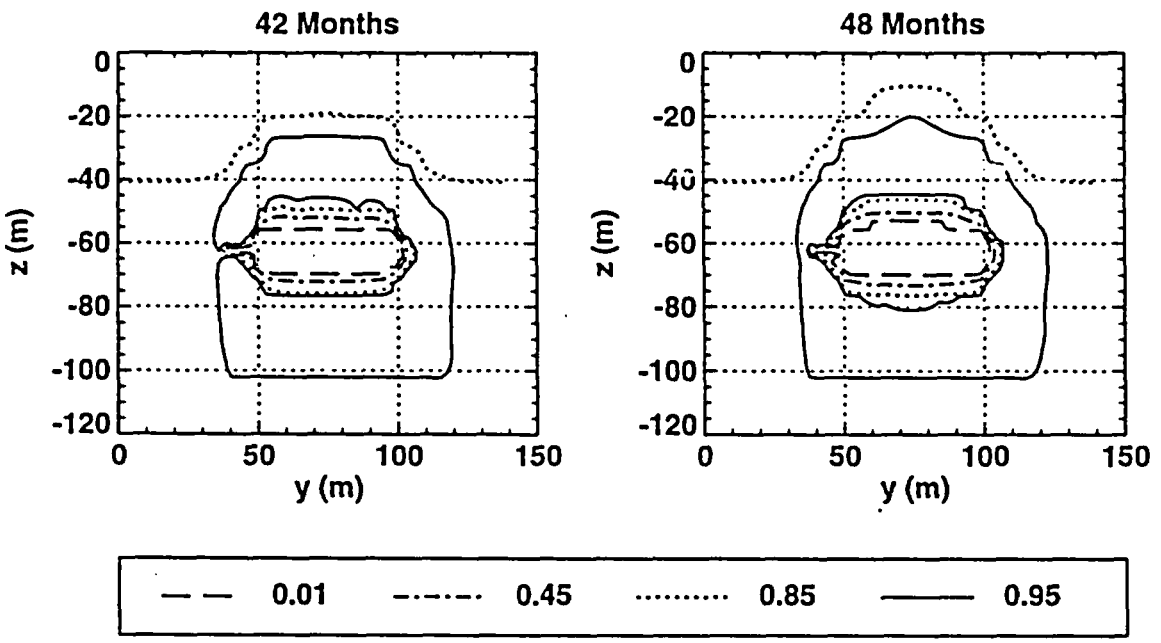

Y-Z Longitudinal Model
High Bulk Perm., 4 Year Heating, 2 Year Cooling
Liquid Saturation

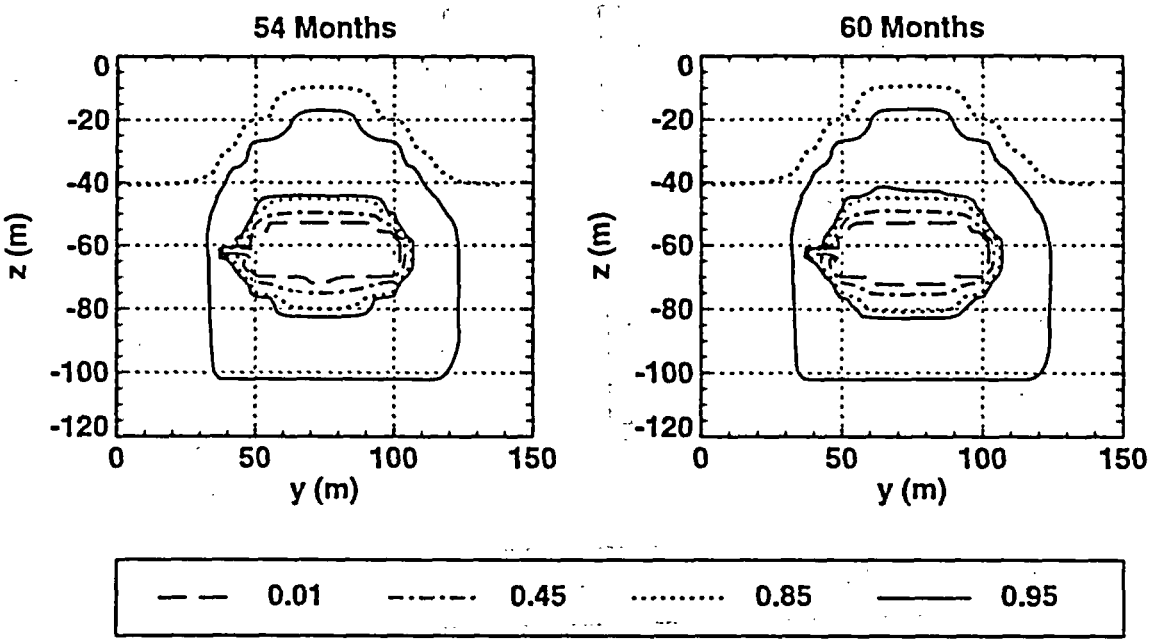

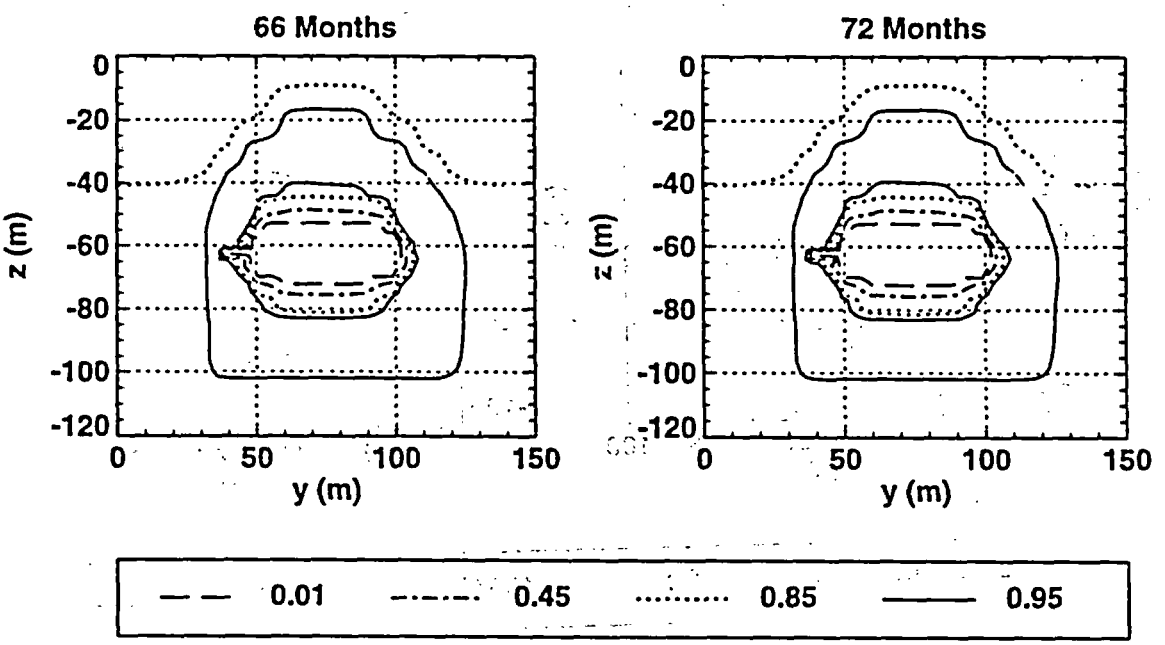

3-D X-Y-Z Model
Low Bulk Perm., 2 Years Heating, 2 Years Cooling
Temperature

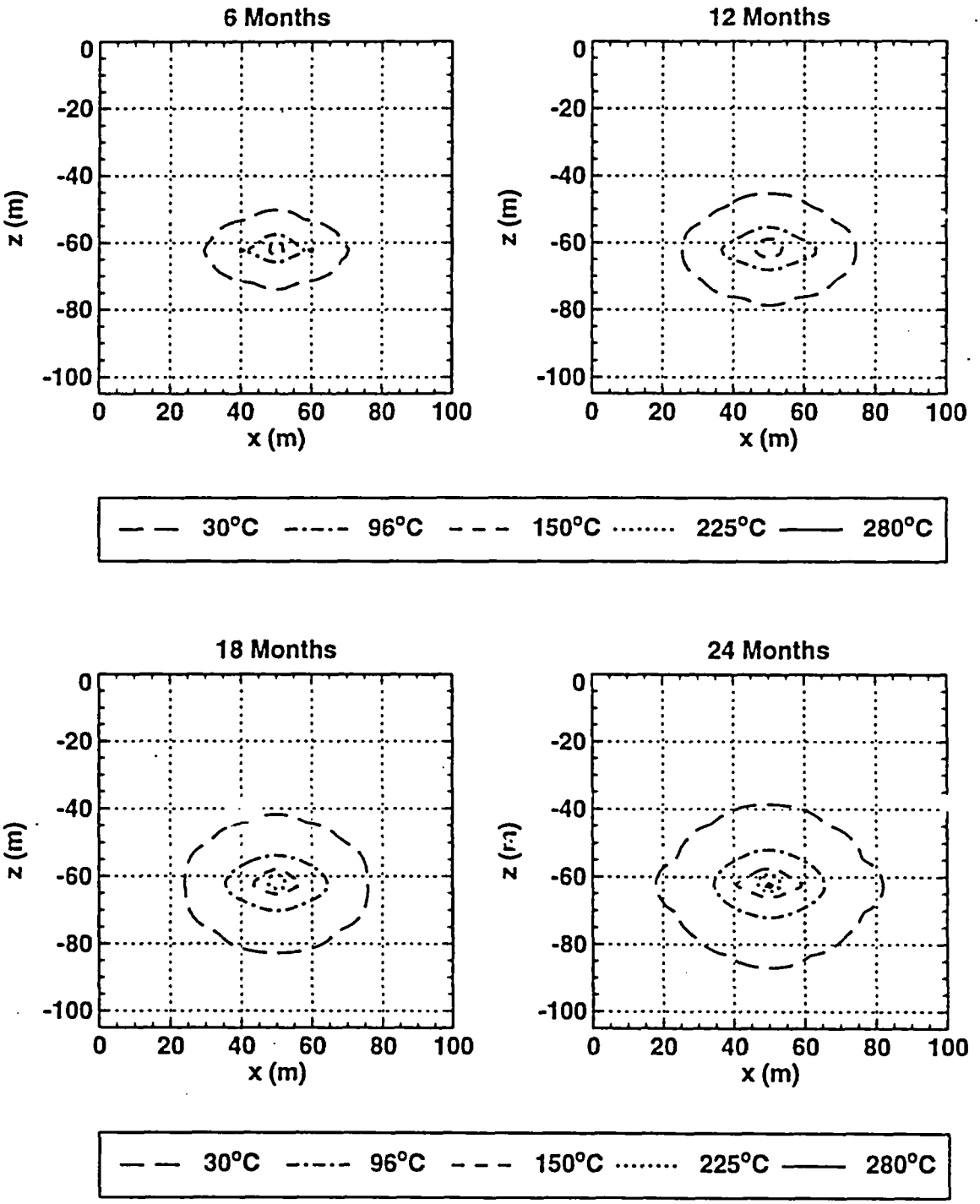

3-D X-Y-Z Model
Low Bulk Perm., 2 Years Heating, 2 Years Cooling
Temperature

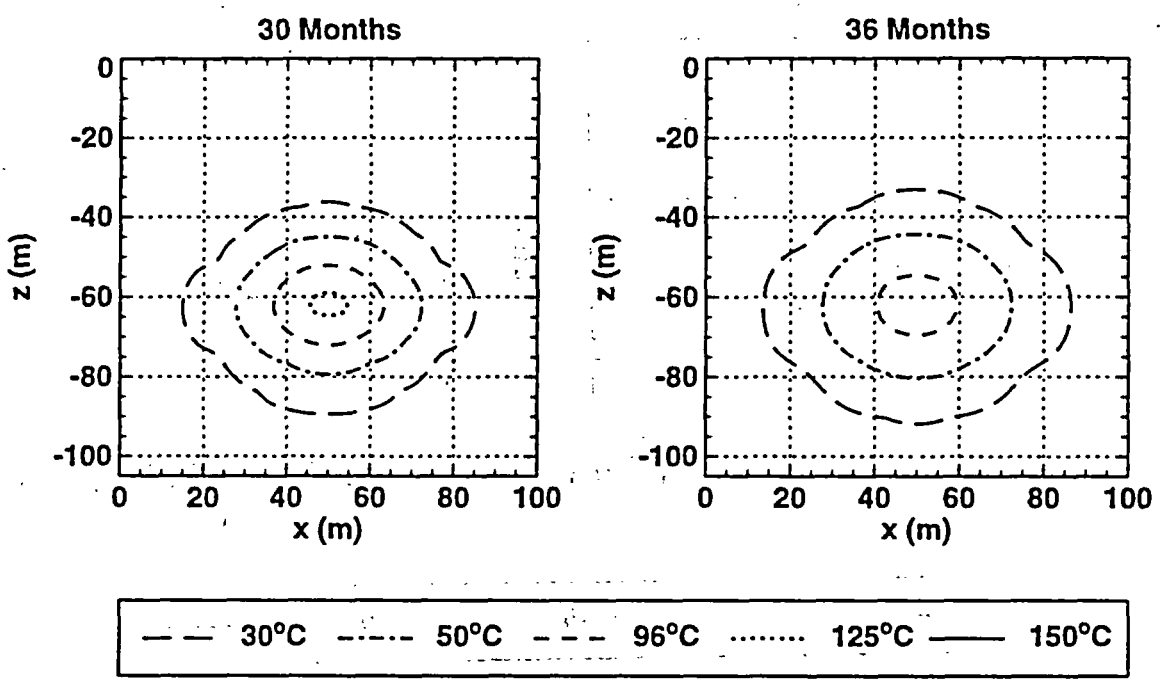

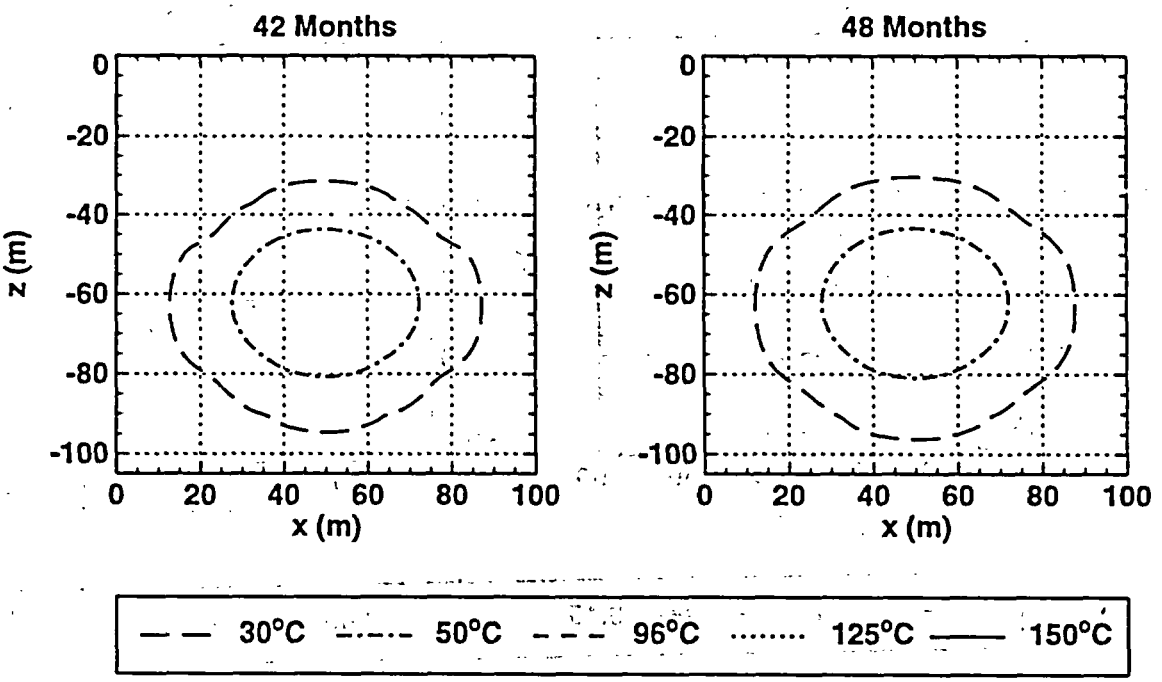

3-D X-Y-Z Model
Low Bulk Perm., 2 Years Heating, 2 Years Cooling
Liquid Saturation

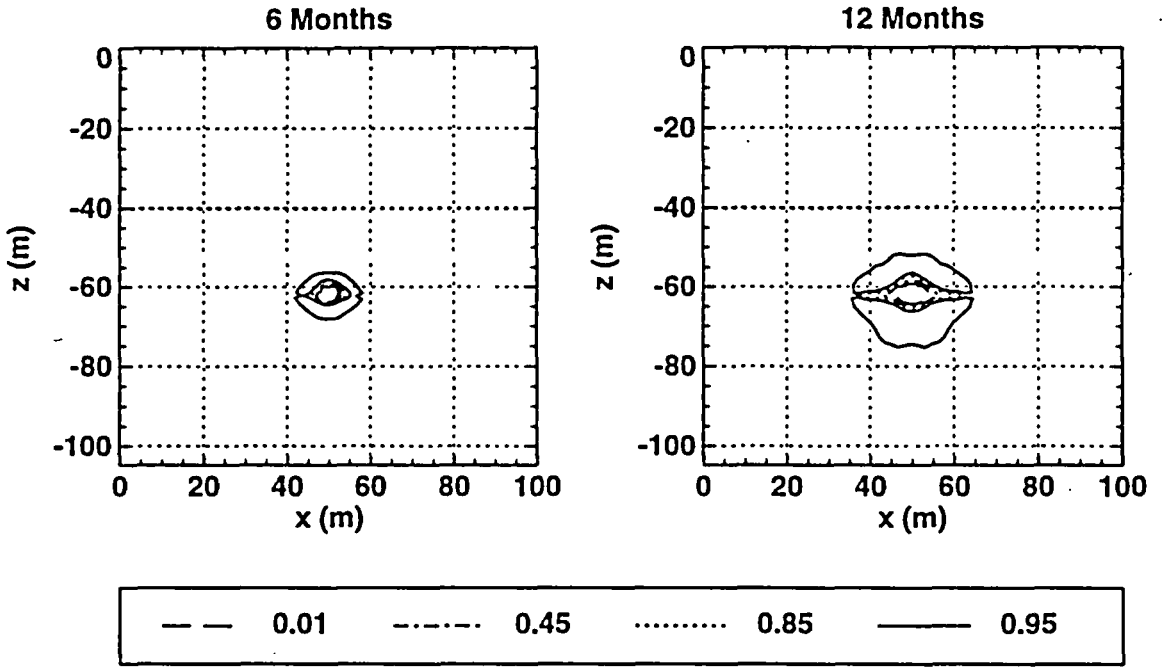

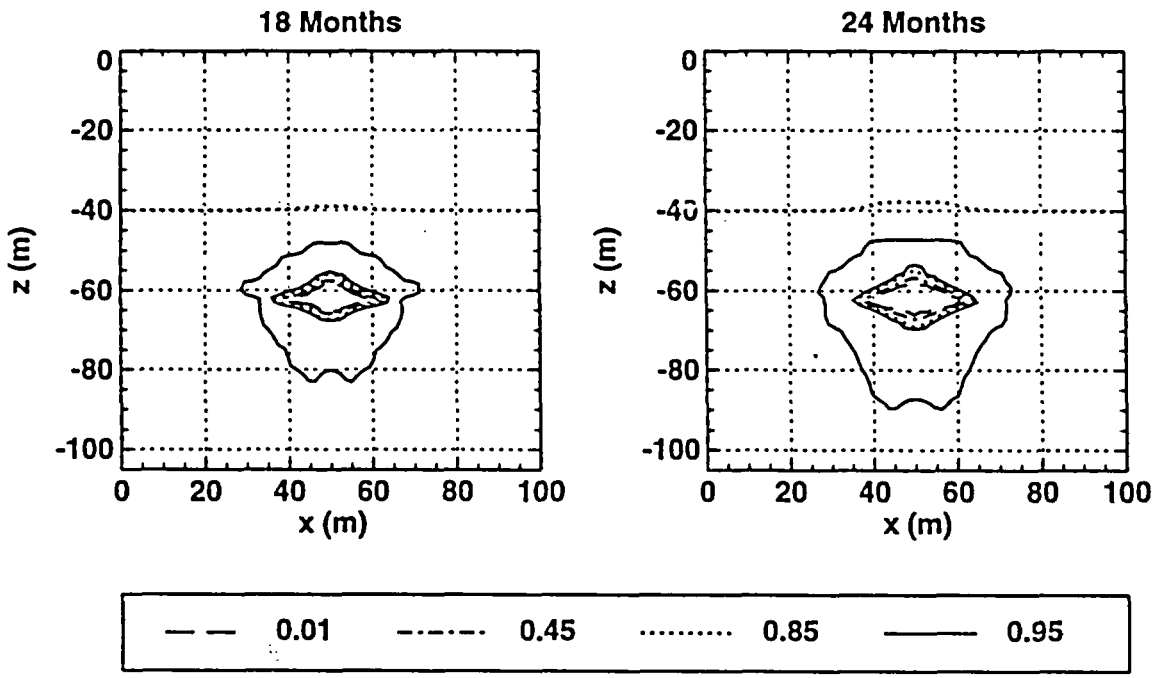

3-D X-Y-Z Model
Low Bulk Perm., 2 Years Heating, 2 Years Cooling
Liquid Saturation

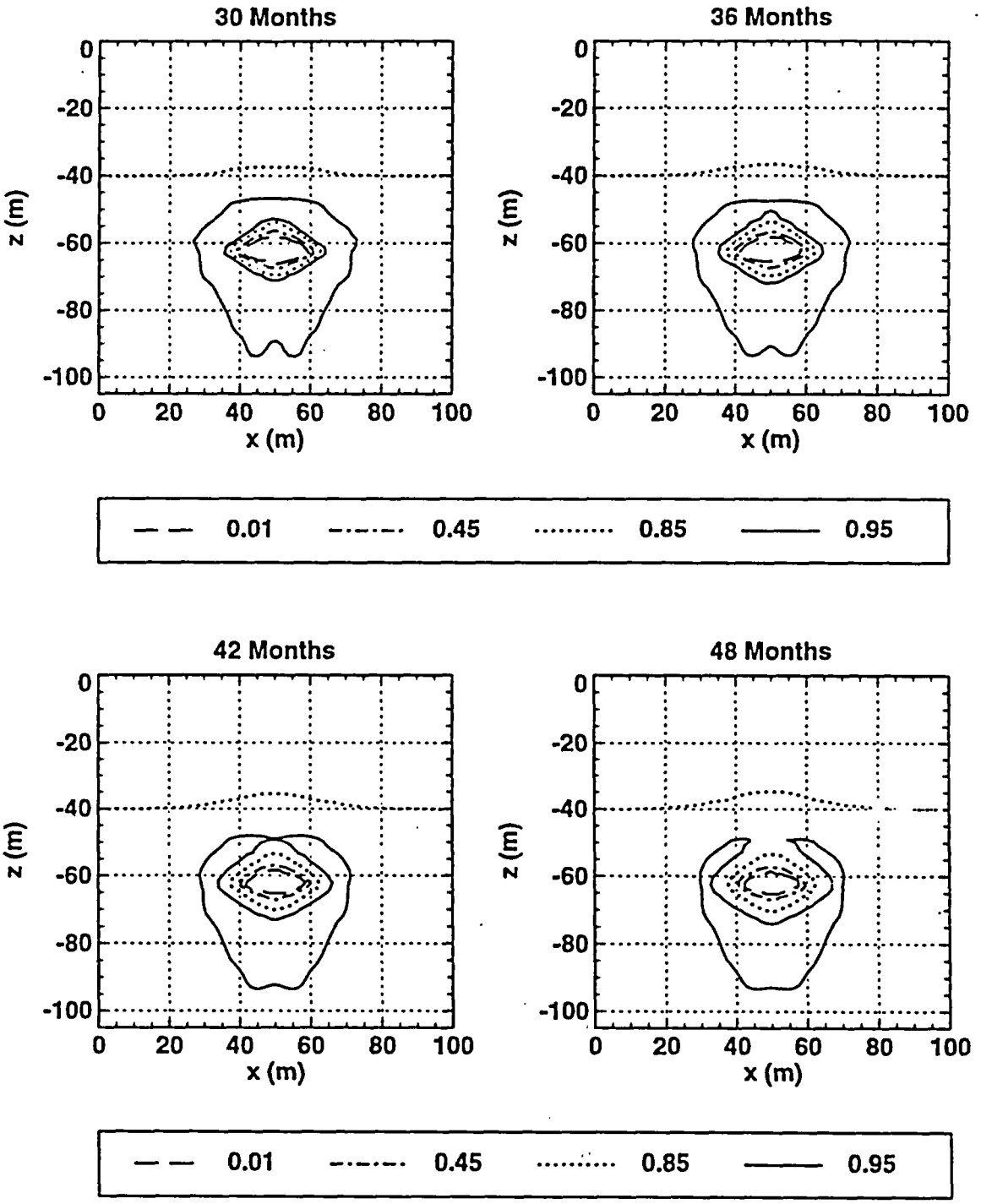

Appendix C: Selected Three-Dimensional Temperature Fields Interpolated from 2-D Thermal-Hydrologic Calculations, and Used as Inputs to the Thermal-Mechanical Calculations

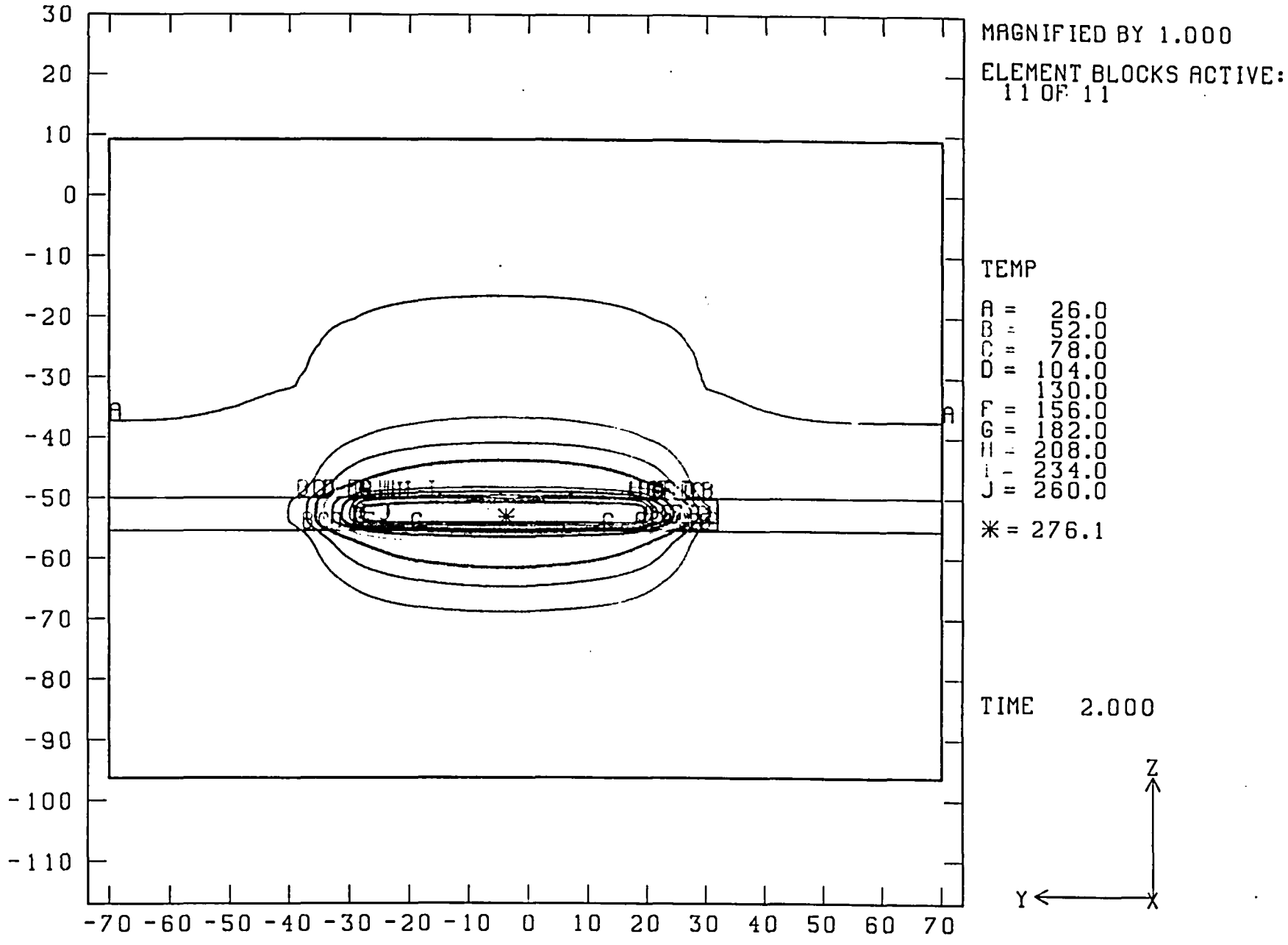

Figure C-1: Temperature contours on heated drift vertical symmetry plane (through 2 years of heating)

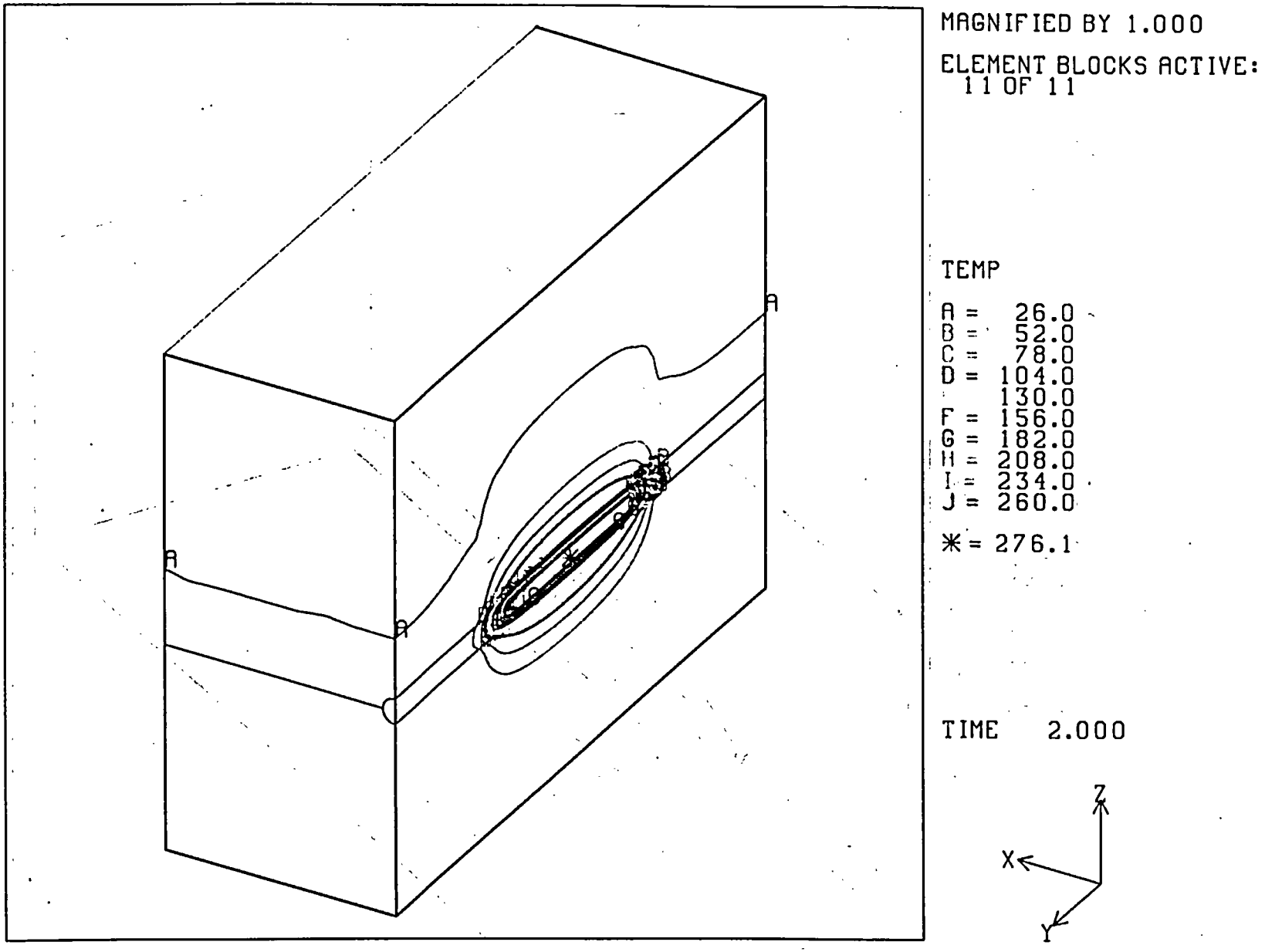

Figure C-2: Orthogonal view along heated drift vertical symmetry plane (through 2 years of heating)

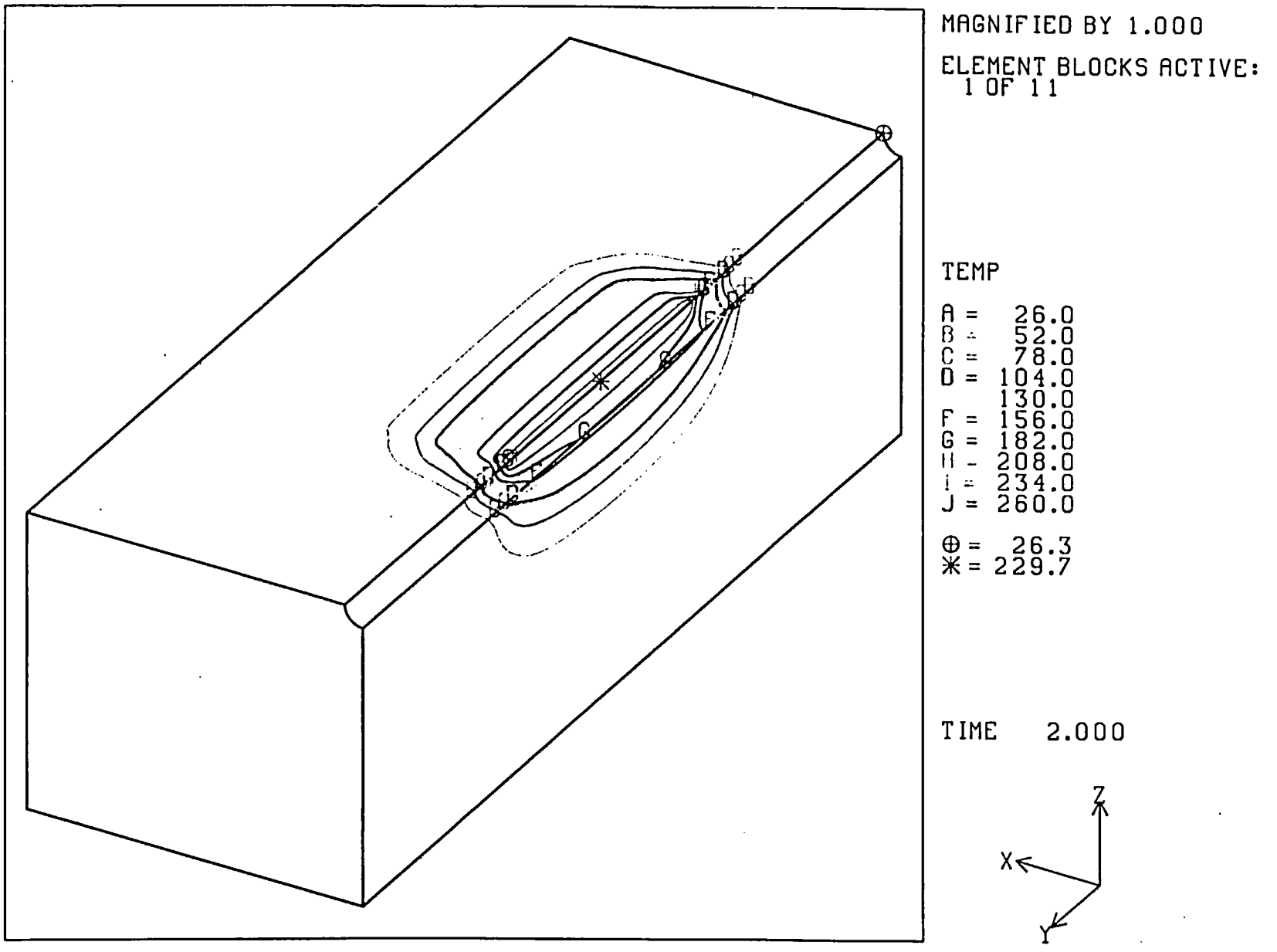

Figure C-3: Cut away view - lower half of computational domain (through 2 years of heating)

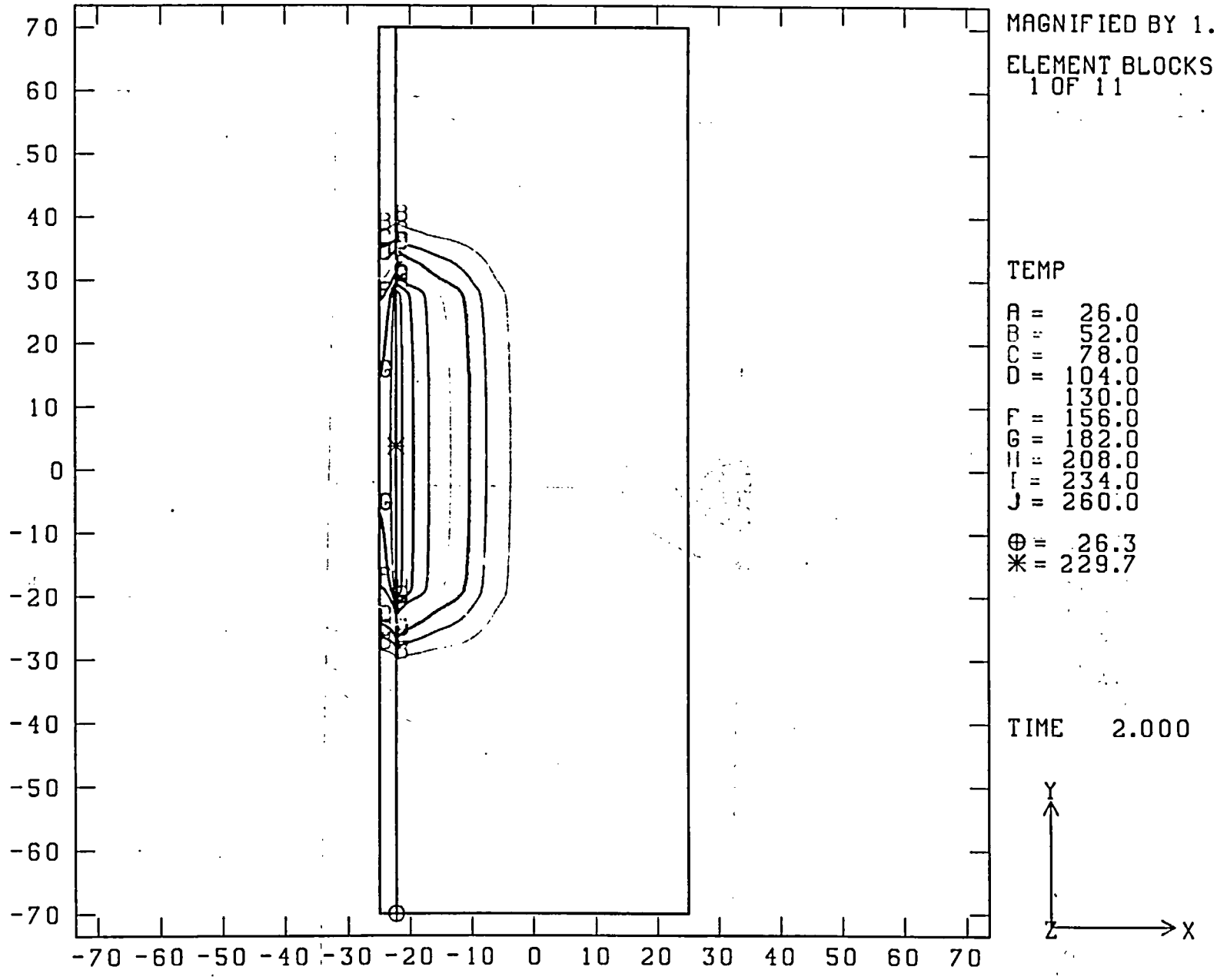

Figure C-4: Top view looking down at horizontal cut-away (through 2 years of heating)

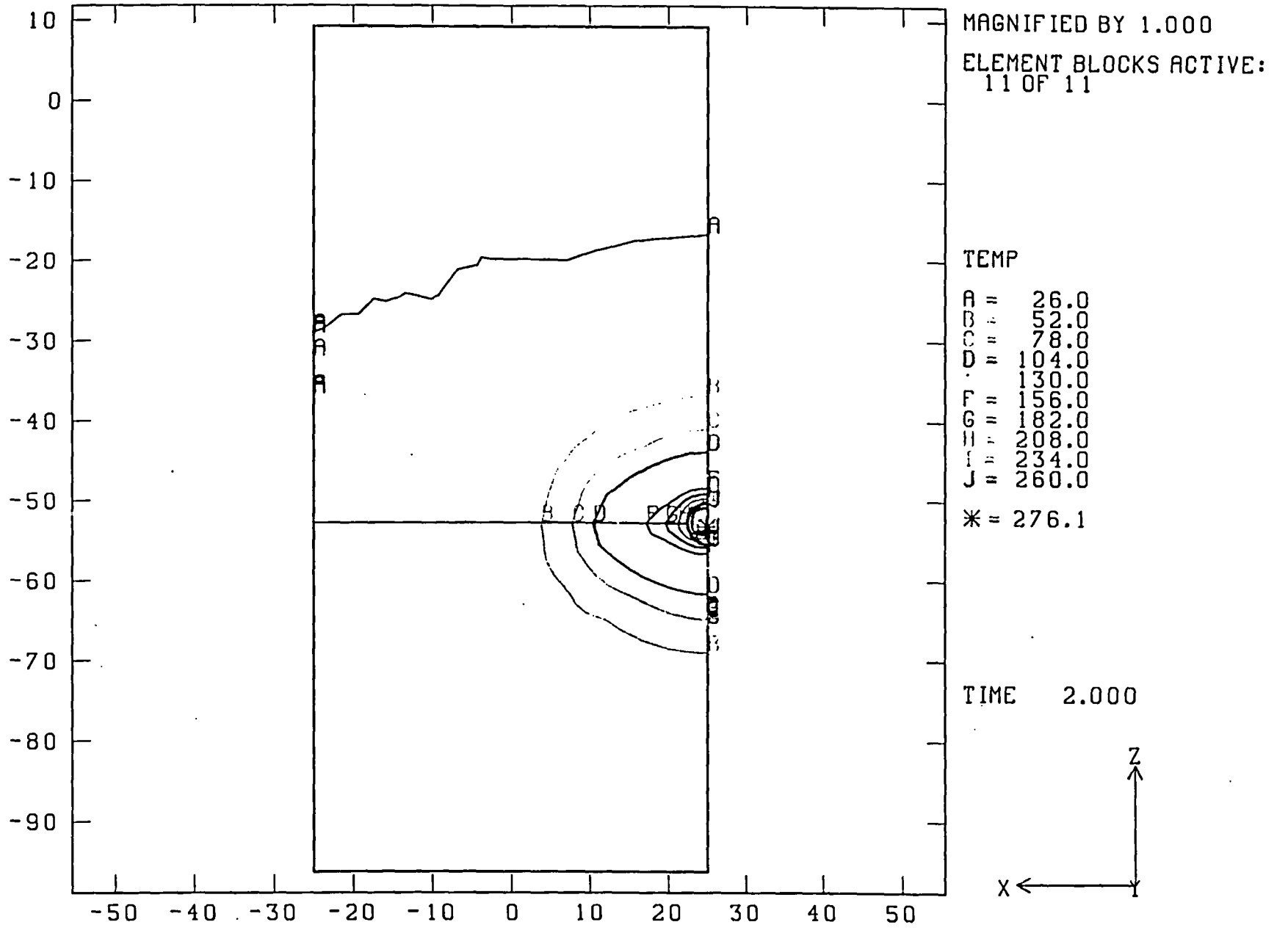

Figure C-5: Cut away through midpoint of tunnel (through 2 years of heating)

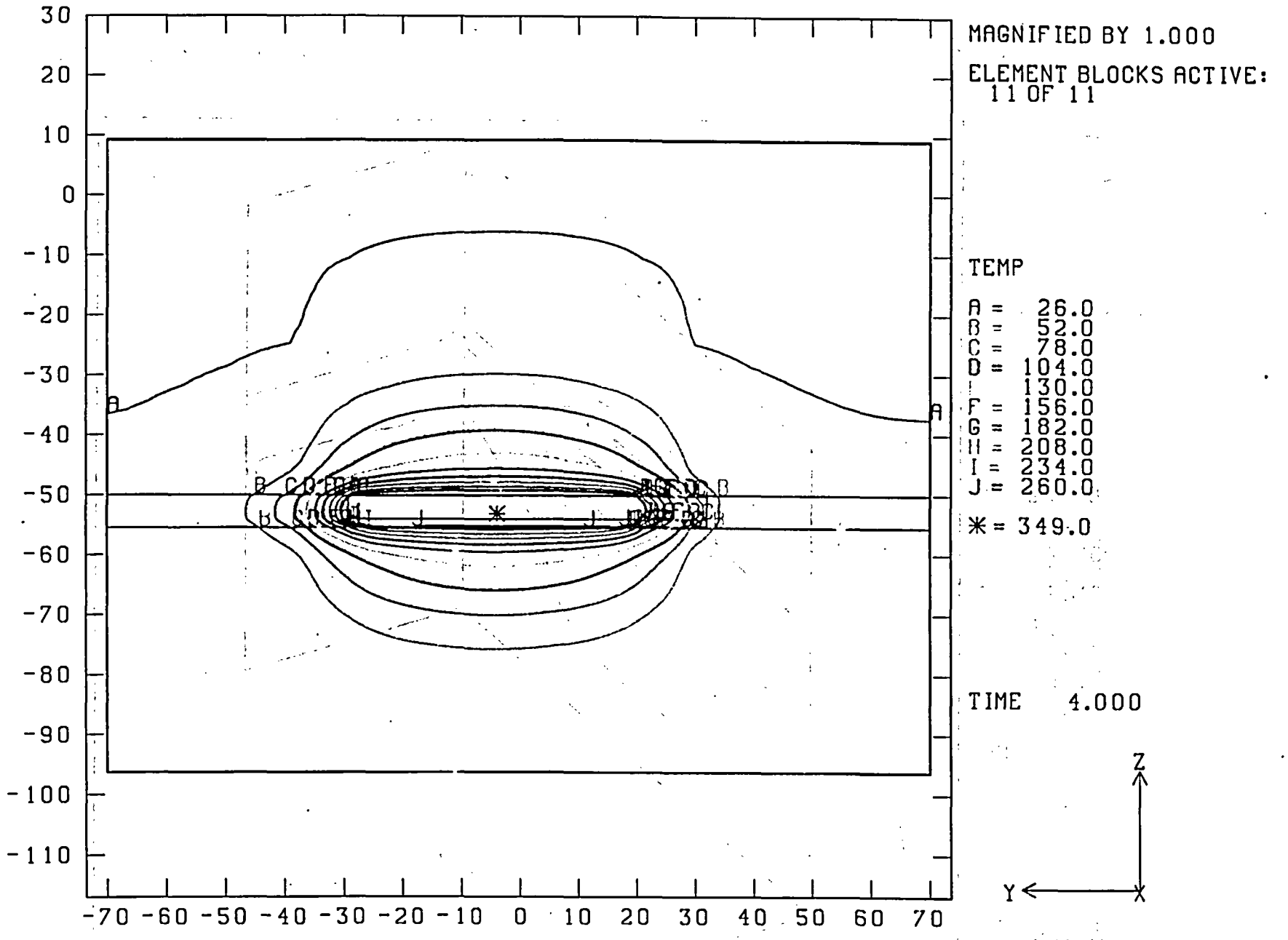

Figure C-6: Temperature contours on heated drift vertical symmetry plane (through 4 years of heating)

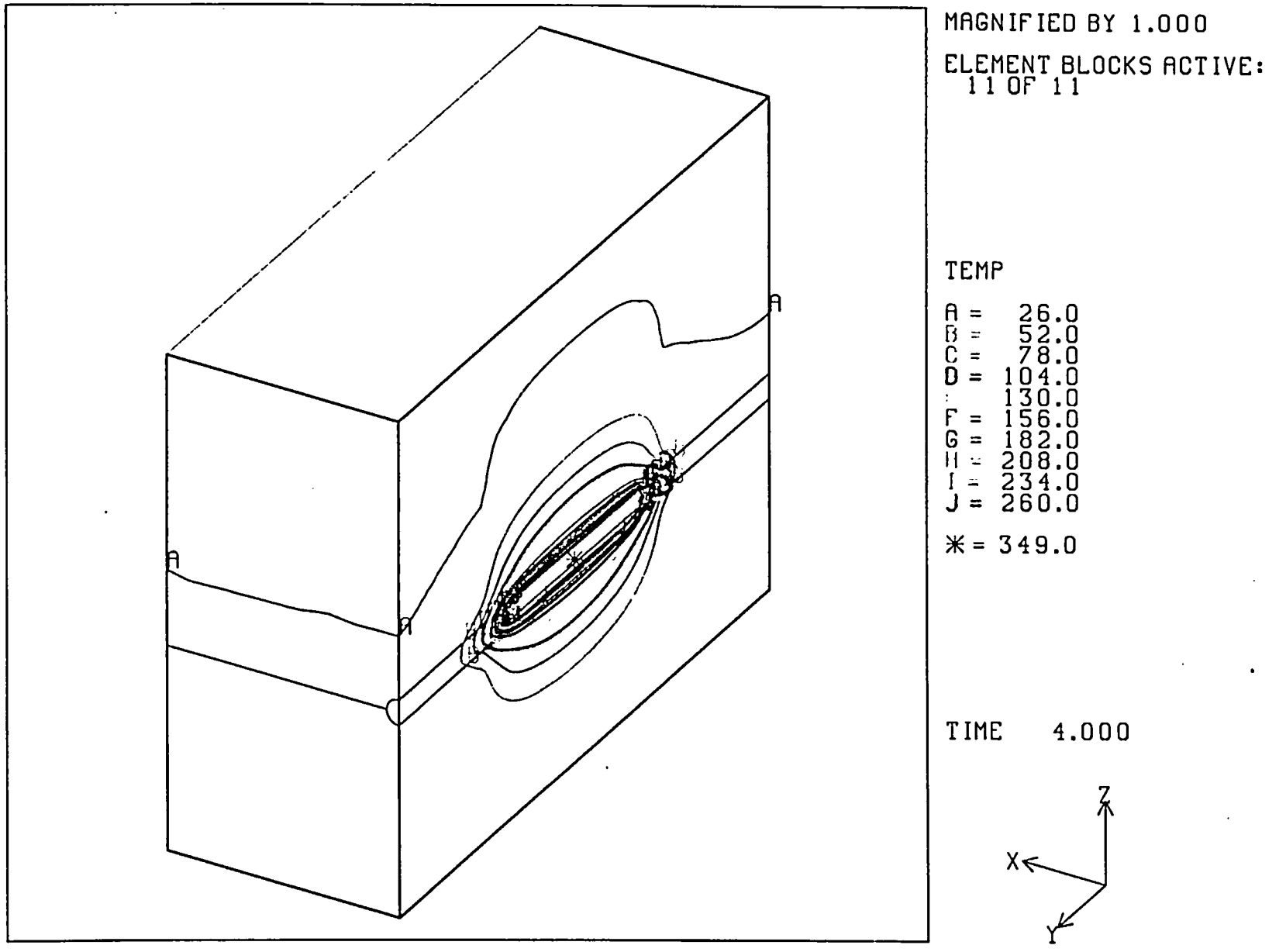

Figure C-7: Orthogonal view along heated drift vertical symmetry plane (through 4 years of heating)

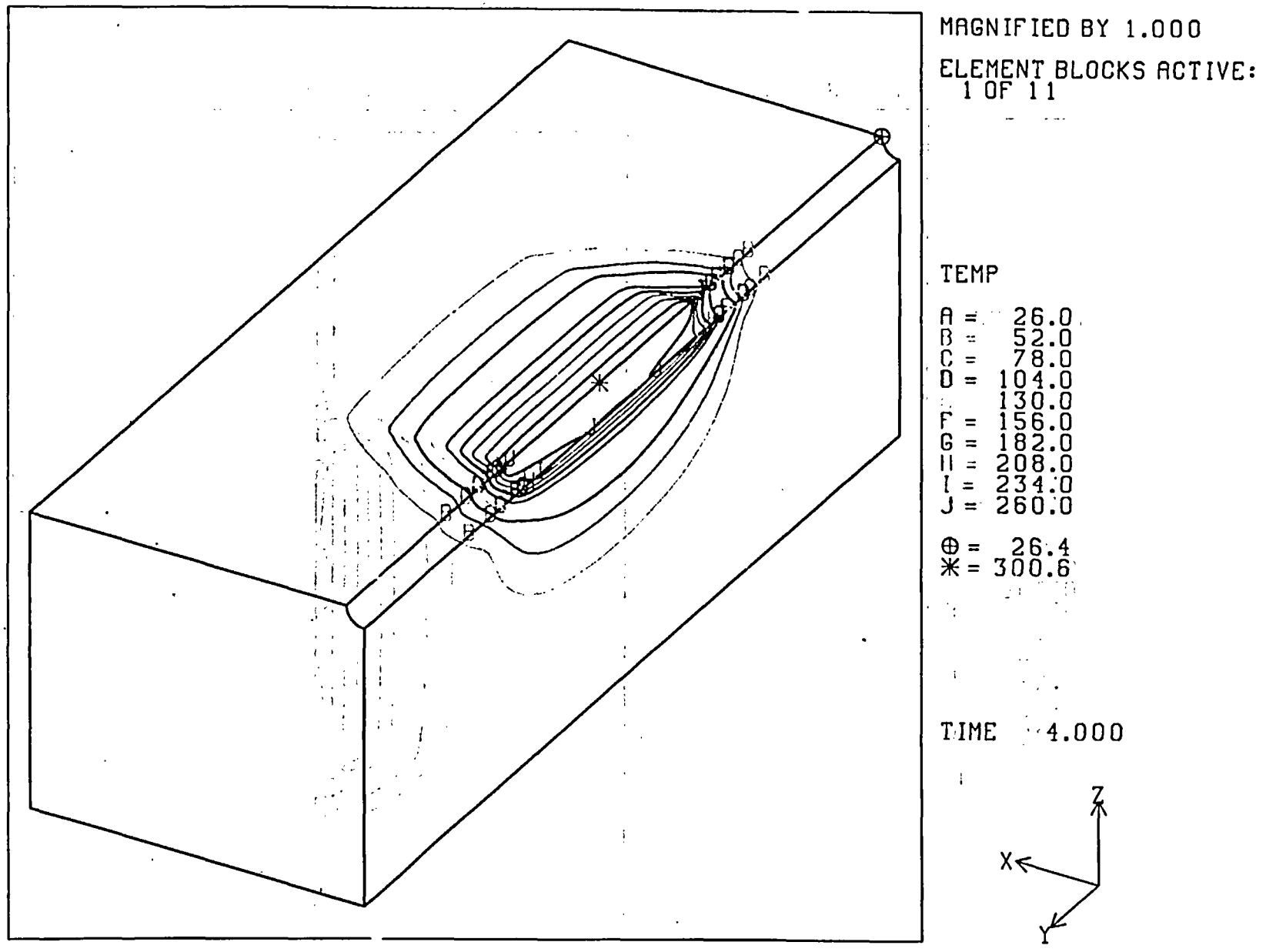

Figure C-8: Cut away view - lower half of computational domain (through 4 years of heating)

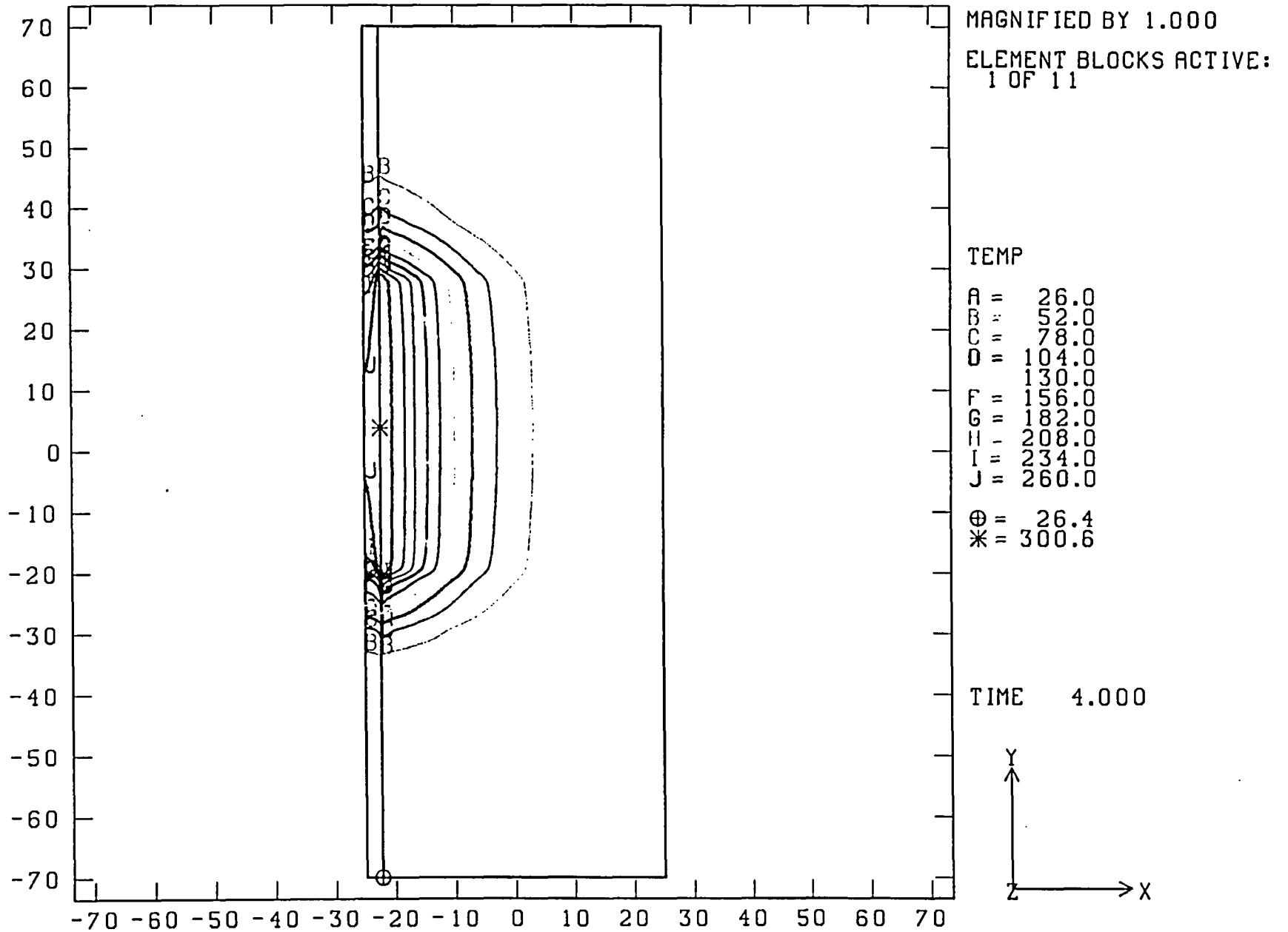

Figure C-9: Top view looking down at horizontal cut-away (through 4 years of heating)

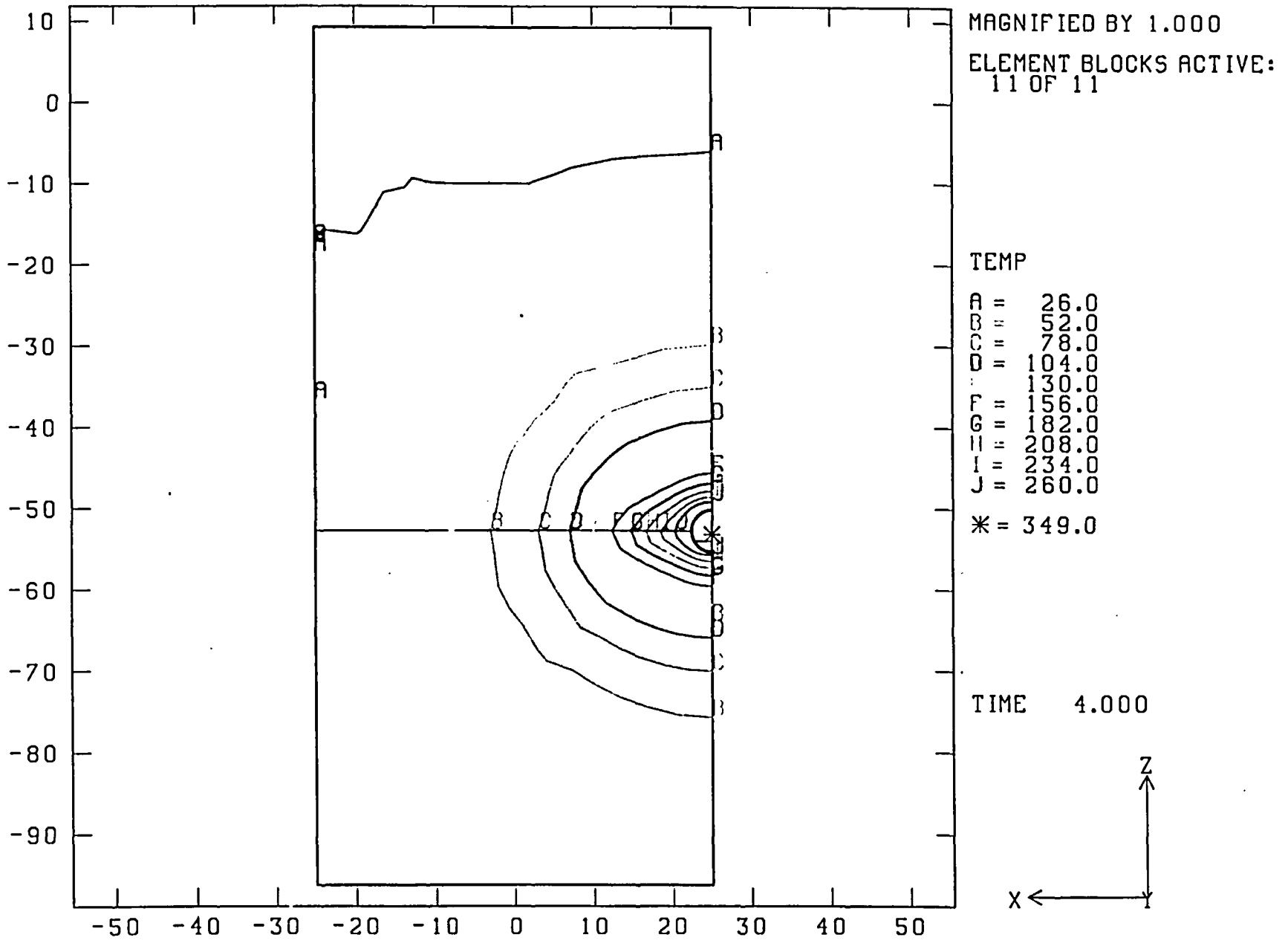

Figure C-10: Cut away through midpoint of tunnel (through 4 years of heating)

Appendix D: Predicted Displacement-Time Histories at Selected MPBX Anchor Locations

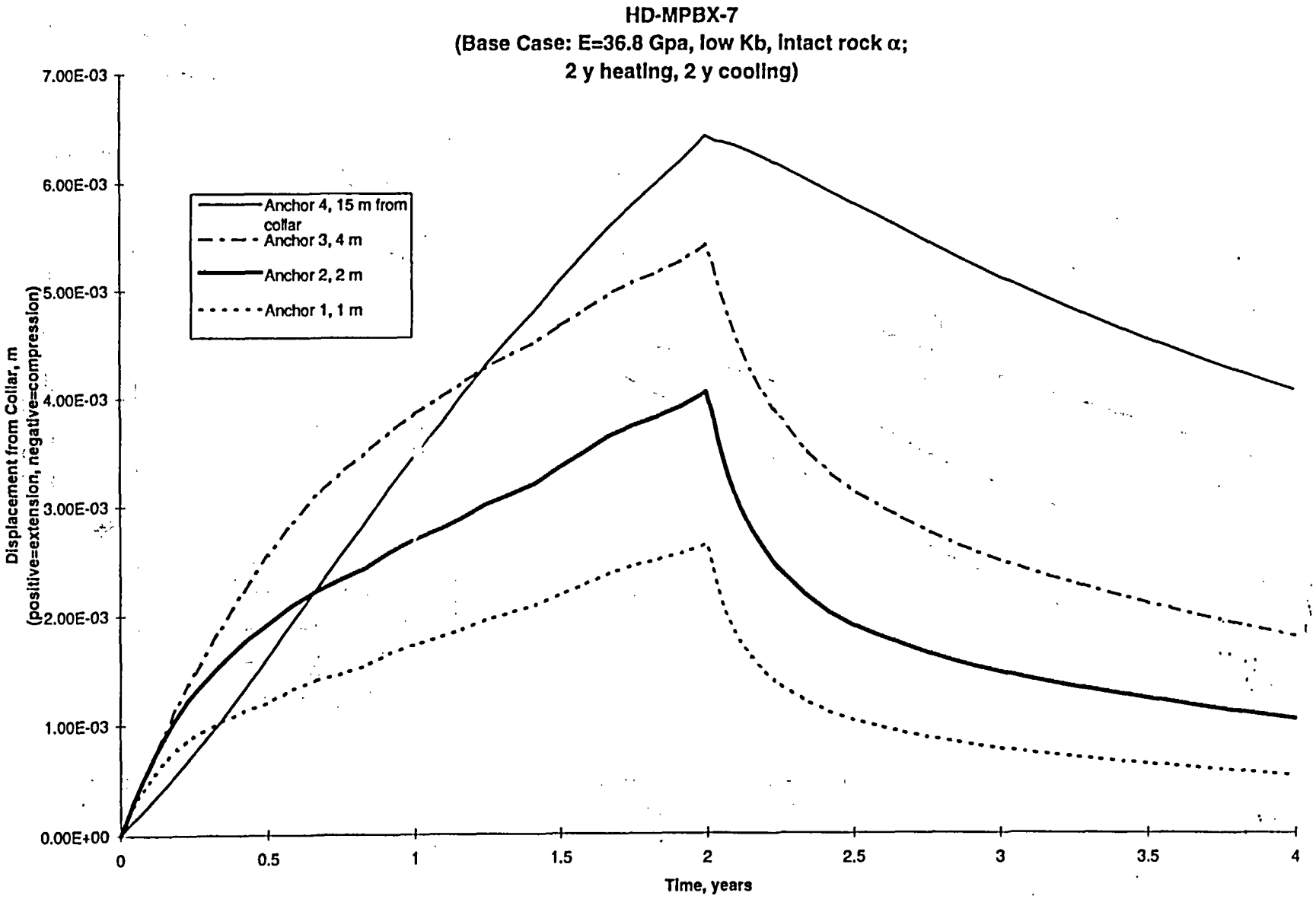
HD-MPBX-7
(Base Case: E=36.8 Gpa, low Kb, intact rock α;
2 y heating, 2 y cooling)
Anchor 4, 15 m from collar
Anchor 3, 4 m
Anchor 2, 2 m
Anchor 1, 1 m
Displacement from Collar, m
(positive=extension, negative=compression)
7.00E-03
6.00E-03
5.00E-03
4.00E-03
3.00E-03
2.00E-03
1.00E-03
0.00E+00
0
0.5
1
1.5
2
2.5
3
3.5
4
Time, years

Figure D-1

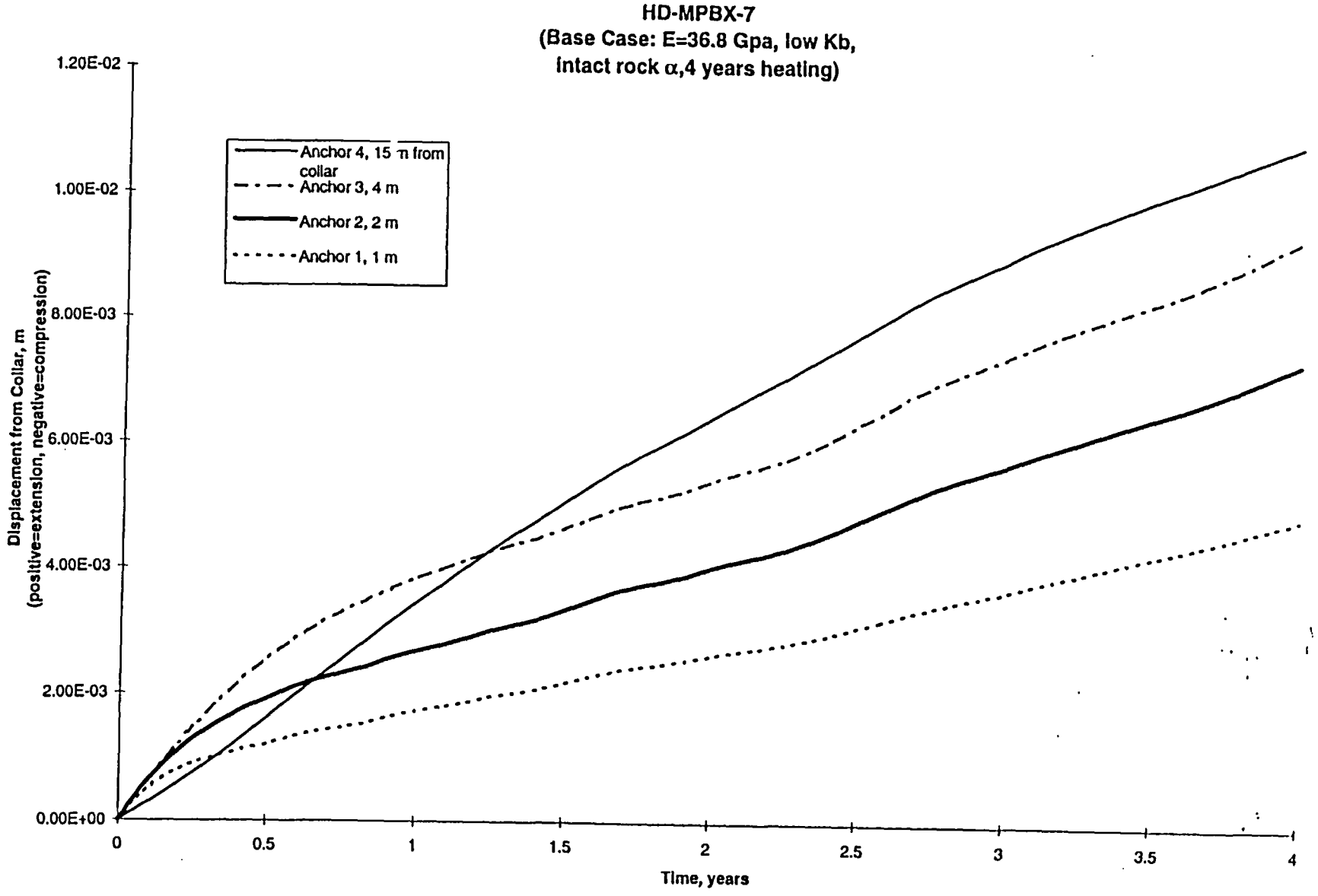
HD-MPBX-7
(Base Case: E=36.8 Gpa, low Kb,
Intact rock α,4 years heating)
Anchor 4, 15 m from collar
Anchor 3, 4 m
Anchor 2, 2 m
Anchor 1, 1 m
Displacement from Collar, m
(positive=extension, negative=compression)
1.20E-02
1.00E-02
8.00E-03
6.00E-03
4.00E-03
2.00E-03
0.00E+00
0
0.5
1
1.5
2
2.5
3
3.5
4
Time, years

Figure D-2

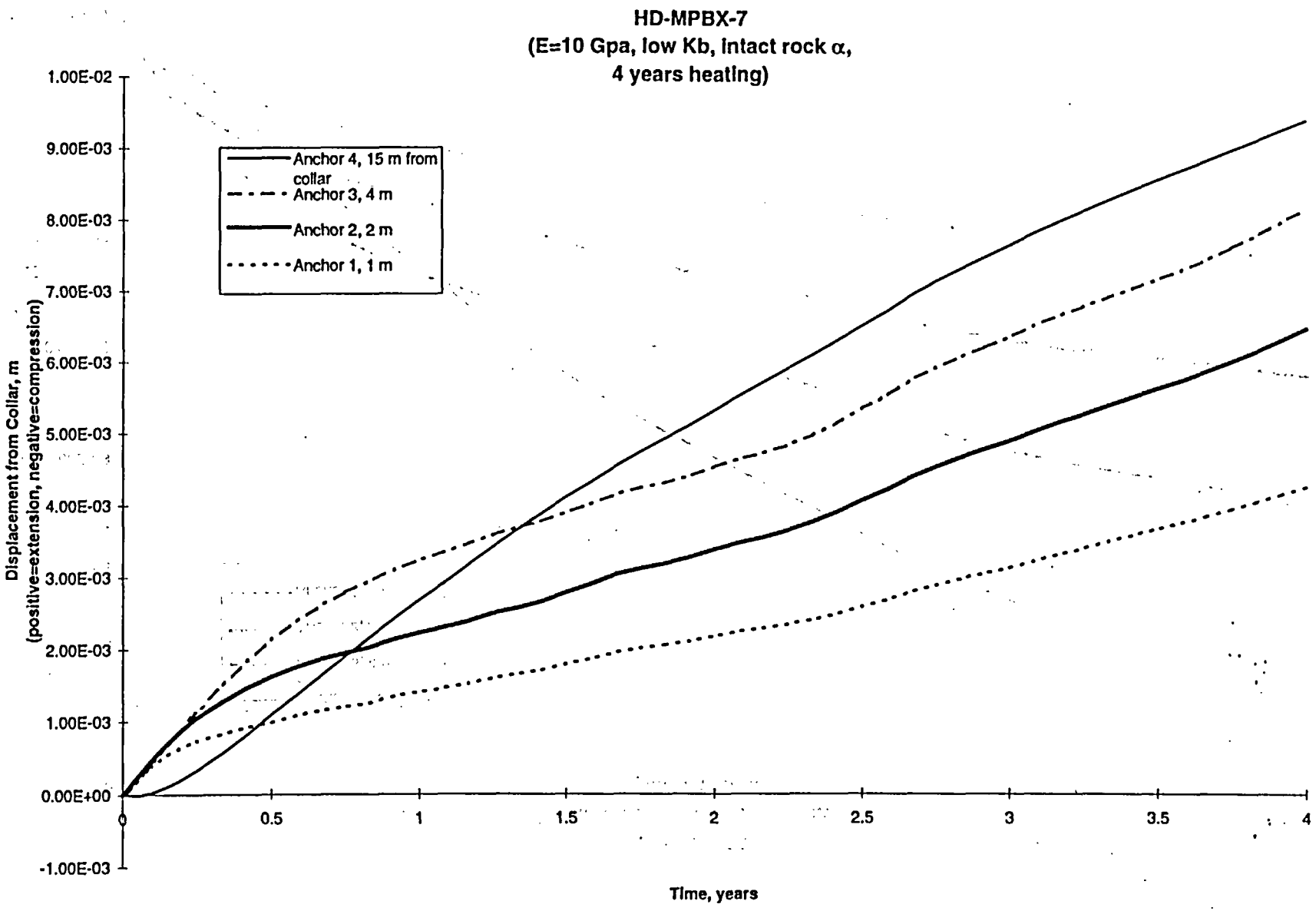
HD-MPBX-7
(E=10 Gpa, low Kb, intact rock α,
4 years heating)
Anchor 4, 15 m from collar
Anchor 3, 4 m
Anchor 2, 2 m
Anchor 1, 1 m
Displacement from Collar, m
(positive=extension, negative=compression)
1.00E-02
9.00E-03
8.00E-03
7.00E-03
6.00E-03
5.00E-03
4.00E-03
3.00E-03
2.00E-03
1.00E-03
0.00E+00
-1.00E-03
0
0.5
1
1.5
2
2.5
3
3.5
4
Time, years

Figure D-3

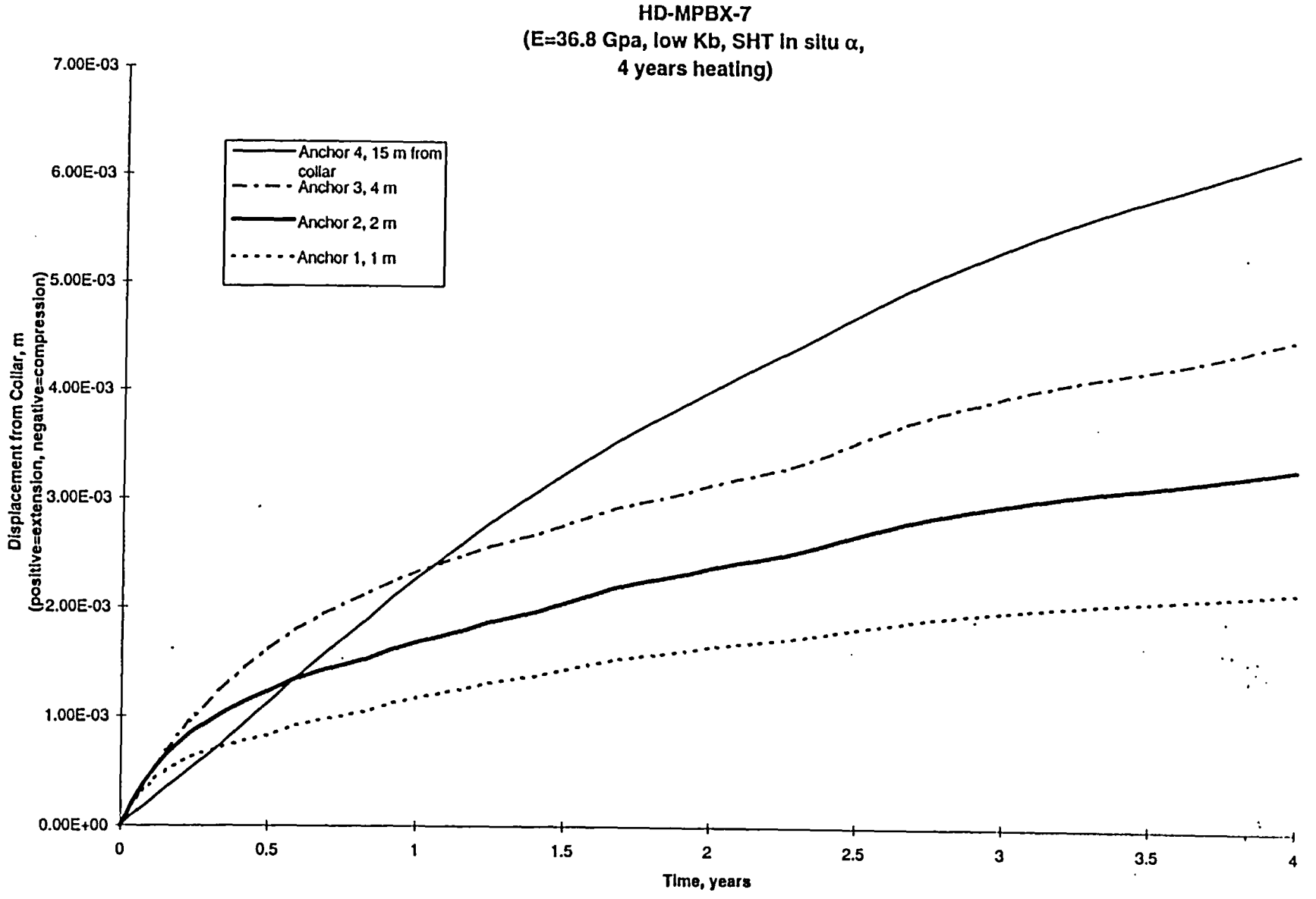
HD-MPBX-7
(E=36.8 Gpa, low Kb, SHT in situ α,
4 years heating)
Anchor 4, 15 m from collar
Anchor 3, 4 m
Anchor 2, 2 m
Anchor 1, 1 m
Displacement from Collar, m
(positive=extension, negative=compression)
7.00E-03
6.00E-03
5.00E-03
4.00E-03
3.00E-03
2.00E-03
1.00E-03
0.00E+00
0
0.5
1
1.5
2
2.5
3
3.5
4
Time, years

Figure D-4

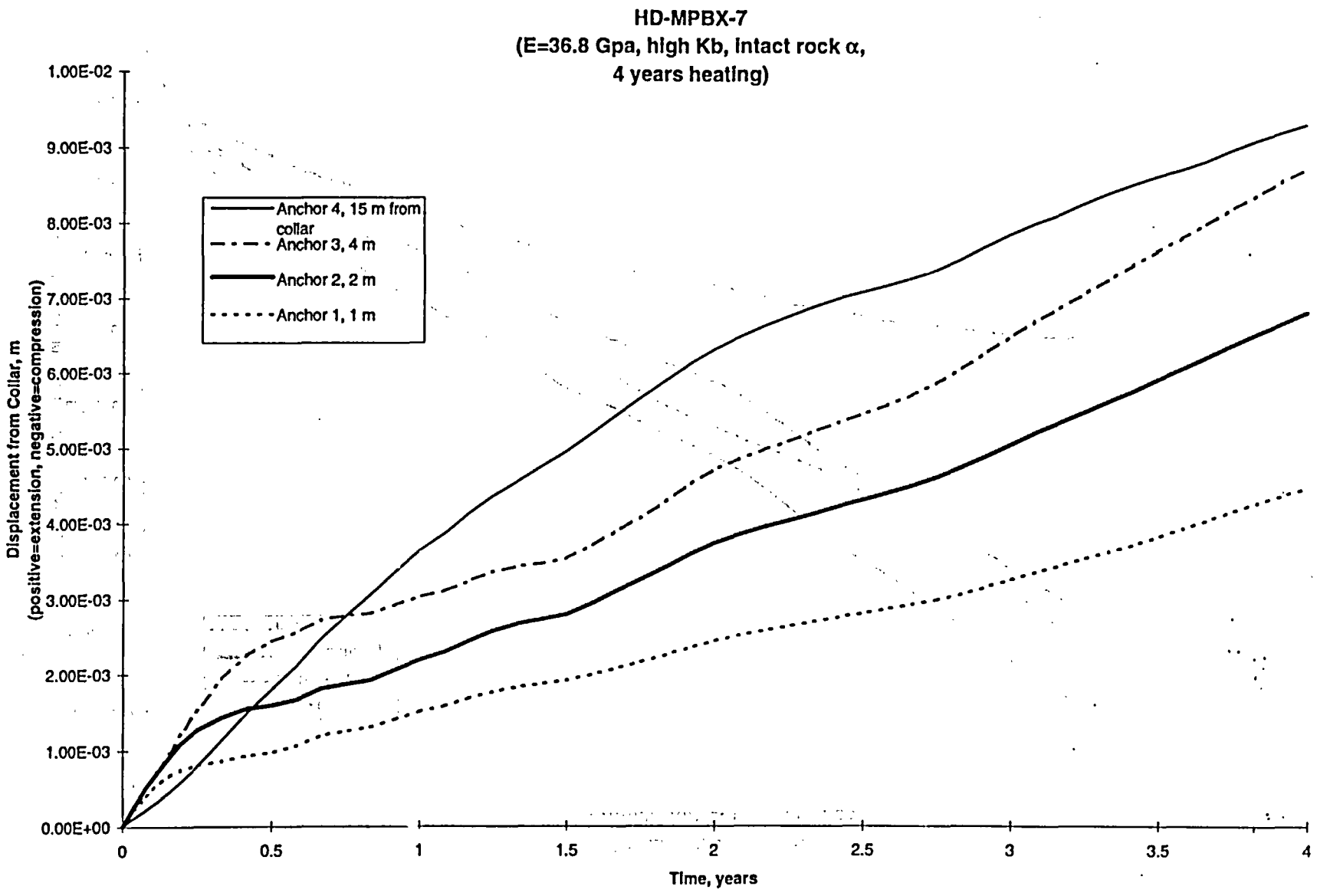
HD-MPBX-7
(E=36.8 Gpa, high Kb, intact rock α,
4 years heating)
Anchor 4, 15 m from collar
Anchor 3, 4 m
Anchor 2, 2 m
Anchor 1, 1 m
Displacement from Collar, m
(positive=extension, negative=compression)
1.00E-02
9.00E-03
8.00E-03
7.00E-03
6.00E-03
5.00E-03
4.00E-03
3.00E-03
2.00E-03
1.00E-03
0.00E+00
0
0.5
1
1.5
2
2.5
3
3.5
4
Time, years

Figure D-5

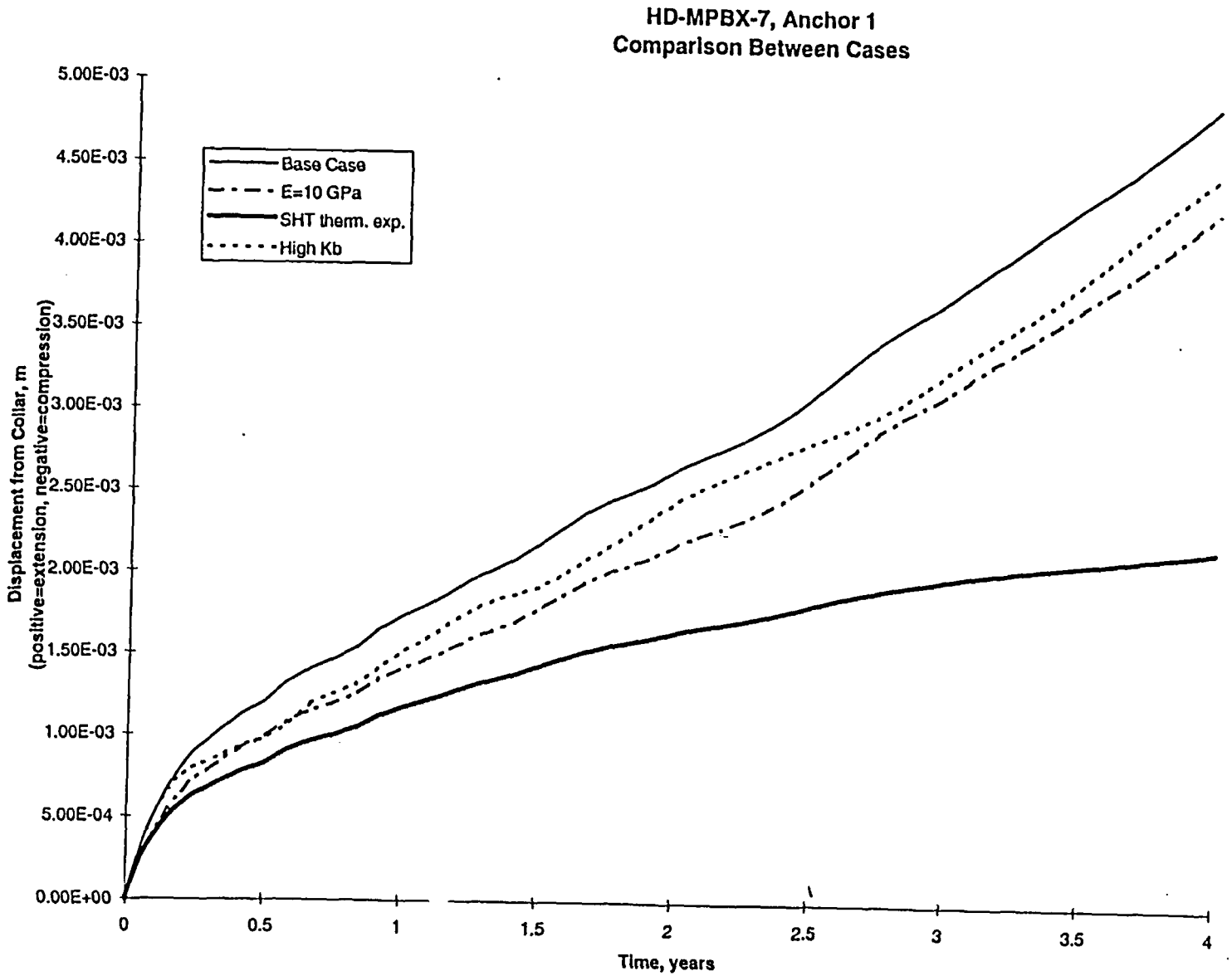
HD-MPBX-7, Anchor 1
Comparison Between Cases
Base Case
E=10 GPa
SHT therm. exp.
High Kb
Displacement from Collar, m
(positive=extension, negative=compression)
5.00E-03
4.50E-03
4.00E-03
3.50E-03
3.00E-03
2.50E-03
2.00E-03
1.50E-03
1.00E-03
5.00E-04
0.00E+00
0
0.5
1
1.5
2
2.5
3
3.5
4
Time, years

Figure D-6

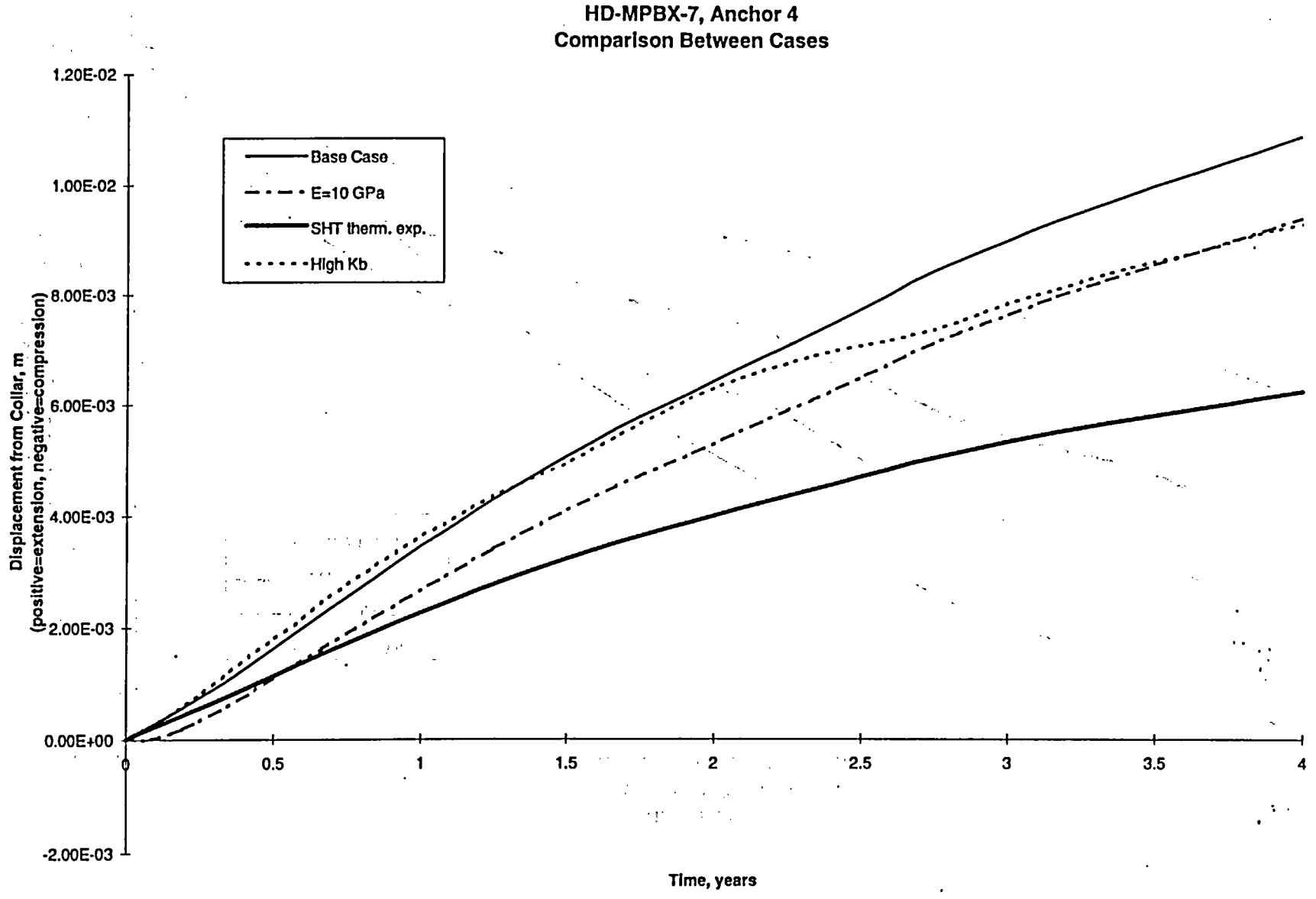
HD-MPBX-7, Anchor 4
Comparison Between Cases
Base Case
E=10 GPa
SHT therm. exp.
High Kb
Displacement from Collar, m
(positive=extension, negative=compression)
1.20E-02
1.00E-02
8.00E-03
6.00E-03
4.00E-03
2.00E-03
0.00E+00
-2.00E-03
0
0.5
1
1.5
2
2.5
3
3.5
4
Time, years

Figure D-7

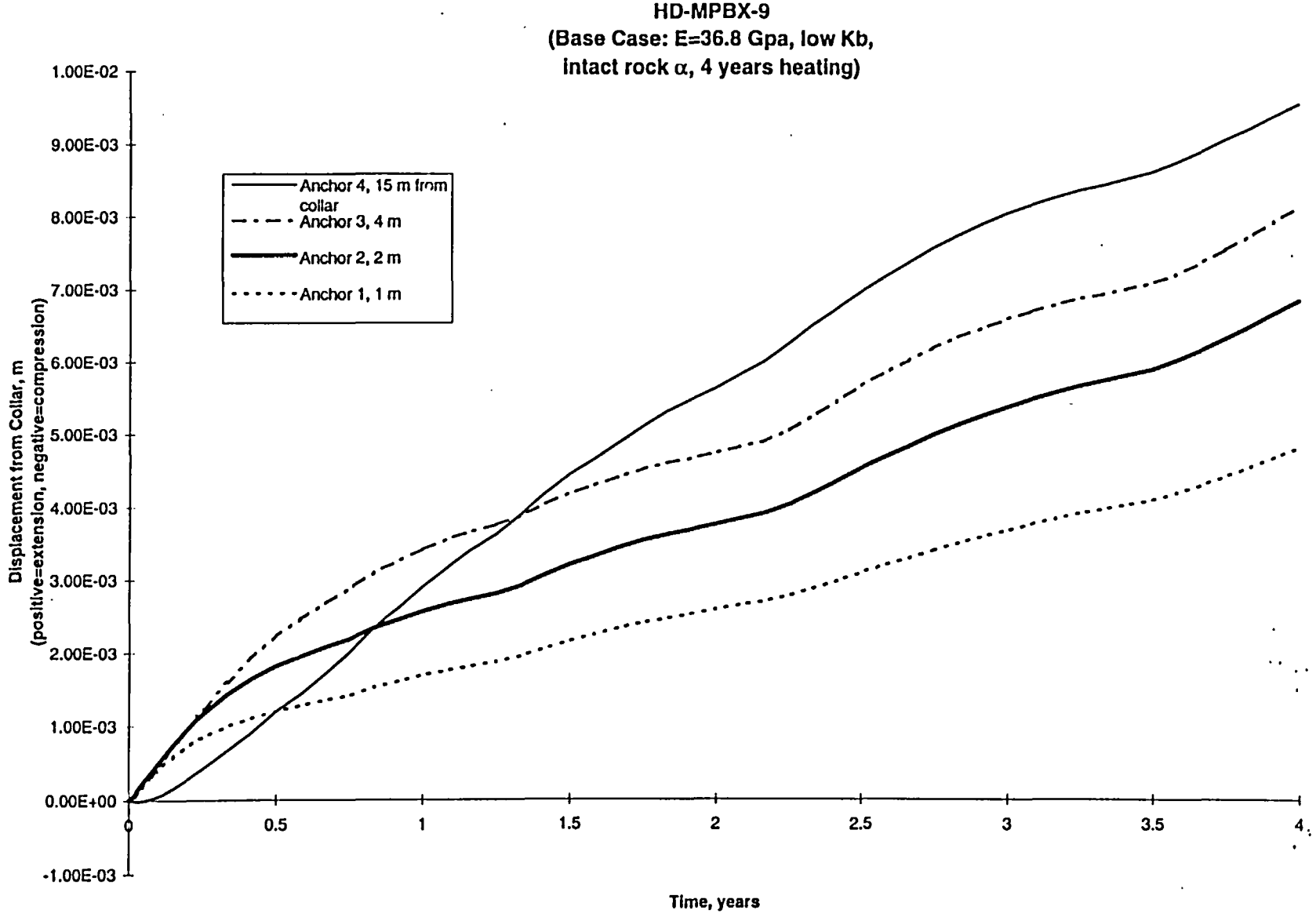
HD-MPBX-9
(Base Case: E=36.8 Gpa, low Kb,
intact rock α, 4 years heating)
Anchor 4, 15 m from collar
Anchor 3, 4 m
Anchor 2, 2 m
Anchor 1, 1 m
Displacement from Collar, m
(positive=extension, negative=compression)
1.00E-02
9.00E-03
8.00E-03
7.00E-03
6.00E-03
5.00E-03
4.00E-03
3.00E-03
2.00E-03
1.00E-03
0.00E+00
-1.00E-03
0
0.5
1
1.5
2
2.5
3
3.5
4
Time, years

Figure D-8

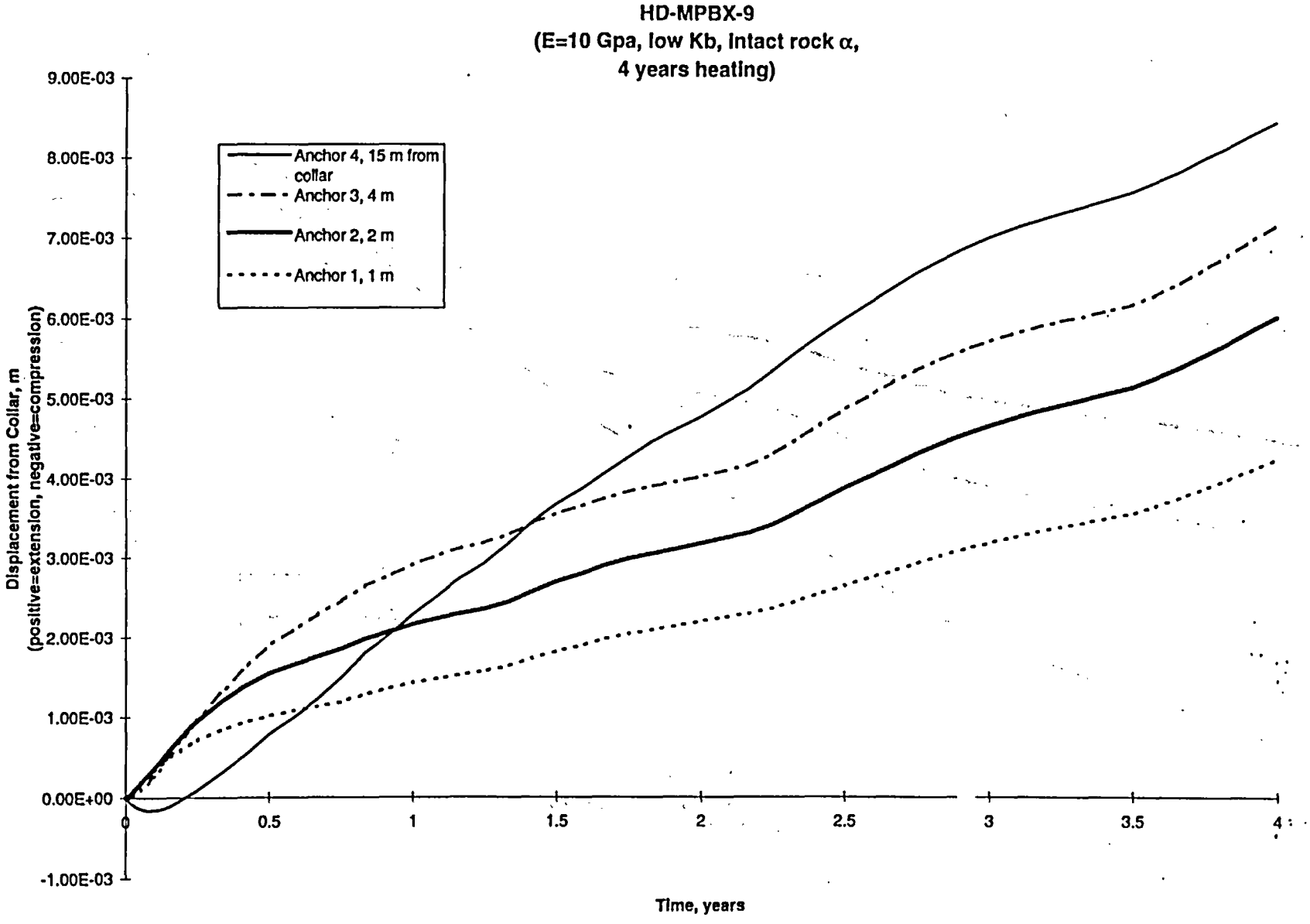
HD-MPBX-9
(E=10 Gpa, low Kb, intact rock α,
4 years heating)
Anchor 4, 15 m from collar
Anchor 3, 4 m
Anchor 2, 2 m
Anchor 1, 1 m
Displacement from Collar, m
(positive=extension, negative=compression)
9.00E-03
8.00E-03
7.00E-03
6.00E-03
5.00E-03
4.00E-03
3.00E-03
2.00E-03
1.00E-03
0.00E+00
-1.00E-03
0
0.5
1
1.5
2
2.5
3
3.5
4
Time, years

Figure D-9

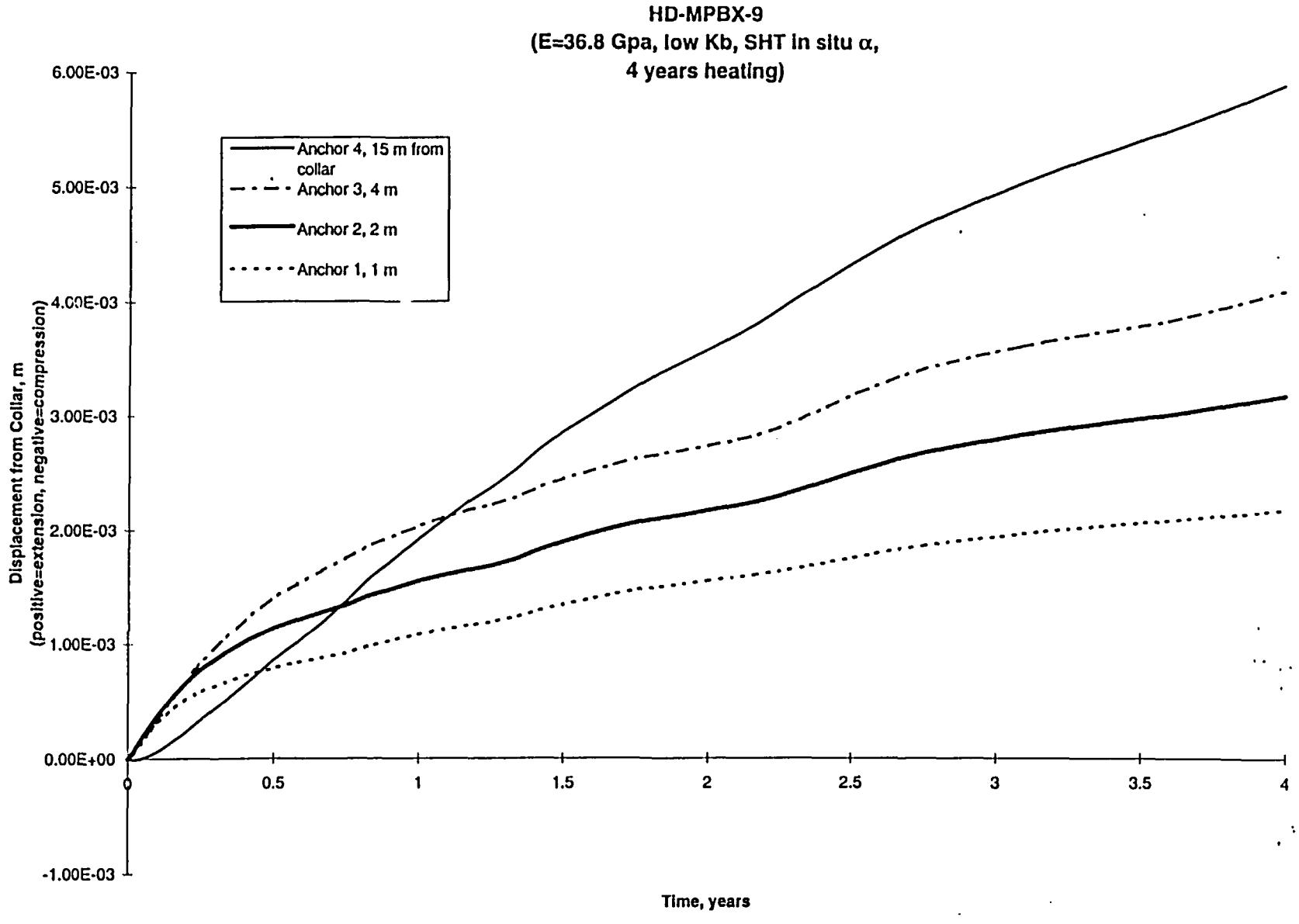
HD-MPBX-9
(E=36.8 Gpa, low Kb, SHT in situ α,
4 years heating)
Anchor 4, 15 m from collar
Anchor 3, 4 m
Anchor 2, 2 m
Anchor 1, 1 m
Displacement from Collar, m
(positive=extension, negative=compression)
6.00E-03
5.00E-03
4.00E-03
3.00E-03
2.00E-03
1.00E-03
0.00E+00
-1.00E-03
0
0.5
1
1.5
2
2.5
3
3.5
4
Time, years

Figure D-10

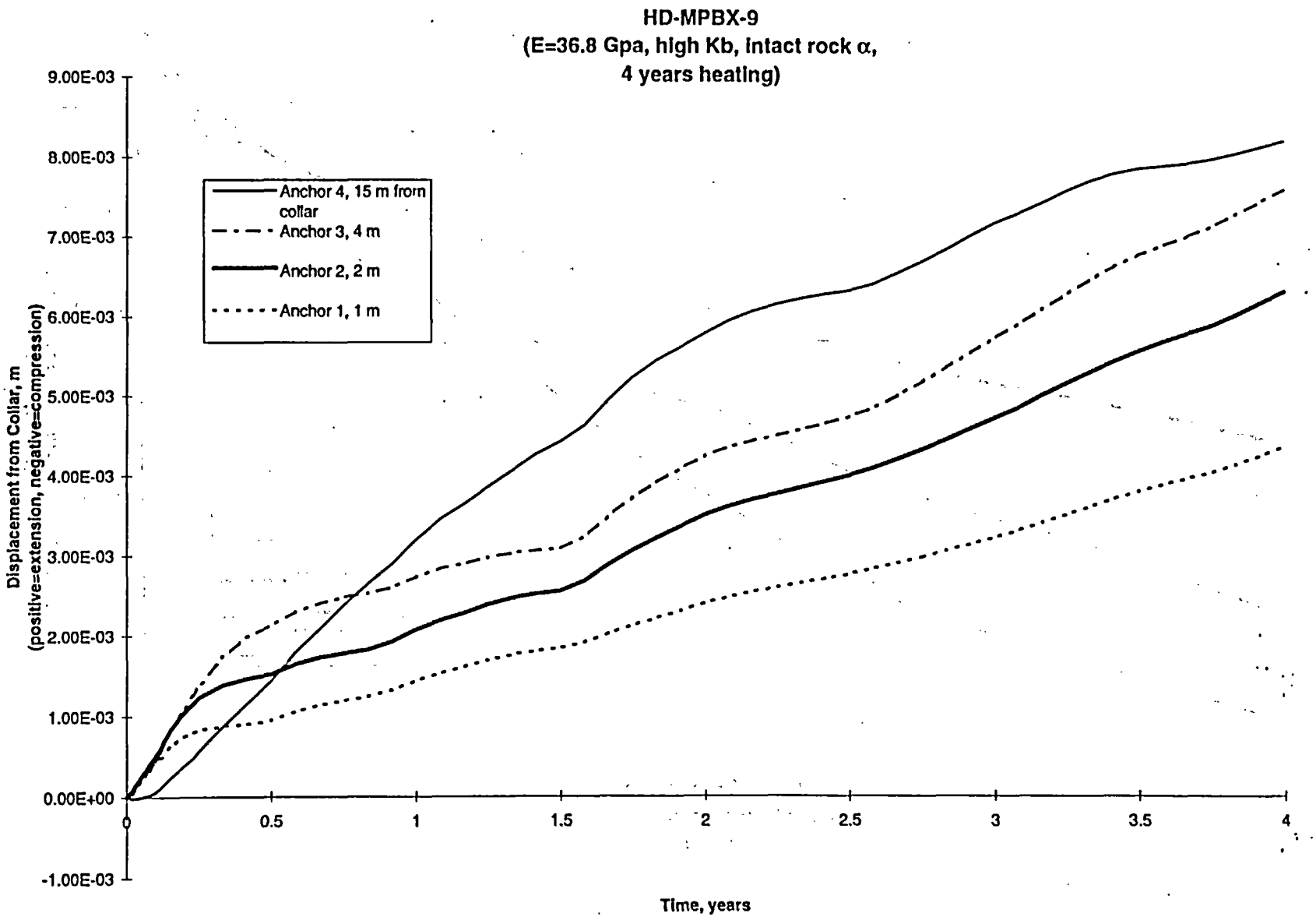
HD-MPBX-9
(E=36.8 Gpa, high Kb, intact rock α,
4 years heating)
Anchor 4, 15 m from collar
Anchor 3, 4 m
Anchor 2, 2 m
Anchor 1, 1 m
Displacement from Collar, m
(positive=extension, negative=compression)
9.00E-03
8.00E-03
7.00E-03
6.00E-03
5.00E-03
4.00E-03
3.00E-03
2.00E-03
1.00E-03
0.00E+00
-1.00E-03
0
0.5
1
1.5
2
2.5
3
3.5
4
Time, years

Figure D-11

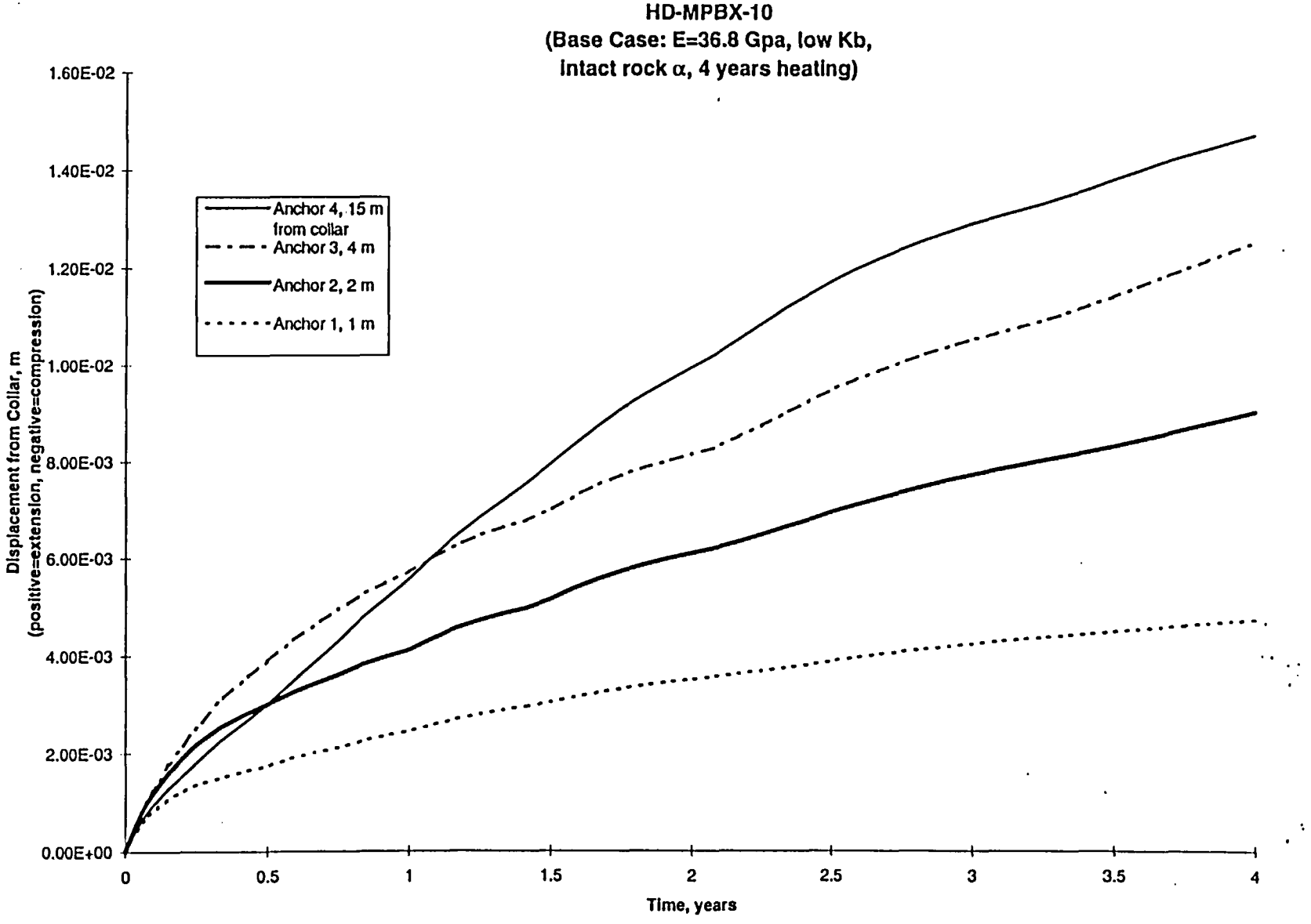
HD-MPBX-10
(Base Case: E=36.8 Gpa, low Kb,
Intact rock α, 4 years heating)
Displacement from Collar, m
(positive=extension, negative=compression)
1.60E-02
1.40E-02
1.20E-02
1.00E-02
8.00E-03
6.00E-03
4.00E-03
2.00E-03
0.00E+00
Anchor 4, 15 m from collar
Anchor 3, 4 m
Anchor 2, 2 m
Anchor 1, 1 m
0
0.5
1
1.5
2
2.5
3
3.5
4
Time, years

Figure D-12

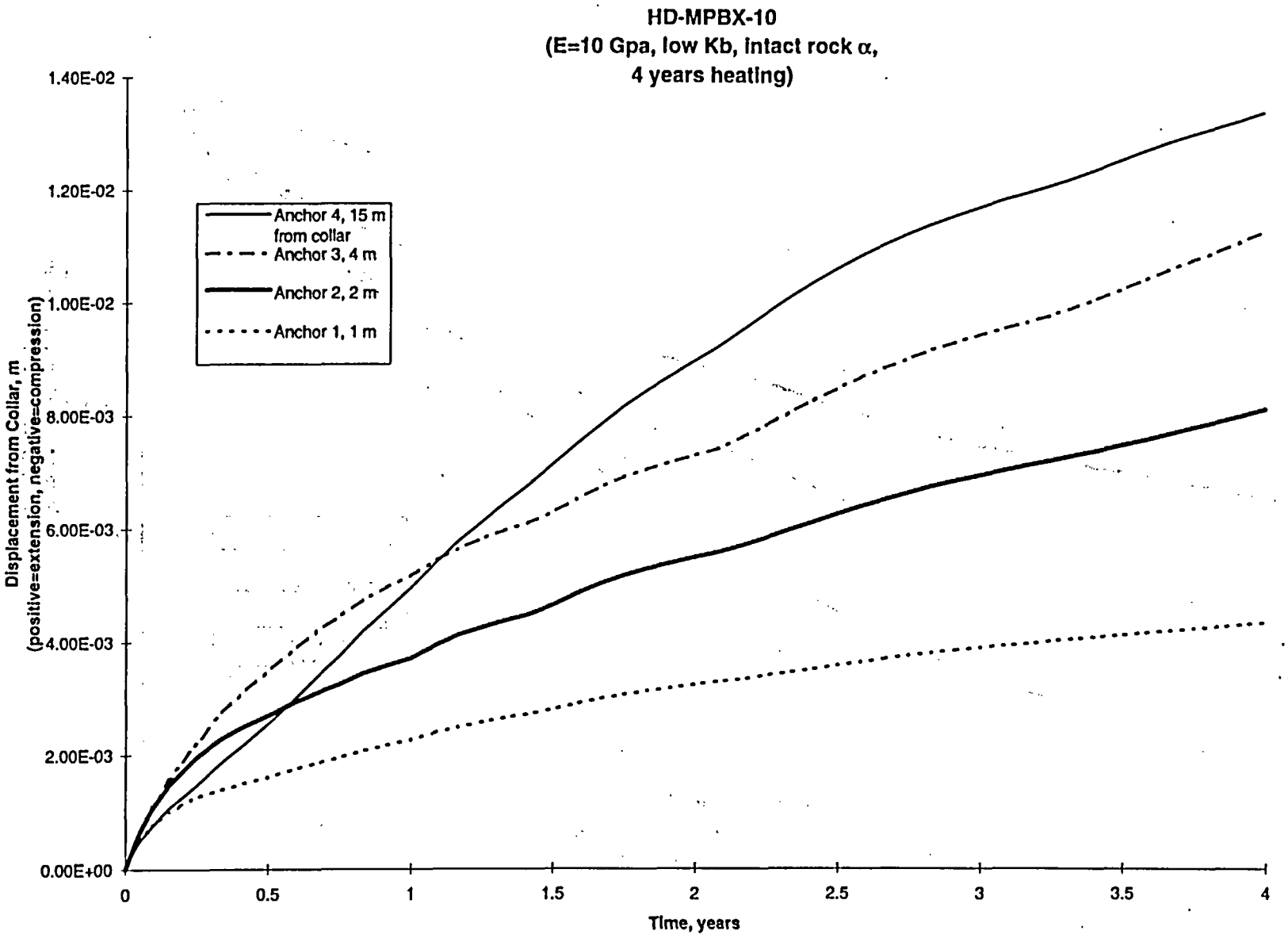
HD-MPBX-10
(E=10 Gpa, low Kb, intact rock α,
4 years heating)
Anchor 4, 15 m from collar
Anchor 3, 4 m
Anchor 2, 2 m
Anchor 1, 1 m
Displacement from Collar, m
(positive=extension, negative=compression)
1.40E-02
1.20E-02
1.00E-02
8.00E-03
6.00E-03
4.00E-03
2.00E-03
0.00E+00
0
0.5
1
1.5
2
2.5
3
3.5
4
Time, years

Figure D-13

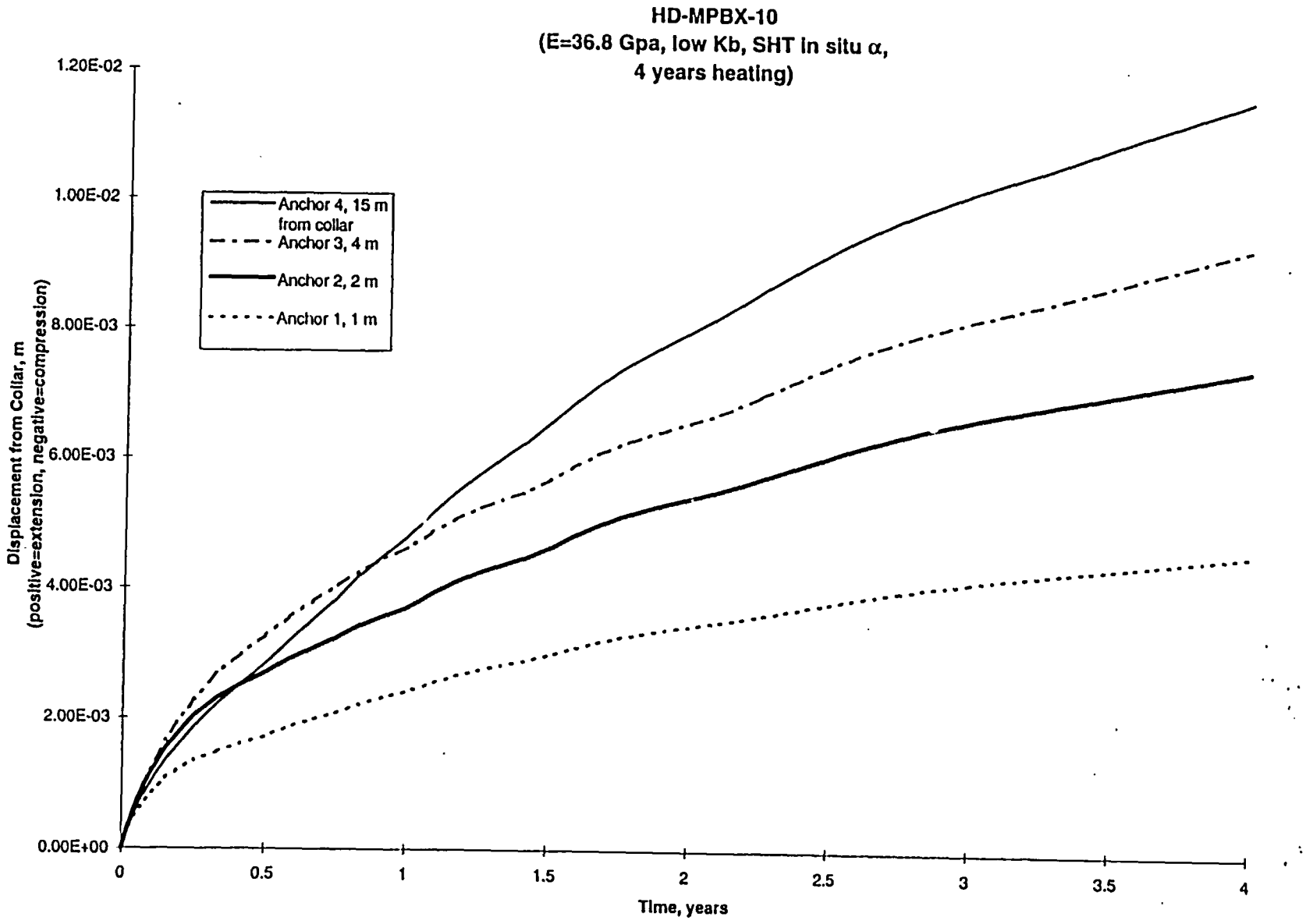
HD-MPBX-10
(E=36.8 Gpa, low Kb, SHT in situ α,
4 years heating)
Anchor 4, 15 m from collar
Anchor 3, 4 m
Anchor 2, 2 m
Anchor 1, 1 m
Displacement from Collar, m
(positive=extension, negative=compression)
1.20E-02
1.00E-02
8.00E-03
6.00E-03
4.00E-03
2.00E-03
0.00E+00
0
0.5
1
1.5
2
2.5
3
3.5
4
Time, years

Figure D-14

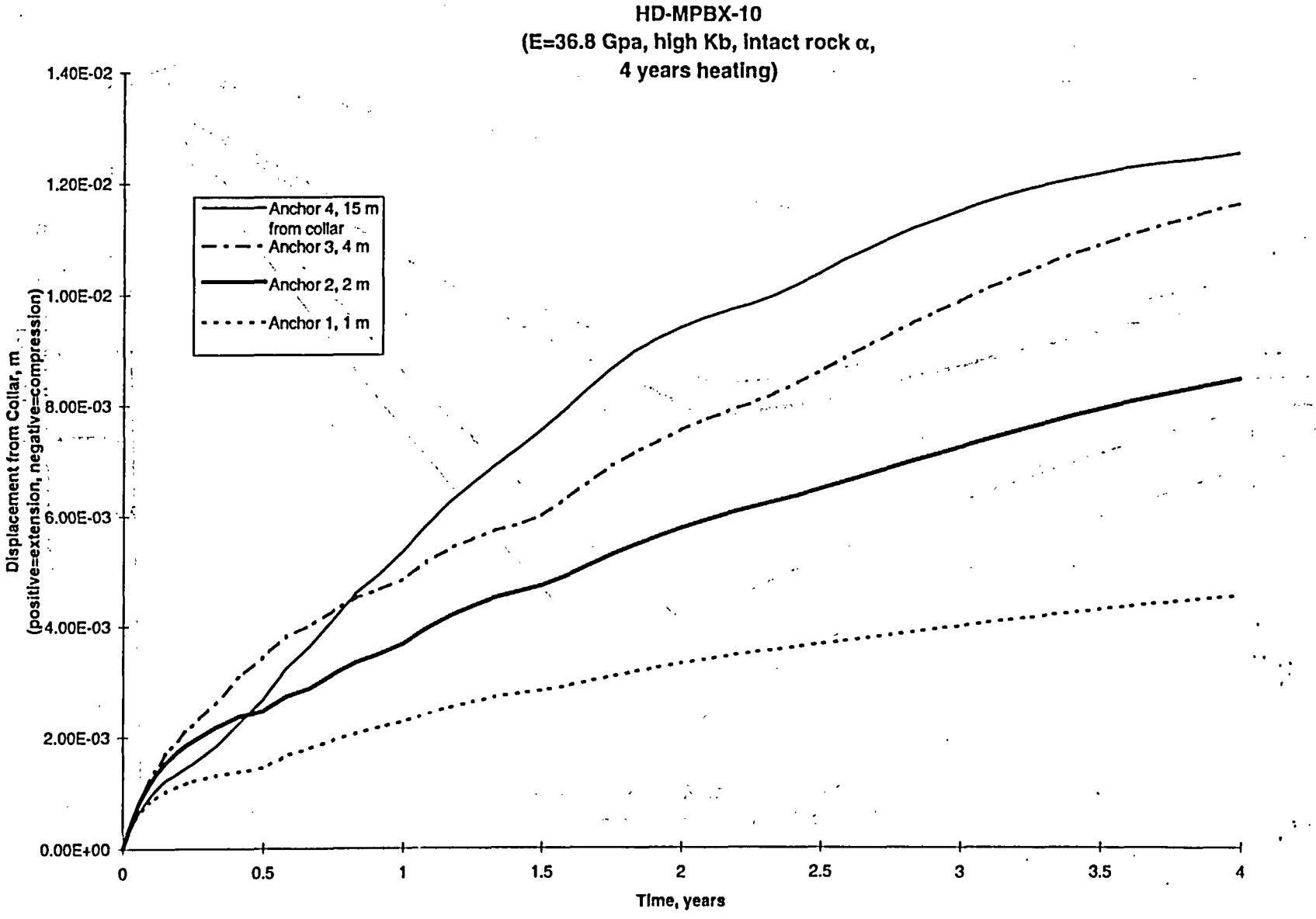
HD-MPBX-10
(E=36.8 Gpa, high Kb, intact rock α,
4 years heating)
Displacement from Collar, m
(positive=extension, negative=compression)
1.40E-02
1.20E-02
1.00E-02
8.00E-03
6.00E-03
4.00E-03
2.00E-03
0.00E+00
Anchor 4, 15 m from collar
Anchor 3, 4 m
Anchor 2, 2 m
Anchor 1, 1 m
0
0.5
1
1.5
2
2.5
3
3.5
4
Time, years

Figure D-15

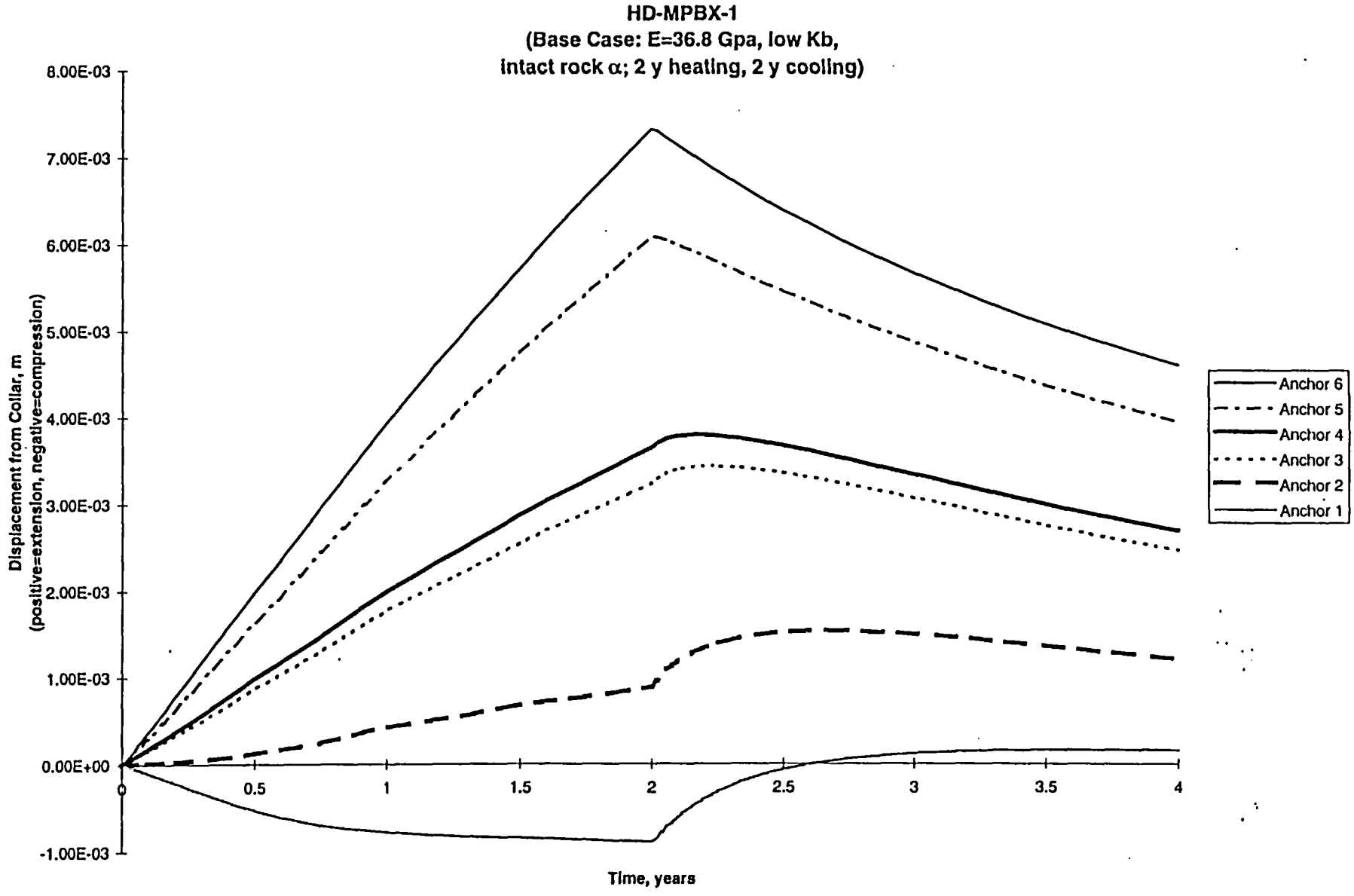
HD-MPBX-1
(Base Case: E=36.8 Gpa, low Kb,
Intact rock α; 2 y heating, 2 y cooling)
Displacement from Collar, m
(positive=extension, negative=compression)
8.00E-03
7.00E-03
6.00E-03
5.00E-03
4.00E-03
3.00E-03
2.00E-03
1.00E-03
0.00E+00
-1.00E-03
0
0.5
1
1.5
2
2.5
3
3.5
4
Time, years
Anchor 6
Anchor 5
Anchor 4
Anchor 3
Anchor 2
Anchor 1

Figure D-16

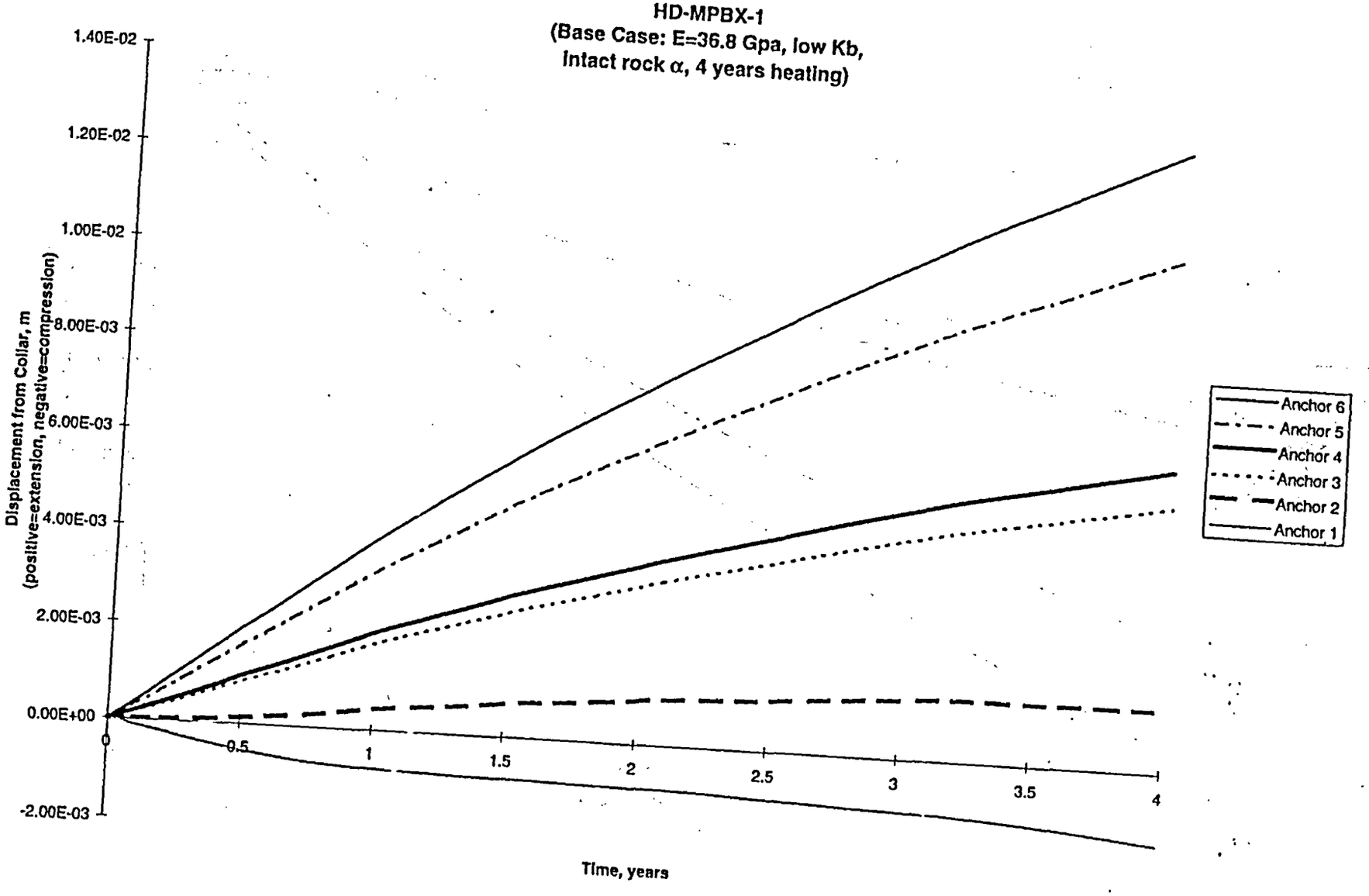
HD-MPBX-1
(Base Case: E=36.8 Gpa, low Kb,
Intact rock α, 4 years heating)
1.40E-02
1.20E-02
1.00E-02
8.00E-03
6.00E-03
4.00E-03
2.00E-03
0.00E+00
-2.00E-03
Displacement from Collar, m
(positive=extension, negative=compression)
0
0.5
1
1.5
2
2.5
3
3.5
4
Time, years
Anchor 6
Anchor 5
Anchor 4
Anchor 3
Anchor 2
Anchor 1

Figure D-17

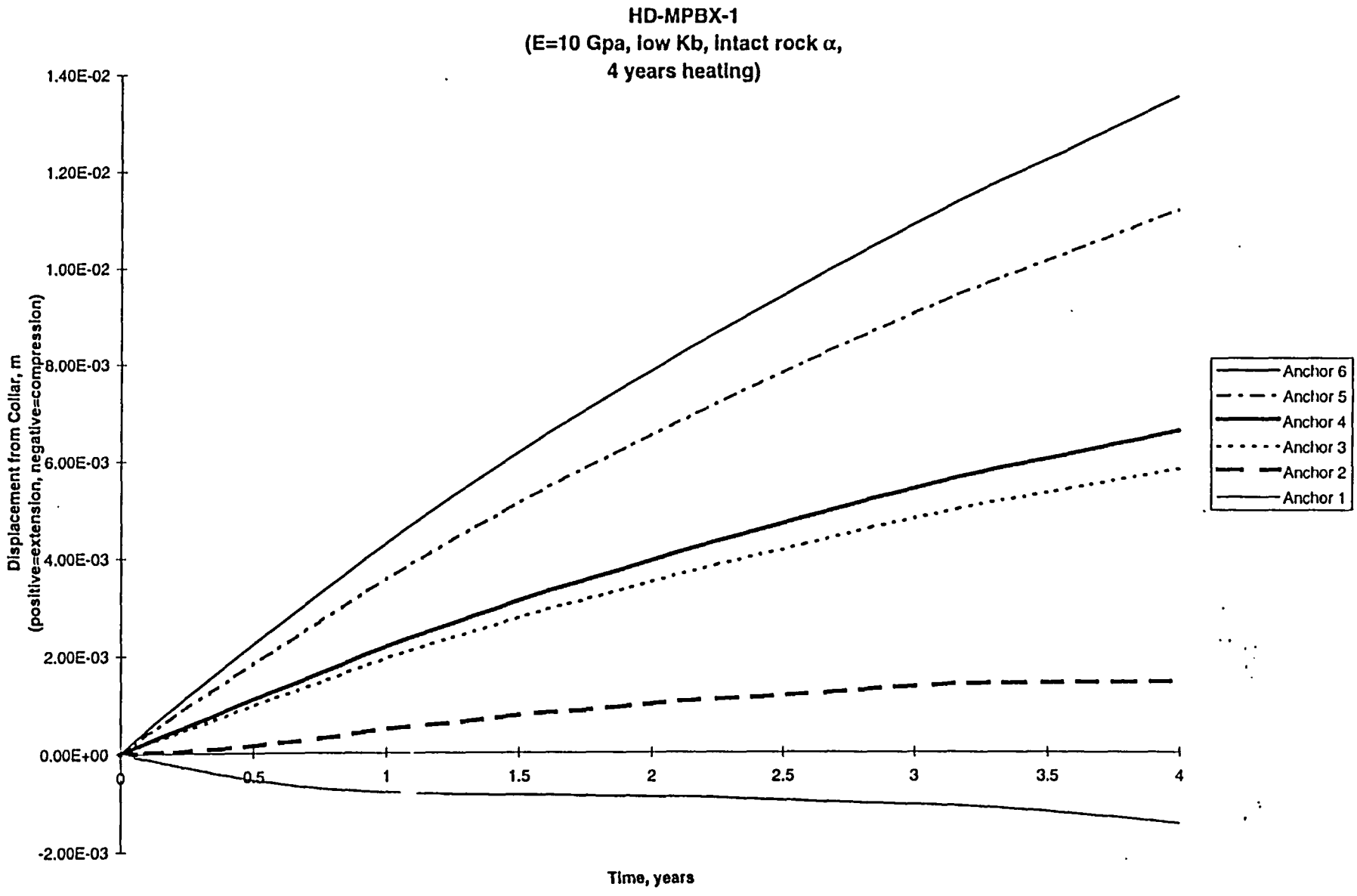
HD-MPBX-1
(E=10 Gpa, low Kb, intact rock α,
4 years heating)
Displacement from Collar, m
(positive=extension, negative=compression)
1.40E-02
1.20E-02
1.00E-02
8.00E-03
6.00E-03
4.00E-03
2.00E-03
0.00E+00
-2.00E-03
0
0.5
1
1.5
2
2.5
3
3.5
4
Time, years
Anchor 6
Anchor 5
Anchor 4
Anchor 3
Anchor 2
Anchor 1

Figure D-18

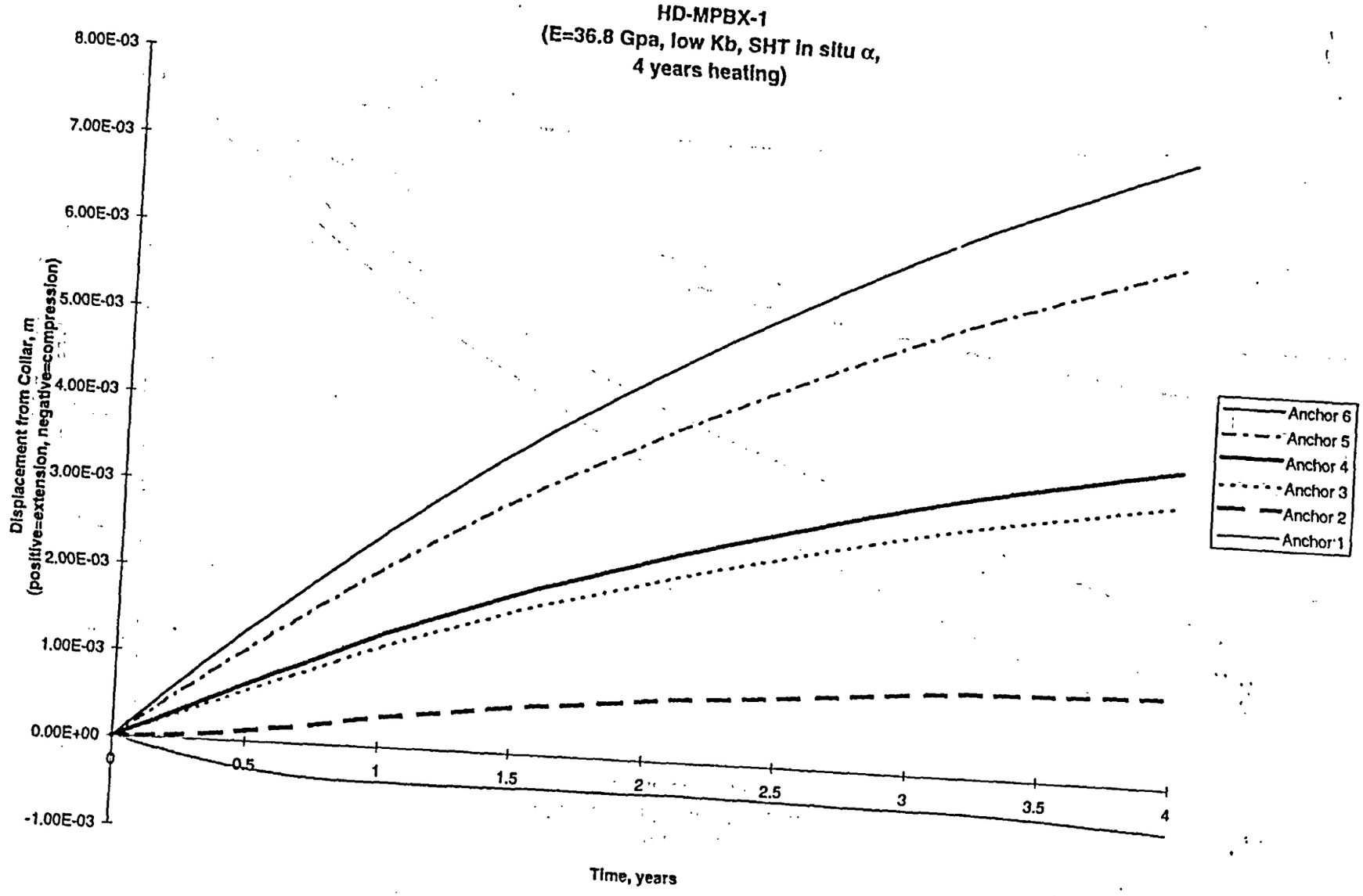
HD-MPBX-1
(E=36.8 Gpa, low Kb, SHT in situ α,
4 years heating)
8.00E-03
7.00E-03
6.00E-03
5.00E-03
4.00E-03
3.00E-03
2.00E-03
1.00E-03
0.00E+00
-1.00E-03
Displacement from Collar, m
(positive=extension, negative=compression)
0
0.5
1
1.5
2
2.5
3
3.5
4
Time, years
Anchor 6
Anchor 5
Anchor 4
Anchor 3
Anchor 2
Anchor 1

Figure D-19

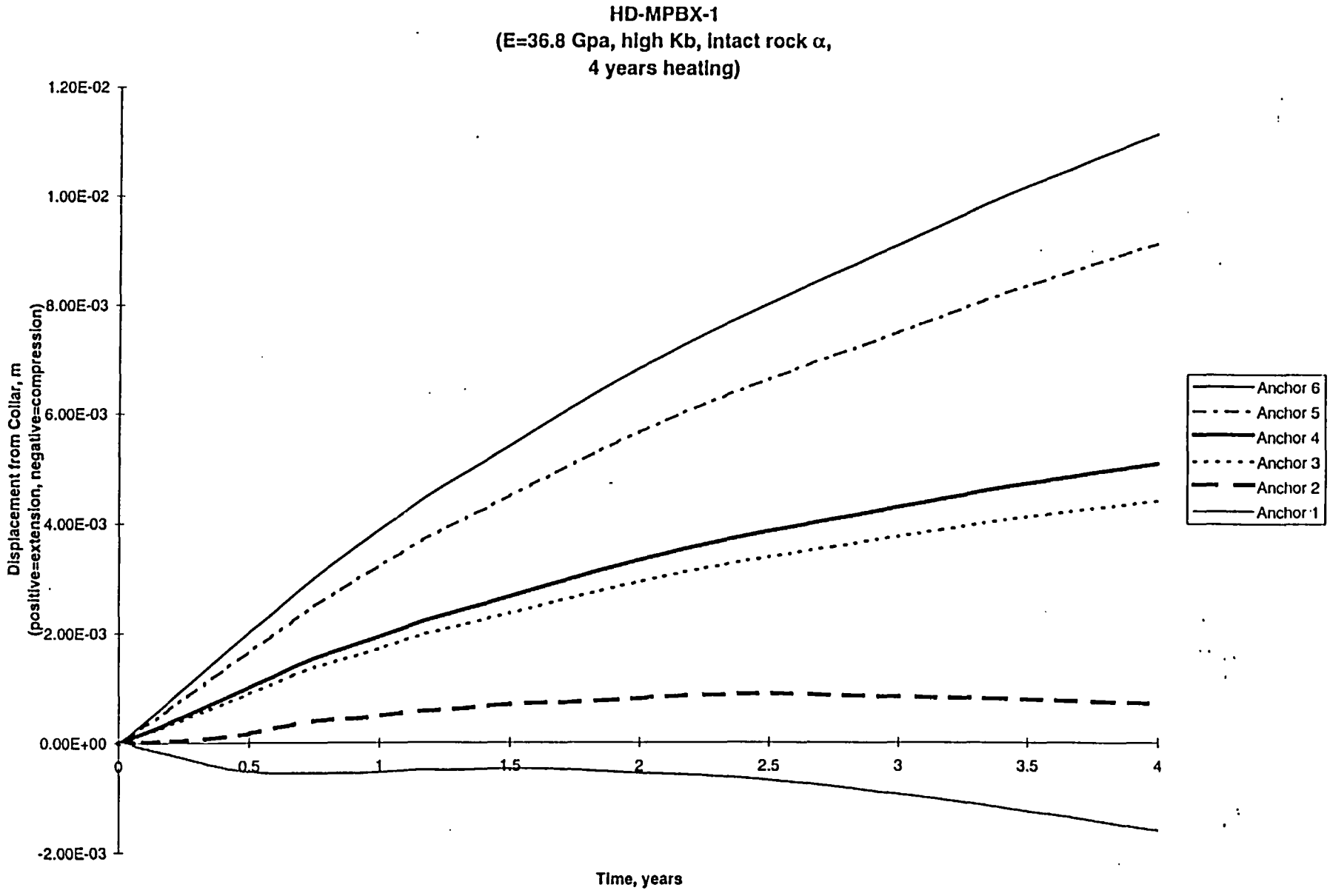
HD-MPBX-1
(E=36.8 Gpa, high Kb, intact rock α,
4 years heating)
1.20E-02
1.00E-02
8.00E-03
6.00E-03
4.00E-03
2.00E-03
0.00E+00
-2.00E-03
Displacement from Collar, m
(positive=extension, negative=compression)
0
0.5
1
1.5
2
2.5
3
3.5
4
Time, years
Anchor 6
Anchor 5
Anchor 4
Anchor 3
Anchor 2
Anchor 1

Figure D-20

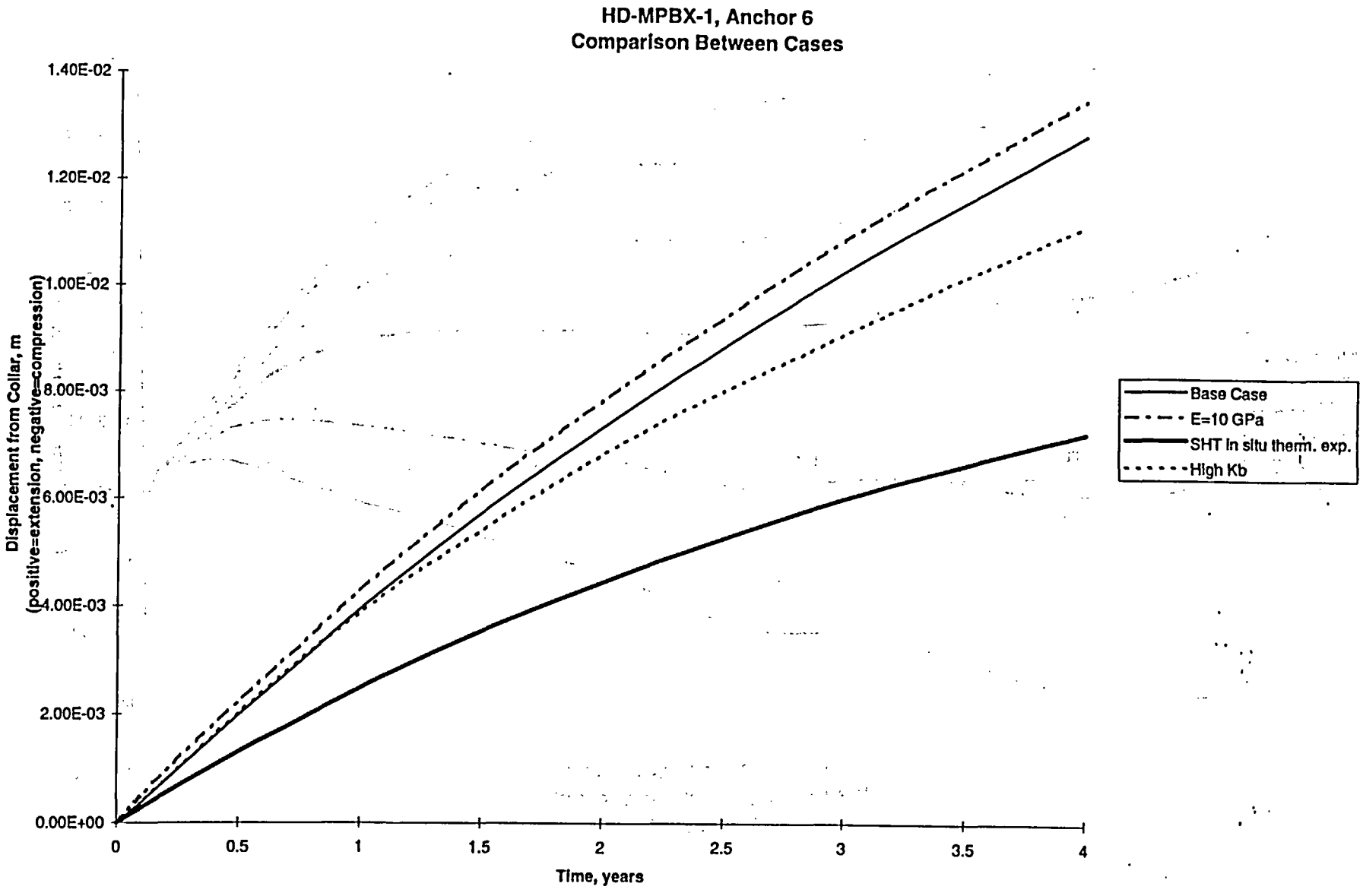
HD-MPBX-1, Anchor 6
Comparison Between Cases
1.40E-02
1.20E-02
1.00E-02
8.00E-03
6.00E-03
4.00E-03
2.00E-03
0.00E+00
Displacement from Collar, m
(positive=extension, negative=compression)
0
0.5
1
1.5
2
2.5
3
3.5
4
Time, years
Base Case
E=10 GPa
SHT In situ therm. exp.
High Kb

Figure D-21

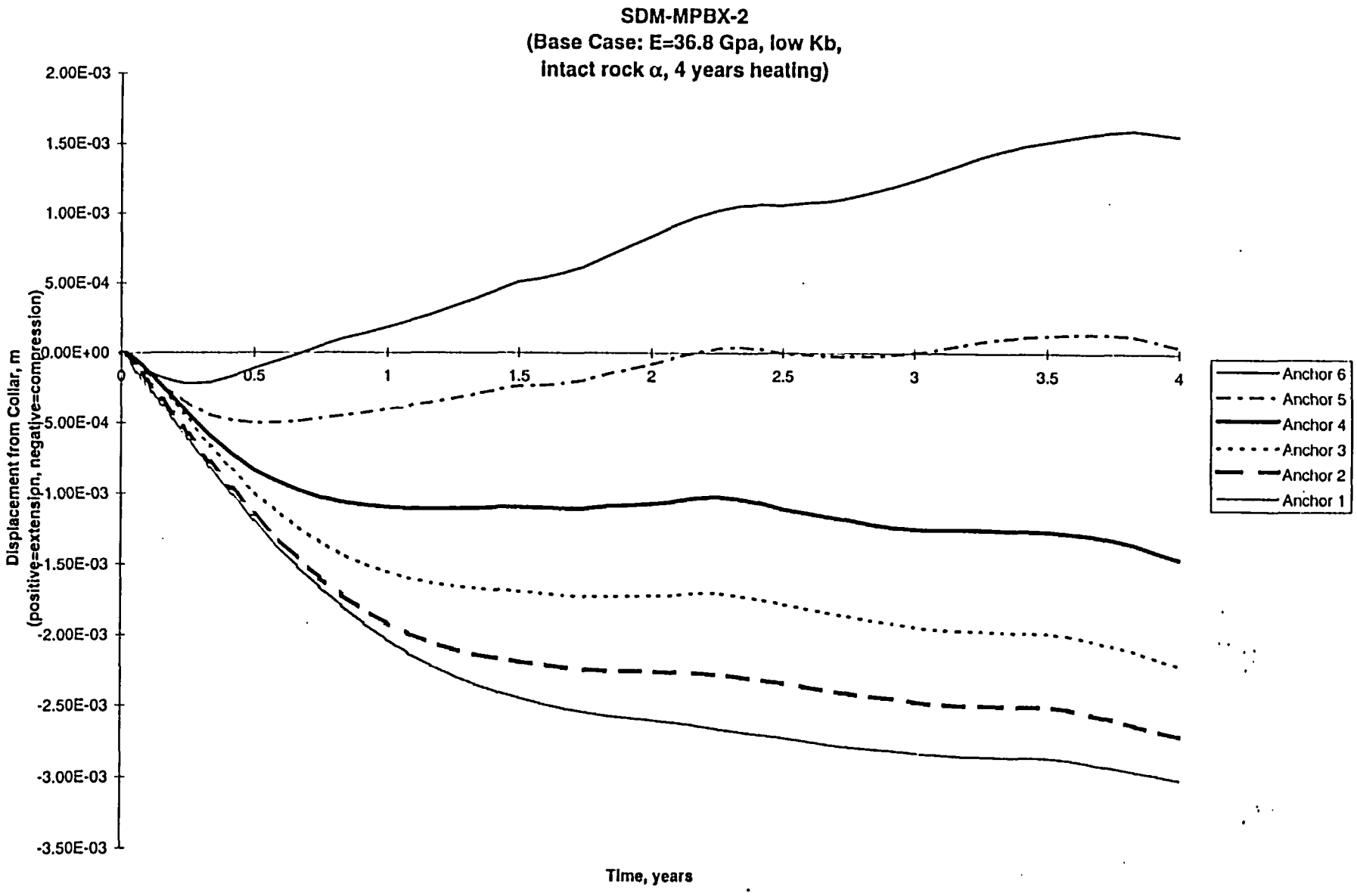
SDM-MPBX-2
(Base Case: E=36.8 Gpa, low Kb,
Intact rock α, 4 years heating)
2.00E-03
1.50E-03
1.00E-03
5.00E-04
0.00E+00
-5.00E-04
-1.00E-03
-1.50E-03
-2.00E-03
-2.50E-03
-3.00E-03
-3.50E-03
0
0.5
1
1.5
2
2.5
3
3.5
4
Displacement from Collar, m
(positive=extension, negative=compression)
Time, years
Anchor 6
Anchor 5
Anchor 4
Anchor 3
Anchor 2
Anchor 1

Figure D-22

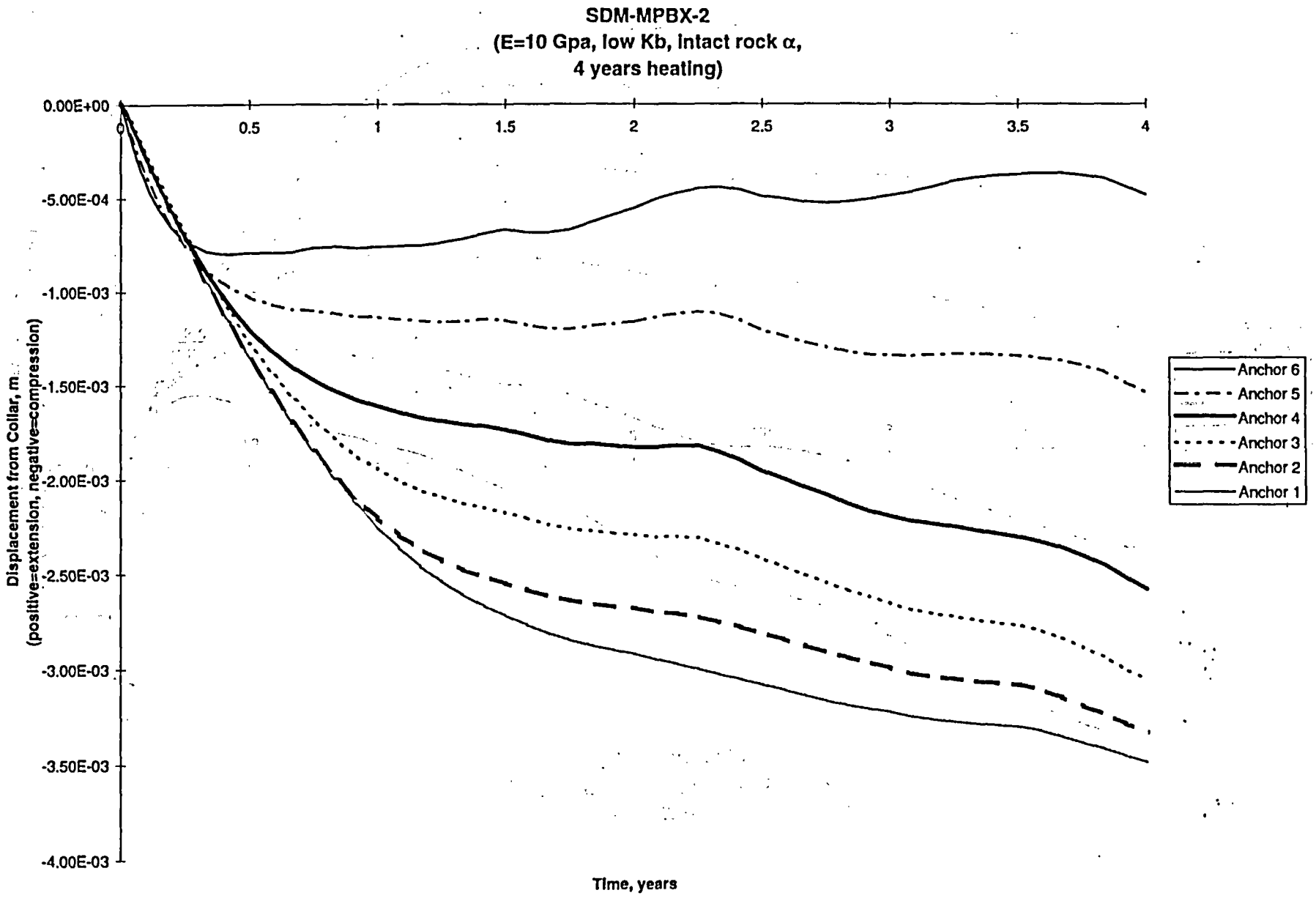
SDM-MPBX-2
(E=10 Gpa, low Kb, intact rock α,
4 years heating)
0.00E+00
-5.00E-04
-1.00E-03
-1.50E-03
-2.00E-03
-2.50E-03
-3.00E-03
-3.50E-03
-4.00E-03
0
0.5
1
1.5
2
2.5
3
3.5
4
Displacement from Collar, m
(positive=extension, negative=compression)
Time, years
Anchor 6
Anchor 5
Anchor 4
Anchor 3
Anchor 2
Anchor 1

Figure D-23

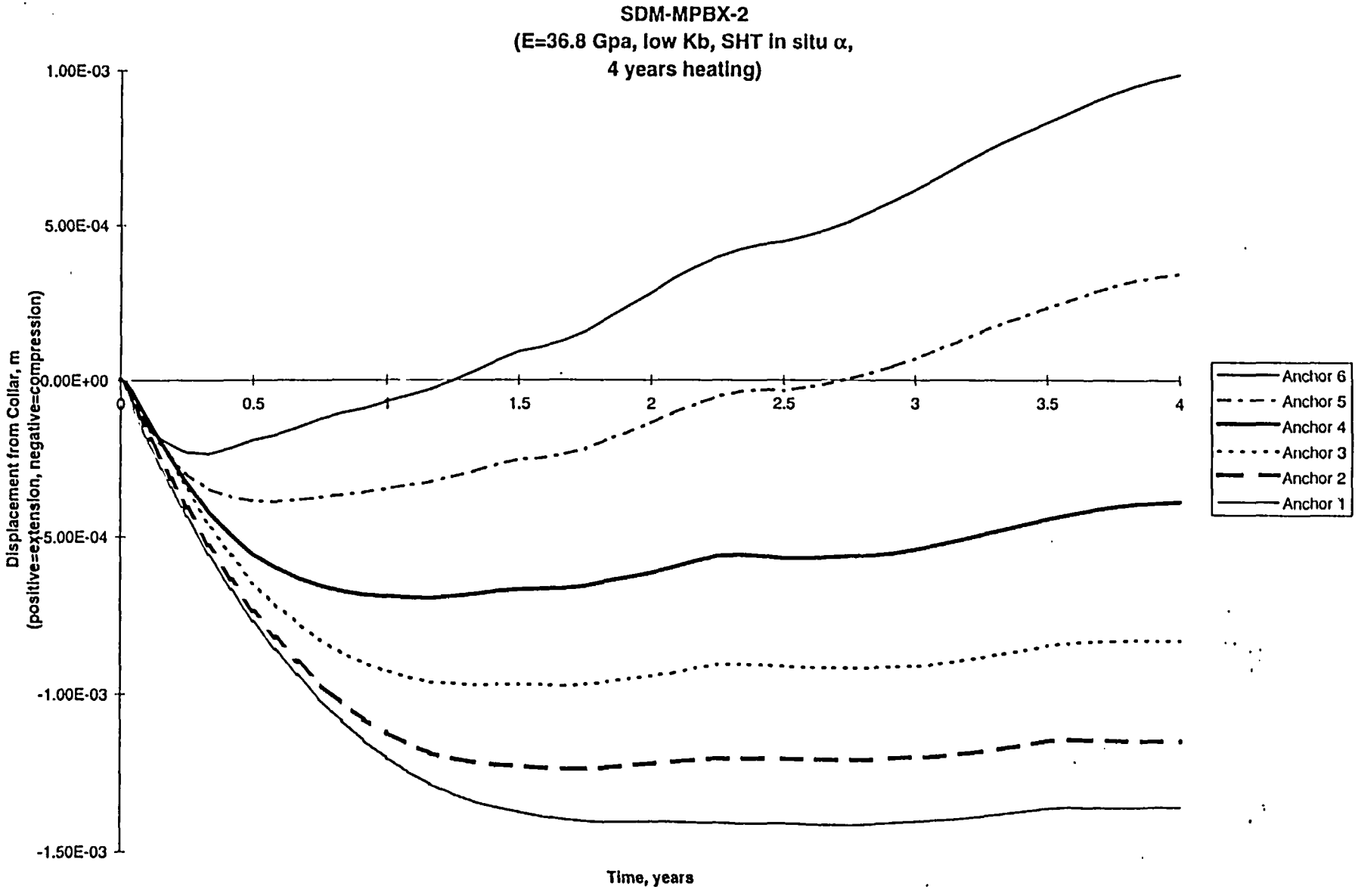
SDM-MPBX-2
(E=36.8 Gpa, low Kb, SHT in situ α,
4 years heating)
1.00E-03
5.00E-04
0.00E+00
-5.00E-04
-1.00E-03
-1.50E-03
Displacement from Collar, m
(positive=extension, negative=compression)
0
0.5
1
1.5
2
2.5
3
3.5
4
Time, years
Anchor 6
Anchor 5
Anchor 4
Anchor 3
Anchor 2
Anchor 1

Figure D-24

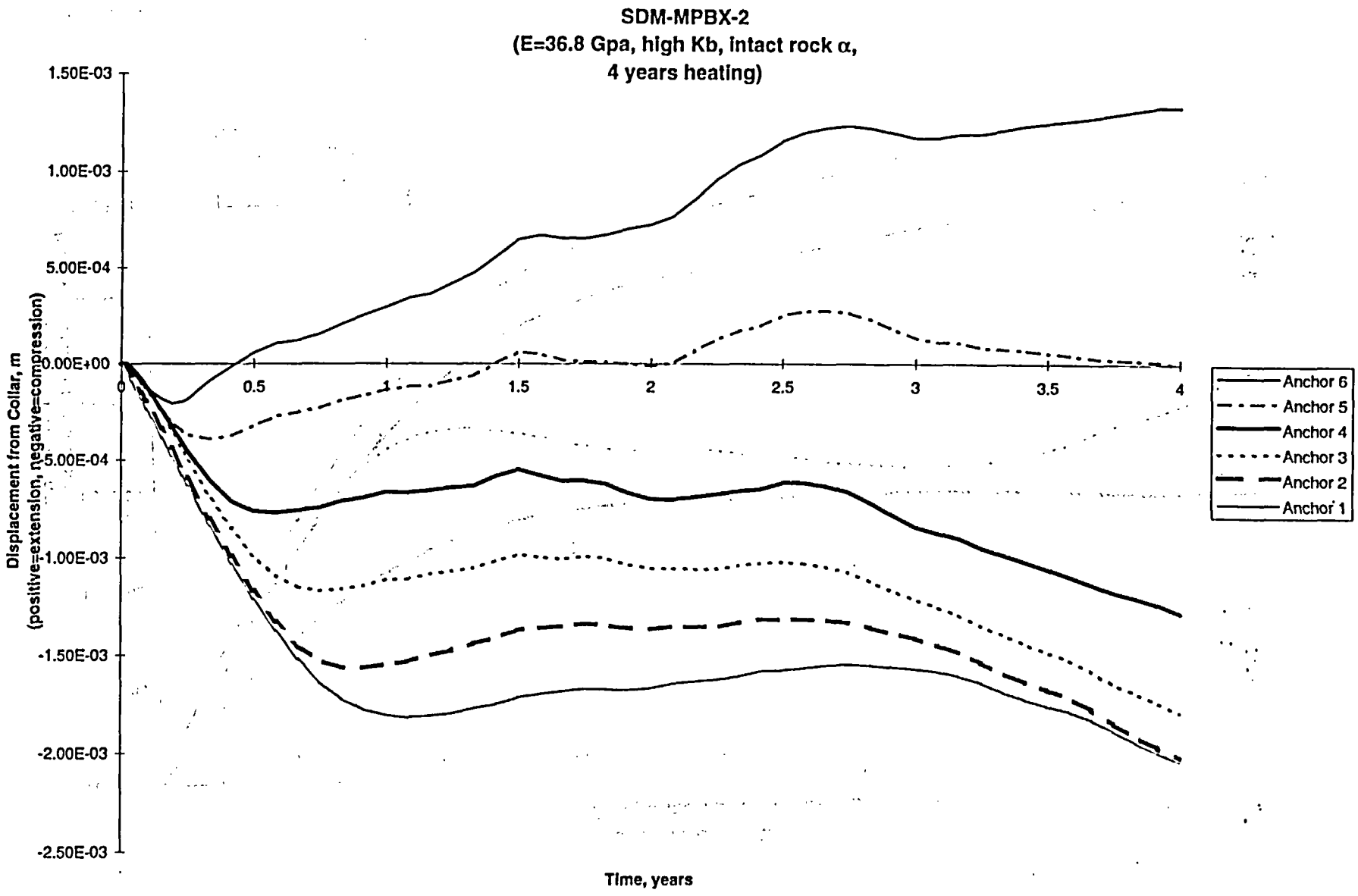
SDM-MPBX-2
(E=36.8 Gpa, high Kb, intact rock α,
4 years heating)
1.50E-03
1.00E-03
5.00E-04
0.00E+00
-5.00E-04
-1.00E-03
-1.50E-03
-2.00E-03
-2.50E-03
0
0.5
1
1.5
2
2.5
3
3.5
4
Displacement from Collar, m
(positive=extension, negative=compression)
Time, years
Anchor 6
Anchor 5
Anchor 4
Anchor 3
Anchor 2
Anchor 1

Figure D-25

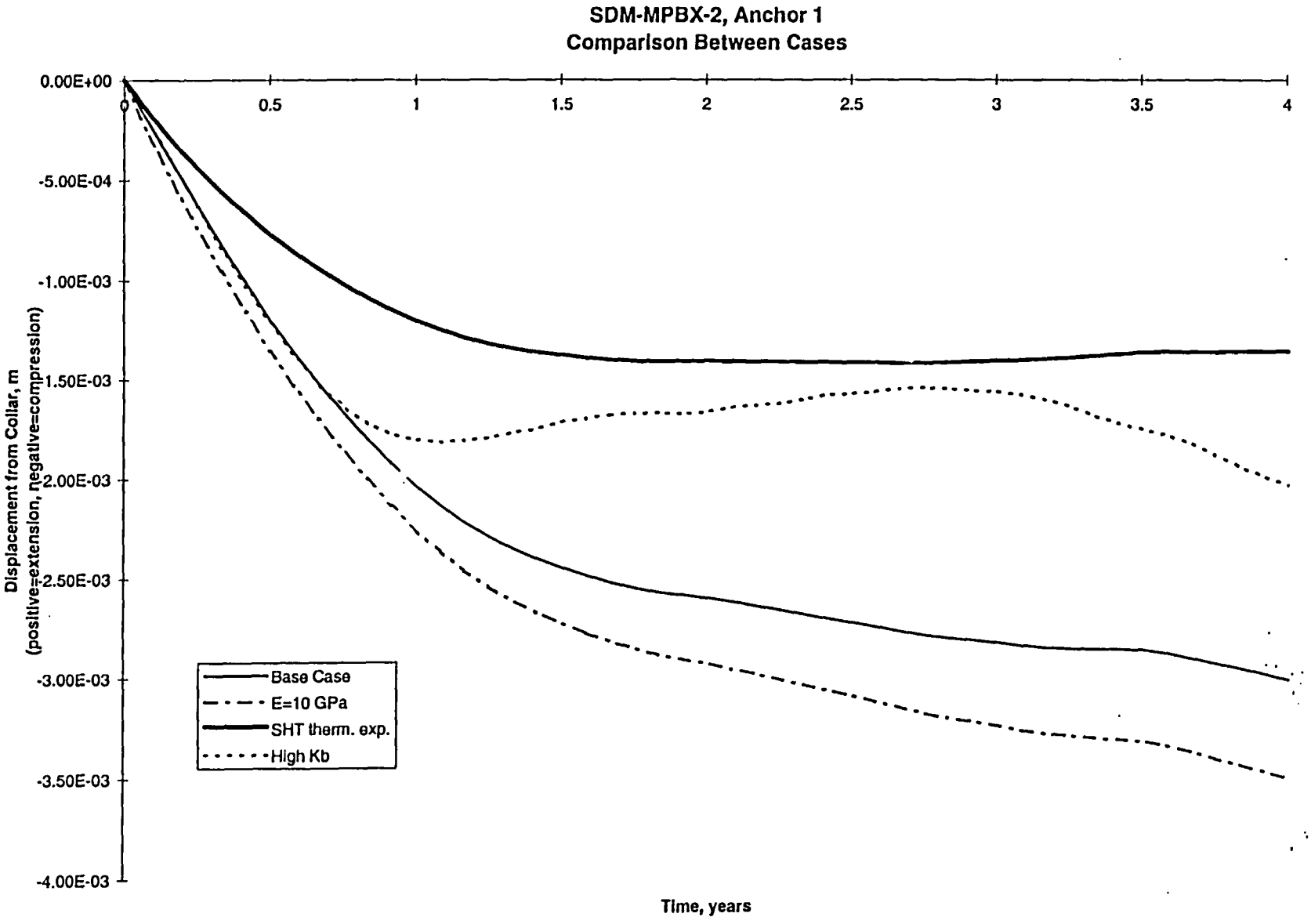
SDM-MPBX-2, Anchor 1
Comparison Between Cases
0.00E+00
-5.00E-04
-1.00E-03
-1.50E-03
-2.00E-03
-2.50E-03
-3.00E-03
-3.50E-03
-4.00E-03
0
0.5
1
1.5
2
2.5
3
3.5
4
Displacement from Collar, m
(positive=extension, negative=compression)
Time, years
Base Case
E=10 GPa
SHT therm. exp.
High Kb

Figure D-26

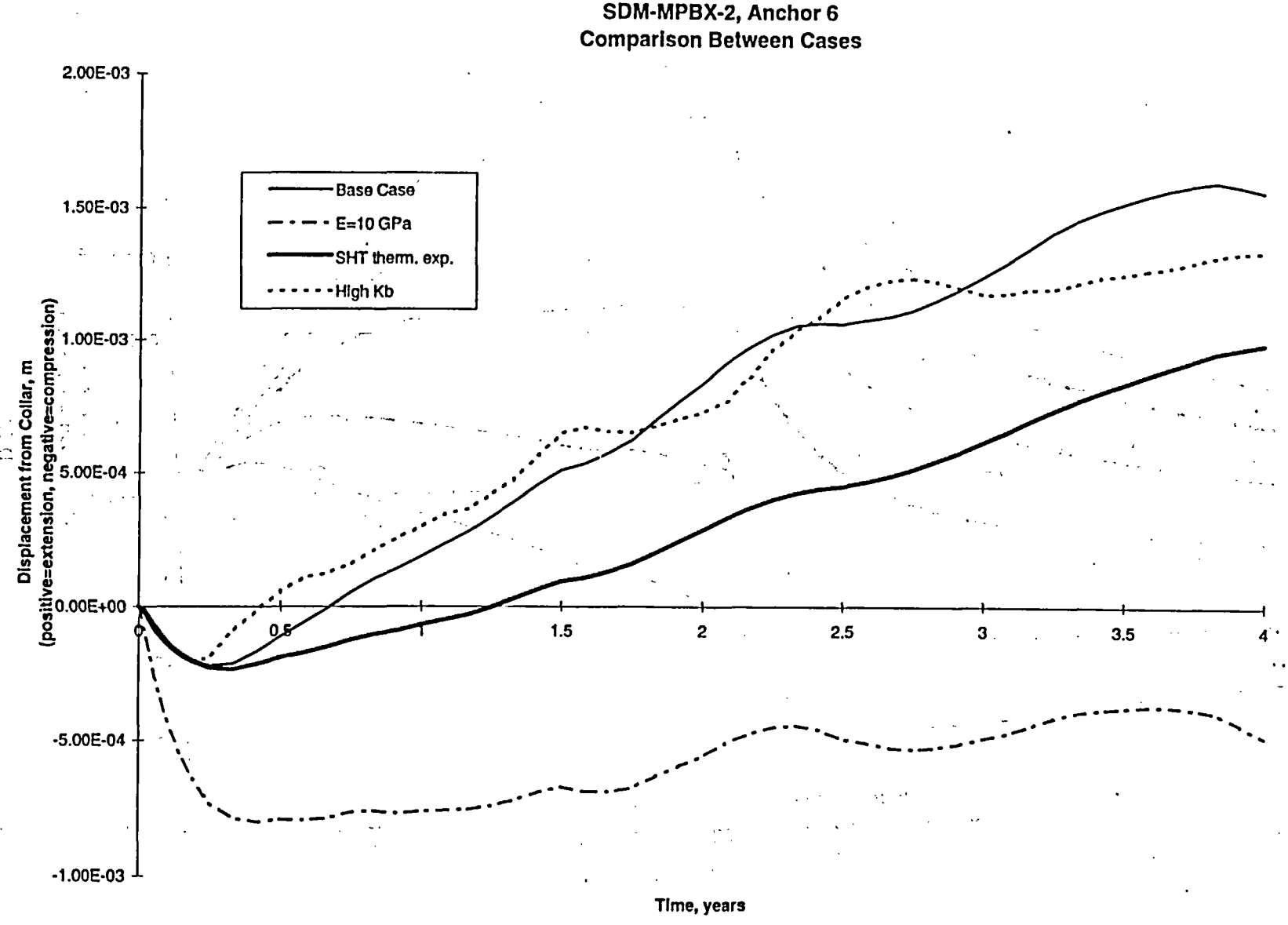
SDM-MPBX-2, Anchor 6
Comparison Between Cases
Base Case
E=10 GPa
SHT therm. exp.
High Kb
2.00E-03
1.50E-03
1.00E-03
5.00E-04
0.00E+00
-5.00E-04
-1.00E-03
Displacement from Collar, m
(positive=extension, negative=compression)
0
0.5
1.5
2
2.5
3
3.5
4
Time, years

Figure D-27

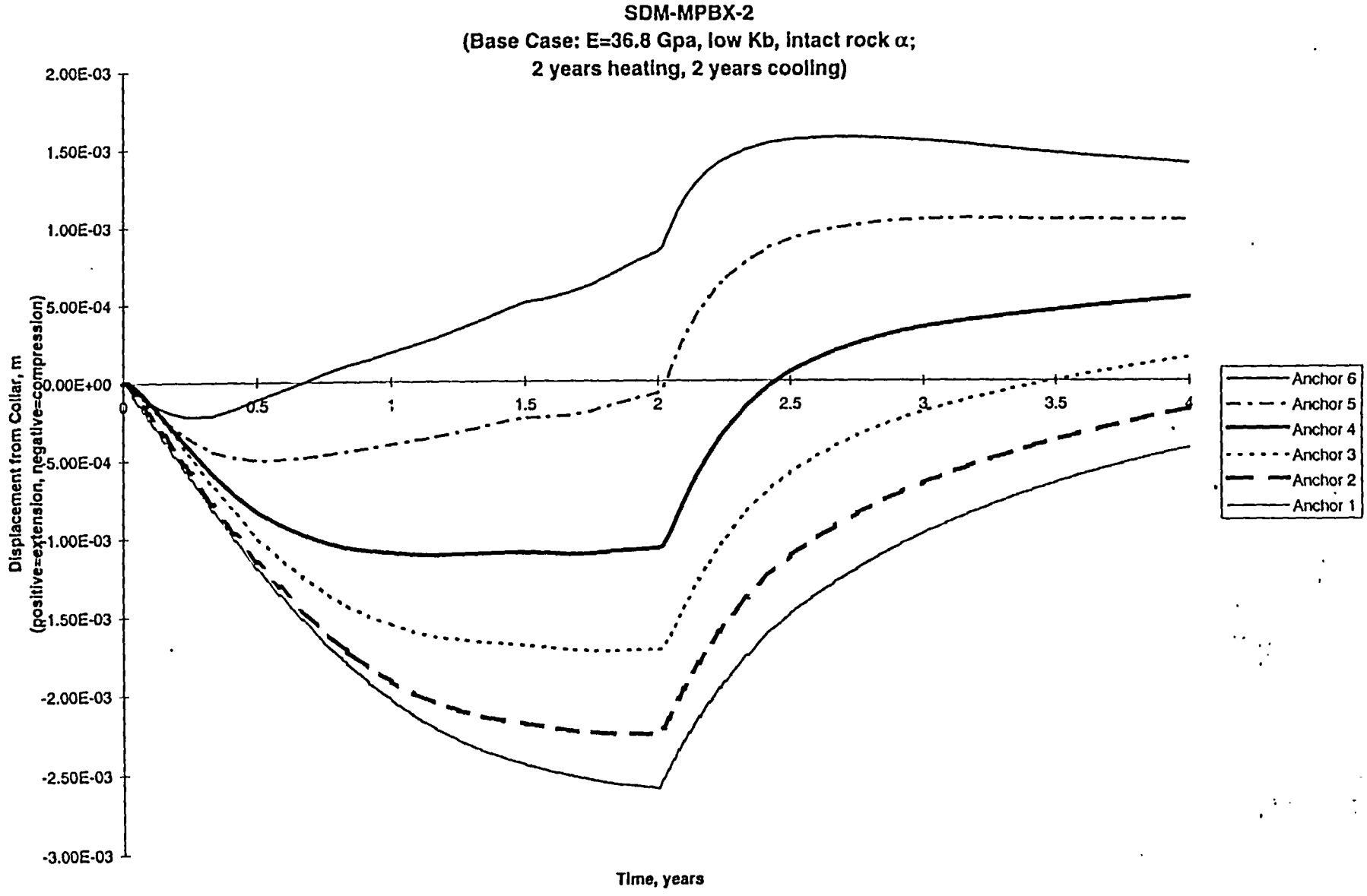
SDM-MPBX-2
(Base Case: E=36.8 Gpa, low Kb, intact rock α;
2 years heating, 2 years cooling)
2.00E-03
1.50E-03
1.00E-03
5.00E-04
0.00E+00
-5.00E-04
-1.00E-03
-1.50E-03
-2.00E-03
-2.50E-03
-3.00E-03
Displacement from Collar, m
(positive=extension, negative=compression)
0
0.5
1
1.5
2
2.5
3
3.5
4
Time, years
Anchor 6
Anchor 5
Anchor 4
Anchor 3
Anchor 2
Anchor 1

Figure D-28